APPLICATIONS OF REVERSIBLE AND SUSTAINABLE AMINE-BASED CHEMISTRIES: CARBON DIOXIDE CAPTURE, IN SITU AMINE PROTECTION AND NANOPARTICLE SYNTHESIS

A Thesis
Presented to
The Academic Faculty

By

Amy Lynn Ethier

In Partial Fulfillment
Of the Requirements for the Degree
Doctor of Philosophy in Chemical Engineering

Georgia Institute of Technology

December 2013

APPLICATIONS OF REVERSIBLE AND SUSTAINABLE AMINE-BASED CHEMISTRIES: CARBON DIOXIDE CAPTURE, IN SITU AMINE PROTECTION AND NANOPARTICLE SYNTHESIS

Approved By:

Dr. Charles Eckert
School of Chemical and Biomolecular Engineering
Georgia Institute of Technology

Dr. Amyn Teja
School of Chemical and Biomolecular Engineering
Georgia Institute of Technology

Dr. Charles Liotta
School of Chemistry and Biochemistry
Georgia Institute of Technology

Dr. Andrei Fedorov
School of Mechanical Engineering
Georgia Institute of Technology

Dr. Carson Meredith
School of Chemical and Biomolecular Engineering
Georgia Institute of Technology

Date Approved: 24 July 2013

For Dr. Nikhil Bhiwankar, who helped me to see my potential

ACKNOWLEDGEMENTS

TABLE OF CONTENTS

LIST OF TABLES

LIST OF FIGURES

LIST OF ABBREVIATIONS

α,αDMe-TEtSA	2-methyl-4-(triethylsilyl)-butyl-2-amine
αMe-TEtSA	4-(triethylsilyl)-butyl-2-amine
βMe-TEtSA	2-methyl-3-(triethylsilyl)propylamine
γ	surface tension
λ	wavelength at maximum absorption
ρ	density
ΔH_{rxn}	enthalpy of reaction
ACN	acetonitrile
Al_2O_3	alumina
ATR-FTIR	Attenuated Total Reflectance Fourier-Transform Infrared
AuNP	gold nanoparticles
CMC	critical micelle concentration
CO_2	carbon dioxide
COSMO-RS	conductor-like screening model for realistic solvation
Cp	heat capacity
DBU	1,8-diazabicyclo[5.4.0]undec-7-ene
DLS	dynamic light scattering
DIPEA	diisopropyl ethylamine
DLaTGS	deuterated L-alanine doped triglycene sulphate
DMESA	3-(aminopropyl)dimethylethylsilane
DMF	dimethyl formamide
DMSO	dimethyl sulfoxide
DOE	Department of Energy
DSC	differential scanning calorimetry

GC-MS	gas chromatography – mass spectrometry
h	height of capillary rise
$HAuCl_4$	gold (III) chloride trihydrate, or tetrachloroauric acid
HPLC	high-performance liquid chromatography
LC-MS	liquid chromatography – mass spectrometry
MEA	monoethanolamine
N_2H_4	hydrazine
$NaBH_4$	sodium borohydride
Na_2CO_3	sodium carbonate
NMR	nuclear magnetic resonance (spectroscopy)
NSF	National Science Foundation
PTC	phase transfer catalyst
r	inner radius of capillary
RevIL	reversible ionic liquid
r_h	hydrodynamic radius
RI	refractive index
RT	room temperature
SAXS	small angle X-ray scattering
$scCO_2$	supercritical carbon dioxide
SDMESA	N-methyl-3-(aminopropyl)dimethylethylsilane
SiO_2	silica
SPR	surface plasmon resonance band
STEtSA	N-methyl-3-(triethylsilyl)propan-1-amine
TEM	transmission electron microscopy/microscope
TESA	triethoxysilylpropylamine
TEtSA	3-(aminopropyl) triethylsilane

TEtSBA	4-(aminobutyl) triethylsilane
TEtSEtA	2-(aminoethyl) triethylsilane
TEtSMA	1-(aminomethyl) triethylsilane
THF	tetrahydrofuran
THSA	3-(aminopropyl) trihexylsilane
TiO_2	titania
TMBG	tetramethyl-butyl guanidine
TMG	1,1,3,3-tetramethylguanidine
TMSA	trimethoxysilylpropylamine
TPSA	3-(aminopropyl) tripropylsilane
trans-TEtSA	(trans)-3-(triethylsilyl)prop-2-en-1-amine
trans-α,αDMe-TEtSA	2-methyl-4-(triethylsilyl)-butyl-2-amine
trans-α,αDMe-TPSA	2-methyl-4-(tripropylsilyl)-butyl-2-amine
TSIL	task-specific ionic liquid
UV-vis	ultraviolet-visible (spectroscopy)

SUMMARY

Sustainability principles guided the development of technology surrounding three research projects. The first project centered on the development of silylamines for post-combustion carbon capture. Silylamines react with CO_2 to form reversible ionic liquids (RevILs). The silylamines were evaluated in terms of performance parameters such as CO_2 capacity, viscosity of the RevIL, and enthalpy of regeneration. Through iterative molecular design, structure-property relationships were established and the proposed solvent system optimized for CO_2 capture.

Three strategies for the use of CO_2, as a reversible, *in-situ* protecting group for amines were investigated in the second project. The utility of the amine protection strategy was determined by performing a chemoselective reaction using CO_2 to protect a reactive amine and direct the reaction to a less reactive site on the same molecule. The reversible, *in-situ* protection of amines using CO_2 has significant impact in industrial syntheses, as it would eliminate the need for separate protection and deprotection unit operations.

The properties and potential applications of gold nanoparticles (AuNP) are highly dependent on their size and shape. For this reason, much effort has been devoted to establish specific and controlled methodologies for nanoparticle synthesis. Producing nanomaterials in a sustainable manner has become a key prospect for nanotechnologies, and was the focus of the third project. Gold nanoparticles were successfully synthesized using reversible ionic liquids. The reversible ionic liquid system offers strong advantages over the existing nanoparticle synthetic techniques in that it provides both stabilization

and size control, and an additional surfactant is not required. The unique, reversible nature of the ionic liquids facilitated the deposition of the nanoparticles on a solid support by heating the solution.

CHAPTER 1 - INTRODUCTION

1.1 Green Chemistry Principles

Green chemistry is the design of processes to incorporate principles that reduce waste and minimize or eliminate the use or generation of hazardous species.[1] Twelve principles of green chemistry were outlined in a book titled *Green Chemistry: Theory and Practice by* Paul Anastas and John Warner.[2] The principles of green chemistry guide the development of methodologies that reduce or eliminate the use and generation of hazardous substances while maintaining an economically driven approach.[3] There are challenges and opportunities associated with the implementation of these principles, and the successful application of sustainable practices will first require an understanding of the drivers for change.[4] The three cornerstones of practical development -- economic, environmental and social -- direct research and industry towards the design of environmentally sustainable processes.

The reduction of waste is a common goal in the projects presented in this thesis. Waste disposal, regulation on pollution, and the cost of raw material have become increasingly expensive for industry. Waste reduction can be achieved through decreased or selected solvent use, more efficient processes that minimize energy loss, identifying recyclability strategies, and improving atom economy.[4, 5] These are all strategies that have been incorporated into the research completed in the Eckert-Liotta group.

Research on CO_2 capture with reversible ionic liquids addresses a need for neat solvents that efficiently capture CO_2, and can be regenerated (release CO_2) with minimal

addition of heat. The development of these capture agents aims to eliminate the need for a co-solvent, while minimizing energy loss and achieving solvent recyclability. Chapter 3 presents the investigation into the use of CO_2 as a temporary protecting group of amine functionalities during chemical syntheses. Amine protection is widely used in almost all sectors of the chemical and pharmaceutical industry. The use of CO_2 as a reversible protecting group reduces solvent waste during protection and deprotection and improves the atom economy of existing processes. The principles of green chemistry have also been applied to the use of reversible ionic liquids as switchable surfactants for nanoparticle synthesis. This synthetic approach reduces solvent waste by eliminating the need for solvent washes and presents a potential for recyclability of the system.

A multidisciplinary approach has been applied to the development of sustainable technologies with an understanding that societal and environmental considerations are only two drivers of change. For the successful implementation of any process, including those presented here, the economics of the technology are significant and must be considered.

1.2 CO_2 Capture with Reversible Ionic Liquids

Energy consumption in the United States is projected to increase from 98 quadrillion BTUs (consumed in 2011) to 108 quadrillion BTUs in 2040.[6] Despite increasing effort to develop clean, alternative energy technologies, there will be a continued dependence on the combustion of fossil fuels to meet the increasing energy demand in the U.S. and globally. In 2011 coal provided 46% of the electricity generated in the U.S. and is projected to remain the predominant fuel for electricity generation through 2035.[7]

CO$_2$ has been identified as a greenhouse gas that is contributing to global warming.[8] A significant source of CO$_2$ emissions in energy related industries is the combustion of coal.[9] The combustion of coal accounted for 79% of the CO$_2$ emissions from power plants in the United States in 2011, as shown Figure 1.1.[6]
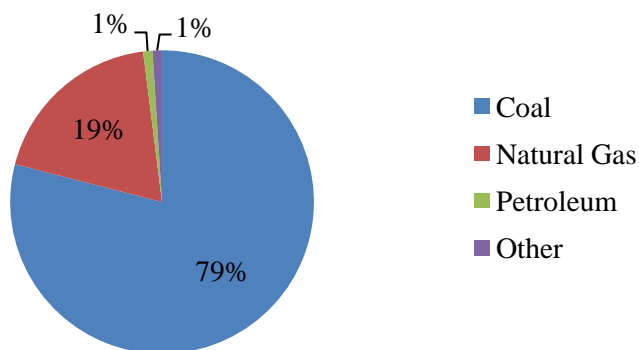
Figure 1.1. CO$_2$ emissions by U.S. electricity generation by source in 2011

CO$_2$ capture technologies must be developed and employed to minimize greenhouse gas emissions.

There are many CO$_2$ capture technologies being developed, including physical and/or chemical absorption using liquid solvents, swing adsorption with MOF's, zeolites, membrane technology, and chemical looping.[10] CO$_2$ capture with aqueous amines is the most developed technology and the current benchmark for CO$_2$ capture.[11] Aqueous monoethanolamine has been used extensively in natural gas sweetening applications, but is also the most mature technology for CO$_2$ capture from dilute, low pressure streams. Liquid solvents such as monoethanolamine react with CO$_2$ to recover 75-90% of CO$_2$ from the inlet source and produce a high purity CO$_2$ outlet stream.[12]

Presented in Chapter 2 is the development of novel CO$_2$ capture solvents. Non-aqueous silylamines react with CO$_2$ to form a reversible ionic liquid. The reversible ionic

3

liquid is capable of additional CO_2 capture through physical absorption. A spectroscopic technique has been developed to determine the chemical and physical absorption capacity. Additional physical properties of the RevIL such as enthalpy of reaction and viscosity were investigated as properties that influence the feasibility of use in capture applications. Optimal solvents for CO_2 capture from high and low pressure streams will be presented.

1.3 In-situ, Reversible Amine Protection with CO_2

Organic syntheses are often multi-step processes with molecules containing more than one reactive site. The reactivity of the functional groups dictates the synthetic pathway unless a protecting group is used. Protective groups serve to block reactive sites to prevent reaction, to reduce unwanted products, or to drive reactivity toward a less reactive group.[13] The use of protecting groups allows for the synthesis of molecules that would otherwise be impossible and has contributed to the successful growth in syntheses of complex molecules.[14]

The use of protecting groups requires protection of the functional group and deprotection following reaction. The addition of these two steps in the synthetic procedure results in a loss in material and generation of waste; specifically during deprotection when the product must be separated. Many efforts have been made to increase synthetic efficiency without the use protecting groups.[15] It is acknowledged, however, that the construction of molecules without protecting groups is a major challenge. One strategy that avoids the introduction and removal of protecting groups in separate steps is *in-situ* protection and deprotection.[15]

Presented in Chapter 3 is the *in-situ,* reversible protection of an amine functionality with CO_2. CO_2 is an inexpensive and safe protecting group and the protection is achieved in a single, reversible reaction. The ability to remove the CO_2 through thermal reversal, results in a significant reduction in waste during deprotection and product separation.

1.4 Reversible Ionic Liquids as Switchable Surfactants for Gold Nanoparticle Synthesis

Nanoparticle synthesis has attracted heightened interest due to increased use of nanoparticles for advanced technologies and catalytic processes.[16] Gold nanoparticles have been studied and characterized extensively, and as a result these were selected to demonstrate proof of concept experiments. Most of the current syntheses, isolation and purification protocols of nanomaterials are expensive, time- and waste-intensive.[17] A strategy for the synthesis of gold nanoparticles using reversible ionic liquids (RevILs) is presented in Chapter 4. The reversible ionic liquids serve as switchable surfactants to form reverse micelles as a template for nanoparticle synthesis. In the synthesis of gold nanoparticles using reversible ionic liquids, there are a number of conditions that were investigated and optimized to produce monodisperse nanoparticles (e.g., silylamine structure). The goal of this research was to develop an approach to nanoparticle synthesis that would reduce waste while achieving the desired physical characteristics -- size, shape and monodispersity -- of the resulting nanoparticles.

1.5 References

1.   Anastas, P. T.; Heine, L. G.; Williamson, T. C., *Green Chemical Syntheses and Processes*. American Chemical Society: Washington D.C., 2000; Anastas, P. T.;

Kirchhoff, M. M., Origins, current status, and future challenges of green chemistry. *Accounts of Chemical Research* **2002,** *35* (9), 686-694.

2.   Anastas, P. T.; Warner, J. C., *Green chemistry: theory and practice*. Oxford University Press: Oxford, England, 1998.

3.   Manley, J. B.; Anastas, P. T.; Cue, B. W., Frontiers in Green Chemistry: meeting the grand challenges for sustainability in R&D and manufacturing. *Journal of Cleaner Production* **2008,** *16* (6), 743-750.

4.   Clark, J. H., Green chemistry: today (and tomorrow). *Green Chemistry* **2006,** *8* (1), 17-21.

5.   Constable, D. J. C.; Jimenez-Gonzalez, C.; Henderson, R. K., Perspective on solvent use in the pharmaceutical industry. *Organic Process Research & Development* **2007,** *11* (1), 133-137.

6.   EPA *Emissions of Greenhouse Gases in the United States*; Environmental Protection Agency: Washington D.C., 2011.

7.   Administration, U. S. E. I. *Annual Energy Review 2011 with Projections to 2035*; U.S. Energy Information Administration: Washington D.C., 2011.

8.   Cox, P. M.; Betts, R. A.; Jones, C. D.; Spall, S. A.; Totterdell, I. J., Acceleration of global warming due to carbon-cycle feedbacks in a coupled climate model (vol 408, pg 184, 2000). *Nature* **2000,** *408* (6813), 750-750.

9.   EPA *Inventory of U.S. Greenhouse Gas Emissions and Sinks:1990-2011*; Washington D.C., 2013.

10.   Lively, R. P.; Chance, R. R.; Kelley, B. T.; Deckman, H. W.; Drese, J. H.; Jones, C. W.; Koros, W. J., Hollow fiber adsorbents for CO_2 removal from flue gas. *Industrial & Engineering Chemistry Research* **2009,** *48* (15), 7314-7324; Banerjee, R.; Phan, A.; Wang, B.; Knobler, C.; Furukawa, H.; O'Keeffe, M.; Yaghi, O. M., High-throughput synthesis of zeolitic imidazolate frameworks and application to CO2 capture. *Science* **2008,** *319* (5865), 939-943; Mason, J. A.; Sumida, K.; Herm, Z. R.; Krishna, R.; Long, J. R., Evaluating metal-organic frameworks for post-combustion carbon dioxide capture via temperature swing adsorption. *Energy & Environmental Science* **2011,** *4* (8), 3030-3040; Rochelle, G. T., Amine Scrubbing for CO2 Capture. *Science* **2009,** *325* (5948), 1652-1654; Brennecke, J. F.; Gurkan, B. E., Ionic Liquids for CO2 Capture and Emission Reduction. *The Journal of Physical Chemistry Letters* **2010,** *1* (24), 3459-3464; Anderson, J. L.; Dixon, J. K.; Maginn, E. J.; Brennecke, J. F., Measurement of SO_2 solubility in ionic liquids. *Journal of Physical Chemistry B* **2006,** *110*, 15059-15062; Kronberger, B.; Johansson, E.; Löffler, G.; Mattisson, T.; Lyngfelt, A.; Hofbauer, H., A Two-Compartment Fluidized Bed Reactor for CO2 Capture by Chemical-Looping Combustion. *Chemical Engineering & Technology* **2004,** *27* (12), 1318-1326.

11. MacDowell, N.; Florin, N.; Buchard, A.; Hallett, J.; Galindo, A.; Jackson, G.; Adjiman, C. S.; Williams, C. K.; Shah, N.; Fennell, P., An overview of CO2 capture technologies. *Energy & Environmental Science* **2010,** *3* (11), 1645-1669; Rubin, E. S.; Mantripragada, H.; Marks, A.; Versteeg, P.; Kitchin, J., The outlook for improved carbon capture technology. *Progress in Energy and Combustion Science* **2012,** *38* (5), 630-671; Rao, A. B.; Rubin, E. S., A Technical, Economic, and Environmental Assessment of Amine-Based CO2 Capture Technology for Power Plant Greenhouse Gas Control. *Environmental Science & Technology* **2002,** *36* (20), 4467-4475.

12. Kohl, A.; Nielsen, R., *Gas Purification*. 5th ed.; Gulf Publishing Company: Houston, Texas, 1997.

13. Wuts, P., G. M.; Greene, T. W., *Greene's Protective Groups in Organic Synthesis*. Fourth Ed. ed.; John Wiley & Sons Inc.: Hoboken, NJ, 2007.

14. Young, I. S.; Baran, P. S., Protecting-group-free synthesis as an opportunity for invention. *Nature Chemistry* **2009,** *1* (3), 193-205.

15. Hoffmann, R. W., Protecting-group-free synthesis. *Synthesis-Stuttgart* **2006,** (21), 3531-3541.

16. Jain, P. K.; Huang, X. H.; El-Sayed, I. H.; El-Sayed, M. A., Noble Metals on the Nanoscale: Optical and Photothermal Properties and Some Applications in Imaging, Sensing, Biology, and Medicine. *Accounts of Chemical Research* **2008,** *41* (12), 1578-1586; El-Sayed, M. A., Some interesting properties of metals confined in time and nanometer space of different shapes. *Accounts of Chemical Research* **2001,** *34* (4), 257-264; Eustis, S.; El-Sayed, M. A., Why gold nanoparticles are more precious than pretty gold: Noble metal surface plasmon resonance and its enhancement of the radiative and nonradiative properties of nanocrystals of different shapes. *Chemical Society Reviews* **2006,** *35* (3), 209-217; Dreaden, E. C.; El-Sayed, M. A., Detecting and Destroying Cancer Cells in More than One Way with Noble Metals and Different Confinement Properties on the Nanoscale. *Accounts of Chemical Research* **2012,** *45* (11), 1854-1865.

17. Murphy, C. J., Sustainability as an emerging design criterion in nanoparticle synthesis and applications. *Journal of Materials Chemistry* **2008,** *18* (19), 2173-2176; Raveendran, P.; Fu, J.; Wallen, S. L., Completely "green" synthesis and stabilization of metal nanoparticles. *Journal of the American Chemical Society* **2003,** *125* (46), 13940-13941.

CHAPTER 2 - SILYLAMINES AS REVERSIBLE IONIC LIQUIDS FOR CO_2 CAPTURE

2.1 Introduction

Carbon dioxide (CO_2) emissions are considered to be a major contributor to global warming. CO_2 accounts for approximately 84% of the of the anthropogenic greenhouse gas emissions, making the capture of CO_2 a primary concern to mitigate harmful environmental impact.[1] Despite increasing efforts to develop renewable (carbon neutral) energy resources, it is projected that coal will remain the principal fuel for electricity generation through 2035.[2] As coal-fired power plants produce approximately one-third of the CO_2 emissions in the United States, the potential for CO_2 capture from large point sources exists.[3]

The flue gas that is produced from burning fossil fuels has a number of components including nitrogen, carbon dioxide, water, oxygen and trace amounts of NO_X and SO_X that remain after desulfurization. The bulk of the flue gas is nitrogen with CO_2 contributing 16 vol%.[4] The dilute concentration of CO_2 in the flue gas stream requires a capture solvent with high selectivity for CO_2.[4, 5] The solvent system must also be recyclable; the large volume of flue gas produced annually makes a single-use sorbent unfeasible.[4]

Traditionally, primary and secondary amines have been used for the capture of CO_2. Upon reaction with CO_2, the amines form an ammonium-carbamate ion pair, presented in Figure 2.1.

R₁=H, Alkyl
R₂=Alkyl
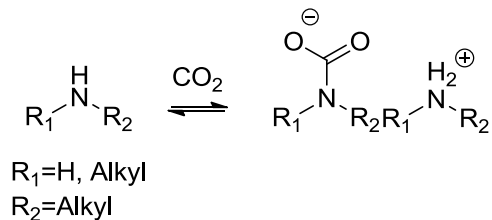
Figure 2.1. Reversible reaction of a primary and secondary amine with CO_2

One example of a primary alkanol amine is monoethanolamine, shown below in Figure 2.2.
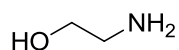
Figure 2.2. Monoethanolamine, a primary alkanolamine used for CO_2 capture

Monoethanolamine has been used for the separation of CO_2 from natural gas and is the most industrialized method of CO_2 capture.[6,7] The use of monoethanolamine for CO_2 has challenges including the high viscosity of the ammonium-carbamate ion pair and the susceptibility of monoethanolamine to degradation. The degradation of monoethanolamine is complex, but it is estimated to result in significant loss in capture capacity. It has been reported that sorbent replacement can range between 2.2-3.1 kilograms of amine per ton of CO_2 captured.[7,8] Due to the high viscosity of the ammonium-carbamate ion pair, and the corrosive nature of amines, monoethanolamine is generally used as a 30% aqueous solution.[8,9] In an amine-based CO_2 capture process, the flue gas enters the absorber where it is contacted with the capture solvent, as shown in Figure 2.3.
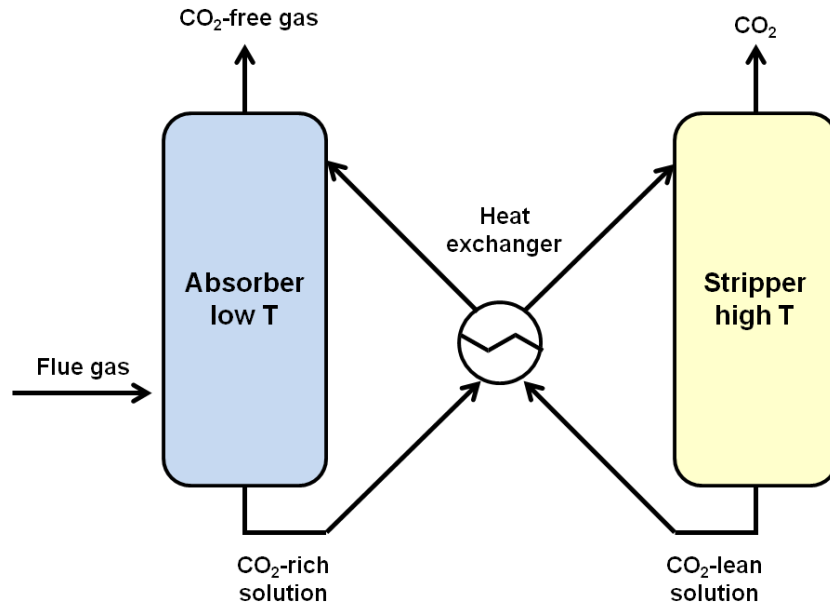
Figure 2.3. Schematic of CO_2 capture and release by a recyclable alkanolamine solution

The solvent is then regenerated by steam heating which releases the CO_2. The capture solvent is then recycled back to the absorber where it again reacts with the CO_2 in the flue gas stream. Due to the high heat capacity and heat of vaporization, it has been estimated that the regeneration of the aqueous amine solution accounts for 70-80% of the energy consumed by the entire capture process.[10]

To address the shortcomings associated with the use of aqueous amine solutions for CO_2 capture, alternative technologies are being developed. These technologies include swing adsorption with MOF's,[11] zeolites,[12] membrane technology,[13] chemical looping[14] and physical and/or chemical absorption using liquid solvents such as ionic liquids.[15]

Traditional ionic liquids capture CO_2 though physical absorption and are attractive solvents due to their negligible vapor pressure, thermal stability and chemical tunability.[16] The properties of the ionic liquid are highly dependent on the anion or cation

species, and much effort has been focused on designing ionic liquids for specific CO_2 separations.[17] Enhancing CO_2 solubility and selectivity has been a primary goal and may be achieved by through structural modification. Such modifications include increasing the alkyl chain length on the cation, or through fluorination of the anion as shown in the ionic liquids in Figure 2.4.[18, 19]
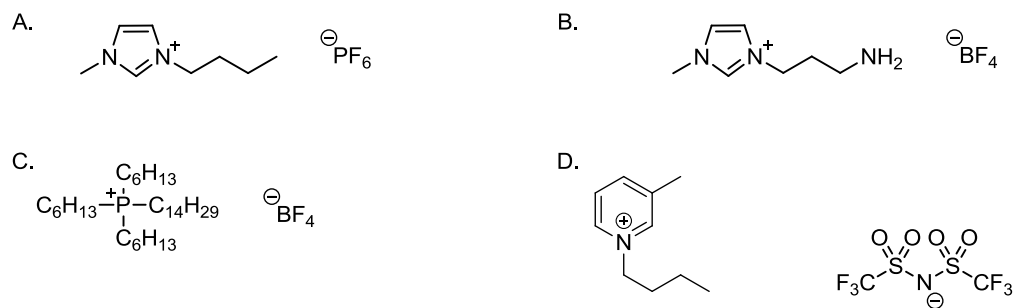
Figure 2.4. Traditional ionic liquids for CO$_2$ capture

The weak van der Waal's forces of interaction result in a very low energy requirement for CO_2 release; however, for low pressure capture conditions such as flue gas (0.16 bar), the CO_2 capacities are limited.[20] To increase the CO_2 capacity of traditional ionic liquids, amine-functionalized anions (task-specific ionic liquids) have been studied. Equimolar CO_2 absorption has been reported for the anion-functionalized ionic liquids shown below in Figure 2.5.
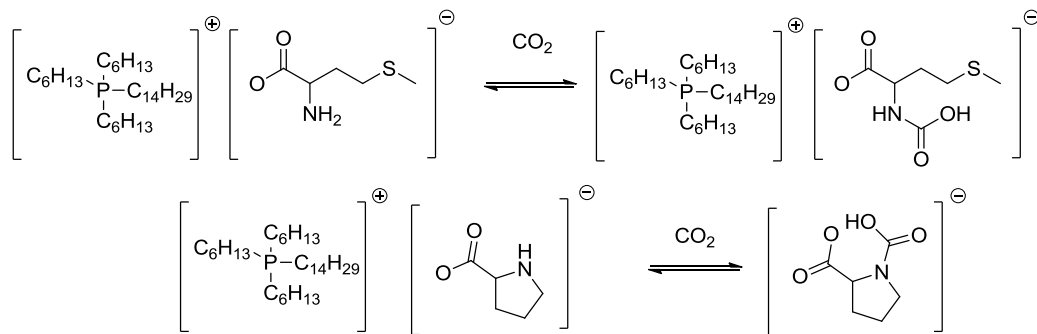
Figure 2.5. Equimolar CO$_2$ capture by anion-functionalized ionic liquids

11

The molar CO_2 capture capacity is significantly increased with the addition of a CO_2-reactive amine group on the ionic liquid backbone.[16, 21] However, ionic liquids typically have very high viscosities, which limits their industrial feasibility. Furthermore, the large molecular weight of the amine-functionalized ionic liquids is prohibitive as the pertinent measure of CO_2 capture capacity is moles of CO_2 captured per kg solvent. The drawbacks of the anion-functionalized ionic liquids result from both the starting species and the reacted species being an ionic liquid. Our group has designed a novel class of switchable solvents in which a low viscosity silylamine reacts with CO_2 forming a reversible ionic liquid that is further capable of physically absorbing CO_2.

2.2 Background

Preliminary studies on reversible ionic liquids (RevILs) focused on commercially available trialkoxysilylamines. These solvents, shown below in Figure 2.6 were initially used to extract hydrocarbons from tar sands.[22]

(3-aminopropyl)trimethoxysilane
TMSA

(3-aminopropyl)triethoxysilane
TESA
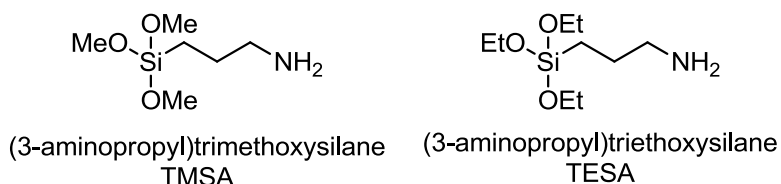
Figure 2.6. Trialkoxysilylamines for CO₂ capture

It has been reported that silane-containing ionic liquids have decreased viscosities, likely due to bond lengthening in the silylated derivatives as well as electronic effects. Upon reaction with CO_2, these trialkoxysilylamines formed liquids that were thermally reversible. The results of these studies using commercially available solvents were promising, although TMSA and TESA are susceptible to hydrolysis. The next generation

reversible ionic liquid systems focused on trialkylsilylamines as the carbon-silicon bond is stable against hydrolytic cleavage. This class of reversible ionic liquids is capable of chemical absorption through reaction with CO_2, and physical absorption of CO_2 by the reversible ionic liquid, as shown in Figure 2.7.
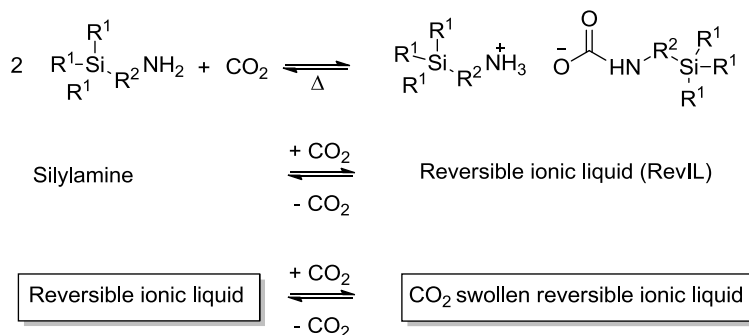
Figure 2.7. Reversible ionic liquid system for CO_2 capture

The properties of the reversible ionic liquid system are highly dependent on the structure of the silylamine. There are a number of properties of the reversible ionic liquid system that influence the viability of these solvents for commercial implementation. Over 15 silylamines were synthesized to study the effect of structure on the (1) CO_2 capture capacity (2) viscosity of the reversible ionic liquid system and (3) temperature at which CO_2 is released from the reversible ionic liquid and the silylamine reformed and (4) the enthalpy of reaction.

2.3 Experimental Methods

2.3.1 Materials

The silylamines presented in this chapter are synthesized by members of the Eckert-Liotta group. Silylamines are kept under inert conditions in a glove box until use. Carbon dioxide was supercritical fluid chromatography (SFC) grade (Air Gas, 99.999%)

and further purified via a Matheson gas purifier and filter cartridge (Model 450B, Type 451 filter).

2.3.2 <u>Instrumentation</u>

^{1}H and ^{13}C NMR spectra were collected on a Varian Mercury Vx 400, using CDCl$_3$ as the lock solvent. Silylamines were diluted directly with CDCl$_3$. Due to the high viscosities of the ionic forms, the RevILs were synthesized in the NMR tube under solvent-free conditions, and a capillary tube containing CDCl$_3$ was placed inside the sample. To conduct quantitative ^{13}C NMR, three important experimental changes were made from the standard ^{13}C NMR procedure. A full 90° pulse was required to insure complete excitation of the nucleus. An extended delay time allows for full relaxation after the pulse is applied. Complete relaxation was determined by performing an inversion recovery T_1 experiment. For 3-(aminopropyl)tripropylsilane RevIL, the carbonyl carbon (162.73 ppm) had the longest T_1 time at 4.027 seconds. It is generally recommended that the delay time used be 5 times the longest T_1 time, so for the quantitative experiments performed, a delay time of 20 seconds was used. Proton decoupling was done only during the acquisition period to avoid a false and disproportional signal buildup as a result of the Nuclear Overhauser Effect. Inverse gated decoupling with 2000 scans was performed for each experiment over a period of 12 hours to increase the signal to noise ratio.

Viscosities of all RevILs were obtained using a Rheosys Merlin II viscometer with a 2° cone and plate system; RevILs were pre-formed, allowed to thermally equilibrate on the instrument, and measured in triplicate.

Differential scanning calorimetry (DSC) measurements were used to determine the reversal temperatures of the RevILs and the temperature of evaporation of the silylamines. The instrument used was a Q20 TA Instruments DSC. 2 mg of the RevIL sample was sealed in an aluminum pan. The temperature was ramped from -40°C to 400°C with a ramp rate of 5°C·min^{-1}, and the temperatures of the reversal or evaporation were determined by the intersect of the baseline of the event and the line tangent to the peak of the event. A DSC thermogram of the TEtSA reversible ionic liquid system is shown in Figure 2.8
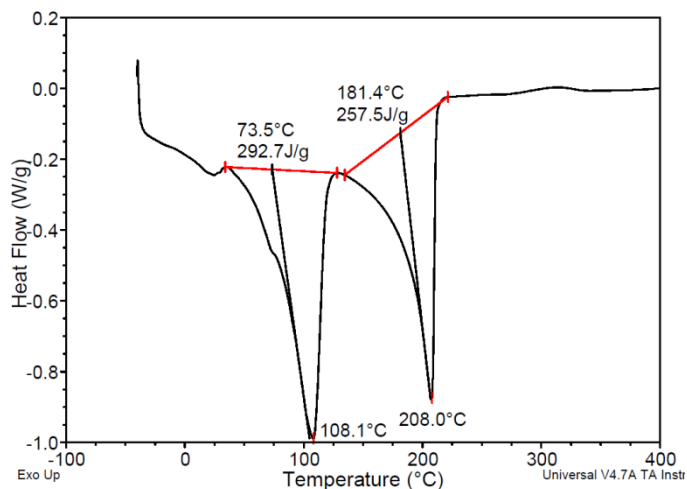
Figure 2.8. DSC thermogram of TEtSA reversible ionic liquid system

For refractive index (RI) measurements, a Reichert Arias 500 Abbe-style refractometer was used, with a circulated cooling bath (heat transfer fluid: glycol). The refractometer is a semi-automatic design which eliminates the need for users to interpret the shadowline intercept, resulting in an accuracy of ±0.0001 regardless of user. Refractive index measurements were determined in triplicate. Density measurements were performed using an Anton Paar DMA 38 density meter capable of measurements from 15°C to 40°C with an accuracy of ±0.001 g/mL.

15

Attenuated Total Reflectance Fourier Transform Infrared spectroscopy (ATR-FTIR) data were collected using a Shimadzu IRPrestige21 with a DLaTGS detector. 32 scans were collected with a resolution of 1 cm^{-1} for each IR spectrum. The FTIR was used in combination with a Specac heated Golden Gate^{TM} ATR accessory with a diamond crystal and zinc selenide lenses. The IR beam is passed through the ATR crystal which results in total internal reflection and the propagation of an evanescent wave along the boundary surface.

2.3.3 Apparatus and Procedures

2.3.3.1 RevIL Synthesis

The formation of the reversible ionic liquid from the silylamine was carried out as follows. A 2 dram vial was weighed; approximately one gram of the silylamine was added to the vial and was weighed again. A 24-50 micron porosity (porosity C) diffuser tube was weighed. The sand bath was set to the required temperature, and the temperature allowed to stabilize. Dry carbon dioxide was sparged through the silylamine for 75 minutes at a flow rate of 200 mL·min^{-1} at 25°C and 1 bar using the diffuser tube. The resulting reversible ionic liquid in the vial and the diffuser tube were then weighed to determine CO_2 capture capacity. In cases where the silylamine formed a solid upon reaction with CO_2 the diffuser tube could not be used. Instead, a stainless steel needle was used to sparge CO_2 through the sample.

2.3.3.2 Reactor Cell for ATR-FTIR Measurements

The Heated Golden Gate^{TM} ATR was used in conjunction with a custom built high pressure stainless steel reactor cell developed through collaboration of the Eckert-

Liotta group and Dr. Kazarian of Imperial College London. The ATR and the reactor cell are shown below in Figure 2.9.
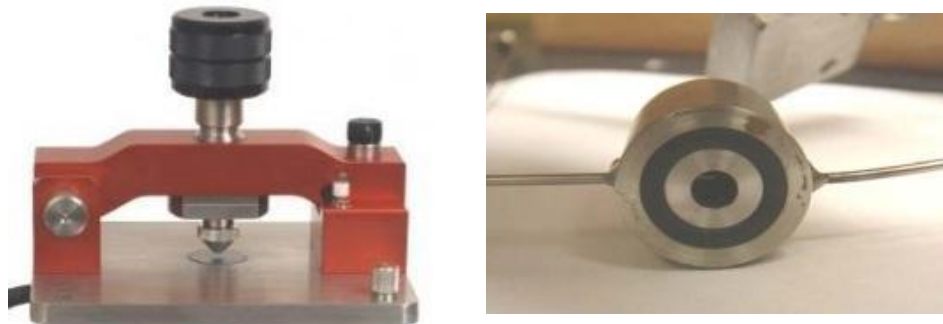
Figure 2.9. ATR accessory (left) and high pressure reactor cell (right)

The reactor cell was designed with approximately 12 in. of HiP 1/16 in. 316 stainless steel tubing attached to the 0.065 in. inlet port of the reactor cell fixed with silver solder. The inlet line was attached to an Isco syringe pump (Model 500D) and the pressure monitored with an Omega 1000 psia pressure transducer. A 0.075 in. recess was used for the placement of a Kalrez O-ring that sealed the base of the reactor to the diamond-embedded tungsten carbide puck on the ATR top plate. The apparatus was tested at 150°C and 70 bar. Physical absorption measurements were completed by placing approximately 0.05 mL of reversible ionic liquid (pre-formed ex-situ to ensure complete conversion of the silylamine to the RevIL) on the diamond crystal. The sample was capped with the high pressure reactor cell and CO_2 pressure applied using an Isco syringe pump. The sample remained under CO_2 pressure for 60 minutes prior to collecting the IR spectrum to ensure vapor-liquid equilibrium had been reached.

Equilibrium conversion at temperatures above 25°C was measured using a Reaction Cell Golden Gate™ ATR reactor cell supplied by Specac, shown in Figure 2.10.

Figure 2.10. High pressure ATR reactor cell accessory

The reactor cell was used to extend the capabilities of the custom built stainless steel reactor cell. The Reaction Cell Golden Gate^{TM} ATR was tested to pressures of 70 bar, but is capable of spectral analysis at pressures up to 210 bar and temperatures up to 200˚C. The temperature of the reaction cell is controlled by an external temperature controller and outfitted with a cooling jacket to prevent overheating. The reactor cell was equipped with an inlet and outlet port for flow-through experiments. The reversible ionic liquid was preformed *ex-situ* in a sand bath equilibrated to the setpoint temperature. The RevIL sample was then transferred to the Reaction Cell Golden Gate^{TM} maintained at the setpoint temperature. CO_2 flowed over the sample to sustain a CO_2 pressure in the headspace equal to one bar. ATR-FTIR measurements were collected and used to determine the equilibrium conversion of the silylamine to the RevIL at temperatures between 40˚C and 85˚C.

2.3.3.3 Swelling Measurements Using the Sapphire Cell

The equilibrium cell consists of a hollow sapphire cylinder with a movable stainless steel piston. The piston separated the cylinder into two cells, one containing the sample and the bottom cell containing water as the pressurizing fluid. The sapphire cell was placed inside a temperature controlled air bath, and the temperature maintained by a digital temperature controller (Omega CN76000). The temperature probes were calibrated against a platinum resistance temperature detector (Omega PRP-4) with a DP251 precision resistance temperature detector bench top thermometer (DP251 Omega). The sapphire cell was mounted on a rotating shaft to facilitate mixing. A schematic of the sapphire cell is shown below in Figure 2.11.
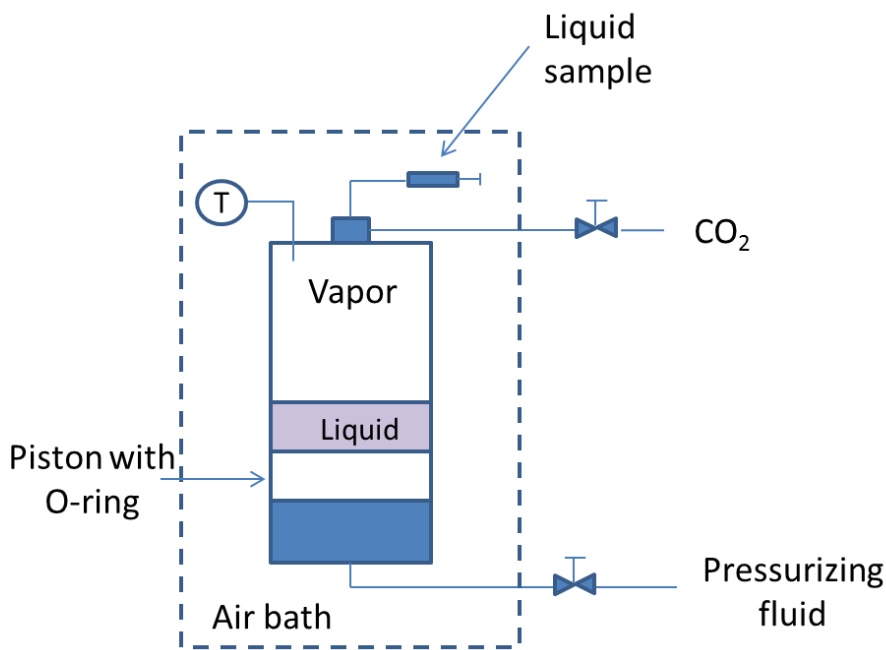
Figure 2.11. Sapphire cell apparatus

A 10 mL sample of the silylamine was added to the sapphire cell, and contacted with CO_2 by charging the cell with CO_2 supplied by an Isco pump. The silylamine was completely

converted to the RevIL when there was no observable decrease in CO_2 pressure. The pressure inside the sapphire cell was measured with a pressure transducer and digital read-out (Druck, DPI 260, PDCR 910). The transducer was calibrated against a hydraulic piston pressure gauge (Ruska) to an uncertainty of $\pm$ 0.01 MPa. Volume measurements were made by measuring height change of the liquid meniscus using a micrometer cathetometer.

2.4 Results and Discussion

The characterization of the reversible ionic liquids (RevILs) is critical in the design of a solvent system for CO_2 capture. The analysis of the reversible ionic liquids will center on the effect of silylamine structure on the (1) chemical and physical absorption of CO_2, and a spectroscopic technique used for the differentiation of the two modes of capture; (2) viscosity of the reversible ionic liquids; (3) thermodynamic properties pertinent to capture and release of CO_2 from a low pressure stream and (4) use of the reversible ionic liquids for capture for high pressure CO_2 capture.

2.4.1 CO$_2$ Capture Capacity of Silylamines

One of the pillars in the design of solvent systems for CO_2 capture is the CO_2 absorption capacity. The total CO_2 capacity for the silylamines was measured gravimetrically at one bar CO_2 pressure to demonstrate the effect of structural changes on the absorption of CO_2.

2.4.1.1 CO$_2$ Capacity from Gravimetric Analyses

The reaction of the silylamines with CO_2 is an equilibrium reaction. The conversion of the silylamine to the RevIL affects the physical properties, and therefore, to

20

achieve consistent results in the analysis of the silylamines it was necessary to achieve

reaction equilibrium for each silylamine. For the silylamines presented in this study, a

reaction time of 75 minutes was required to achieve equilibrium. This reaction time was

established by monitoring gravimetric uptake of CO_2 by 3-(aminopropyl)tripropylsilane

as a function of time as shown in Figure 2.12.
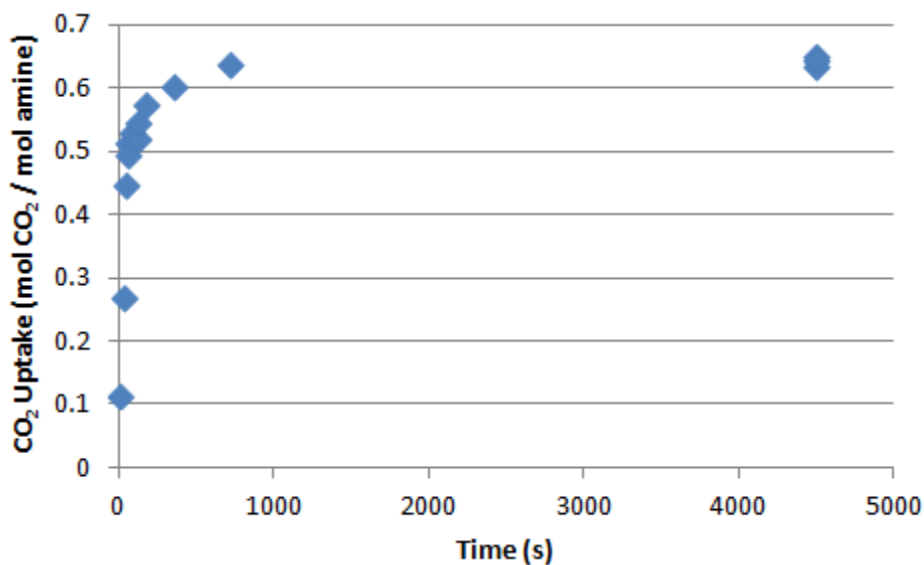
Figure 2.12. Capacity of 3-(aminopropyl)tripropylsilane as a function of time measured by gravimetric uptake

The equilibrium capacity of 3-(aminopropyl)tripropylsilane was reached after about 13

minutes. A reaction time of 75 minutes was used to make certain equilibrium had been

reached for each silylamine system presented here. Complete conversion of the

silylamine to the reversible ionic liquid was also verified using ^{13}C NMR. The ^{13}C NMRs

of 3-(aminopropyl)tripropylsilane and RevIL are shown in Figure 2.13.
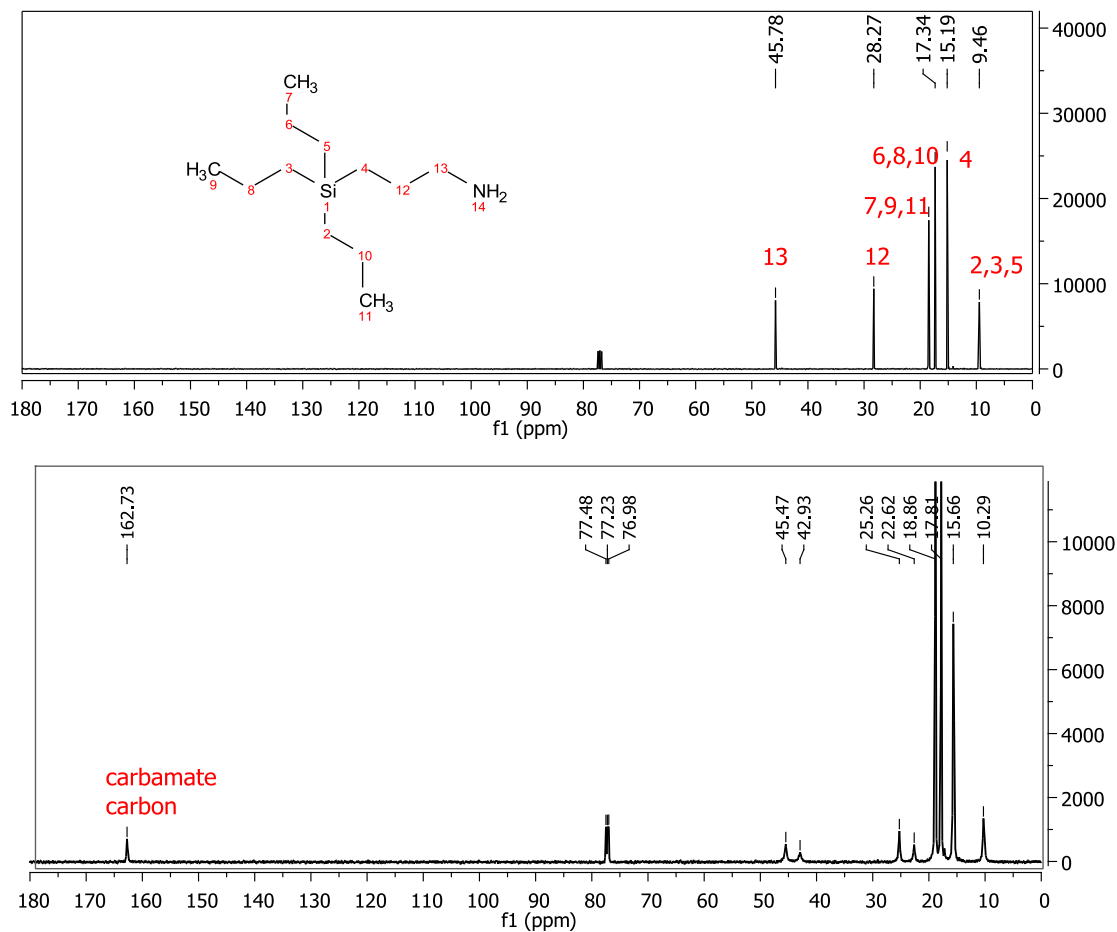
Figure 2.13. Comparison of ^{13}C NMR spectra of 3-(aminopropyl)tripropylsilane (top) and RevIL (bottom)

Upon reaction with CO_2, the silylamine (six characteristic carbons) forms the RevIL (nine characteristic carbons). The carbonyl of the carbamate species appears at 162 ppm. The complete conversion of the silylamine to the reversible ionic liquid is evident as there are no remaining silylamine peaks in the ^{13}C NMR of the RevIL.

A third measure of conversion of the silylamine to the RevIL is refractive index. Refractive index measurements are an easy approach to determine sample composition,

and conversion of the silylamine to the RevIL. Shown in Figure 2.14 are the refractive

index measurements of the 3-(aminopropyl)tripropylsilane reversible ionic liquid system.
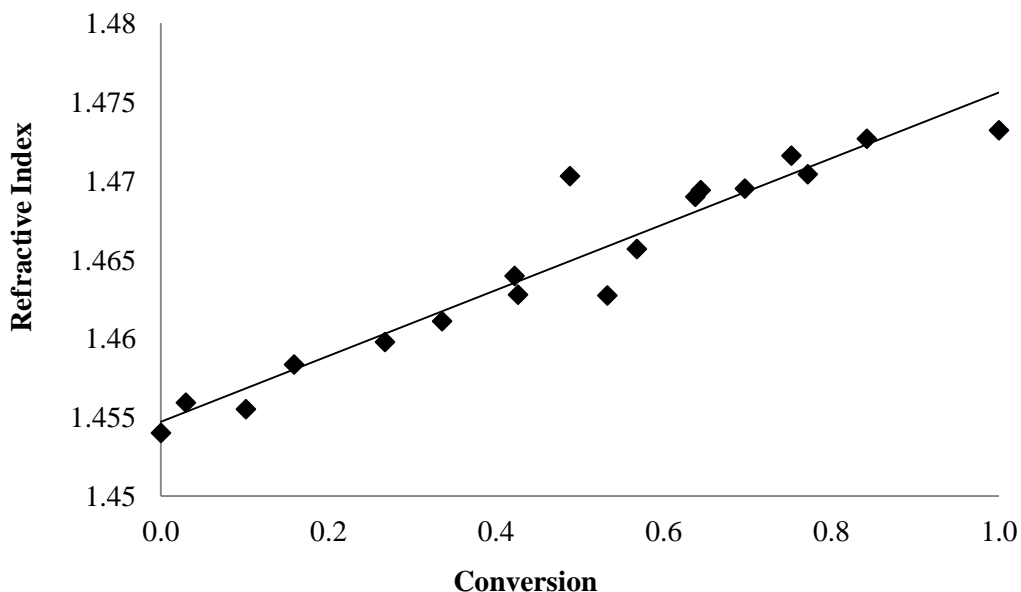
Figure 2.14. Relationship between refractive index and extent of conversion from silylamine to the reversible ionic liquid for 3-(aminopropyl)tripropylsilane

The relationship between refractive index and conversion is linear and the

refractive index was used to confirm complete conversion of the silylamine to the RevIL.

One element of the CO_2 capacity of the reversible ionic liquids that was considered was

the recyclability of the system. Recyclability is the capture and release of CO_2 over

multiple cycles. Refractive index measurements were particularly useful in studying the

recyclability of the RevIL system. Shown below in Figure 2.15 is the recyclability study

of 3-(aminopropyl)tripropylsilane. The refractive index of the silylamine was measured at

the beginning of the study (refractive index of 3-(aminopropyl)tripropylsilane equal to

1.454). CO_2 was sparged through the sample forming the RevIL (refractive index equal to

1.474). The sample was then heated at 100°C for one hour and the refractive index was

23

again measured. The cycle was repeated five times. The silylamine was analyzed using ^{1}H NMR after the fifth cycle, and was found to be identical to that at the beginning of the experiment. With almost negligible loss of activity over five cycles we expect that the reversible ionic liquid system can be effectively recycled over several more cycles.
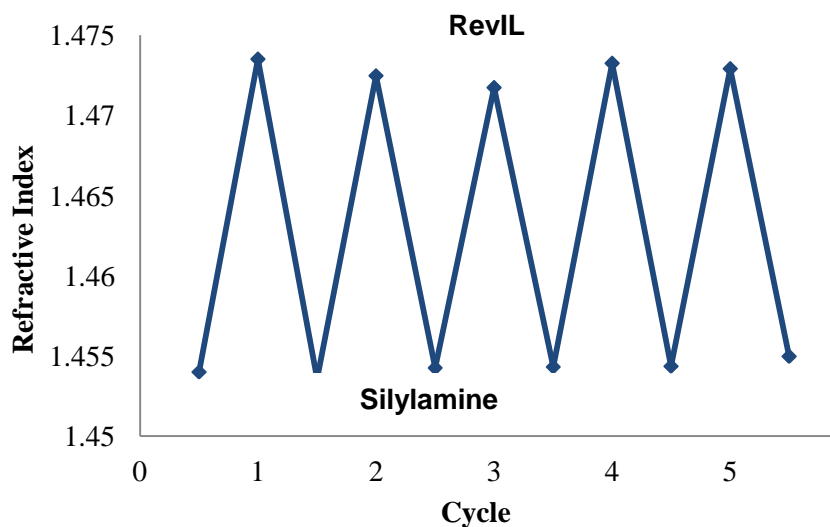
Figure 2.15. Recyclability of the 3-(aminopropyl)tripropylsilylamine RevIL system demonstrated by refractive index measurements

The influence of structure on CO_2 capture capacity was a primary goal of the study. The effect of molecular changes on CO_2 absorption was observed when CO_2 capacity was calculated in moles of CO_2 per mole of silylamine. The CO_2 capture capacities of three of the reversible ionic liquid systems are reported in Table 2.1.

Table 2.1. Gravimetrically determined CO_2 capacities

Silylamine	Abbreviation	Structure	Capacity (mol CO_2/mol amine)
3-(aminopropyl)triethylsilane	TEtSA	Et_3Si ⌒⌒ NH_2	0.63±0.01
3-(aminopropyl)tripropylsilane	TPSA	Pr_3Si ⌒⌒ NH_2	0.64±0.01
3-(aminopropyl)trihexylsilane	THSA	Hex_3Si ⌒⌒ NH_2	0.67±0.01

As shown in Table 2.1, the CO_2 uptake of the presented silylamines exceeds the theoretical uptake of CO_2 if two moles of amine react with one mole of CO_2. A number of possibilities were investigated to identify the source of enhanced CO_2 uptake, including physical absorption of CO_2 at atmospheric CO_2 pressure. In addition to the chemical reaction with CO_2, the reversible ionic liquid systems are also capable of physically absorbing CO_2 which would result in additional CO_2 uptake. The gravimetric measurements, however, do not provide a distinction between the chemical and physical absorption of CO_2, and therefore a spectroscopic approach was developed to understand better the chemistry of the additional capacity.

2.4.1.2 Decoupling Chemical and Physical Absorption

The measurement of chemical and physical CO_2 capture capacity is fundamental to the development of solvents for a capture process with specific inlet conditions (e.g., pressure, concentration and temperature). Our group has developed a spectroscopic

technique that enables the differentiation between chemical and physical absorption of CO_2 using Attenuated Total Reflectance Fourier Transform Infrared (ATR-FTIR).

2.4.1.3 ATR-FTIR Instrument for Measurement of Chemical and Physical Absorption

Attenuated Total Reflectance-Fourier Transform Infrared (ATR-FTIR) is particularly useful for studying the reversible ionic liquid system because it facilitates spectroscopic measurements of liquid samples without the preparation that is required with FTIR analysis alone. The reflection from the evanescent wave extends only microns into the sample, thereby requiring a very small sample size for analysis. The small sample size is ideal for laboratory scale reactions of silylamines synthesized "in-house" and reduces the time required for the samples to reach equilibrium during chemical and physical absorption. In addition, this analytical technique offers a number of advantages over tradition gravimetric[19, 23] and volumetric[24, 25] techniques including the (1) ability to take *in-situ* measurements without sampling and (2) capability to monitor the formation of additional peaks (i.e., chemical species) under CO_2 pressure using a high pressure reactor cell.

The measurement of the chemical and physical absorption of three of our selected silylamines, TEtSA, TPSA and THSA demonstrates the utility of the measurement technique. Each system has a distinct infrared spectrum; and characteristic peaks provide information on the extent of chemical and physical CO_2 absorption for each silylamine. An infrared spectrum of TPSA silylamine and RevIL is shown in Figure 2.16.
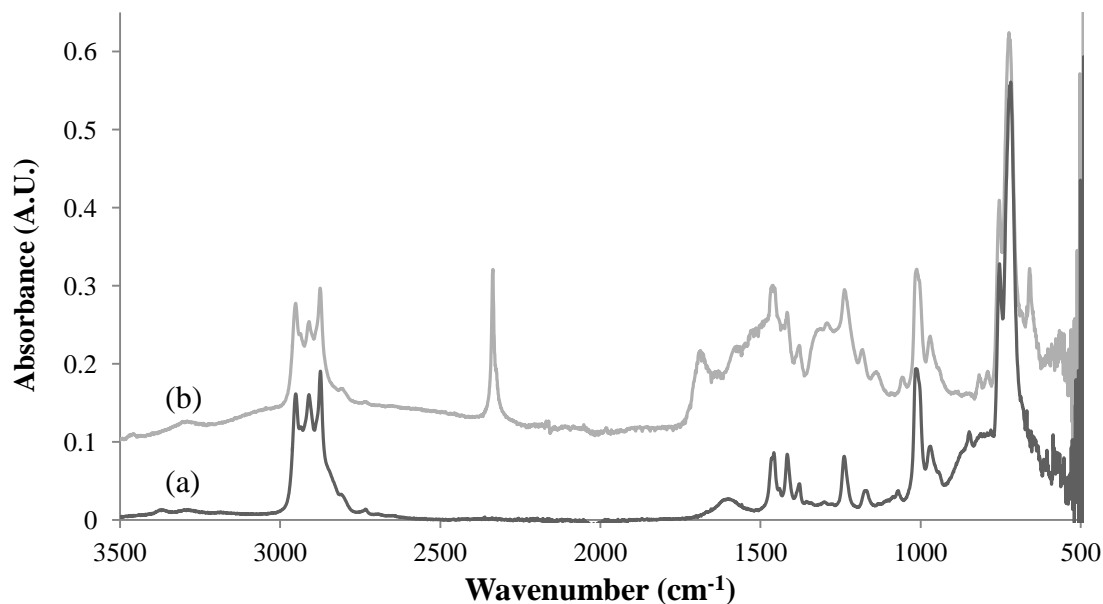
Figure 2.16. Infrared spectrum of TPSA RevIL system (a) silylamine (b) RevIL with physically absorbed CO$_2$ at 25°C

Characteristic peaks of the silylamine appear in two regions. The C-H stretch is observed between 3100-2600 cm^{-1} and the weakly absorbing N-H deformation band falls between 1650-1590 cm^{-1}. The reaction of the silylamine to RevIL from chemical absorption of CO$_2$ is monitored by the appearance of (1) a broad ammonium (-NH$_3^+$) peak that covers the range of 2600-3100 cm^{-1} (2) the asymmetric CO$_2^-$ stretch of the carbamate anion and (3) a carbonyl stretch at 1700 cm^{-1}. Assignments are in agreement with those in literature.[16,26] It is ideal to use an isolated peak for quantitative analysis using FTIR, but the characteristic peaks of the silylamine and the reversible ionic liquid overlap. However, it is possible to measure the total absorbance as the sum of the contributing parts (silylamine and RevIL).[27] Using the additive nature of absorbance with the Beer-Lambert Law, shown below in Equation 2.1, the conversion of the silylamine to the RevIL may be determined.

$$A_T = \sum_i \varepsilon_i b c_i \qquad \text{Equation 2.1}$$

In Equation 2.1, ε is extinction coefficient ($cm^2 \cdot mol^{-1}$), b is pathlength (cm), and c is concentration ($mol \cdot cm^{-3}$). Additional details about the calculation of the pathlength and molar absorptivity may be found in Appendix B.

FTIR measurements at 25°C indicate complete conversion of the silylamine to the RevIL. The use of this IR technique to measure the equilibrium conversion of the silylamine-RevIL system at temperatures above 25°C will be presented during the discussion of thermodynamic properties of this system. The ATR-FTIR technique was also used to measure physical absorption of CO_2 by the RevIL under pressure. Measuring the physical absorption of a reversible ionic liquid provides insight into structural changes that may be made to enhance capture capacity. Additional discussion will follow on enhanced CO_2 capture from high pressure streams. However, as presented, the gravimetric uptake of CO_2 exceeds the theoretical uptake, and for this reason it becomes necessary to identify CO_2 uptake due to chemical and physical absorption at 1 bar CO_2 pressure.

2.4.1.4 Physical Absorption Capacities of Reversible Ionic Liquids

Physical absorption is calculated by measuring the absorbance of the asymmetric CO_2 stretch of the reversible ionic liquid as a function of CO_2 pressure, as shown below in Figure 2.17.
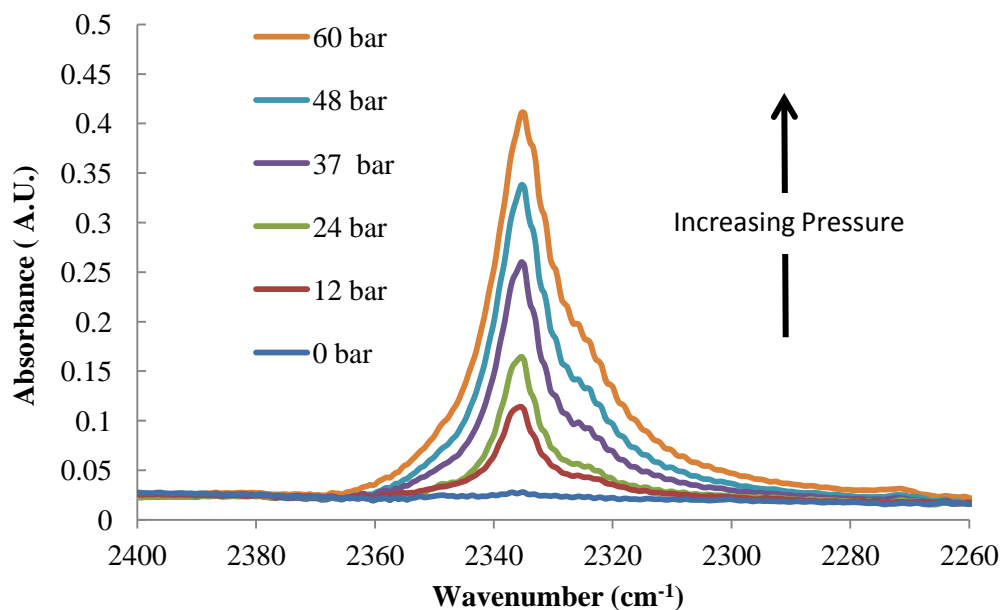
Figure 2.17. Asymmetric CO₂ stretch of TPSA RevIL as a function of CO₂ pressure

The reversible ionic liquid also undergoes a density change as a result of swelling under applied CO_2 pressure. Swelling will affect concentration measurements of CO_2 in the reversible ionic liquid, and therefore must be accounted for in the physical absorption calculations. Swelling, S % is calculated as

$$S = \left(1 - \frac{\rho_S}{\rho_{RevIL}}\right) \cdot 100 \qquad \text{Equation 2.2}$$

where ρ_s (g·cm^{-3}) is the density of the swollen RevIL under CO_2 pressure and ρ_{RevIL} (g·cm^{-3}) is the density of the RevIL. Initially, swelling measurements were calculated by measuring the decrease in absorbance of the region between 3100-2600 cm^{-1} (Figure 2.16) which contains the C-H stretch. This approach, however, is not a direct measurement of density change and may be influenced by a shift in reaction equilibrium

29

(silylamine and RevIL or the formation of additional species under CO_2 pressure). To directly measure density change as a function of CO_2 pressure, a high pressure sapphire cell was employed.

2.4.1.5 Sapphire Cell for High Pressure Volume Expansion Measurements

Volume expansion and phase behavior measurements were completed using a sapphire cell apparatus. Liquid volume of the RevIL was calculated by measuring the height of the liquid meniscus with a micrometer cathetometer. For displacements less than 50 mm the accuracy was 0.01 mm. The swelling was calculated by measuring the volume change of the RevIL sample under CO_2 pressure as shown in Equation 2.3. V_s is the volume of the swollen RevIL under CO_2 pressure and V_{RevIL} is the volume of the RevIL at atmospheric pressure.

$$S = \left(\frac{V_S - V_{RevIL}}{V_{RevIL}} \right) \cdot 100 \qquad \text{Equation 2.3}$$

Swelling measurements for the three reversible ionic liquid samples are shown below in Figure 2.18. The swelling of many conventional solvents under CO_2 pressure has been reported to be dependent on solvent properties and can range from 2% (dichloromethane) to 9% (acetonitrile) at 40°C and approximately 6 bar CO_2 pressure.[28]

30
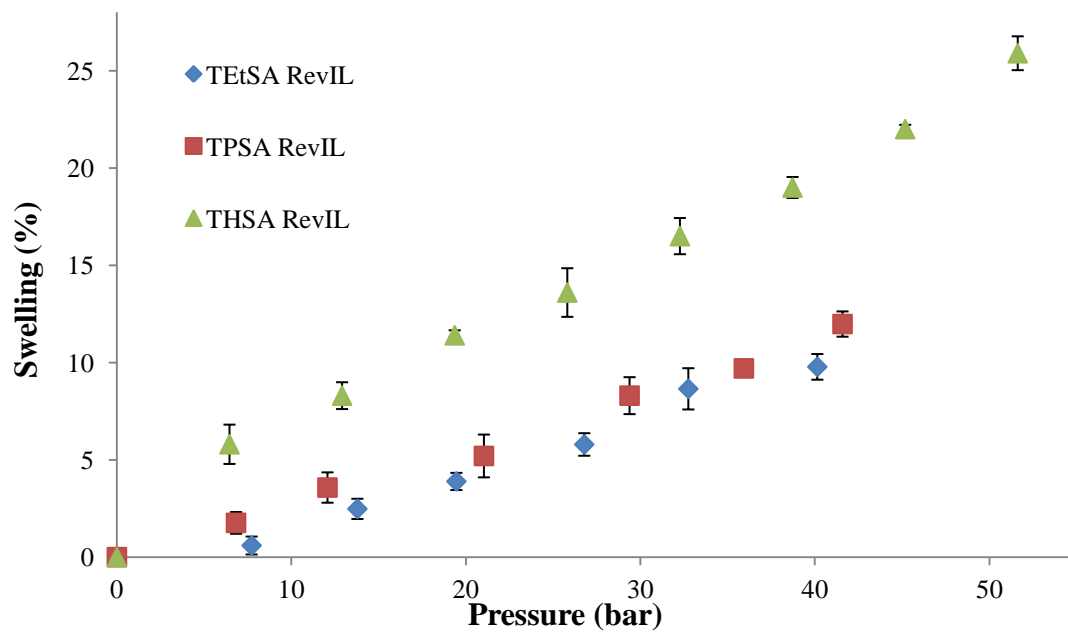
Figure 2.18. RevIL swelling as a result of applied CO_2 pressure measured with a sapphire cell apparatus at 25°C

The importance of directly measuring swelling, as opposed to using the decrease in absorbance of the C-H stretch as a measure of density change, can be seen below in Figure 2.19.
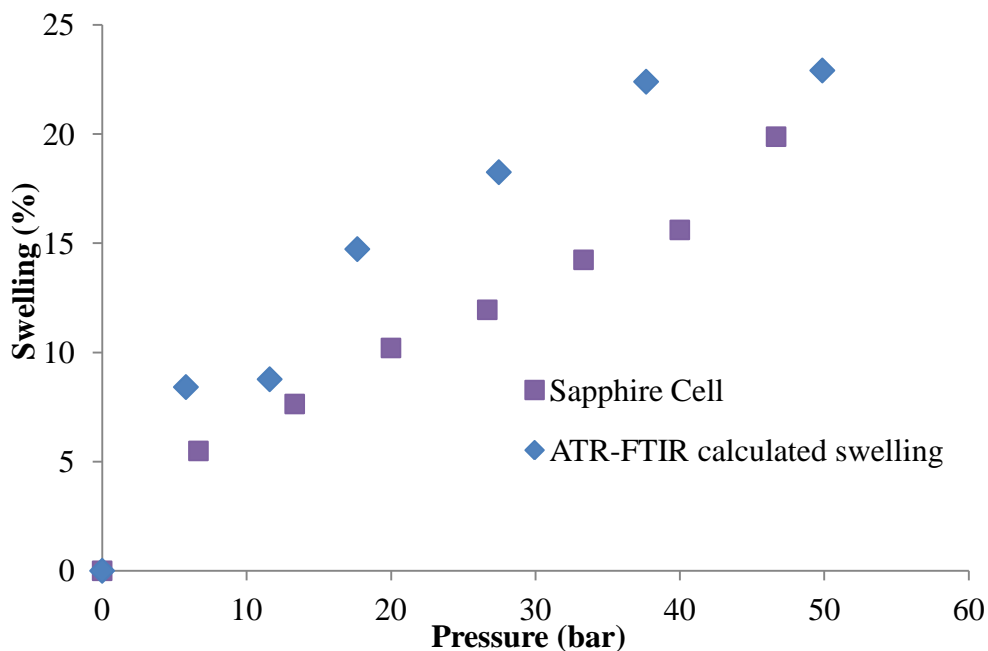
Figure 2.19. Swelling measurements calculated by ATR-FTIR and a sapphire cell apparatus at 25°C

The calculated swelling from ATR-FTIR measurements is consistently higher than the swelling measured by volume expansion in the sapphire cell. These results would indicate that there is an additional reaction or shift in equilibrium of the RevIL system as a result of applied CO_2 pressure.

Using sapphire cell swelling measurements in addition to the absorbance measurements of the asymmetric CO_2 stretch, the concentration of CO_2 in the RevIL is calculated as follows:

$$A_{II}^s = \varepsilon_{CO2}b_{II}c_{CO2} + A_{II}^0(1-S)$$

Equation 2.4

where A_{II}^s (cm^{-1}) is the integrated absorbance area of the asymmetric CO_2 stretch, ε_{CO2} ($cm \cdot mol^{-1}$) is the extinction coefficient of the physically absorbed CO_2, b_{II} (cm) is the effective pathlength for the IR region containing the asymmetric CO_2 stretch (2400-2260 cm^{-1}), c_{CO2} ($mol \cdot cm^{-3}$) is the concentration of physically absorbed CO_2, and the $A_{II}^0(1-S)$

32

(cm^{-1}) term is the correction for swelling. Information on the calculation of the extinction coefficient for physically absorbed CO_2 and the effective pathlength may be found in Appendix B. The mole fraction of CO_2 in the RevIL is calculated from the ATR-FTIR concentration measurements and the molecular weight and density of the RevIL. The mole fraction of CO_2 in the RevIL as a function of CO_2 pressure is shown below in Figure 2.20.
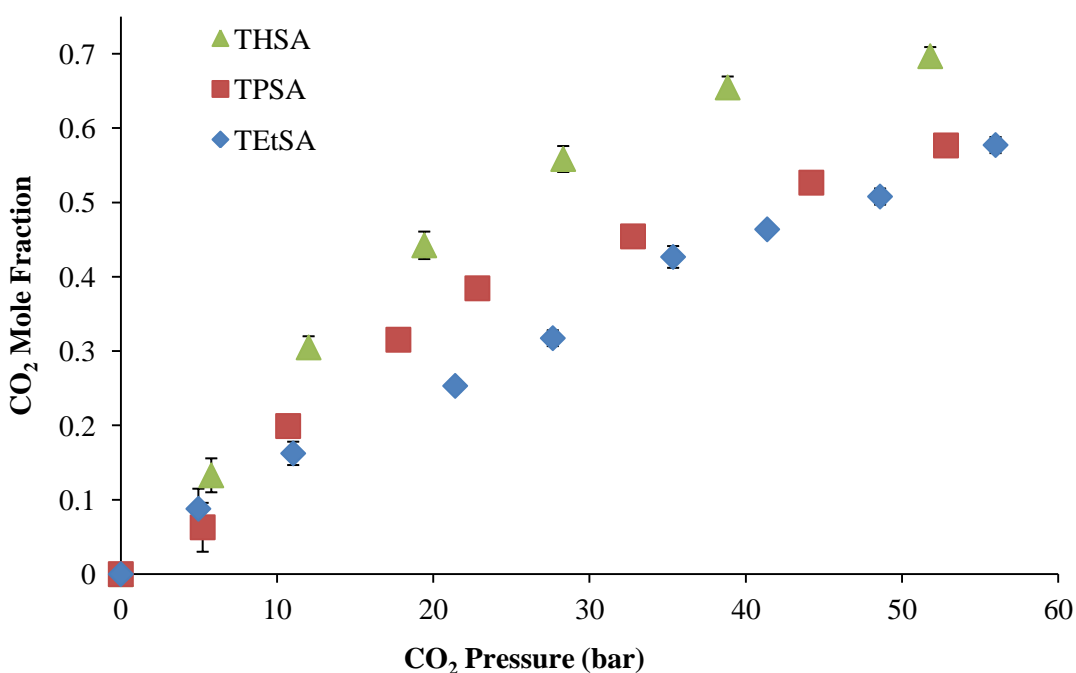
Figure 2.20. CO_2 mole fraction in the RevIL as function of CO_2 pressure

At one bar CO_2 pressure, the mole fraction of CO_2 in the RevIL is between $1.3x10^{-2}$ and $2.0 x10^{-2}$ depending on the RevIL structure. THSA exhibited the highest CO_2 solubility ($x_{CO2}=2.0x10^{-2}$), while TEtSA and TPSA have comparable but lower CO_2 physical absorptions ($x_{CO2}=1.3x10^{-2}$ to $1.7x10^{-2}$). CO_2 solubilities in traditional ionic liquids have been reported in the literature and exhibit comparable solubility values. For example, [bmim][PF6], [emim][Tf_2N], and [emim][CF_3SO_3] exhibit comparable solubility values

between 1.4×10^{-2} and 2.7×10^{-2} mole CO_2 per mole of ionic liquid at 30˚C. To measure the effect of RevIL structure on the physical absorption of CO_2 at one bar CO_2 pressure, Henry's Law constants were calculated. Henry's Law is a limiting case of vapor-liquid equilibrium, valid for systems at sufficiently low solubility to preclude any effects of solute-solute interactions. Henry's Law states that the solubility of a gas in equilibrium with a liquid phase is directly proportional to the partial pressure of the gas in the vapor phase, as shown in Equation 2.5. Henry's law is both solute and solvent specific. If the vapor phase is assumed ideal, it can be written as:

$$y_{CO_2} P = x_{CO_2} H_{CO_2}$$

Equation 2.5

Henry's Law constants were found by a straight-line fit (through the origin) of data points below 30 bar. An example is shown below in Figure 2.21 for TEtSA.
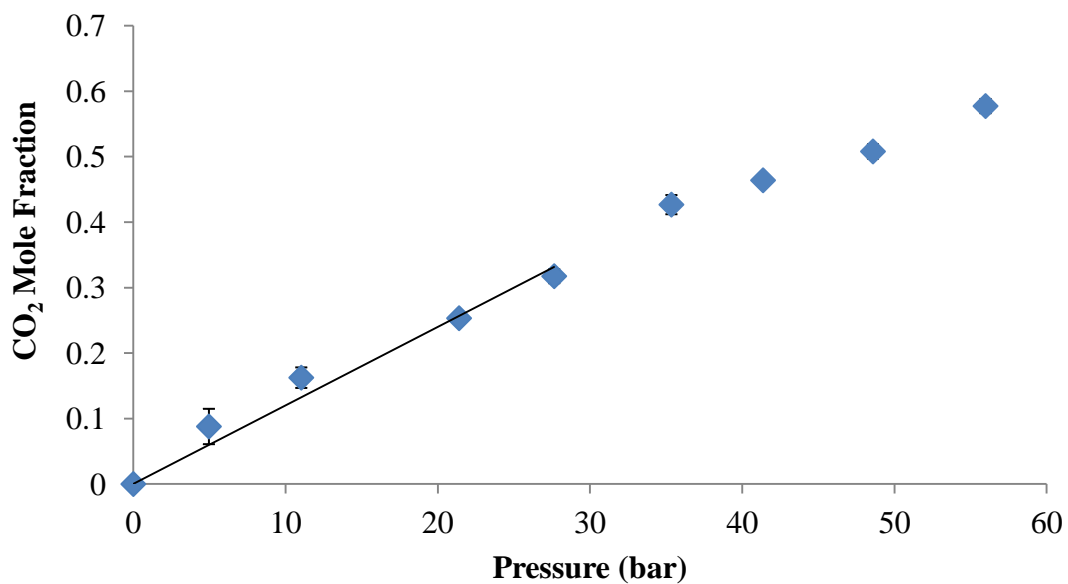
Figure 2.21. CO$_2$ mole fraction measurements used to calculate Henry's Law constants of TEtSA RevIL system at 25°C

Henry's law constants at were calculated at 25°C and 35°C as shown below in Table 2.2.

Table 2.2. Henry's Law constants of select RevILs at 25°C and 35°C

RevIL	Henry's Law Constant at 25°C (bar)	Henry's Law Constant at 35°C (bar)
TEtSA	69±2	77
TPSA	52±2	60
THSA	44±3	50

From these data, we conclude that the physical absorption capacity at one bar CO$_2$ pressure is not the only contributor to the enhanced CO$_2$ capacity of the reversible

35

ionic liquid systems.

Conventional 2:1 amine to CO_2 stoichiometry would dictate 0.50 moles of CO_2 per mole of amine; however, the CO_2 capacities are on average 30% greater than 2:1 stoichiometry. This corresponds to 0.15 moles of additional CO_2 uptake per mole of amine not accounted for by the conventional chemical reaction. The physical absorption of CO_2 at one bar along with the conventional chemical reaction, gives a theoretical CO_2 capacity of 0.51 moles of CO_2 per mole of amine.

2.4.1.6 Enhanced CO_2 Capacity through Formation of Stable Carbamic Acid Species

One possibility that would result in enhanced CO_2 capacity is entrapment of CO_2 bubbles while forming the RevIL by sparging CO_2 through the reversible ionic liquid system. The high viscosity of the RevILs could entrain additional CO_2 in microbubbles that could contribute to the gravimetric uptake of CO_2. There were no visible bubbles that remained after bubbling and Dynamic Light Scattering (DLS) experiments did not show any evidence of microbubbles. The DLS experiments did not completely rule out the possibility of entrapped CO_2; however, it is unlikely that these small bubbles could enhance the uptake of CO_2 by 25%. We also proposed that the enhanced CO_2 capture capacity could result from small amounts of water that were being introduced to the silylamine while sparging with CO_2. One product of the chemical reactions that would result in the presence of water is shown in Figure 2.22.
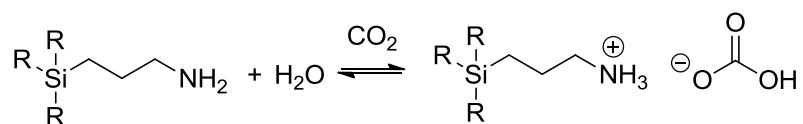
Figure 2.22. Reaction of a silylamine with CO_2 in the presence of water

36

This is not likely to be the cause of the enhanced capacity as the presence of water is limited to ppb levels in the CO_2, and the introduction of a drying tube along the CO_2 line did not change the resulting capacity.

Two additional reactions could result in enhanced CO_2 capacity, as presented in Figure 2.23. The first species is a carbamic anhydride. The second species results from an additional mole of CO_2 reacting with the available electrons on the nitrogen of the carbamate.
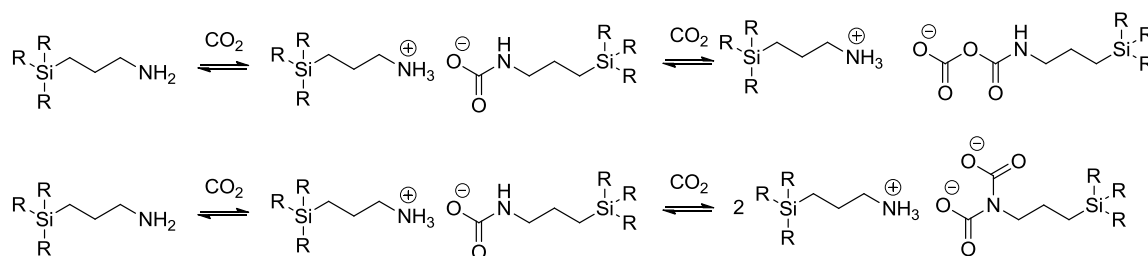
Figure 2.23. Two additional proposed reaction schemes resulting in enhanced CO_2 capacity

The presence of these species is unlikely, however, due to the mild conditions under which the RevIL is formed. Additionally, the carbamic anhydride is asymmetric, which would result in two distinguishable carbonyl peaks. The additional adduct of CO_2 to one molecule of amine will be discussed in the amine protection chapter of this thesis and has been reported in literature at -30˚C.[29] However, the quantitative ^{13}C NMR does not support this hypothesis. Although the diamide species is symmetric, with equivalent carbonyls, we would still expect two carbonyl species in the ^{13}C NMR from the carbamate and diamide species. Additionally, if two molecules of CO_2 were attached to the amine nitrogen to form the diamide, two ammonium cations would be required to counterbalance the negative charge. The carbamic anhydride and diamide species were ruled out as sources of enhanced CO_2 capacity through ^{13}C NMR experiments.

37

Revisiting the reaction equilibrium between the silylamine and CO_2 (Figure 2.24), the amine reacts with one mole of CO_2 forming the carbamic acid species. The carbamic acid is then deprotonated by an additional mole of amine forming the ammonium-carbamate ion pair. If the reaction does not proceed completely to the ion pair at equilibrium, the presence of carbamic acid may be the contributing intermediate. The stabilization of the carbamic acid through hydrogen bonding would result in enhanced CO_2 capacity.
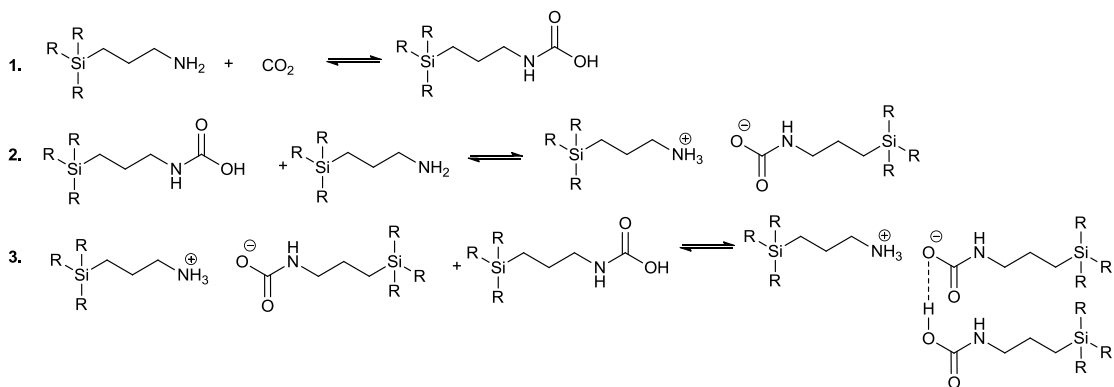
Figure 2.24 Proposed equilibria for the reaction of CO_2 with silylamines

Quantitative ^{13}C NMR was used to further investigate the reaction equilibrium. The ^{13}C

NMR spectrum of the stabilized carbamic acid is shown below in Figure 2.25.
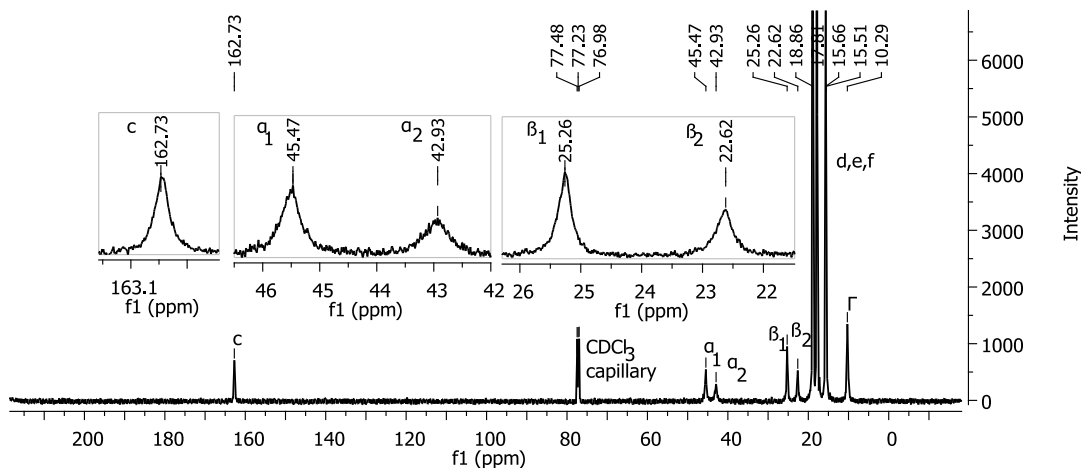
Figure 2.25. Quantitative ^{13}C NMR of TPSA RevIL

Distinct signals exist for the alpha and beta carbon (relative to the amine) on the propyl

backbone. This result is expected due to the different chemical environment of the

ammonium cation and the carbamic acid-carbamate anion. The alpha and beta peaks of

the ammonium cation have been labeled α_2 and β_2 and the hydrogen-bonded carbamic

acid-carbamate anion labeled α_1 and $\beta_1,$ as shown below in Figure 2.26.
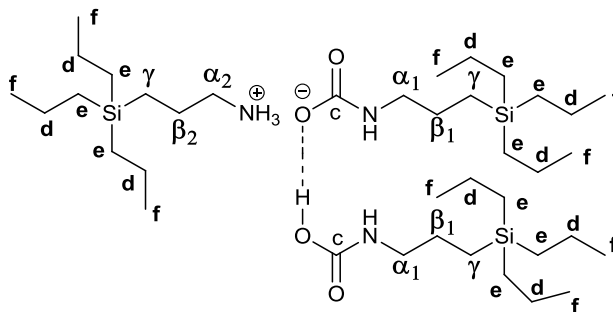
Figure 2.26. Hydrogen bonded network of carbamate-carbamic acid species

For clarification, the peak assignments and integrations of the above ^{13}C NMR are shown in Table 2.3 .

Table 2.3. Quantitative ^{13}C NMR areas of TPSA RevIL

^{13}C peak	Relative integration
c – 162.73 ppm	1.92±0.08
α_1 – 45.47 ppm	1.69±0.08
α_2 – 42.93 ppm	1.00[a]
β_1 – 25.26 ppm	1.81±0.11
β_2 – 22.62 ppm	1.12±0.05

If the silylamine was completely reacted to the ammonium-carbamate ion pair, the integration of the α and β peaks should integrate to the same values. However, α_1 and β_1 of the hydrogen-bonded carbamic acid-carbamate anion integrate to 1.69±0.08 and 1.81±0.11 respectively. These integrations are approximately 65% greater than the integration of the alpha and beta carbon of the ammonium cation (α_2 and β_2) which integrate to 1.00 and 1.12±0.05 respectively. The increased areas of the α_1 and β_1 carbon peaks further support the hydrogen-bonded carbamic acid-carbamate anion complex.

During the collection of ATR-FTIR spectra of the RevIL as a function of CO_2 pressure, it was observed that the peak absorbance at 1700 cm^{-1} increased as pressure was increased above one bar (Figure 2.27).
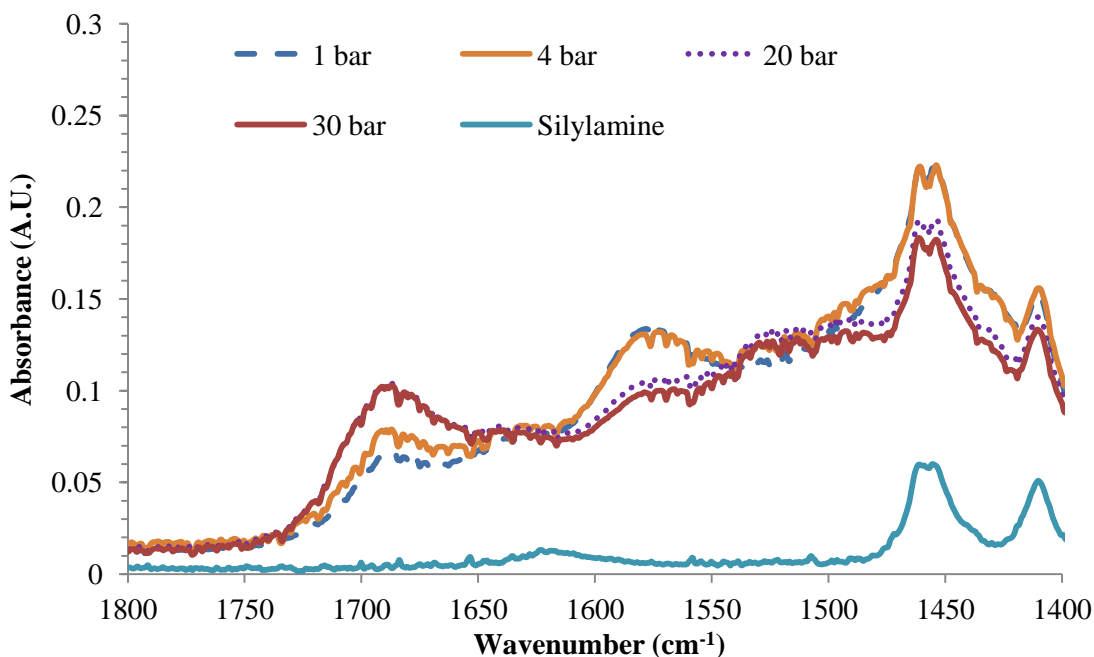
Figure 2.27. FTIR spectrum of a) TPSA silylamine and b) the TPSA reversible ionic liquid as a f(CO₂) pressure

As previously discussed, the N-H bend is observed at 1646 cm^{-1}. The absorption at 1575 cm^{-1} is assigned to the asymmetric CO_2^- stretch of the carbamate anion, and we postulate that the absorption at 1700 cm^{-1} is the carbonyl stretch of the carbamic acid species. As CO_2 pressure is increased, this carbonyl stretch increases and the asymmetric CO_2^- stretch of the carbamate anion decreases. This observation is consistent with an increase in concentration of carbamic acid and a decrease in concentration of carbamate under applied CO_2 pressure. From the IR spectrum, it may be seen that at pressures above 20 bar, the absorbance does not continue to increase. Additional experiments may be completed to determine the maximum achievable concentration of carbamic acid achievable by increasing CO_2 pressure.

2.4.1.7 Effect of Structural Changes on CO_2 Chemical Capacity

A next generation of silylamines was synthesized that further demonstrates the use of molecular design to optimize silylamine structure for CO_2 capture. Shown in Table

41

2.4 are 15 silylamines and their CO_2 capture capacity including TEtSA, TPSA and THSA presented above.

Table 2.4. Gravimetric CO_2 capture capacities at 25°C and 1 bar CO_2 pressure
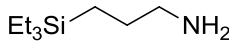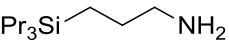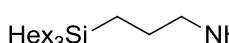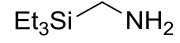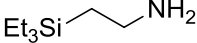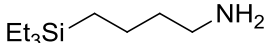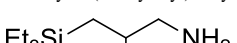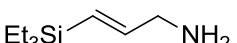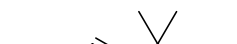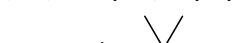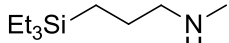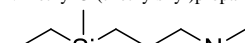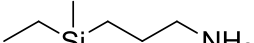
Silylamine	Abbreviation	CO$_2$ Uptake (mol CO_2/mol amine)	CO$_2$ Uptake (mol CO_2/kg amine)
Varying the alkyl chain length on the silicon atom			
Et$_3$Si〜NH$_2$ 1-(aminopropyl)triethylsilane	TEtSA	0.63±0.01	3.66±0.03
Pr$_3$Si〜NH$_2$ 1-(aminopropyl)tripropylsilane	TPSA	0.64±0.01	2.99±0.03
Hex$_3$Si〜NH$_2$ 1-(aminopropyl)trihexylsilane	THSA	0.67±0.01	1.96±0.02
Varying the alkyl chain length between the silicon atom and amine			
Et$_3$Si〜NH$_2$ 2-(aminomethyl)triethylsilane	TEtSMA	0.59±0.01	4.09±0.08
Et$_3$Si〜NH$_2$ 3-(aminoethyl)triethylsilane	TEtSEtA	0.59±0.01	3.67±0.03
Et$_3$Si〜NH$_2$ 4-(aminobutyl)triethylsilane	TEtSBA	0.35±0.03	1.9±0.2
Branching along the alkyl chain backbone			
Et$_3$Si〜NH$_2$ 4-(triethylsilyl)-butyl-2-amine	αMe-TEtSA	0.63±0.03	3.36±0.15
Et$_3$Si〜NH$_2$ 2-methyl-4-(triethylsilyl)-butyl-2-amine	α,αDMe-TEtSA	0.48±.03	2.4±0.2
Et$_3$Si〜NH$_2$ 2-methyl-3-(triethylsilyl)propylamine	βMe-TEtSA	0.59±0.01	3.15±0.07
Unsaturation in the alkyl chain backbone			
Et$_3$Si〜NH$_2$ (*trans*)-3-(triethylsilyl)prop-2-en-1-amine	*trans*-TEtSA	0.61±0.03	3.56±0.20
Et$_3$Si〜NH$_2$ (*trans*)-2-methyl-4-(triethylsilyl)-butyl-2-amine	*trans*-α,αDMe-TEtSA	0.47±0.03	2.35±0.16
Pr$_3$Si〜NH$_2$ (*trans*)-2-methyl-4-(tripropylsilyl)-butyl-2-amine	*trans*-α,αDMe-TPSA	0.40±0.000	1.65±0.000
Secondary silylamines			
Et$_3$Si〜N(H) N-methyl-3-(triethylsilyl)propan-1-amine	STEtSA	0.65±0.01	3.49±0.05
Si〜N(H) N-methyl-3-(aminopropyl)dimethylethylsilane	SDMESA	0.62±0.02	3.87±0.11
Additional			
Si〜NH$_2$ 3-(aminopropyl)dimethylethylsilane	DMESA	0.42±0.04	2.85±0.24

Table 2.4 shows that increasing the alkyl chain length on the silicon atom, does not have a strong influence on the uptake of CO_2 on a molar basis. However, when developing solvents for CO_2 capture, the industrially relevant capacity measure is in terms of moles of CO_2 per kg of amine. In this regard, the THSA silylamine, due to its larger molecular weight, results in a CO_2 capacity that is significantly lower per kg of silylamine than TPSA and TEtSA. The effect of molecular weight on CO_2 capacity is best illustrated in Figure 2.28.
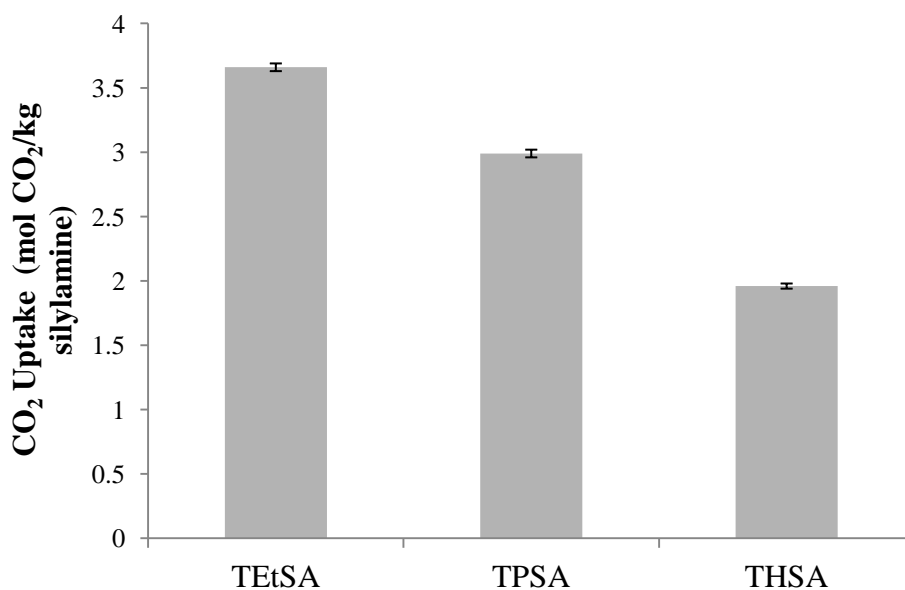
Figure 2.28. Effect of alkyl chain length on the silicon atom on CO_2 capacity

The next generation silylamines were synthesized using TEtSA as the base structure, and structural changes resulted in little to no increase in the molecular weight of the silylamine. For example, three silylamines were synthesized to understand the effect of varying the distance between the amine and the silicon atom (TEtSMA, TEtSEtA and TEtSBA). Changing the length of the backbone of the silylamine from a propyl group (TEtSA) does not strongly influence the CO_2 capacity until the amine-

silicon link is increased to a butyl chain. TEtSBA forms a low-melting solid upon reaction with CO_2. As a result of the solid formation, mass transfer limitations exist that limit the uptake of CO_2 to 0.35 ± 0.03 mol CO_2 per mol of amine.

Introducing one methyl group alpha to the amine (αMe-TEtSA) did not affect the CO_2 uptake. Although the effect is very small, moving the methyl group to the beta position (βMe-TEtSA) results in a capture capacity of 0.59 moles of CO_2 per mole of amine compared to 0.63 moles CO_2 per mole of amine captured by TEtSA. Capacity is affected when two methyl groups were added alpha to the amine (α,αDMe-TEtSA). The steric hindrance that results from the proximity of the methyl groups to the amine caused a 25% decrease in CO_2 capacity over TEtSA. Unsaturation along the propyl backbone of the silylamine did not influence the CO_2 capacity of *trans*-TEtSA or *trans*-α,αDMe-TEtSA; however, the capacity of *trans*-α,αDMe-TPSA was only 70% of the saturated analog. The secondary amines synthesized for this study exhibited a capture capacity equivalent to TEtSA. DEMSA, an asymmetric silylamine forms a solid upon reaction with CO_2. As with other silylamines that formed solids in their ionic form, the capture capacity of DMESA was less than TEtSA. However, by placing a methyl group on the amine of DMESA, forming the secondary amine (SDMESA), the RevIL formed is a liquid and CO_2 capacity is increased to 0.62 ± 0.02 moles of CO_2 per mole of amine. Candidates for CO_2 capture must exhibit a high capacity; the best candidates for CO_2 capture based on capacity are shown in Table 2.5 below.

Table 2.5. Optimal CO$_2$ capture solvents based on maximum CO$_2$ capacity

Silylamine	CO$_2$ Uptake (mol CO$_2$/kg amine)	Silylamine	CO$_2$ Uptake (mol CO$_2$/kg amine)
TEtSA	3.66±0.03	*trans*-TEtSA	3.56±0.20
TEtSMA	4.09±0.08	STETSA	3.49±0.05
TEtSEtA	3.67±0.03	SDMESA	3.87±0.11
αMe-TEtSA	3.36±0.15		

Capacity is only one of the criteria in the selection of CO$_2$ capture solvents. The viscosity plays a significant role in the determining industrial viability and has been investigated for the reversible ionic liquid systems.

2.4.2 Viscosity of Reversible Ionic Liquid Systems

The energy required to pump the silylamine and the reversible ionic liquid is strongly influenced by viscosity; for this reason, much attention has been focused on developing approaches to minimize viscosity. The viscosities were measured with one bar CO$_2$ pressure at 25°C and 40°C.

2.4.2.1 Effect of Structure on RevIL Viscosity

RevIL viscosities at 25°C are shown in Table 2.6. Many of the viscosity values reported are outside of the range of industrially relevant capture solvents. However, as evident in Table 2.6, there is a strong influence of silylamine structure on the resulting RevIL viscosity, and the RevILs exhibit viscosities of <100 cP to greater than 6,000 cP.

Table 2.6. RevIL viscosities at 25°C

Abbreviation	Viscosity at 25°C (cP)	Abbreviation	Viscosity at 25°C (cP)
TEtSA	6088±36	TEtSMA	2373±206
TPSA	3700±180	TEtSEtA	solid
THSA	2400±88	TEtSBA	solid
αMe-TEtSA	6915±431	α,αDMe-TEtSA	1257±338
βMe-TEtSA	5075±141	*trans*-TEtSA	3889±252
trans-α,αDMe-TEtSA	<100[a]	*trans*-α,αDMe-TPSA[d]	<100[a]
STEtSA	135±14	SDMESA	117±16
DMESA	solid		

[a] Measurements below 100 cP are below the reliable detection limits of the instrument

The length of the alkyl chain on the silicon atom has marked effect on RevIL viscosity. Increasing the chain length from ethyl groups to propyl groups decreases the viscosity by half. Although not as significant, the decrease in viscosity from TPSA to THSA is 1,300 cP. The RevIL network is held together in part by Coulombic forces. Increasing the bulkiness of the RevIL decreases the charge density likely decreasing the RevIL viscosity.

The length of the alkyl link between the silicon atom and the amine had a significant effect on RevIL viscosity. The silylamine with a methyl linker has a viscosity of approximately 2,000 cP. Increasing the linker to a propyl chain results in a viscosity of 6,000 cP; and the butyl linker forms a solid upon reaction with CO_2. From the results of the three RevIL viscosities, it was expected that a trend between the alkyl linker and the

RevIL viscosity existed and an ethyl linker (TEtSEtA) would have a viscosity between 2,000 and 6,000 cP. This was not the case, and the ethyl linker formed a solid.

Although the addition of a single methyl group alpha or beta to the amine (αMe-TEtSA and βMe-TEtSA) does not significantly affect RevIL viscosity, the addition of two methyl groups alpha to the amine resulted in the decrease in viscosity by approximately 4,800 cP from TEtSA. Although this decrease in viscosity is significant, it is important to consider that the ααDMe-TEtSA silylamine does not fully convert to the RevIL, and therefore the lower viscosity is due in part to the presence of unreacted silylamine (viscosity <100 cP).

The viscosity of the unsaturated TEtSA analog (*trans*-TEtSA) was very promising. *trans*-TEtSA achieves complete conversion to the RevIL, and yet exhibits a viscosity 36% less than TEtSA. Likewise, the viscosities of the unsaturated RevILs, *trans*-ααDMe-TEtSA and *trans*-ααDMe-TPSA, were less than the saturated RevILs, however, this is again due to the presence of unreacted silylamine.

The secondary amines (STEtSA and SDMESA) had viscosities over 95% less than TEtSA. Presented here was the demonstration of the strong influence on silylamine structure on the resulting RevIL viscosity upon reaction of CO_2. Based on RevIL viscosity, the most suitable candidates as CO_2 capture solvents are shown in Figure 2.29. TEtSA is included as a reference.
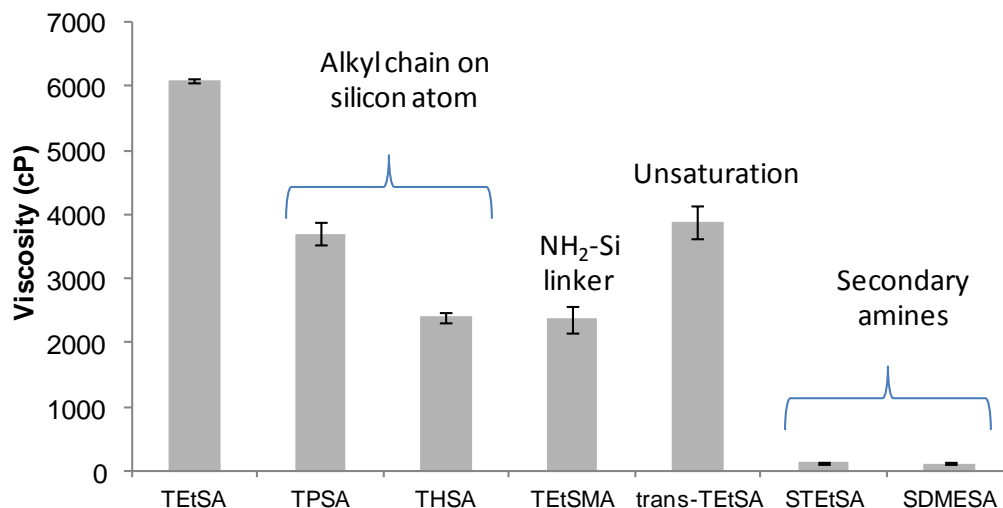
Figure 2.29. Effect of RevIL structure on viscosity at 25°C

The structure of the silylamine, however, is just one tuning parameter available with the RevIL system to achieve viscosities that are nearing industrial viability.

2.4.2.2 Temperature as an Additional Parameter to Decrease RevIL Viscosity

In the design of solvents for CO_2 capture from coal fired power plants, 40°C is often the standard operating temperature for absorption, as this is the temperature of the flue gas as it exits the desulfurization unit. This is advantageous for the RevIL system as temperature may be used as an additional tuning parameter to control RevIL viscosity. Not shown in Figure 2.30 are the RevILs that formed solids at 25°C and 40°C and RevILs with viscosities below 100cP as a decrease in viscosity could not be accurately measured with the viscometer used in these studies.
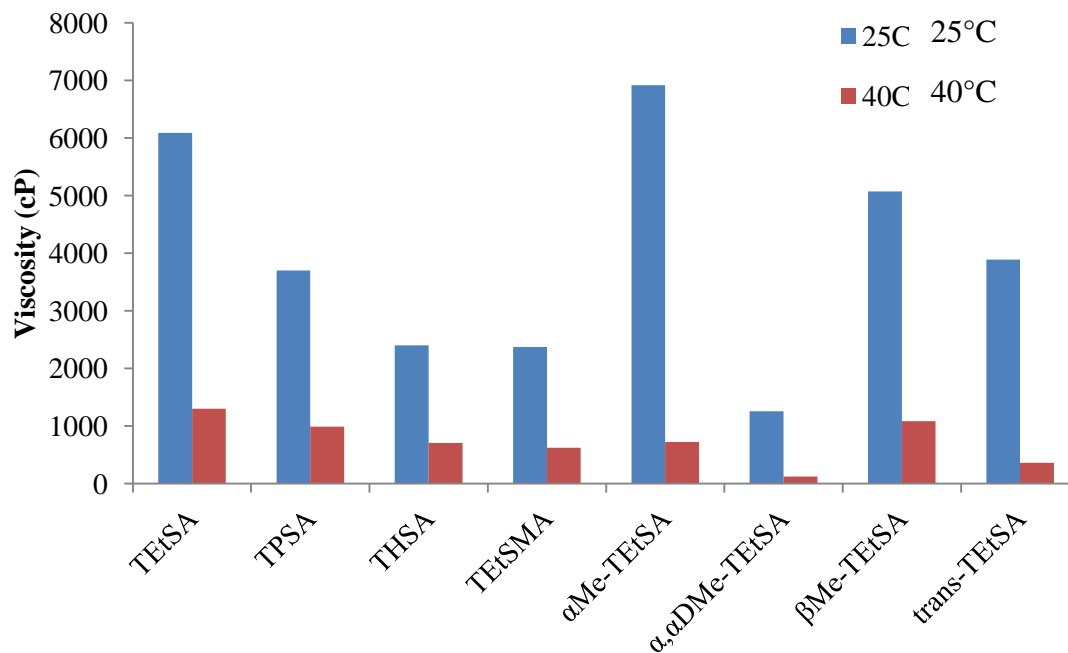
Figure 2.30. RevIL viscosity as a function of temperature

In fact, as presented in Table 2.7, the decrease in RevIL viscosity as temperature is increased from 25°C to 40°C can be as much as 90% in the case of αMe-TEtSA. From this table, it may be seen that there are a number of RevILs including *trans*-TEtSA with viscosities nearing that of industrial viability (100 cP).

Table 2.7. RevIL viscosities at 40°C

Abbreviation	Viscosity at 40°C (cP)	Abbreviation	Viscosity at 40°C (cP)
TEtSA	1303±100	TEtSMA	625±58
TPSA	990±29	TEtSEtA	solid
THSA	710±79	TEtSBA	solid
αMe-TEtSA	725±164	α,αDMe-TEtSA	125±22
βMe-TEtSA	1084±62	*trans*-TEtSA	362±19
trans-α,αDMe-TEtSA	<100[a]	*trans*-α,αDMe-TPSA[d]	<100[a]
STEtSA	<100[a]	SDMESA	<100[a]
DMESA	solid		

[a] Measurements below 100 cP are below the reliable detection limits of the instrument used

There are other considerations in designing solvents for post-combustion capture but the increased capture temperature has proven to be highly advantageous for reducing RevIL viscosity.

2.4.2.3 Conversion of the Silylamine to the RevIL as an Approach to Control Viscosity

A unique feature of this RevIL system is the capability to control viscosity by regulating conversion of the silylamine to the reversible ionic liquid. As shown in Figure 2.31, the viscosity of TPSA is a function of CO_2 capacity, or conversion of the silylamine to the RevIL.
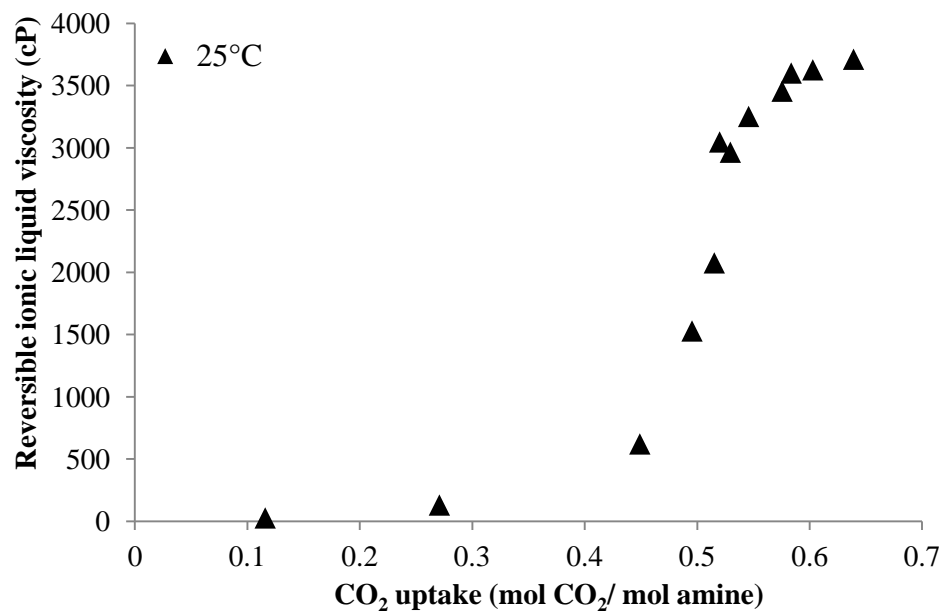
Figure 2.31. Viscosity at 25°C as a function of CO_2 capacity of the TPSA reversible ionic liquid system

The viscosity follows a hockey stick-like curve in which the viscosity stays below 620 cP

until the capacity reaches 0.45 moles of CO_2 per mole of amine. This point on the curve

lies just before the viscosity significantly increases as a function of conversion, and at 0.5

moles of CO_2 per mole of amine, the viscosity increases to 1528 cP. This study was also

completed at 40°C, also shown in Figure 2.32.
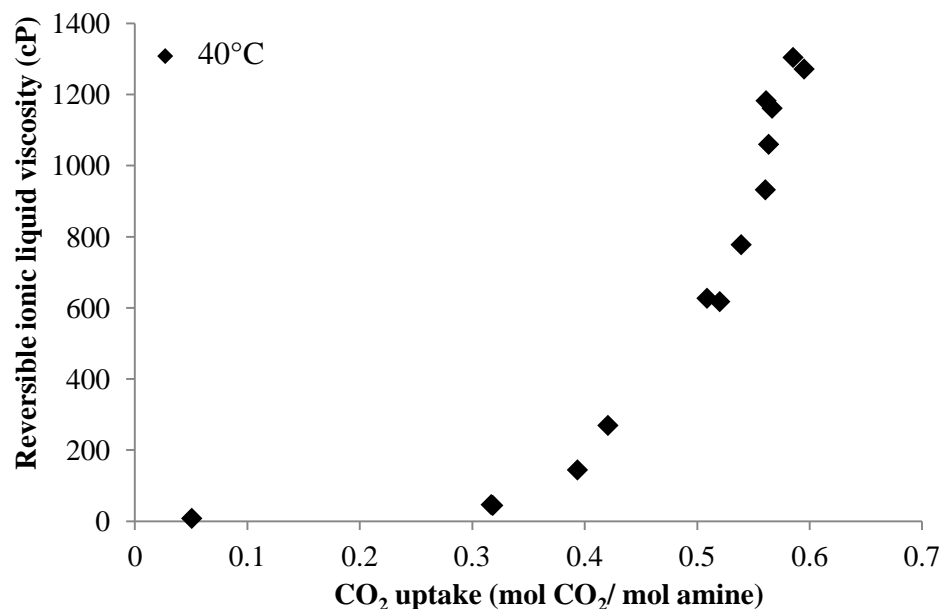
Figure 2.32. Viscosity at 40°C as a function of CO₂ capacity of the TPSA reversible ionic liquid system

At 40°C, a viscosity of 620 cP is not reached until 0.52 moles of CO_2 are captured per mole of amine. Furthermore, if the CO_2 conversion is limited to a capacity of 0.39 moles of CO_2 per mole of amine, the viscosity remains below 150 cP. Although there isn't a definitive value for viscosities of industrial viable solvents, a viscosity below 150 cP results in a significant decrease in energy required for pumping.

2.4.3 Thermodynamic Properties of the Reversible Ionic Liquid Systems

In the development of reversible ionic liquids for CO_2 capture, thermodynamic properties are significant in determining the most promising candidate for CO_2 capture applications. The thermodynamic properties that have been investigated include the (1) extent of reaction of the silylamine to the RevIL as a function of temperature, (2) temperature at which CO_2 is released and the reversible ionic liquid reverts back to the silylamine form, (3) enthalpy of regeneration and (4) enthalpy of physical absorption.

In post combustion CO_2 capture processes, there are three components to the reversal of the RevIL and release of CO_2 as shown below in Equation 2.6.

$$Q = mC_p\Delta T + \Delta H_{regeneration} + \Delta H_{physical\ reversal}$$ **Equation 2.6**

The first term is the energy required to heat the RevIL from 40°C—the temperature at which the flue gas exits the desulfurization unit—to the reversal temperature, or the onset of CO_2 release. Preliminary calculations indicate that the heat capacity of the reversible ionic liquid systems are not highly dependent on structure, however, the reversal temperature is strongly influenced by small structural changes to the silylamine. As was done in developing silylamines with maximum chemical capacity, TEtSA was used as a reference molecule to compare the effect of changes to the silylamine structure on the reversal temperature. The DSC thermogram (sample shown in the experimental section of this chapter) shows two endothermic events. The first event is the release of CO_2 and regeneration of the silylamine, and the second event is the evaporation of the silylamine. The structural modifications to the silylamine were intended to develop structure-property relationships to minimize energy required to regenerate the silylamine and release CO_2 (i.e., decrease reversal temperature and enthalpy of regeneration), however, the evaporation of the silylamine remains an important consideration. It is critical that significant loss of the silylamine is not incurred during the regeneration of the reversible ionic liquid system. The difference in the temperature of evaporation and reversal temperature of each of the silylamines is over 60°C, therefore minimizing loss of the silylamine due to evaporation.

2.4.3.1 Reversal Temperature of Reversible Ionic Liquids

The temperatures of the reversal events were determined by the intersection of the baseline of the event and the line tangent to the peak of the event. Reversal temperatures of the 15 reversible ionic liquids are shown in Table 2.8.

Table 2.8. Reversal temperatures of RevILs as determined by DSC

Abbreviation	Reversal Temperature (°C)	Abbreviation	Reversal Temperature (°C)
TEtSA	71±3	TEtSMA	78±5
TPSA	64±2	TEtSEtA	109±3[a]
THSA	51±1	TEtSBA	84±4[b]
αMe-TEtSA	52±2	α,αDMe-TEtSA	41±6
βMe-TEtSA	57±7	*trans*-TEtSA	48±2
trans-α,αDMe-TEtSA	11[c]	*trans*-α,αDMe-TPSA[d]	15±2
STEtSA	30±3	SDMESA	37±2
DMESA	80±8[e]		

[a] Formed solid (MP 49±1°C); [b] Formed solid (MP 66±4°C); [c] Reversal temperature difficult to measure due to broad events in the DSC thermogram; [d] Bottom of reversal curve at 48°C; [e] Formed solid (MP 66±3°C)

Of the structural modifications made, increasing the alkyl chain length on the silicon atom, branching along the alkyl backbone, unsaturation of the propyl backbone and the order of the amine (1° or 2°) showed the strongest influence on reversal temperature.

The reversal temperature of THSA is 20°C less than TEtSA. This decrease in reversal temperature may easily be explained by entropic effects; THSA has more degrees of freedom than the much smaller molecule TEtSA. Interestingly, decreasing the alkyl linker chain between the silicon atom and the amine from an ethyl group to a

methyl group did not have a significant effect on the reversal temperature. However, the change in structure is more subtle than increasing the three alkyl chains attached to the silicon atom. Both TEtSEtA and TEtSBA first undergo a phase change from a solid to a liquid at 49°C and 66°C, respectively, prior to releasing CO_2.

Introducing a methyl group alpha or beta to the amine decreases the reversal temperature by 19°C (αMe-TEtSA) and 14°C (βMe-TEtSA). This effect is much more significant when two methyl groups are added alpha to the amine. α,αDMe-TEtSA reverses at 43°C. When designing solvents for CO_2 capture, it is important to balance maximum capture capacity with reduced reversal temperature; and as dictated by capture conditions, solvents with reversal temperatures at 40°C would result in incomplete conversion to the RevIL.

The decrease in reversal temperature of the unsaturated RevILs compared to their saturated analogs is significant. *trans*-TEtSA reversed at 48°C, over 20°C less than TEtSA. In the synthesis of the unsaturated silylamines, it was found that only the *trans* isomers were present. As a result, it is postulated that the locked conformation may also decrease the reversal temperature of the unsaturated RevILs.

The secondary amines also had a decreased reversal temperature. Although both secondary amines reached complete conversion at 25°C, reversal temperatures of 30°C (STEtSA) and 37°C (SDMESA) make these silylamines less suitable for CO_2 capture from flue gas streams at 40°C.

56

2.4.3.2 Enthalpy of Regeneration

The next—and most significant—term in the energy required for release the capture CO_2 is the enthalpy of regeneration. In the development of the reversible ionic liquid systems presented here, the first structural modifications made to the silylamine structure was the increase of alkyl chain length on the silicon atom from ethyl groups (TEtSA) to propyl groups (TPSA) and finally to hexyl groups (THSA). As discussed, increasing the alkyl chain length decreases reversal temperature as a result of an increase in entropy of the larger, bulkier molecules. The enthalpy of regeneration, however, was not significantly changed. It was proposed that the reaction between a primary amine -- with minimal steric hindrance -- and CO_2 will result in a heat of reaction that is independent to the changes made around the silicon atom. This was not the case however, for the branched, unsaturated, and secondary amines that were investigated. Shown below in Table 2.9 is a compilation of the enthalpy of regeneration for the reversible ionic liquid systems.

Table 2.9. Enthalpy of regeneration of RevILs

Abbreviation	Heat of Regeneration (kJ·mol CO_2^{-1})	Abbreviation	Heat of Regeneration (kJ·mol CO_2^{-1})
TEtSA	83±6	TEtSMA	76±7
TPSA	89±3	TEtSEtA	91±16[a]
THSA	81±3	TEtSBA	152±19[b]
αMe-TEtSA	90±5	α,αDMe-TEtSA	114±16
βMe-TEtSA	89±8	*trans*-TEtSA	85±7
trans-α,αDMe-TEtSA	7[c]	*trans*-α,αDMe-TPSA[d]	21±6
STEtSA	77±6	SDMESA	76±2
DMESA	130±14[e]		

[a] Formed solid (MP 49±1°C); [b] Formed solid (MP 66±4°C); [c] Enthalpy difficult to measure due to broad events in the DSC thermogram; [d] Bottom of reversal curve at 48°C; [e] Formed solid (MP 66±3°C) Note – Heat of regeneration of reversible ionic liquids that formed solids includes both melting and CO_2 release DSC events.

Increasing the alkyl linker from a propyl chain (TEtSA) to a butyl chain resulted in a doubling of the enthalpy of regeneration. It is proposed that this may be due to intramolecular interactions that would result in a stabilization of the ammonium-carbamate ion pair. This 6-membered ring would be achieved only with TEtSBA.

Introducing two methyl groups alpha to the amine resulted in incomplete conversion, or a decrease in capacity. This effect is likely due to destabilization of the carbamate species which would decrease the enthalpy of regeneration. However, the enthalpy of regeneration of α,αDMe-TEtSA (calculated in terms of kJ per mole of CO_2) is higher as a result of this decreased capacity. The unsaturated amines with branching alpha to the amine also have a decreased enthalpy of regeneration, although the

measurement of these values was difficult due to the presence of broad events in the DSC thermogram.

The results of the effect of structure on reversal temperature and enthalpy of regeneration were combined assuming negligible physical absorption. The reversible ionic liquid systems that show a significant reduction in energy for regeneration over traditional CO_2 capture technologies are shown in Figure 2.33. The energy for regeneration of an aqueous solution of MEA has been reported as approximately 140 kJ per mol CO_2.[30]
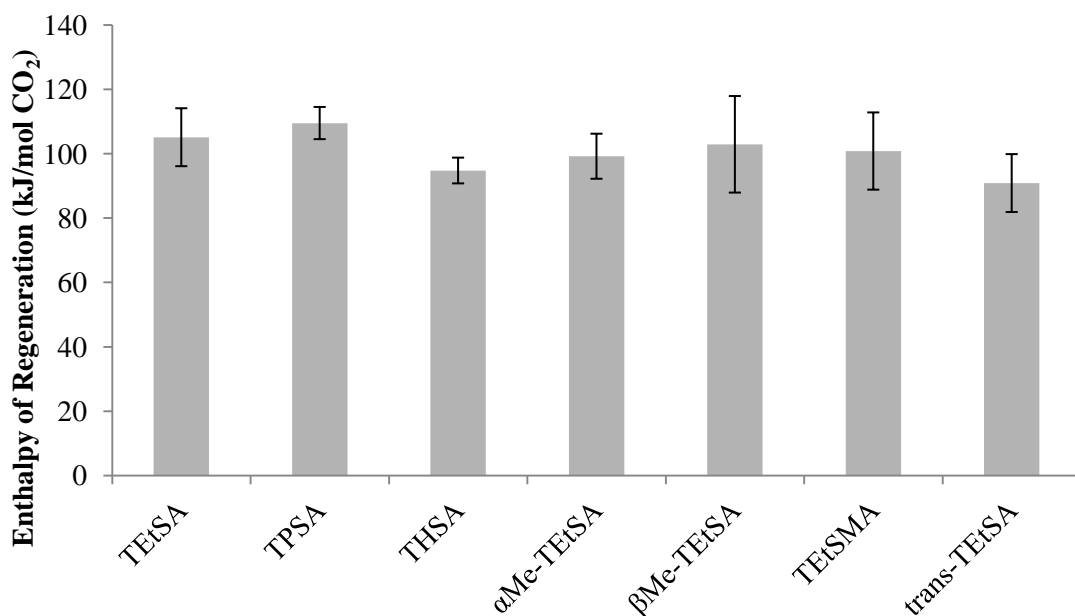
Figure 2.33. Total energy of regeneration of select reversible ionic liquid systems

2.4.3.3 Equilibrium Conversion of the Silylamine to the RevIL at Elevated Temperature

The capture temperature of the absorption process has an effect on almost all elements of the design of solvents for CO_2 capture. Reversible ionic liquids with reversal temperatures above 40°C would be expected to have only a slight decrease in capture

capacity at 40°C. This is the case for a select group of silylamines for which the capture capacity was determined at 40°C, as shown in Table 2.10.

Table 2.10. CO_2 uptake capacity at 40°C for a select group of silylamines

Abbreviation	CO_2 Uptake at 40°C (mol CO_2/mol amine)	CO_2 Uptake at 40°C (mol CO_2/kg amine)
TEtSA	0.603±0.002	3.48±0.01
α,αDMe-TEtSA	0.46±0.02	2.29±0.08
βMe-TEtSA	0.599±0.003	3.19±0.01

These three silylamines showed CO_2 capture capacity of over 95% the maximum capacity at 25°C. These results were very promising as they indicate that capacity for these RevILs will not be negatively affected by capture conditions for flue gas applications.

The reversal temperatures of 15 silylamines have been presented. These values provided information on how the structure of the silylamine may be changed to decrease the reversal temperature of the resulting RevIL. To understand better the equilibrium concentration of the silylamine-RevIL system, equilibrium conversions were calculated using TPSA as a model compound at one bar CO_2 pressure using ATR-FTIR.

The equilibrium conversion was measured by forming the reversible ionic liquid at each temperature being investigated. The gravimetric measurement of capacity at 40°C provided insight on the CO_2 capacity of three selected silylamines at temperatures above 25°C, however, this technique is sensitive to any losses of the silylamine as a result of evaporation at elevated temperature. Using the IR technique ensures the accuracy of the conversion measurement with one bar applied CO_2 pressure. The sample was quickly

60

transferred to the ATR-FTIR reaction cell, as described in the experimental section of this chapter. Measuring the absorbance of the broad ammonium peak and the carbonyl region produced conversion values at temperatures between 40°C and 80°C as shown below in Table 2.11.

Table 2.11. Equilibrium conversions of TPSA RevIL system at 1 bar CO_2 pressure

Temperature (°C)	Equilibrium Conversion (%)	Temperature (°C)	Equilibrium Conversion (%)
40	100±0	75	75±3
60	100±0	80	70±6
65	94±4	85	64±7
70	82±3		

These data provide valuable information on the temperature at which the stripper must be operated to release CO_2 and regenerate the silylamine.

2.4.4 <u>CO_2 Capture from High Pressure Streams</u>

An optimal solvent for CO_2 capture depends highly on the capture conditions. In a process selection chart adapted from Tennyson and Schaaf, 1977 for CO_2 removal with no H_2S present, recommended solvents for CO_2 removal range from amines, activated hot potassium carbonate to strictly physical solvents based on partial pressure of CO_2 in the feed and product.[31] The unique capability of the reversible ionic liquid system is that it can chemically absorb CO_2 (ideal for low pressure streams) and physically absorb CO_2; which takes advantage of enhanced CO_2 capture with low energy requirements for regeneration. Modifications that may be made to the silylamine structure that will

enhance physical absorption capacity at CO_2 pressures above one bar were investigated experimentally and computationally.

2.4.4.1 CO_2 Capacity of RevIL System at Pressures Above Atmospheric

Candidates for CO_2 capture from high pressure streams must (1) feature a high affinity for CO_2 (i.e., achieve increased physical absorption of CO_2 compared to conventional solvents) and (2) be highly selective towards CO_2. To study the selectivity of three of our reversible ionic liquids, Henry's law constants of various gases in the RevIL system were calculated using COSMO-RS,[1] and are presented in Figure 2.34.
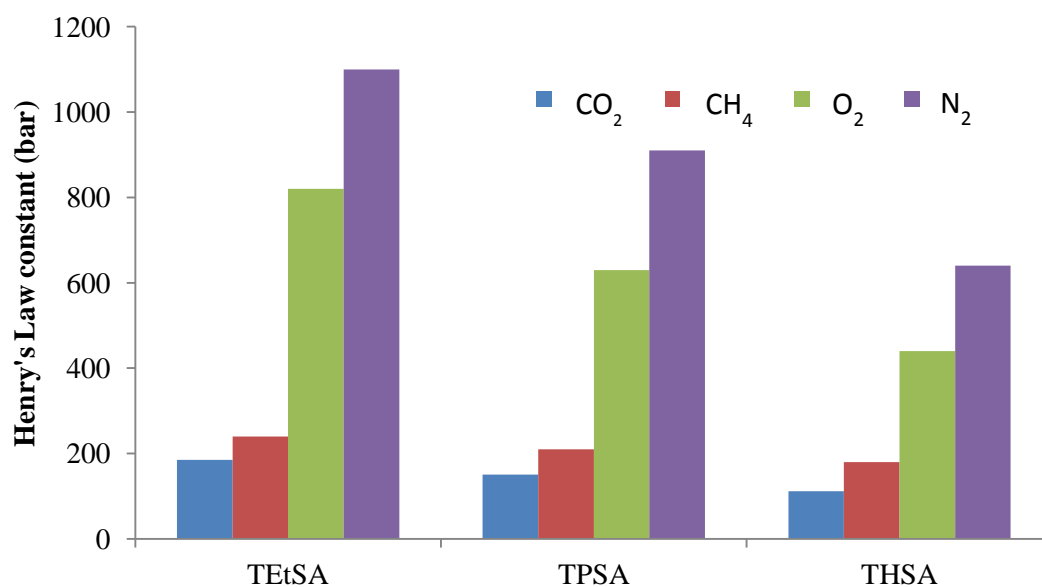
Figure 2.34. Henry's Law constants of gases in the RevIL systems at 25°C predicted by COSMO-RS

The COSMO-RS predicted Henry's Law constants of CO_2 in the RevIL are higher than the experimentally determined values. However, the trends predicted by COSMO-RS closely match trends derived from the experimental results. The results of the COSMO-

---

[1] This work was completed in collaboration with a visiting scholar from the Universidad Complutense de Madrid. The results of the COSMO-RS studies were published

RS study showed that the Henry's Law constants were much higher for methane, oxygen and nitrogen. These results are particularly important for CO_2 separation from methane-CO_2 mixtures, indicating that the RevILs will preferentially capture CO_2. The results of the experimentally and theoretically determined Henry's Law constants show that the silylamine structure influences the physical absorption capacity of the RevIL. One way to understand this effect of structure on physical absorption capacity is by calculating the theoretical void volumes of the RevIL systems.

The void volume (V_V) of a RevIL is defined as the "empty" space between the molecules, and was calculated by subtracting the theoretical van der Waals volume (V_{vdW}) from the experimentally determined molar volume (V_M).[32] The relationship between void volume and physical absorption capacity has been reported for traditional ionic liquids, and may prove to be beneficial in designing capture solvents for high pressure CO_2 separation.[25] The effect of void volumes, ($cm^3 \cdot mol^{-1}$) on Henry's law constants ($H_{CO2, RevIL}$ at 35°C) is presented in Figure 2.35 for four of the RevIL systems.
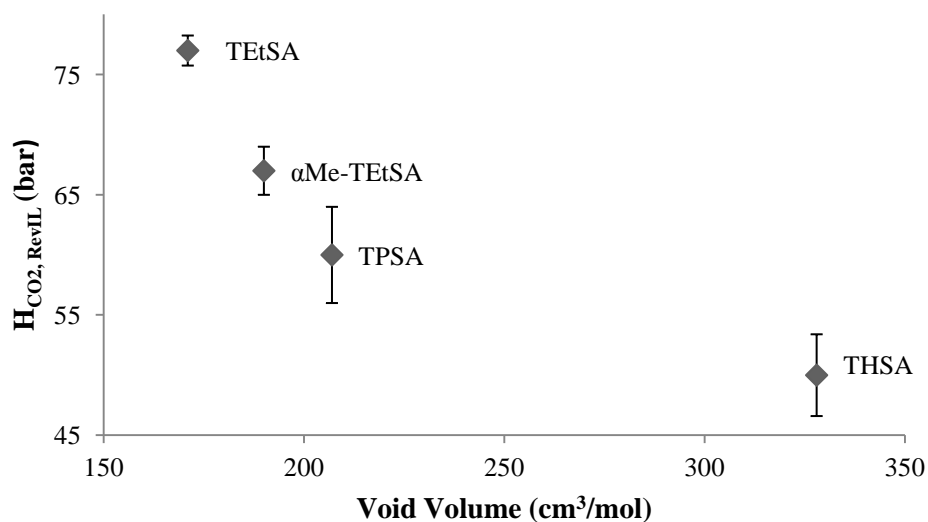
Figure 2.35. Henry's law constants of RevILs at 35°C versus void volume

63

It appears that the Henry's law constants, $H_{CO2,RevIL}$, correlate with V_V. Longer alkyl chains on the silicon atom disrupt packing ability, hence provide greater void space and greater CO_2 solubility. Likewise, the presence of a methyl group alpha to the amine (αMe-TEtSA) also increases the void volume and CO_2 solubility accordingly. These results are consistent with the increase in the physically absorbed CO_2 observed from TEtSA to THSA. From this data, it may also be observed that CO_2 solubility as a function of void volume appears to be linear in the range of 171-207 $cm^3 \cdot mol^{-1}$. The relationship between void volume and CO_2 solubility does not remain linear as the void volume is increased to 328 $cm^{3.} mol^{-1}$ in the case of THSA. This is an important piece of information, as it appears that the effect of alkyl chain length on the silicon atom is less significant at chain lengths greater than six carbon atoms.

The effect of structure on CO_2 capture capacity is very different for high and low pressure applications; this is best seen in Figure 2.36. Whereas at 0.15 bar CO_2 pressure, the physical absorption capacity is negligible; at 25 bar, the physical absorption capacity accounts for 27-43% of the total capacity.
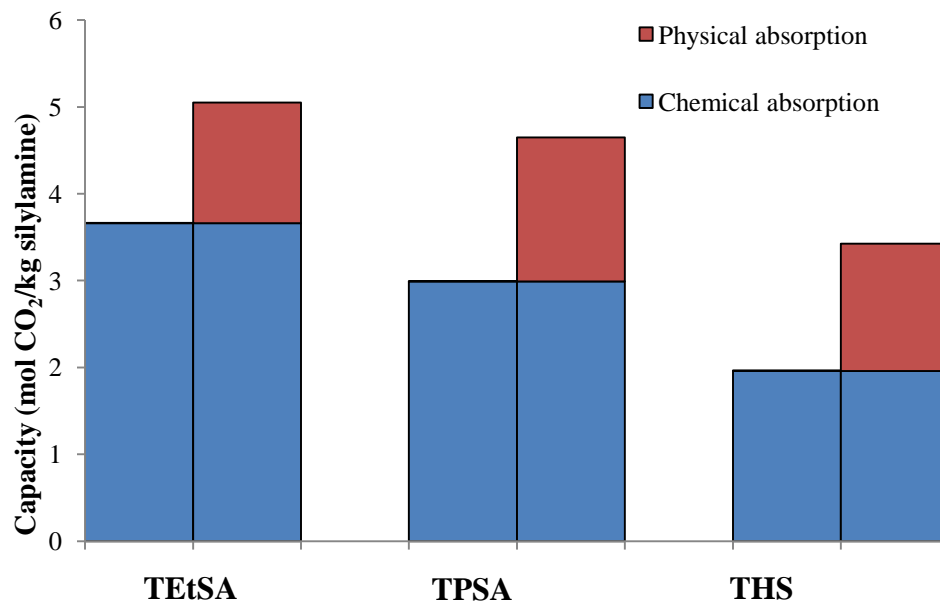
Figure 2.36. CO$_2$ capture capacity of three RevIL systems at 25°C

Inlet conditions for CO$_2$ separation from methane deposits covers a very broad range of CO$_2$ pressures.[31] Shown below is the total CO$_2$ capacity of the RevIL system at 35°C as a function of CO$_2$ pressure.
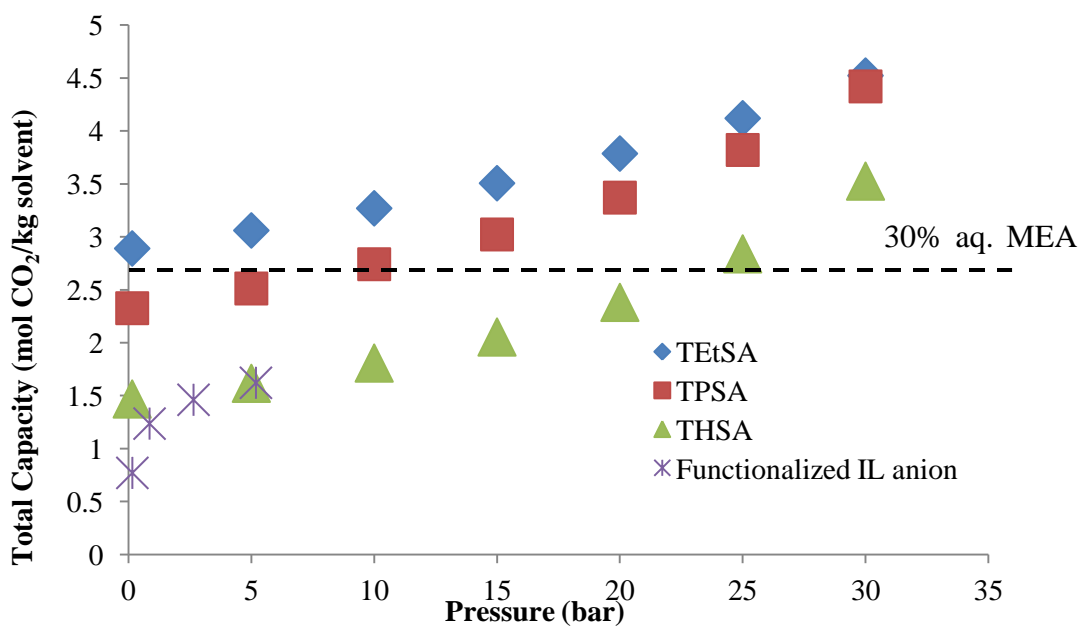
Figure 2.37. Total CO$_2$ capture capacity of RevIL systems as a function of pressure

65

As a benchmark, an aqueous solution of monoethanolamine and the capacity of a functionalized ionic liquid are included.[7, 16] The aqueous solution of monoethanolamine has a high capacity for low pressure applications (as it is often used). The functionalized ionic liquid has a low Henry's law constant, or high CO_2 solubility, but when measuring capacity in terms of moles of CO_2 captured per kg solvent, the large molecular weight is highly disadvantageous. This data also demonstrates that the enhanced physical absorption capacity of TPSA compared to TEtSA. This increased physical absorption of CO_2 by TPSA results in a total capacity essentially equivalent to TEtSA at 30 bar.

2.4.4.2 Energy Required for Regeneration of Silylamines

In addition to the enhanced CO_2 capture capacity at pressures above one bar; the additional uptake of CO_2 via physical absorption also results in a decreased energy for regeneration. Again referring to Equation 2.6, the total energy required for regeneration includes three terms. The energy to heat the RevIL from the capture temperature (40°C) to the reversal temperature (dependent on RevIL structure); the enthalpy of regeneration and the enthalpy of physically absorbed CO_2. The effect of structure on the reversal temperature and the enthalpy of regeneration of the RevIL systems has been presented. To determine the enthalpy of physically absorbed CO_2, Henry's Law constants were calculated as a function of temperature. The data for TPSA RevIL is shown below.
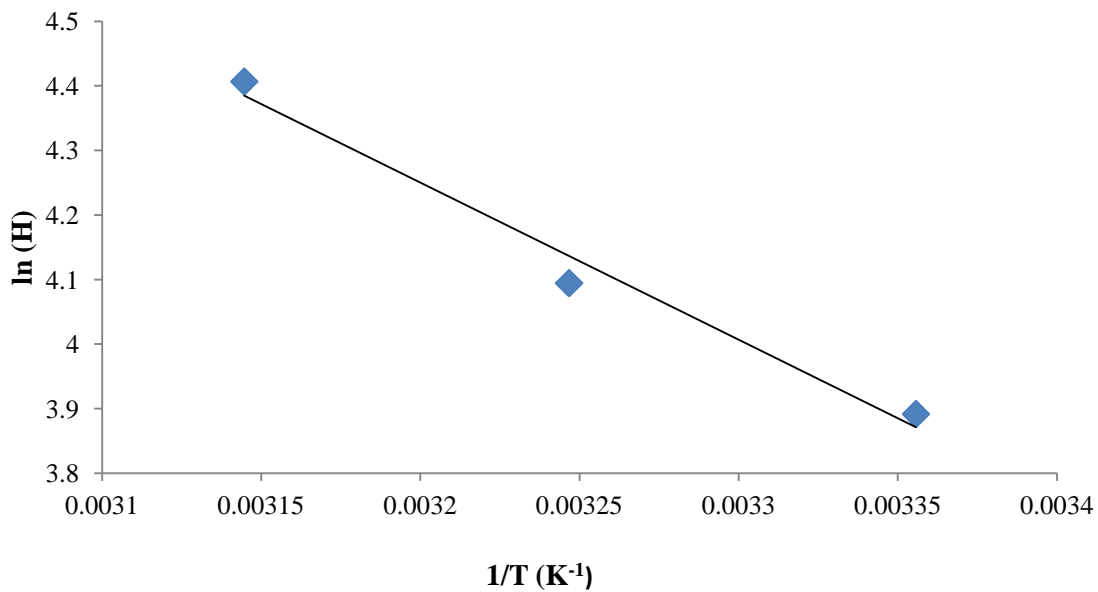
Figure 2.38. Physical absorption of CO$_2$ as a function of temperature

The enthalpy of physically absorbed CO$_2$ was calculated from these data using the following equation.

$$\Delta H_{abs} = R \left(\frac{d(lnP)}{d(1/T)} \right)$$

Equation 2.7

The enthalpy of physically absorbed CO$_2$ of TEtSA, TPSA and THSA was equal to 20±4 kJ per mole. Using this value in addition to the enthalpy of reaction and reversal temperature, the total energy required for regeneration was calculated as a function of CO$_2$ pressure as shown in Figure 2.39.
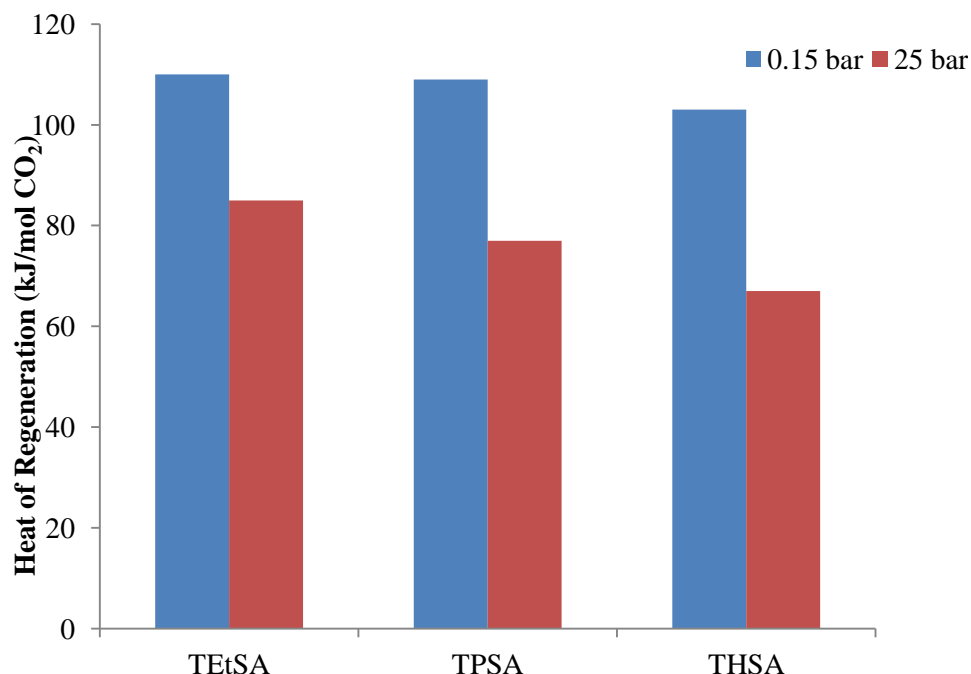
Figure 2.39. Total energy required for regeneration of three RevIL systems at 0.15 bar and 25 bar and 35°C

As is evident from the data, there is a significant decrease in the total energy required for regeneration at 25 bar CO_2 pressure as a result of the enhanced physical absorption of CO_2 at pressures above one bar. As expected, increasing the physical absorption capacity by increasing the alkyl chain length on the silicon atom decreases the heat of regeneration per mole of CO_2 captured.

2.5 Conclusions
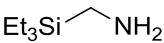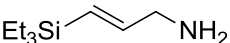
Reversible ionic liquids are a novel class of switchable solvents that have been used in coupling reaction and separation, crude oil separation and now CO_2 capture. The reversible ionic liquid system consists of a silylamine that upon reaction with CO_2 forms an ammonium-carbamate ion pair. Heating the reversible ionic liquid releases the captured CO_2, reforming the silylamine. In addition, the reversible ionic liquid is further capable of physically absorbing additional CO_2, thus giving enhanced capacity

particularly at pressures above one bar. In the design of CO_2 capture solvents, the industrially relevant properties that must be considered are the CO_2 capture capacity, viscosity, reversal temperature and enthalpy of regeneration. These properties are strongly influenced by the structure of the silylamine, and a process for screening reversible ionic liquids that present high CO_2 capture capacity while minimizing the viscosity and energy for reversal has been presented.

Using iterative molecular design and theoretical modeling, the influence of adding or changing the position of one or more methyl groups in the silylamine structure, the alkyl chain length on the silicon atom and unsaturation along the backbone of the silylamine was determined.

The capture conditions are an important consideration in the selection of a CO_2 capture solvent; for example a high pressure CO_2 capture application would benefit from a reversible ionic liquid system with high physical absorption capacity (TPSA or THSA). For low pressure CO_2 capture (e.g., CO_2 capture from flue gas), two silylamine solvents have capture properties that distinguish them from the remaining silylamines synthesized for this study. The properties of these reversible ionic liquid systems are shown below in Table 2.12.

Table 2.12. Structures and properties of TEtSMA and *trans*-TEtSA

Property	TEtSMA $Et_3Si \frown NH_2$	*trans*-TEtSA $Et_3Si \diagup\!\!\diagdown\frown NH_2$
CO$_2$ uptake (mol CO$_2$/mol amine, 25°C)	0.59±0.01	0.61±0.03
CO$_2$ uptake (mol CO$_2$/kg amine, 25°C)	4.09±0.08	3.56±0.20
Reversal temperature (°C)	78±5	48±2
Enthalpy of regeneration (kJ/mol CO$_2$)	76±7	85±7
RevIL viscosity at 25°C (cP)	2373±206	3889±252
RevIL viscosity at 40°C (cP)	625±58	362±19

TEtSMA and *trans*-TEtSA both have high CO$_2$ capture capacities, viable reversal temperatures and comparable enthalpies of regeneration. The reversible ionic liquid viscosities are significantly lower than many of the RevILs investigated, and by controlling conversion of the silylamine to the reversible ionic liquid, an industrially feasible viscosity could be achieved.

2.6 References

1.   U. S. Environmental Protection Agency, *Inventory of U.S. Greenhouse Gas Emissions and Sinks:1990-2011*; Washington D.C., 2013.

2.   *Annual Energy Outlook 2011 with Projections to 2035*; U.S. Energy Information Administration: Washington, 2011; Administration, E. I. *Annual Energy Outlook 2001 With Projections to 2020*; Washington, DC, 2000.

3.   Olajire, A. A., CO$_2$ capture and separation technologies for end-of-pipe applications - A review. *Energy* **2010,** *35* (6), 2610-2628; Ciferno, J.; Litynski, J.,

DOE/NETL Advanced Carbon Dioxide Capture R&D Program: Technology Update. National Energy Technology Laboratory, 2011.

4.   D'Alessandro, D. M.; Smit, B.; Long, J. R., Carbon dioxide capture: Prospects for new materials. *Angewandte Chemie International Edition* **2010,** *49*, 6058-6082.

5.   Fisher, K. S.; Searcy, K.; Rochelle, G. T.; Ziaii, S.; Shubert, C. *Advanced Amine Solvent Formulations and Process Integration for Near-Term CO_2 Capture Success*; Pittsburgh, PA, 2007.

6.   Kohl, A.; Nielsen, R., *Gas Purification*. 5th ed.; Gulf Publishing Company: Houston, Texas, 1997.

7.   Rao, A. B.; Rubin, E. S., A Technical, Economic, and Environmental Assessment of Amine-Based CO2 Capture Technology for Power Plant Greenhouse Gas Control. *Environmental Science & Technology* **2002,** *36* (20), 4467-4475.

8.   Strazisar, B. R.; Anderson, R. R.; White, C. M., Degradation pathways for monoethanolamine in a CO_2 capture facility. *Energy & Fuels* **2003,** *17* (4), 1034-1039.

9.   Bello, A.; Idem, R. O., Comprehensive Study of the Kinetics of the Oxidative Degradation of CO2 Loaded and Concentrated Aqueous Monoethanolamine (MEA) with and without Sodium Metavanadate during CO2 Absorption from Flue Gases. *Industrial & Engineering Chemistry Research* **2005,** *45* (8), 2569-2579; Veawab, A.; Tontiwachwuthikul, P.; Bhole, S. D., Studies of corrosion and corrosion control in a CO_2-2-amino-2-methyl-1-propanol (AMP) environment. *Industrial & Engineering Chemistry Research* **1997,** *36* (1), 264-269.

10.   Aaron, D.; Tsouris, C., Separation of CO_2 from flue gas: A review. *Separation Science and Technology* **2005,** *40* (1-3), 321-348.

11.   Mason, J. A.; Sumida, K.; Herm, Z. R.; Krishna, R.; Long, J. R., Evaluating metal-organic frameworks for post-combustion carbon dioxide capture via temperature swing adsorption. *Energy & Environmental Science* **2011,** *4* (8), 3030-3040.

12.   Banerjee, R.; Phan, A.; Wang, B.; Knobler, C.; Furukawa, H.; O'Keeffe, M.; Yaghi, O. M., High-throughput synthesis of zeolitic imidazolate frameworks and application to CO_2 capture. *Science* **2008,** *319* (5865), 939-943.

13.   Lively, R. P.; Chance, R. R.; Kelley, B. T.; Deckman, H. W.; Drese, J. H.; Jones, C. W.; Koros, W. J., Hollow fiber adsorbents for CO_2 removal from flue gas. *Industrial & Engineering Chemistry Research* **2009,** *48* (15), 7314-7324.

14.   Kronberger, B.; Johansson, E.; Löffler, G.; Mattisson, T.; Lyngfelt, A.; Hofbauer, H., A Two-Compartment Fluidized Bed Reactor for CO_2 Capture by Chemical-Looping Combustion. *Chemical Engineering & Technology* **2004,** *27* (12), 1318-1326.

15.   Rochelle, G. T., Amine Scrubbing for CO$_2$ Capture. *Science* **2009,** *325* (5948), 1652-1654; Brennecke, J. F.; Gurkan, B. E., Ionic Liquids for CO2 Capture and Emission Reduction. *The Journal of Physical Chemistry Letters* **2010,** *1* (24), 3459-3464; Anderson, J. L.; Dixon, J. K.; Maginn, E. J.; Brennecke, J. F., Measurement of SO$_2$ solubility in ionic liquids. *Journal of Physical Chemistry B* **2006,** *110*, 15059-15062; Heldebrant, D. J.; Yonker, C. R.; Jessop, P. G.; Phan, L., Organic liquid CO2 capture agents with high gravimetric CO2 capacity. *Energy & Environmental Science* **2008,** *1* (4), 487-493; Rainbolt, J. E.; Koech, P. K.; Yonker, C. R.; Zheng, F.; Main, D.; Weaver, M. L.; Linehan, J. C.; Heldebrant, D. J., Anhydrous tertiary alkanolamines as hybrid chemical and physical CO2 capture reagents with pressure-swing regeneration. *Energy & Environmental Science* **2011,** *4* (2), 480-484; Heldebrant, D. J.; Koech, P. K.; Rainbolt, J. E.; Zheng, F.; Smurthwaite, T.; Freeman, C. J.; Oss, M.; Leito, I., Performance of single-component CO$_2$-binding organic liquids CO$_2$ BOLs for post combustion CO$_2$ capture. *Chemical Engineering Journal* **2011,** *171* (3), 794-800; Phan, L.; Andreatta, J. R.; Horvey, L. K.; Edie, C. F.; Luco, A.-L.; Mirchandani, A.; Darensbourg, D. J.; Jessop, P. G., Switchable-polarity solvents prepared with a single liquid component. *Journal of Organic Chemistry* **2008,** *73* (1), 127-132.

16.   Gurkan, B. E.; de la Fuente, J. C.; Mindrup, E. M.; Ficke, L. E.; Goodrich, B. F.; Price, E. A.; Schneider, W. F.; Brennecke, J. F., Equimolar CO$_2$ absorption by anion-functionalized ionic liquids. *Journal of the American Chemical Society* **2010,** *132* (7), 2116-2117.

17.   Brennecke, J. E.; Gurkan, B. E., Ionic Liquids for CO$_2$ Capture and Emission Reduction. *Journal of Physical Chemistry Letters* **2010,** *1* (24), 3459-3464.

18.   Muldoon, M. J.; Aki, S.; Anderson, J. L.; Dixon, J. K.; Brennecke, J. F., Improving carbon dioxide solubility in ionic liquids. *Journal of Physical Chemistry B* **2007,** *111* (30), 9001-9009; Aki, S.; Mellein, B. R.; Saurer, E. M.; Brennecke, J. F., High-pressure phase behavior of carbon dioxide with imidazolium-based ionic liquids. *Journal of Physical Chemistry B* **2004,** *108* (52), 20355-20365; Anderson, J. L.; Dixon, J. K.; Brennecke, J. F., Solubility of CO$_2$, CH$_4$, C$_2$H$_6$, C$_2$H$_4$, O$_2$, and N$_2$ in 1-Hexyl-3-methylpyridinium Bis(trifluoromethylsulfonyl)imide: Comparison to Other Ionic Liquids. *Accounts of Chemical Research* **2007,** *40* (11), 1208-1216; Soriano, A. N.; Doma, B. T.; Li, M. H., Carbon dioxide solubility in 1-ethyl-3-methylimidazolium trifluoromethanesulfonate. *Journal of Chemical Thermodynamics* **2009,** *41* (4), 525-529.

19.   Anthony, J. L.; Maginn, E. J.; Brennecke, J. F., Solubilities and Thermodynamic Properties of Gases in the Ionic Liquid 1-n-Butyl-3-methylimidazolium Hexafluorophosphate. *The Journal of Physical Chemistry B* **2002,** *106* (29), 7315-7320.

20.   Shannon, M. S.; Bara, J. E., Reactive and Reversible Ionic Liquids for CO_2 Capture and Acid Gas Removal. *Separation Science and Technology* **2012,** *47* (2), 178-188.

21.   Goodrich, B. F.; de la Fuente, J. C.; Gurkan, B. E.; Zadigian, D. J.; Price, E. A.; Huang, Y.; Brennecke, J. F., Experimental Measurements of Amine-Functionalized Anion-Tethered Ionic Liquids and Carbon Dioxide. *Industrial & Engineering Chemistry Research* **2011,** *50*, 111-118; Wang, C.; Luo, X.; Luo, H.; Jiang, D.-e.; Li, H.; Dai, S., Tuning the Basicity of Ionic Liquids for Equimolar CO_2 Capture. *Angewandte Chemie International Edition* **2011,** *50*, 4918-4922; Bates, E. D.; Mayton, R. D.; Ntai, I.; Davis, J. H., CO_2 capture by a task-specific ionic liquid. *Journal of the American Chemical Society* **2002,** *124* (6), 926-927.

22.   Blasucci, V.; Hart, R.; Mestre, V. L.; Hahne, D. J.; Burlager, M.; Huttenhower, H.; Thio, B. J. R.; Pollet, P.; Liotta, C. L.; Eckert, C. A., Single component, reversible ionic liquids for energy applications. *Fuel* **2010,** *89* (6), 1315-1319.

23.   Babarao, R.; Jiang, J. W., Molecular screening of metal-organic frameworks for CO_2 storage. *Langmuir* **2008,** *24* (12), 6270-6278; Fauth, D. J.; Frommell, E. A.; Hoffman, J. S.; Reasbeck, R. P.; Pennline, H. W., Eutectic salt promoted lithium zirconate: Novel high temperature sorbent for CO2 capture. *Fuel Processing Technology* **2005,** *86* (14-15), 1503-1521.

24.   Camper, D.; Scovazzo, P.; Koval, C.; Noble, R., Gas solubilities in room-temperature ionic liquids. *Industrial & Engineering Chemistry Research* **2004,** *43* (12), 3049-3054.

25.   Blanchard, L. A.; Gu, Z. Y.; Brennecke, J. F., High-pressure phase behavior of ionic liquid/CO_2 systems. *Journal of Physical Chemistry B* **2001,** *105* (12), 2437-2444.

26.   Danon, A.; Stair, P. C.; Weitz, E., FTIR Study of CO_2 Adsorption on Amine-Grafted SBA-15: Elucidation of Adsorbed Species. *The Journal of Physical Chemistry C* **2011,** *115* (23), 11540-11549; Soutullo, M. D.; Odom, C. I.; Wicker, B. F.; Henderson, C. N.; Stenson, A. C.; Davis, J. H., Reversible CO_2 Capture by Unexpected Plastic-, Resin-, and Gel-like Ionic Soft Materials Discovered during the Combi-Click Generation of a TSIL Library. *Chemistry of Materials* **2007,** *19* (15), 3581-3583; Knöfel, C. a. M. C. l. a. H. V. a. L. P. L., Study of Carbon Dioxide Adsorption on Mesoporous Aminopropylsilane-Functionalized Silica and Titania Combining Microcalorimetry and in Situ Infrared Spectroscopy. *The Journal of Physical Chemistry C* **2009,** *113* (52), 21726-21734.

27.   Settle, F., *Handbook of instrumental techniques for analytical chemistry*. Prentive-Hall, Inc.: 1997; p 247-277.

28.   Lazzaroni, M. J.; Bush, D.; Brown, J. S.; Eckert, C. A., High-pressure vapor-liquid equilbria of some carbon dioxide plus organic binary systems. *Journal of Chemical and Engineering Data* **2005,** *50* (1), 60-65.

29. McGhee, W.; Riley, D.; Christ, K.; Pan, Y.; Parnas, B., Carbon dioxide as a phosgene replacement: synthesis and mechanistic studies of urethanes from amines, CO_2, and alkyl chlorides. *Journal of Organic Chemistry* **1995,** *60* (9), 2820-2830.

30. Oexmann, J.; Hensel, C.; Kather, A., Post-combustion CO2-capture from coal-fired power plants: Preliminary evaluation of an integrated chemical absorption process with piperazine-promoted potassium carbonate. *International Journal of Greenhouse Gas Control* **2008,** *2* (4), 539-552; Kim, I.; Svendsen, H. F., Heat of Absorption of Carbon Dioxide (CO_2) in Monoethanolamine (MEA) and 2-(Aminoethyl)ethanolamine (AEEA) Solutions. *Industrial & Engineering Chemistry Research* **2007,** *46* (17), 5803-5809.

31. Kidnay, A. J.; Parrish, W. R., *Fundamentals of Natural Gas Processing*. Taylor & Francis Group, LLC: 2006.

32. Bondi, A., van der Waals Volumes and Radii. *Journal of Physical Chemistry* **1964,** *68* (3), 441-451.

CHAPTER 3 - CARBON DIOXIDE AS A PROTECTING GROUP IN CHEMICAL SYNTHESES

3.1 Introduction

Many pharmaceutical and agrochemical compounds contain basic nitrogen functionalities.[1] The basicity of the nitrogen is influenced by steric hindrance and electronic effects of the substituents.[2] Aryl amines (e.g., aniline) are less reactive than alkyl amines (e.g., propylamine) due to inductive and resonance effects. Pyridines and pyrroles are also less reactive than alkylamines due to reduced nucleophilicity. The reactivity of amines is advantageous for many chemical syntheses; however, amine containing substrates are also prone to participation in side reactions or unwanted interactions. To provide greater control over the chemistry of amine-containing compounds, protecting groups are often used during chemical syntheses.

Careful selection of protecting groups is necessary to achieve a reaction with high yields of the desired product. In Greene's Protective Groups in Organic Synthesis, it is proposed that a protecting group must:[3]

(1) React with the substrate with good yields to achieve sufficient protection

(2) Form a protected species that can be separated from side products

(3) Avoid further sites for reaction

There are several available amine protecting groups, some of which are shown in Figure 3.1.[4]

acetyl   N-tert-butoxycarbonyl   carboxybenzyl

tosyl   trityl   p-methoxybenzyl carbonyl
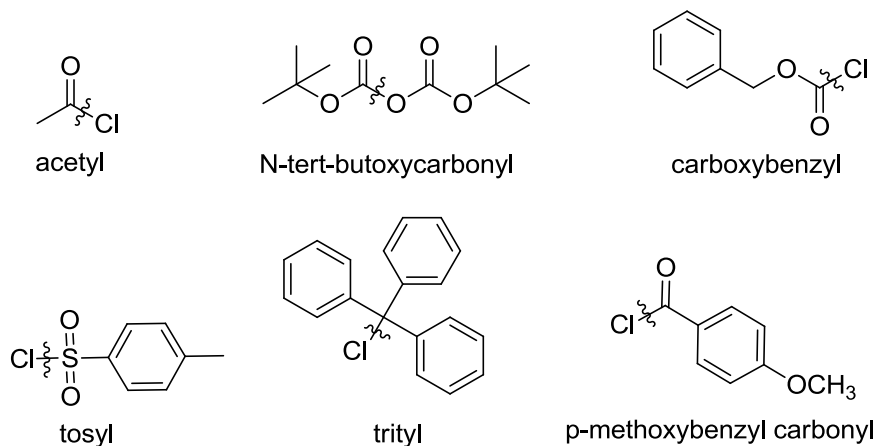
Figure 3.1. Common protecting groups used for amines

Protecting groups react with the amine functionality to form a protected species for subsequent reaction. The simplest approach for acetamide protection is achieved through the reaction of the amine with acetic anhydride or acetyl chloride as shown below in Figure 3.2.
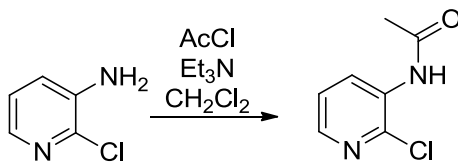
Figure 3.2. Acetamide protection of an amine with acyl chloride under basic conditions

The reactants, reaction conditions and molecule functionalities involved in the synthetic scheme dictate the most suitable protecting group. For example, the protection of an amine with acyl chloride suffers from reduced selectivity due to high reactivity of the protecting species.[5] The reaction of the bulkier N-tert-butoxycarbonyl with an amine functionality is referred to as a Boc protecting group. Boc protecting groups are

considered to be among the most useful protecting groups in synthetic organic chemistry.[6] Careful consideration must be taken when using a Boc protecting group, however, because it is able to react intramolecularly with nucleophiles and electrophiles.[6]

The use of protecting groups to reduce or eliminate unwanted interactions has been presented in literature for a wide range of organic syntheses.[5, 7-9] One example of a class of reactions that utilizes protective strategies is the Suzuki-Miyaura cross-coupling reaction. The Suzuki coupling reaction is one of the most commonly used methodologies for carbon-carbon bond formation of organic halides with organoboron compounds.[10] Many of the organic halides contain an amine functionality, and thus the formation of these complex molecules has been challenging. Literature reports indicate that Pd catalyzed reactions involving free amines suffer from low yields.[11] The low yields of these reactions are attributed to the interaction of the lone pair of electrons on the basic nitrogen with the catalyst. Caron et al. reported improved reaction yields for the Pd catalyzed coupling of 3-amino-2-chloropyridine with phenylboronic acid when the amino group was protected as an acetamide or an imine.[12] Without protection, the reaction did not proceed. The acetamide protection strategy gave an overall yield of 48% and the *in-situ* imine protection resulted in a 99% yield. The inclusion of a protecting group reduced interaction between the palladium catalyst and the amine and thus the reaction yield was improved.

Protecting groups are also used to direct reaction toward a less reactive site in a chemoselective reaction. Oseltamivir phosphate (Tamiflu), shown in Figure 3.3 is synthesized through a series of twelve steps.
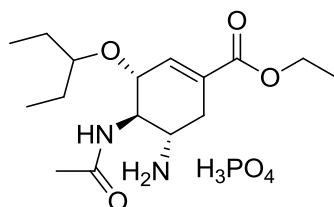
Figure 3.3. Chemical structure of Oseltamivir phosphate (Tamiflu)

The desired product is achieved through the initial protection of the 5-amino group as the benzaldehyde imine as shown in Figure 3.4.[13]
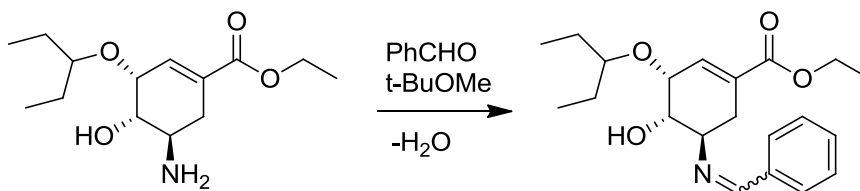
Figure 3.4. Protection of the 5-amino site in the synthesis of Oseltamivir phosphate (Tamiflu)

Protecting groups must be selected carefully for protecting ability as well as for the subsequent removal and separation from the reaction products. Typically the removal of a protecting group requires the use a strong acid or base to cleave the protecting group, causing potential interference with other products or reagents in the reaction mixture.[1, 5]

Despite the challenges associated with the use of protective groups, the elimination of protective groups from synthetic organic chemistry is unlikely.[5] Thus, the development of new methods for the efficient and economical protection of functional groups must be considered. As a consequence, we initiated studies on the use of CO_2 as an *in situ*, reversible protecting reagent.

3.2 Background

A number of publications have discussed supercritical CO_2 as a solvent, reactant and protecting agent.[9, 14, 15] For example, Leitner *et al*. have reported the protection of an amine functionality during ring closing metathesis using supercritical CO_2.[8, 9] Ruthenium catalysts used for ring closing metathesis reactions are deactivated in the presence of amine containing substrates.[9, 16] As a result, the conventional ring closing metathesis route to form cyclic amines involves three steps (protection/cyclization/deprotection). The formation of carbamic acid in supercritical carbon dioxide eliminates the need for an additional protecting group. Additionally, the use of supercritical CO_2 as a solvent for coupling reactions is prevalent in literature.[17] More specifically, Heck reactions (similar to Suzuki coupling reactions) with amine containing substrates showed increased yields when completed in supercritical CO_2 as opposed to conventional reaction solvents. The improved yields were attributed to the interaction of CO_2 with the amine to prevent interaction between the amine and the palladium catalyst.[18]

The use of supercritical CO_2 to direct product distribution of allylic amines has also been presented. Shown in Figure 3.5 is the reaction pathway of an allylic amine under hydroaminomethylation conditions in a conventional solvent and in supercritical CO_2.[7, 8] In a conventional solvent, the nucleophilic nitrogen will directly result in the ring closure at the rhodium acyl intermediate. Reversible carbamic acid formation minimizes ring closure and directs the reaction to the pyrrolidine.
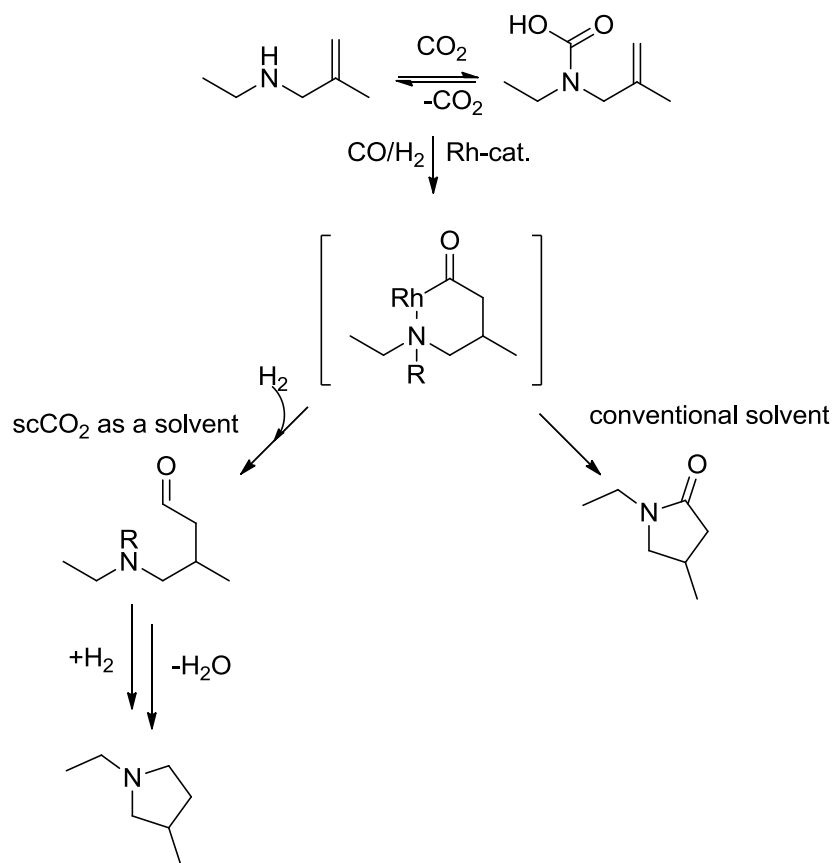
Figure 3.5. Supercritical CO_2 as a solvent and protective medium to direct reaction pathway under hydroaminomethylation conditions

Although supercritical CO_2 is considered green, as it is naturally abundant, non-toxic, nonflammable, and recyclable, the implementation of reactions in supercritical CO_2 requires high pressure equipment. The use of supercritical CO_2 as a reaction medium and protective agent is unlikely to be adopted for large-scale industrial applications. Similar to the reactions between primary silylamines (presented in Chapter 2), we proposed reversible amine protection via reaction with CO_2 at atmospheric (or low) pressure.

The use of CO_2 as a protecting agent at atmospheric pressure is fairly novel. The protection of nucleophilic centers using CO_2 has been published; however this work

involves the use of *n*-Butyllithium to form the lithium salt of the carbamate species.[19] *n*-Butyllithium reacts violently with water, so its use on a large-scale is challenging. Preliminary investigations into the use of added base for CO_2 protection have also been investigated for the large-scale synthesis of an antibiotic, Ertapenem Sodium; the final steps are shown in Figure 3.6.[20] Increased yields with CO_2 protection are attributed to a decrease in Pd-C deactivation, however, the reaction details and confirmation of CO_2 protection are a bit ambiguous.
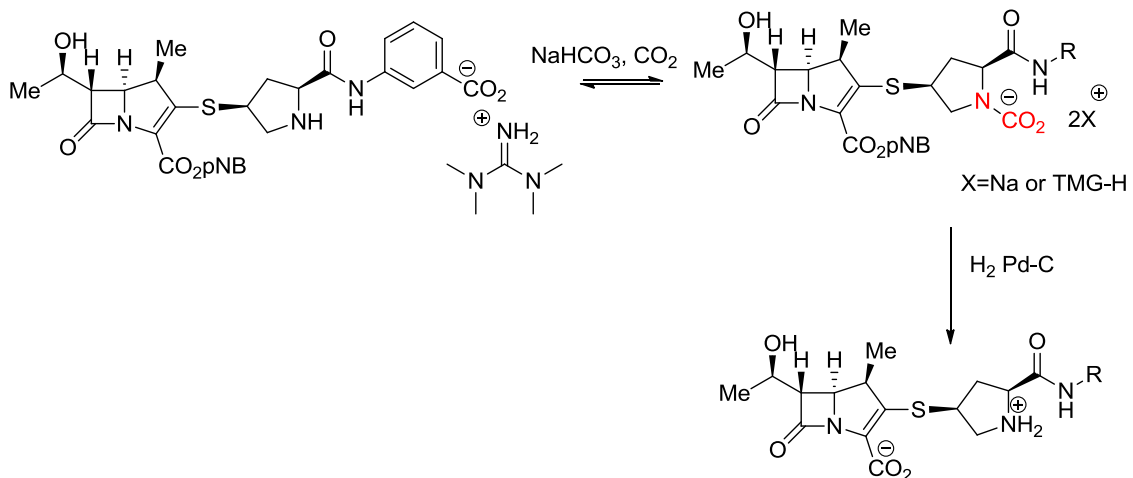
Figure 3.6. Large-scale synthesis of Ertapenem Sodium with CO_2 protection

A discussion of three *in-situ*, reversible amine protection strategies, and evidence supporting the successful protection of a model compound during a chemoselective reaction will be presented.

3.3 Experimental Section

3.3.1 <u>Materials</u>

All chemicals were purchased from Sigma-Aldrich and used as received unless otherwise noted. Chemicals used were: benzylamine (>99.5%); 4-chlorobenzylamine

(98%); 4-bromo-α-methylbenzylamine (≥96.0%); 4-bromoaniline (97%); 1,8-Diazabicyclo[5.4.0]undec-7-ene (98%, purified by distillation); triethylamine (≥99.0%); acetonitrile (ACN, anhydrous); tetrahydrofuran (THF, anhydrous); dichloromethane; Celite® 545 (filter aid, treated with sodium carbonate, flux calcined) 4-(aminomethyl)benzoic acid (97%); lithium aluminum hydride (powder, reagent grade, 95%); 1,2,4-Triazole (98%); isopropenyl acetate (VWR, 99%); pivaloyl chloride (99%); dimethyl sulfoxide (DMSO, >99.5%); dimethylsulfoxide-d_6 (100%, 99.96 atom % D); N,N-dimethylformamide (DMF, anhydrous); N,N-dimethylformamide-d_7 (99.5 atom % D); acetonitrile-d_3 (100%, 99.96 atom % D). Carbon dioxide used was SFE grade from Airgas (99.999%).

 Experimental

3.3.1.1 Synthesis of Benzylcarbamic Acid

0.857 grams (8 mmol) benzylamine was added to 20 mL anhydrous DMSO or DMF to make a 0.4 M solution. The sample was stirred while sparging with CO_2 (rotometer flowrate: 200 mL·min^{-1}) at 25°C and 1 bar for 60 minutes to ensure complete conversion of the benzylamine to the carbamic acid.

3.3.1.2 Synthesis of Benzylcarbamate-Protonated DBU Ion Pair

0.857 grams (8 mmol) benzylamine was added to 8 mL anhydrous acetonitrile to make a 1 M solution. The sample was stirred while adding 1.339 grams (8.8 mmol) 1,8-Diazabicyclo[5.4.0]undec-7-ene under nitrogen. The sample was sparged with CO_2 via a stainless steel needle (rotometer flowrate: 200 mL·min^{-1}) at 25°C and 1 bar for 30 minutes to ensure complete conversion to the ionic species.

3.3.1.3 Synthesis of Pivaloyl Benzotriazole

Pivaloyl benzotriazole was synthesized from benzotriazole and pivaloyl chloride (Figure 3.7). The procedure was adapted from literature report.[21, 22] Anhydrous THF was added to an argon-purged round bottom flask mixed with a stir bar. An equivalent of benzotriazole was added and the solution was cooled to 0°C using an ice bath. An equimolar equivalent of pivaloyl chloride and triethylamine (TEA) were added. The reaction was brought to room temperature and allowed to stir for 4 hours. The mixture was then quenched with methanol and water. The organic layer was extracted with dichloromethane and brine. The collected organic layer was then rotovapped to yield pivaloyl benzotriazole as a yellow oil (68% isolated yield).
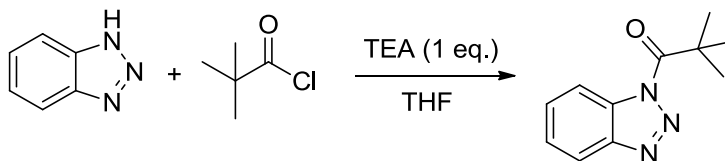
Figure 3.7. Synthesis of pivaloyl benzotriazole

3.3.1.4 Synthesis of 4-(aminomethyl)-phenyl methanol
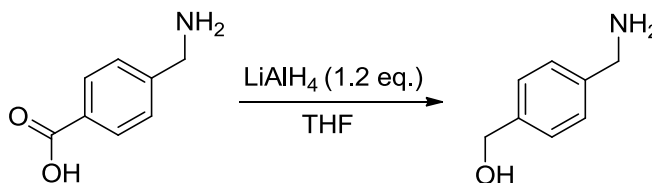
Figure 3.8. Synthesis of 4-(aminomethyl)-phenyl methanol

The model compound, 4-(aminomethyl)-phenyl methanol was prepared from 4-aminomethyl benzoic acid by reduction with LiAlH4 (Figure 3.8) following literature precedent.[23] One equivalent of 4-aminomethyl benzoic acid was added to a round bottom flask with a stir bar and condenser. The flask was sealed and purged with argon and

anhydrous tetrahydrofuran (THF) was added. The solution was cooled to near 0°C using an ice bath. Approximately 1.2 equivalents of LiAlH₄ (powder) was added in portions slowly to limit the exotherm and byproduct H_2 gas produced. Once added, the solution was heated to reflux (66°C). After 12 hours, the reaction mixture was cooled again to 0°C. The remaining LiAlH₄ was quenched slowly with methanol followed by water/30% sodium hydroxide solution. The organic layer was extracted with dichloromethane and rotovapped to yield 4-(aminomethyl)-phenyl methanol as a pale yellow solid in 30% isolated yield.

3.3.1.5 Procedure for the Acylation Reactions with and without CO₂ Protection

The following acylating agents were chosen for use in a model nucleophilic acyl substitution reaction − pivaloyl chloride, pivaloyl benzotriazole, and isopropenyl acetate (Figure 3.9).

pivaloyl chloride   pivaloyl benzatriazoyl   isopropenyl acetate
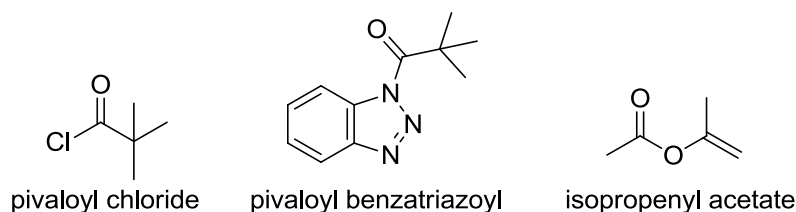
Figure 3.9. Acyl substrates investigated in a nucleophilic substitution reaction

3.3.1.6 Procedure for the Acylation Reactions with Benzylamine

8 mL anhydrous acetonitrile was added to a 15 mL round bottom flask purged with nitrogen. 0.85 grams (8 mmol) of benzylamine was added and stirred. 1.1 equivalents 1,8-Diazabicyclo[5.4.0]undec-7-ene (8.8 mmol) was added and stirred. The sample was sparged with CO_2 (rotometer flowrate: 200 mL·min⁻¹) or N_2 via a stainless steel needle at 25°C and 1 atm for 30 minutes. The acylating agent was added to the

reaction mixture for the two reaction conditions (1 or 2 equivalents of acylating species). Samples were analyzed with ^{1}H and ^{13}C NMR.

3.3.1.7 Procedure for the Acylation Reactions with (4-(aminomethyl)phenyl)methanol

0.22 grams (1.6 mmol) of the solid (4-(aminomethyl)phenyl)methanol was weighed into a 10 mL round bottom flask, and placed under a nitrogen atmosphere. 4 mL anhydrous acetonitrile was added to the solid and stirred to make a 0.4 M solution. 1.1 equivalents 1,8-Diazabicyclo[5.4.0]undec-7-ene (1.8 mmol) was added and stirred. The sample was sparged with CO_2 (rotometer flowrate: 200 mL·min^{-1}) or N_2 via a stainless steel needle at 25°C and 1 atm for 30 minutes. A stock solution of 1,2,4 –triazole was prepared by dissolving 0.11 g 1,2,4 –triazole (1.604 mmol) in 10 mL anhydrous acetonitrile. 1 mL of the stock solution was added to the solution of (4-(aminomethyl)phenyl)methanol. 0.161 g (1.604 mmol) or 0.321 (3.208 mmol) of isopropenyl acetate was added to the reaction mixture for the two reaction conditions (1 or 2 equivalents of acylating species). Samples were analyzed with ^{1}H and ^{13}C.

3.3.2 Instrumentation

^{1}H and ^{13}C NMR spectra were collected on a Bruker AMX-400. To conduct quantitative ^{13}C NMR, a complete relaxation was determined by performing an inversion recovery T_1 experiment. The carbonyl peak at 159.14 had the longest T_1 time of 23 seconds. The recommended delay time is 5 times the longest T_1 time, and therefore a delay time of 125 seconds was used. A full 90° pulse was used to insure complete excitation of the nucleus, and proton decoupling was done only during the acquisition period to avoid a false and disproportional signal buildup.

Differential scanning calorimetry was used to determine the reversal and/or melting temperature of the solid carbamate salts formed. DSC measurements were performed using a Q20 TA DSC Instrument. The DSC method included equilibrating the cell at -40°C and ramping the temperature 5°C per minute until 400°C was reached. The reversal temperature is defined from the DSC thermogram as the intersection of tangent lines drawn from the onset and bottom of the reversal events – as shown in the results section.

3.4 Results and Discussion

A systematic approach to CO_2 protection has been investigated as a means to alter chemical reactivity of a model compound. The demonstration of amine protection was first completed using benzylamine derivatives as shown in Figure 3.10. The halogen containing compounds were chosen as they were of interest for later use as substrates in Suzuki coupling reactions.
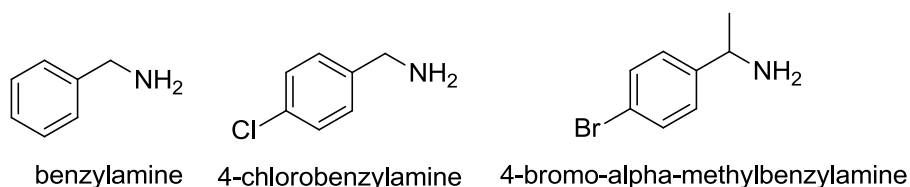
Figure 3.10. Model substrates for amine protection strategies

3.4.1 <u>Amine Protection through the Formation of an Ammonium-Carbamate Ionic Salt</u>

The first protection technique evaluated the reaction of CO_2 with the amine substrate to form an ammonium-carbamate ionic salt shown in Figure 3.11.
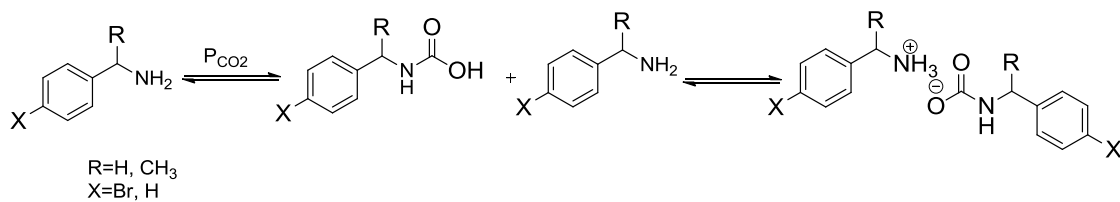
Figure 3.11. Reaction of benzyl-type amines with CO_2 to form an ammonium-carbamate ionic salt

Benzylamine first reacts with CO_2 to form a carbamic acid species. The carbamic acid is rapidly deprotonated in the presence of an additional mole of amine to form an ammonium-carbamate ion pair. The ion pair may be isolated as a white solid, and was analyzed with FTIR and DSC. The IR spectrum of the ammonium-carbamate salt of 4-bromo-α-methylbenzylamine formed after reaction with 1 bar of CO_2 at 25°C is shown in Figure 3.12. There are two characteristic peaks in the IR spectrum. The first is the broad ammonium (NH_3^+) vibration between 2800 and 3200 cm^{-1} and the second is the characteristic carbonyl stretch (C=O) at ~1630 cm^{-1}.
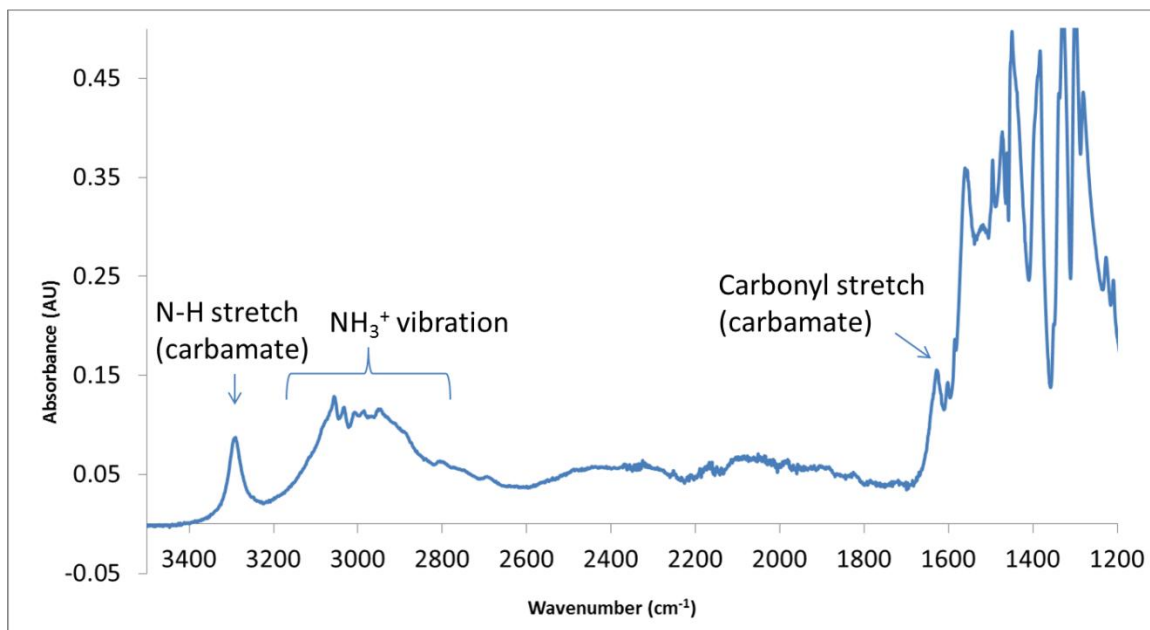
Figure 3.12. FTIR spectrum of 4-bromo-α-methylbenzylamine salt after reaction with 1 bar of CO_2 at 25°C

The DSC thermogram of the CO_2-protected 4-bromo-α-methylbenzylamine salt (Figure 3.13) shows two events.
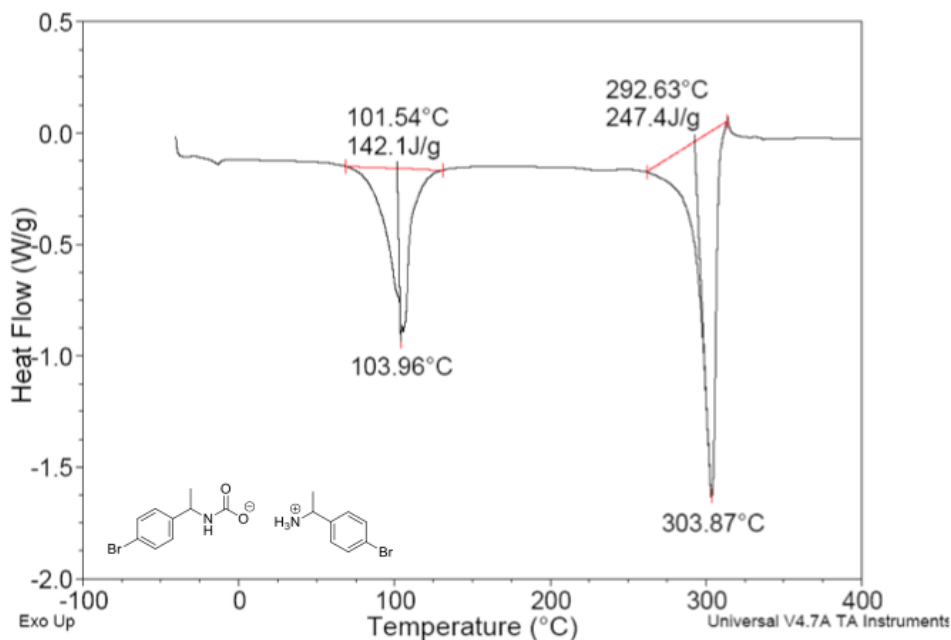
Figure 3.13. DSC thermogram of 4-bromo-α-methylbenzylamine salt after reaction with 1 bar of CO_2 at 25°C

The first event has a small shoulder due to the melting of the solid and subsequent release of CO_2. The second event corresponds to the evaporation of 4-bromo-α-methylbenzylamine. The DSC results indicate the neat protected species would be stable to temperatures approaching 100°C. For use in a chemical synthesis, the properties of the protected species must also be investigated in solution.

3.4.1.1 Ammonium-Carbamate Salt in Solution

The solubility of the protected salt in polar aprotic solvents was studied by sparging CO_2 through a 0.4 M solution of 4-bromo-α-methylbenzylamine in tetrahydrofuran, ethyl acetate, acetone, 1,4 dioxane, chloroform, and acetonitrile. Upon introduction of CO_2 to the solution at 25°C, a white solid precipitated out of solution. At

50°C, the solid dissolves into the solvent; however, NMR suggests significant reversal of the salt back to the starting amine substrate. The ^{13}C NMR is shown in Figure 3.14. The salt was formed by sparging benzylamine with ^{13}C labeled CO_2.
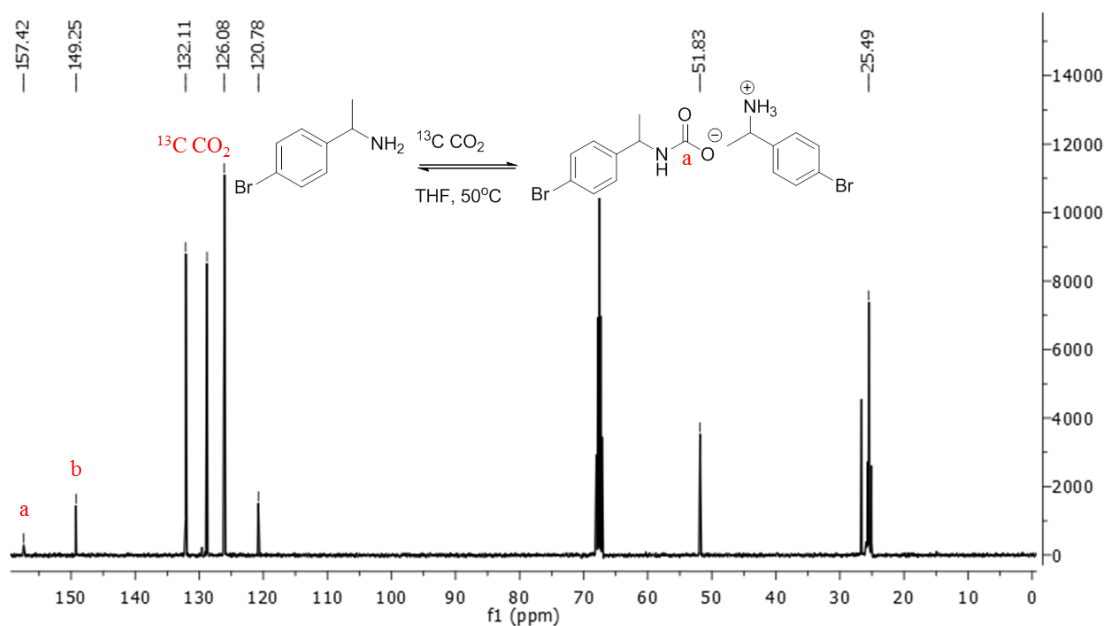
Figure 3.14. ^{13}C NMR spectrum of the 4-bromo-α-methylbenzylamine in THF at 50°C under 1 bar CO_2 pressure

The relatively small size of the carbamate peak at 157.42 ppm suggests that there is minimal amount of protected species in solution. ^{13}C NMR experiments are only semi-quantitative; however, isotopically labeled $^{13}CO_2$ was used to form the protected salt, so the carbonyl of the carbamate should appear much larger than the non-isotopically labeled peaks. The isotopically labeled $^{13}CO_2$ is dissolved in solution as indicated by the peak at 126.08 ppm in the ^{13}C NMR.

The insolubility of the protected ammonium-carbamate species has been reported by Leitner et al. during the iridium-catalyzed enantioselective hydrogenation of imines in supercritical CO_2,[15] and the analysis of the ammonium-carbamate species has been

difficult due to the insolubility of the salt in organic solvents. As a result, alternative solvents have been investigated.[24]

At 25°C the protected 4-bromo-α-methylbenzylamine is soluble in methanol. In the presence of an alcohol, ammonium carbamate and ammonium methyl carbonate ion pairs are formed in nearly equivalent amounts. The ^{13}C NMR is presented in Figure 3.15.
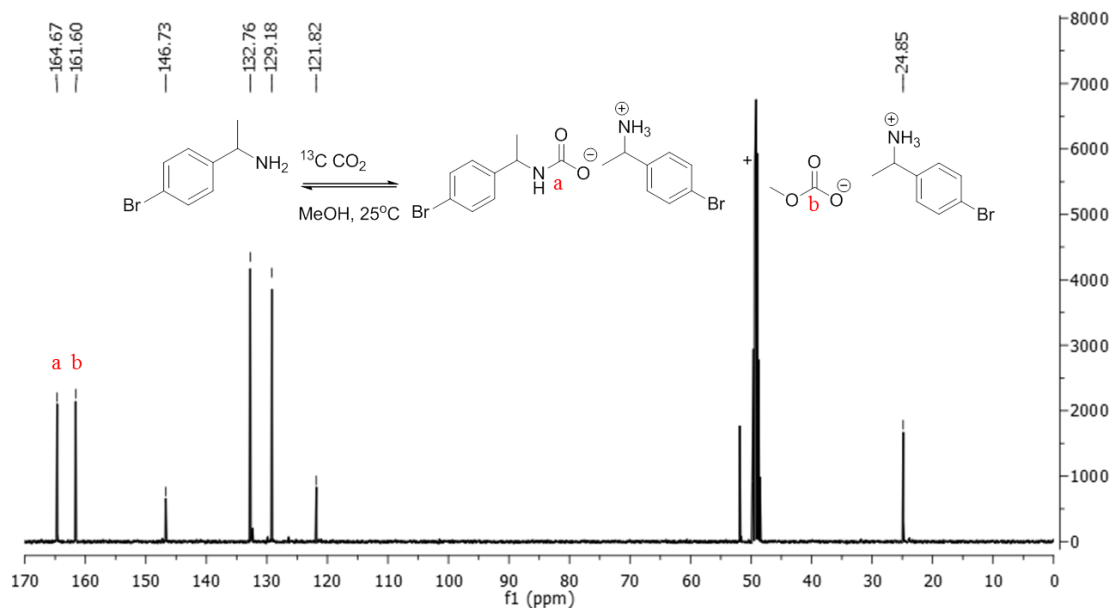
Figure 3.15. ^{13}C NMR spectrum of 4-bromo-α-methylbenzylamine in methanol at 25°C under 1 bar CO$_2$ pressure

An NMR spectrum was also recorded at 50°C to determine the stability of the protected species at elevated temperature. As shown in Figure 3.16, a significant decrease in the carbamate carbonyl carbon is observed.

This is complimented by an increase in the peak at 126 ppm which corresponds to $^{13}CO_2$ in solution. The ammonium-methyl carbonate ion pair appears to have high stability at 50°C, and a significant peak is still observed at 161.60 ppm at 50°C.
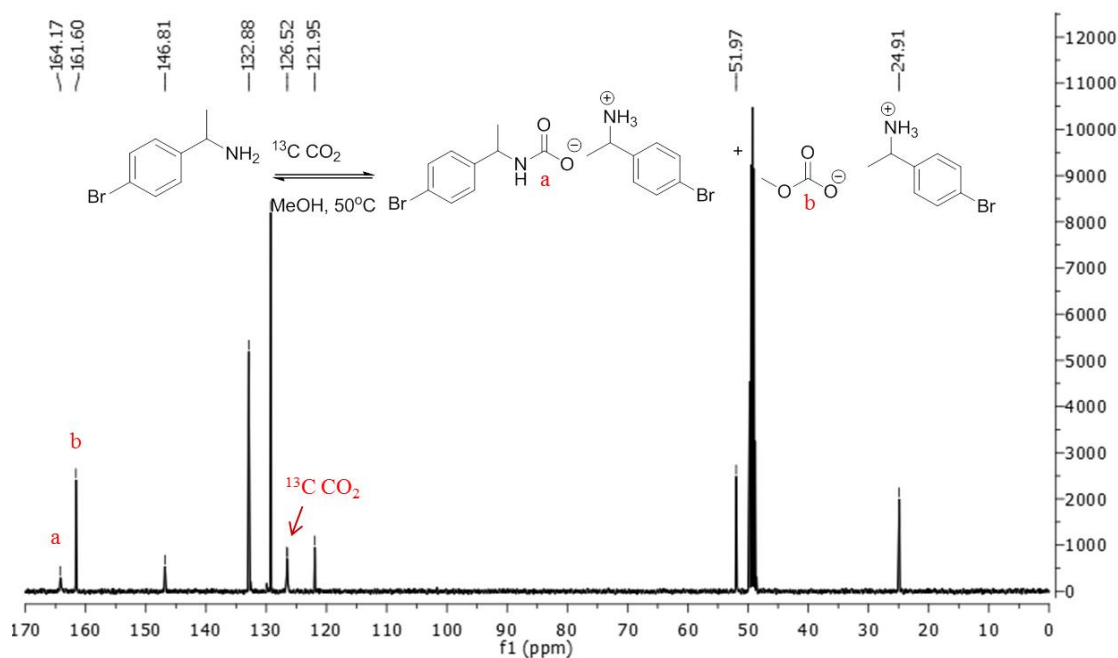
Figure 3.16. NMR spectrum of 4-bromo-α-methylbenzylamine in methanol at 50 °C under 1 bar CO$_2$ pressure

Although there is no evidence of the unprotected 4-bromo-α-methyl benzylamine, it was decided that the formation of one protected species is advantageous for use in chemical syntheses.

3.4.2 Amine Protection through the Formation of a Stabilized Carbamic Acid Species

In an effort to form a single, protected species, the stabilization of a benzylcarbamic acid species in solution was considered. The formation of carbamic acid through reaction of a primary or secondary amine with CO_2 is well known.[25] Referring again to Figure 3.11, the amine first reacts with CO_2 to form the carbamic acid, and then is rapidly deprotonated by another mole of amine to form the ammonium-carbamate ion

pair. The transient nature of carbamic acid makes the isolation very difficult. The complete conversion of alkylamines and naphthylalkylamines to carbamic acid in dimethyl sulfoxide (DMSO) and dimethyl formamide (DMF) has been reported in literature.[26, 27] The formation of carbamic acid (Figure 3.17) in these protophilic, highly dipolar, aprotic solvents can be understood by considering the effect of solvent on the acid–base equilibrium reaction between the amine and carbamic acid.[26]
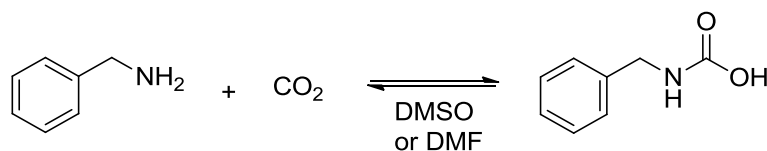
Figure 3.17. Equilibrium reaction of benzylamine to form benzylcarbamic acid

The ^{13}C NMR spectra of the carbamic acid formed in DMSO and DMF respectively are shown in Figure 3.18 and Figure 3.19.
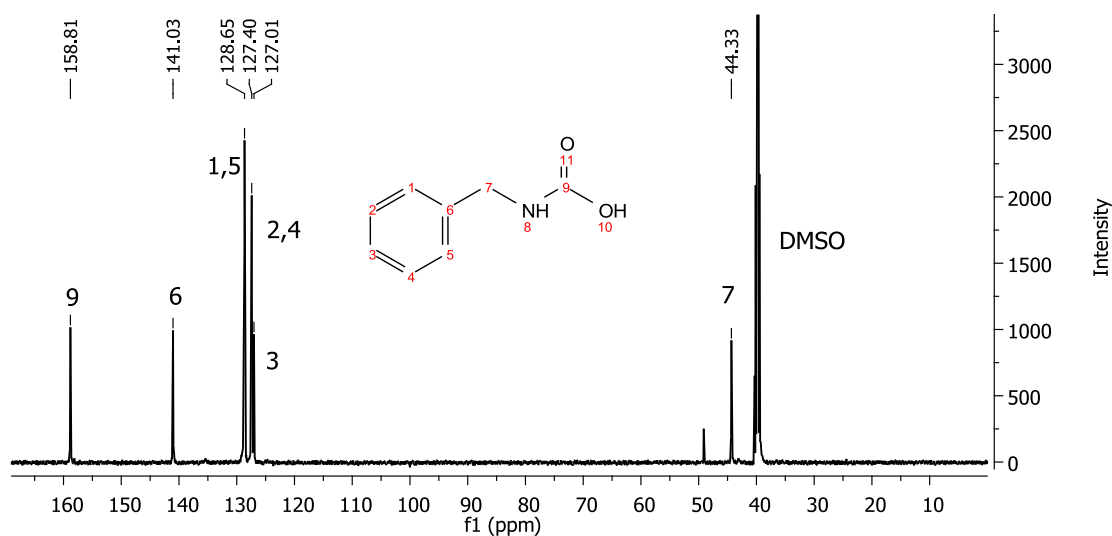
Figure 3.18. ^{13}C NMR of benzylcarbamic acid formed in DMSO

92
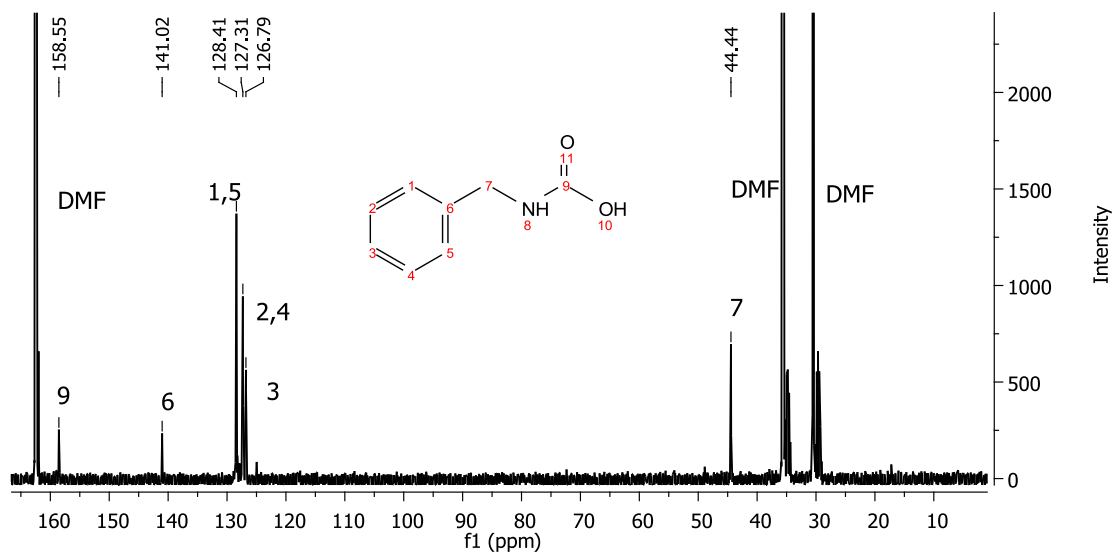
Figure 3.19. ¹³C NMR of benzylcarbamic acid formed in DMF

3.4.2.1 Nucleophilic Acyl Substitution with Pivaloyl Chloride

To determine the ability of the carbamic acid to protect an amine functionality during a nucleophilic acyl substitution, pivaloyl chloride was used as an acylating agent. Without CO_2 protection benzylamine would react with pivaloyl chloride to form N-benzylpivalamide. The control reaction was completed and analyzed by ^{13}C NMR. The NMR indicated the presence of two products shown in Figure 3.20. The first was confirmed as the N-benzylpivalamide; the second species was formed from the reaction of pivaloyl chloride with DMSO. This reaction has been reported in literature and also occurs with pivaloyl chloride and DMF.[28]
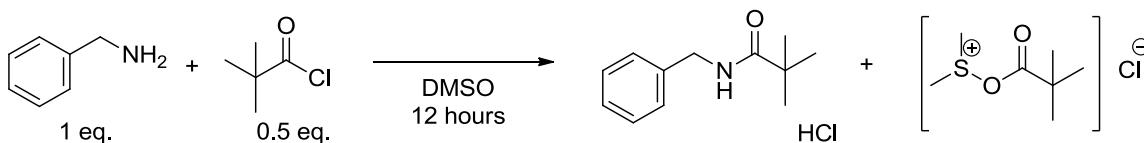
Figure 3.20. Reaction products of benzylamine and pivaloyl chloride in DMSO

93

Despite the unwanted reaction between pivaloyl chloride and DMSO/DMF, the reaction was run with the protected carbamic acid species. A 0.4 M solution of benzylamine in DMSO was sparged with CO_2 for 30 minutes. Following complete conversion of the benzylamine to carbamic acid (confirmed by ^{13}C NMR), the solution was cooled to 0°C and 0.5 equivalents of pivaloyl chloride were added dropwise. The reaction was stirred for three hours. NMR analysis confirmed the presence of unreacted carbamic acid and the DMSO-pivaloyl chloride reacted species, shown in Figure 3.21.
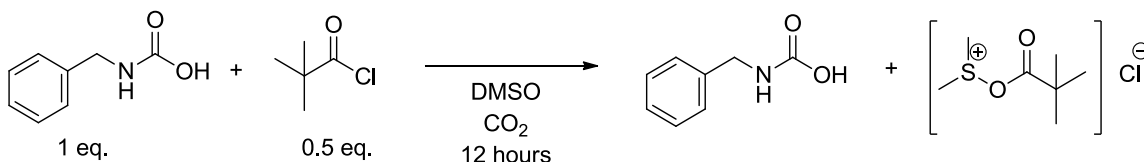
Figure 3.21. Reaction of benzylcarbamic acid with pivaloyl chloride in DMSO

The results were promising in that the benzylamine remained protected and N-benzylpivalamide was not formed. However, the reaction between pivaloyl chloride and DMSO/DMF is undesired from a processing standpoint and thus alternative acylating agents were explored.

3.4.2.2 Nucleophilic Acyl Substitution with Pivaloyl Benzotriazole

In an effort to decrease the reactivity of the acylating agent, 1-(2,2,2-trimethylacetyl)-1H-benzotriazole (pivaloyl benzotriazole) was investigated as substitute for pivaloyl chloride. Again, a control reaction without CO_2 was completed with pivaloyl benzotriazole. After stirring for 24 hours at room temperature, a sample was analyzed by ^{13}C NMR. N-benzylpivalamide and starting material (benzylamine) were observed as shown in Figure 3.22.
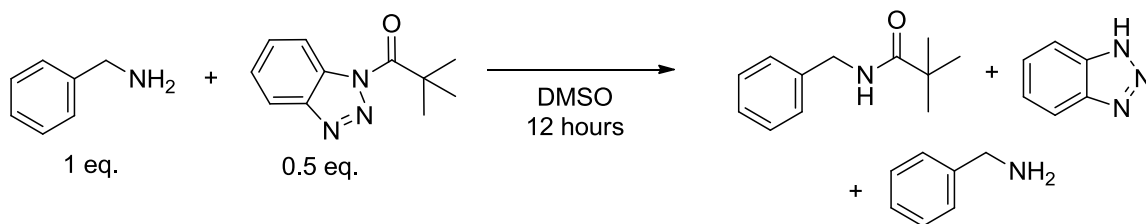
Figure 3.22. Reaction of benzylamine with pivaloyl benzotriazole in DMSO

Reactions were then conducted with CO_2-protected benzylcarbamic acid. As previously described, CO_2 was sparged through a solution of benzylamine in DMSO. Pivaloyl benzotriazole was then added dropwise to the solution of protected amine, and stirred for 12 hours. The reaction was completed with 0.5 and 1 equivalent of pivaloyl benzotriazole. In both reactions, the products were benzylpivalamide and residual benzyl-carbamic acid, as presented in Figure 3.23.
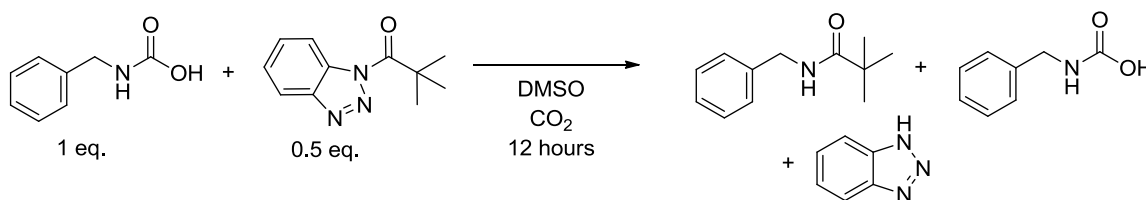
Figure 3.23. Observed reaction of benzylcarbamic acid with pivaloyl benzotriazole in DMSO

The pivaloyl benzotriazole did not react with DMSO; however the undesired product was formed in the above reaction. The formation of benzylpivalamide indicated that the benzylamine did not remain protected upon addition of the acylating agent. One explanation for the complete formation of benzylpivalamide is that benzotriazole (formed upon reaction of the amine with pivaloyl benzotriazole) may have deprotonated the benzylcarbamic acid. The pKa of benzotriazole is 8.2, and therefore a small concentration would lead to the deprotonation of the benzylcarbamic acid and reformation of the amine.[22]

95

3.4.3 Amine Protection through the Stabilization of the Carbamate Salt with Added Base

The formation of the ammonium-carbamate ion pair through neat reaction of benzylamine and the stabilization of benzylcarbamic acid in DMSO/DMF have been presented. These species did not maintain protection during model acylation reactions, and the result was the formation of the undesired product. To shift the reaction equilibrium further toward the protected species, an additional base was added to the solution of benzylamine in a polar aprotic solvent prior to reaction with CO_2. The reaction scheme is shown in Figure 3.24. In the presence of an added base, the carbamic acid formed upon the reaction with CO_2 is rapidly deprotonated by the base to form the carbamate-protonated base ion pair.
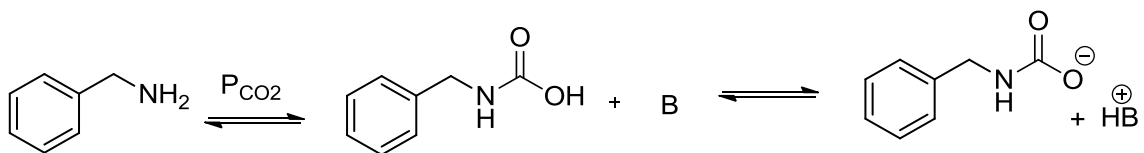
Figure 3.24. Reaction of benzylamine with CO_2 in a polar aprotic solvent with added base.

The base strength has a significant impact on the solubility of the ion pair in conventional solvents, and the stability of the protected species during an acylation reaction. The solubility of the protected species was first examined. Four bases were studied for the protection of benzylamine in acetonitrile. The first two bases tested are commonly used organic bases, triethylamine (TEA) and diisopropylethylamine (DIPEA) shown in Figure 3.25. Upon reaction with CO_2, a white solid was formed that was insoluble in acetonitrile (ACN) or tetrahydrofuran (THF).

triethylamine (TEA)   diisopropylethylamine (DIPEA)
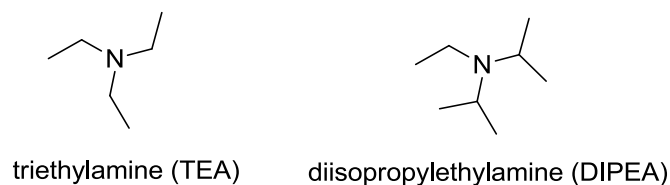
Figure 3.25. Organic bases investigated for the protection of benzylamine in a polar aprotic solvent

The insolubility of the protected species in acetonitrile and tetrahydrofuran prompted the investigation into stronger amidine or guanidine bases, such as 1,1,3,3-tetramethylguanidine (TMG) and 1,8-diazabicyclo[5.4.0]undec-7-ene (DBU) shown in Figure 3.26.

1,8-diazabicyclo[5.4.0]undec-7-ene (DBU)   tetramethylguanidine (TMG)
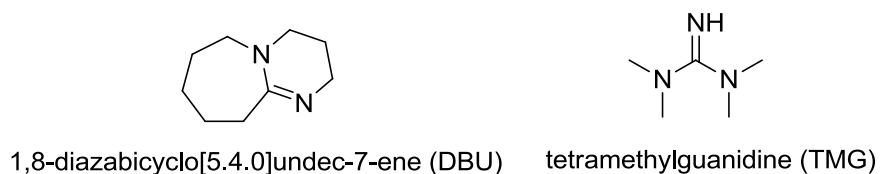
Figure 3.26. Amidine and guanidine bases investigated for the protection of benzylamine in a polar aprotic solvent

Both DBU and TMG have been used in the synthesis of urethanes from amines, CO_2 and alkyl chlorides.[29] Additionally, the concept of a reversible ionic liquid has been applied to the use of DBU and TMG in the reaction of primary alkyl amines, aminoesters and amino alcohols.[30] Upon reaction with CO_2 the resulting carbamate-protonated base ion pair is soluble in acetonitrile, facilitating further analysis. Both TMG and DBU form a protected species upon reaction with CO_2, but the following discussion will focus on experiments with DBU as the added base.

3.4.3.1 Characterization of the CO_2-Protected Benzylamine Using DBU

Figure 3.28 depicts the equilibrium reaction of benzylamine with CO_2 in the presence of DBU.
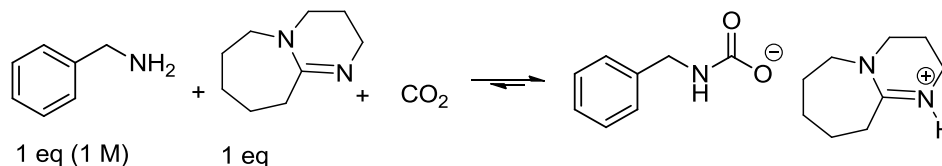
Figure 3.27. Equilibrium reaction of benzylamine with 1,8-diazabicyclo[5.4.0]undec-7-ene (DBU) and CO_2.

The ^{13}C NMR spectrum of the CO_2-protected benzylamine in the presence of DBU showed two carbonyls (163.63 and 159.14 ppm) in addition to the peak at 166 ppm that corresponds to the protonated DBU. The peak labeled "b" in the ^1H NMR spectrum (Figure 3.29) corresponds to the CH_2 of the carbamate.
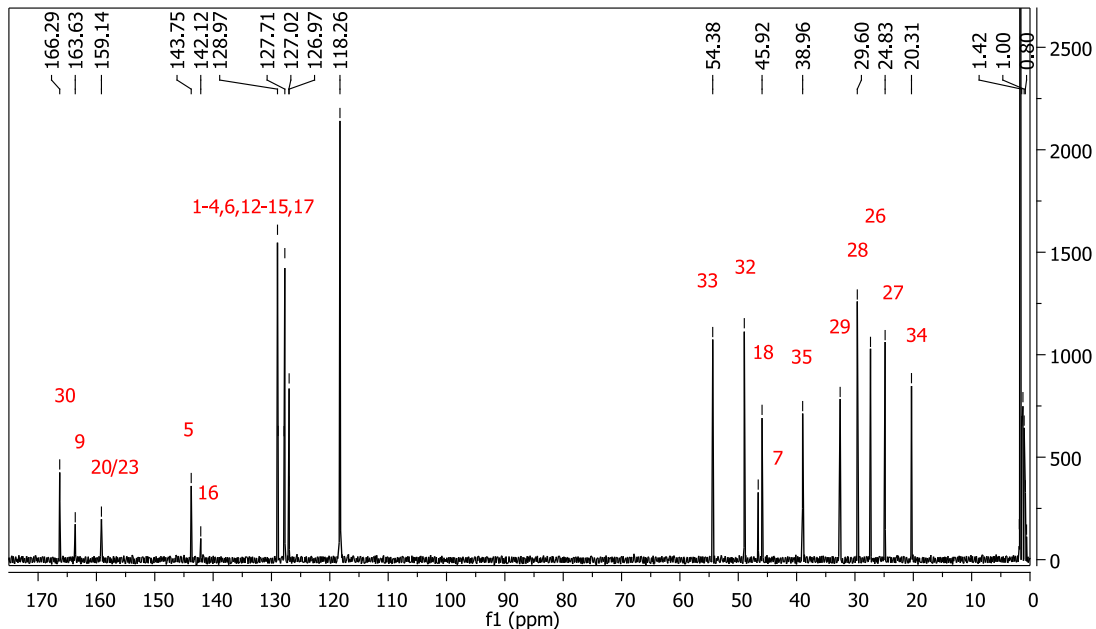
Figure 3.28. ^{13}C NMR of protected benzylamine in the presence of DBU in acetonitrile

98
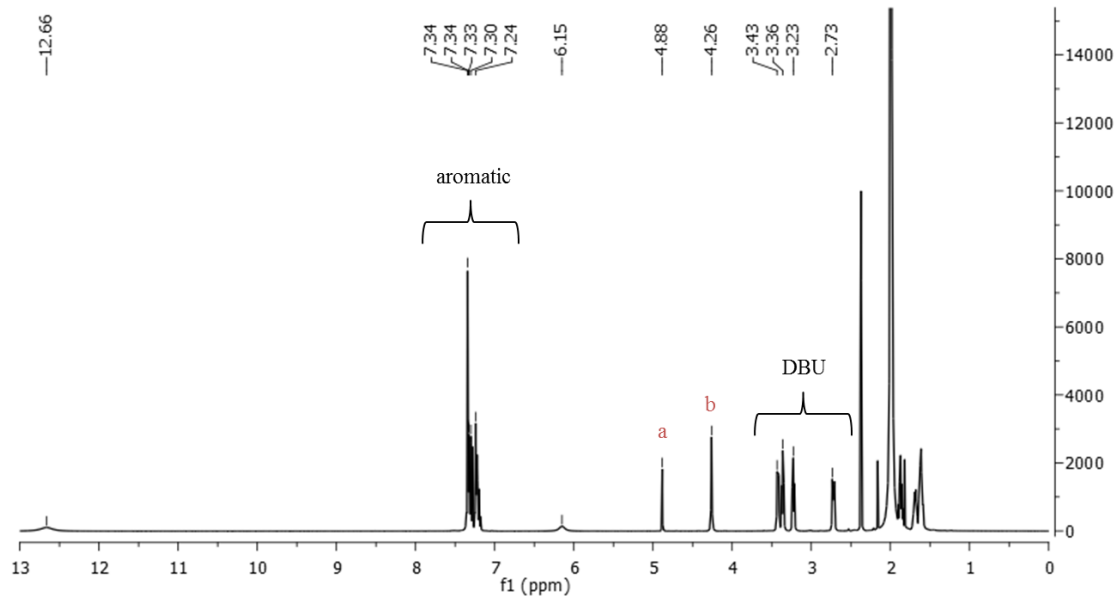
Figure 3.29.¹H NMR of protected benzylamine in the presence of DBU in acetonitrile

The presence of an additional peak could be attributed to the following structures in Figure 3.30.

Species A

Species B

Species C
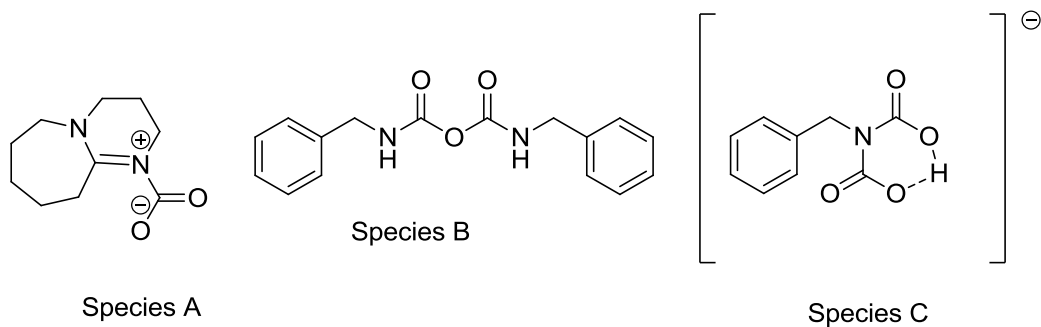
Figure 3.30. Potential products in the protected benzylamine system

The possibility of a DBU-CO_2 adduct was first investigated using ^{1}H-^{13}C HMBC NMR, shown in Figure 3.31. This NMR experiment correlates chemical shifts of the proton and carbon nuclei separated from each other with two or more chemical bonds. From the ^{1}H-^{13}C HMBC NMR it can be seen that the only peak above 150 ppm that corresponds to the DBU protons is at 166.29 ppm. This peak is confirmed as the carbon

double bonded to the nitrogen of the DBU. A prior publication from this group conclusively found that a DBU-CO_2 adduct does not exist.[31] The HMBC NMR also indicated that the unknown carbonyl peak at 158 ppm corresponds to the peak labeled "a" in the ^{1}H NMR spectrum.
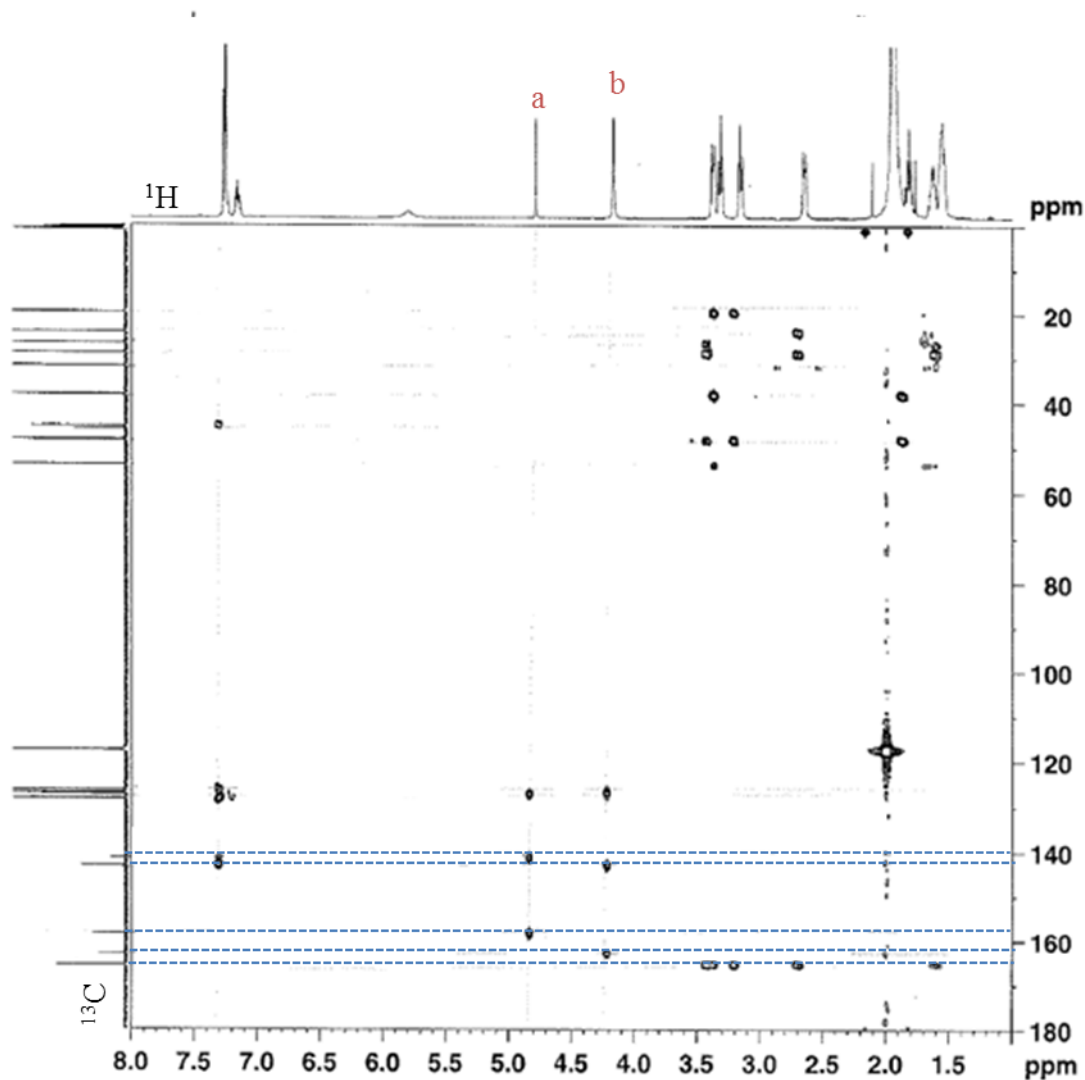
Figure 3.31. ^{1}H-^{13}C HMBC NMR experiment of protected benzylamine with DBU

Quantitative ^{13}C NMR was used to determine whether species B or species C was present in the protected benzylamine system. By integrating the carbon peaks in quantitative ^{13}C

NMR it is possible to determine the approximate ratio of each carbon atom. The ^{13}C NMR integrations are shown below and normalized to the carbon of DBU at 166 ppm. The integrations of the quantitative ^{13}C NMR indicate that for the unknown species, the carbonyl integration is double the integration of the CH_2 or quaternary carbon of the molecule. These results support the diadduct species that is shown in Figure 3.32. This species has been reported only at -30°C with two equivalents of DBU.[29]

Table 3.1. Quantitative ^{13}C NMR integrations for protected species

Peak Assignment	Species	Integration
30	DBUH$^+$	1
9	Carbamate	0.54
20/23	Diadduct	0.57
5	Carbamate	0.48
16	Diadduct	0.23
7	Carbamate	0.49
18	Diadduct	0.21
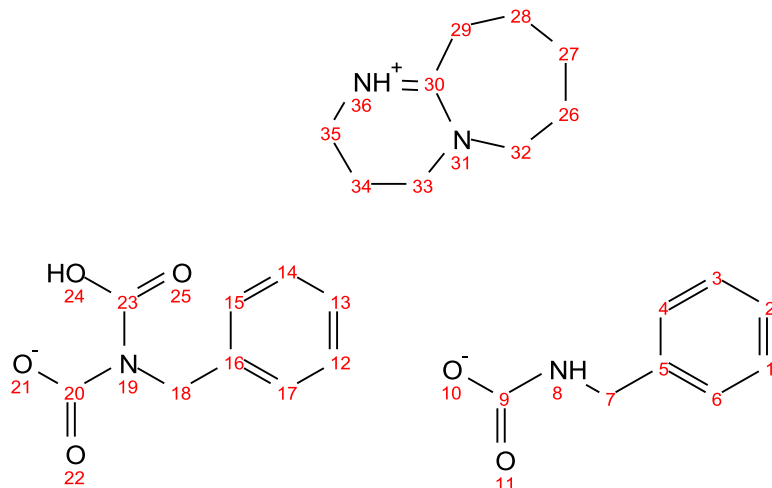
Figure 3.32. Protected benzylamine species in the form of a carbamate and diadduct

The final consideration into the diadduct species was the charge balance. As can be seen in Figure 3.32, the proposed charge balance is achieved through proton sharing of the diadduct and likely the carbamate species. To determine whether the peak at 12 ppm in the ^{1}H spectrum corresponded to a nitrogen, a ^{1}H-^{15}N HSQC NMR experiment was completed at -30°C with ^{15}N labeled benzylamine to minimize proton exchange. As can be seen in Figure 3.33, there is no correlation of the proton at 12 ppm to a nitrogen. These results provide further support of a carbamic acid-carbamate stabilized diadduct species.
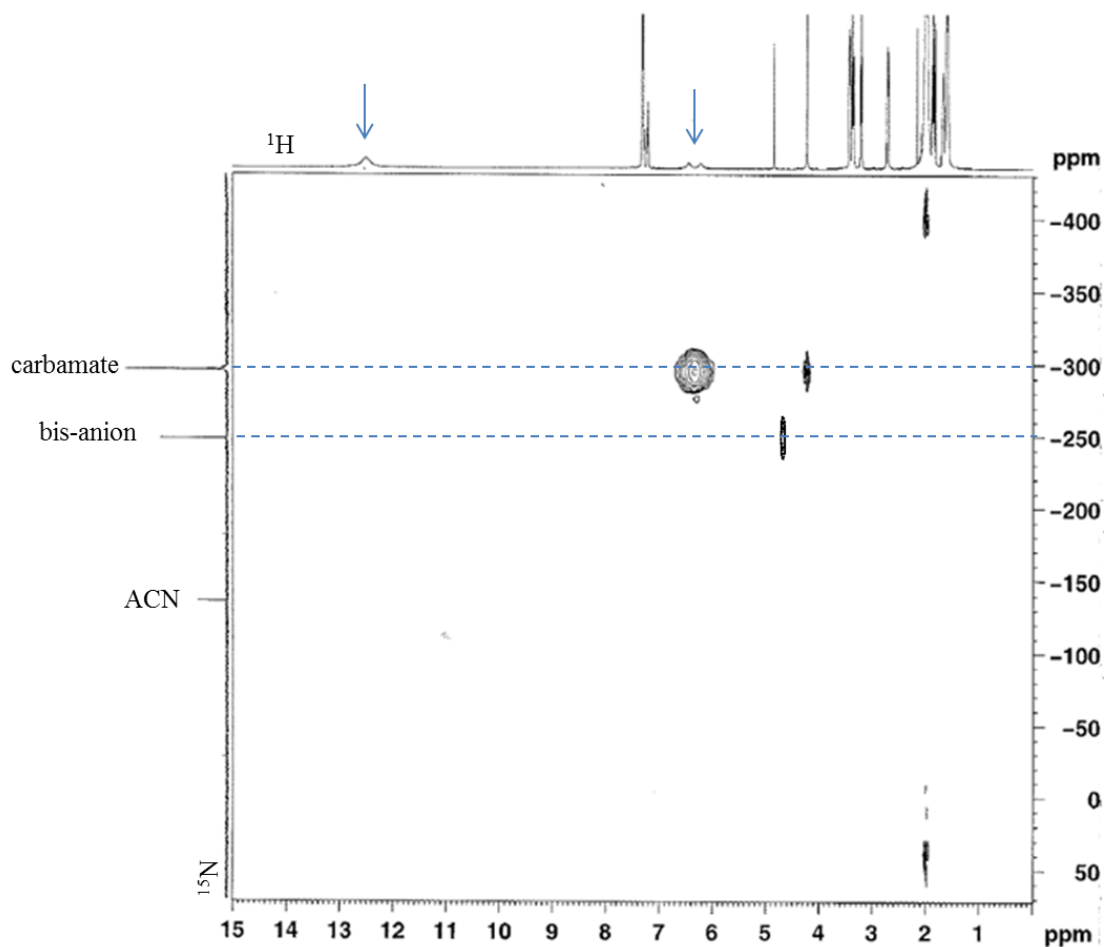
Figure 3.33. ^{1}H-^{15}N HSQC NMR experiment of protected ^{15}N benzylamine at -30°C

The presence of DBU appears to promote the formation of the carbamate-carbamic acid stabilized system. A preliminary experiment was completed in which 0.5 equivalents of DBU were added to a solution of benzylamine in acetonitrile and sparged with CO_2. It was expected that half the benzylamine would form the carbamate-protonated DBU ion pair, and the remaining benzylamine would form the ammonium-carbamate ion pair as shown in Figure 3.34.
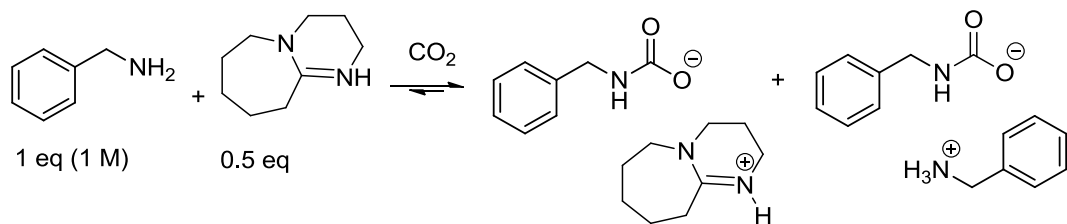
Figure 3.34. Proposed reaction between benzylamine and CO_2 with 0.5 equivalents of added DBU

However, upon sparging with CO_2, no solid precipitated from solution (as would be expected with the formation of the ammonium-carbamate ion pair), and from the ^{1}H and ^{13}C NMR we conclude that a single protected species was formed (Figure 3.35). The reduction in the amount of DBU may provide an economic benefit.
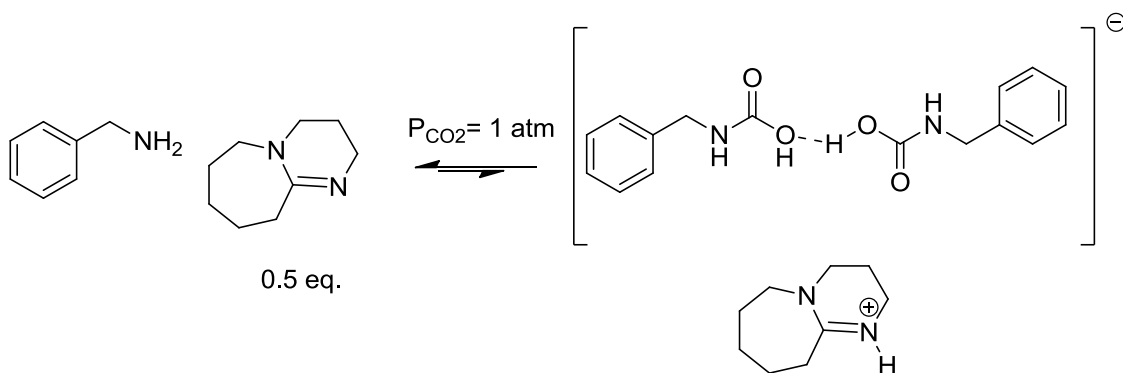
Figure 3.35. Stabilization of carbamic acid-carbamate species upon reaction of benzylamine and CO_2 with 0.5 equivalents of added DBU

With confirmation of the protected species, nucleophilic acyl substitution reactions were again investigated to test the utility of the protection using CO_2 and added DBU.

3.4.4 Model Reaction: Nucleophilic Acyl Substitution

3.4.4.1 Nucleophilic Acyl Substitution with Pivaloyl Chloride

To demonstrate the utility of the in-situ protection of benzylamine using CO_2 and DBU as an added base, a nucleophilic acyl substitution reaction was completed using pivaloyl chloride as the acylating agent. It was proposed that without CO_2 protection, the

benzylamine would react with pivaloyl chloride to form the benzylpivalamide. In the presence of CO_2 and added base, the amine would form a protected species, preventing reaction with pivaloyl chloride at the amine site (Figure 3.36). The carbamate could potentially react with the pivaloyl chloride to form the benzylcarbamic pivalic anhydride.
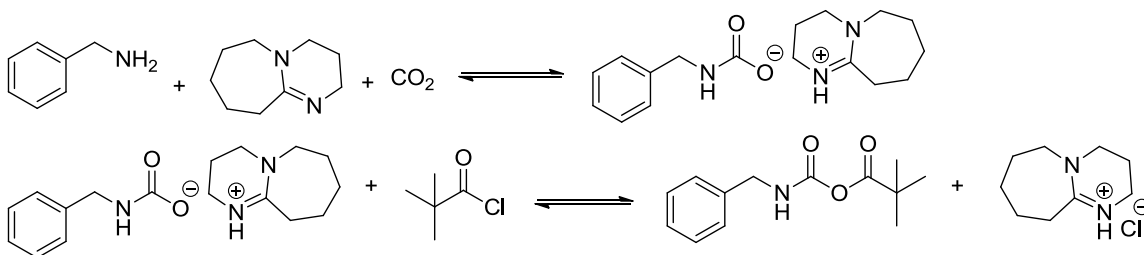
Figure 3.36. Proposed reaction pathway with CO_2 protection

The CO_2-protected benzylamine species was first formed in acetonitrile with 1.2 equivalents of DBU. Although anhydrous acetonitrile was used for these reactions, a small amount of water remained in the system. In the presence of DBU, water and CO_2 are known to react to form a protonated DBU-bicarbonate species.[31] To account for any DBU lost due to this reaction, a slight excess (1.2 equivalents) of DBU was used. The solution was cooled to 0°C and approximately 0.5 equivalents of pivaloyl chloride was added dropwise. After one hour, a sample was taken for NMR analysis. The ^{13}C NMR is shown below in Figure 3.37. From the NMR standards (provided in Appendix E), it was clear that the pivaloyl chloride did not react with the amine to form the benzylpivalamide, however an additional unexpected peak was present at 184 ppm.
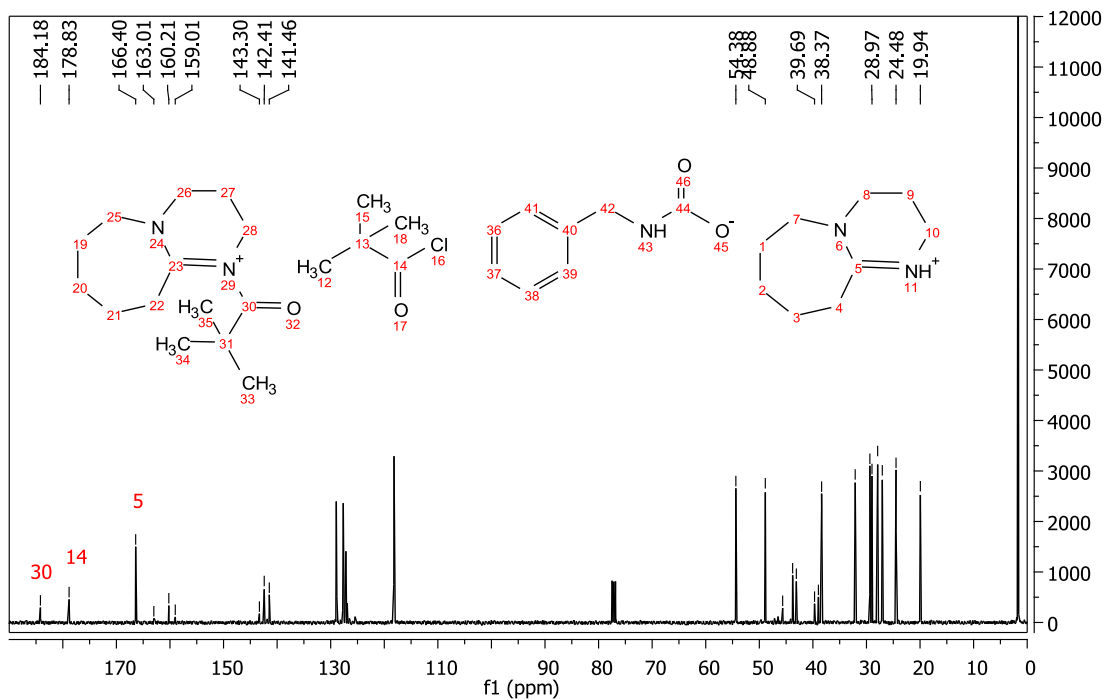
Figure 3.37. ^{13}C NMR of the reaction of CO_2-protected benzylamine using DBU and pivaloyl chloride

A standard solution of pivaloyl chloride and DBU was prepared and stirred for one hour. An NMR sample was taken and the peak at 184 ppm was again present. This result indicated that the pivaloyl chloride reacted with the DBU, forming Species A, shown in Figure 3.38.
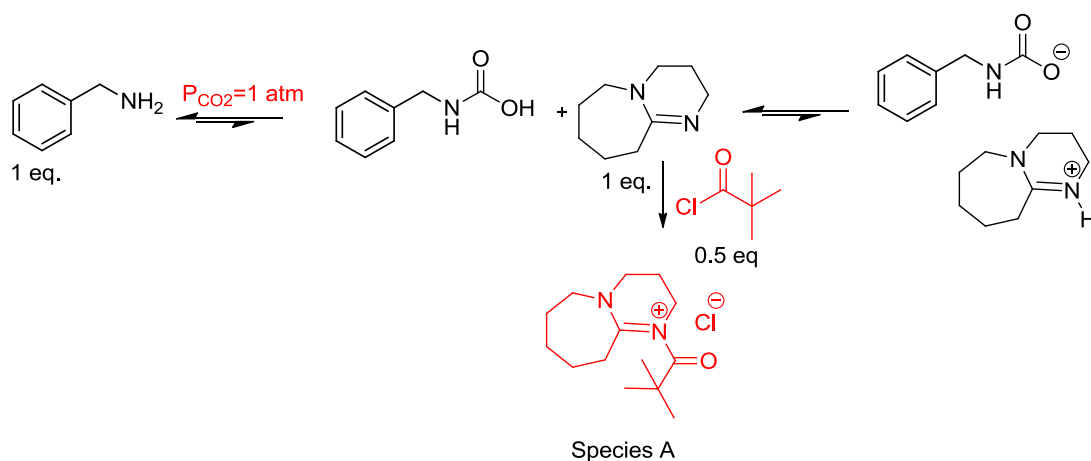
Figure 3.38. Reaction of pivaloyl chloride with DBU during acylation reaction of protected benzylamine

The results from these initial reactions were promising in terms of developing a CO_2 protection strategy using DBU as an added base. Control experiments with no CO_2 protection showed that pivaloyl chloride preferentially reacts with benzylamine, as there was no evidence of the DBU-pivaloyl chloride reacted species in the NMR. The amine protection with CO_2 was therefore a manipulation of the chemistry as the reactivity of the amine was drastically reduced. However, the reaction between DBU and pivaloyl chloride was not desired because ultimately it results in the inability of the pivaloyl chloride to acylate an additional site during a chemoselective reaction. As a result of the high reactivity of pivaloyl chloride, an alternative acylating agent was used to demonstrate amine protection using CO_2 and DBU.

3.4.4.2 Nucleophilic Acyl Substitution with Pivaloyl Benzotriazole

Previous experiments using pivaloyl benzotriazole as the acylating agent indicated that the reactivity of pivaloyl benzotriazole was lower than pivaloyl chloride. We proposed that the use of pivaloyl benzotriazole would mitigate reaction of the acyl substrate with DBU. The protected benzylamine was prepared by sparging CO_2 through a 1 M solution of benzylamine and DBU (1.2 equivalents) in acetonitrile. The reaction solution was cooled to 0°C and 1 equivalent of pivaloyl benzotriazole was added. After one hour a sample was taken for NMR analysis. The ^{13}C NMR (Figure 3.39) indicated that the pivaloyl chloride reacted with DBU in the same manner as the reaction of DBU and pivaloyl chloride. It became clear that a more mild acyl substrate was required that would not react with DBU.
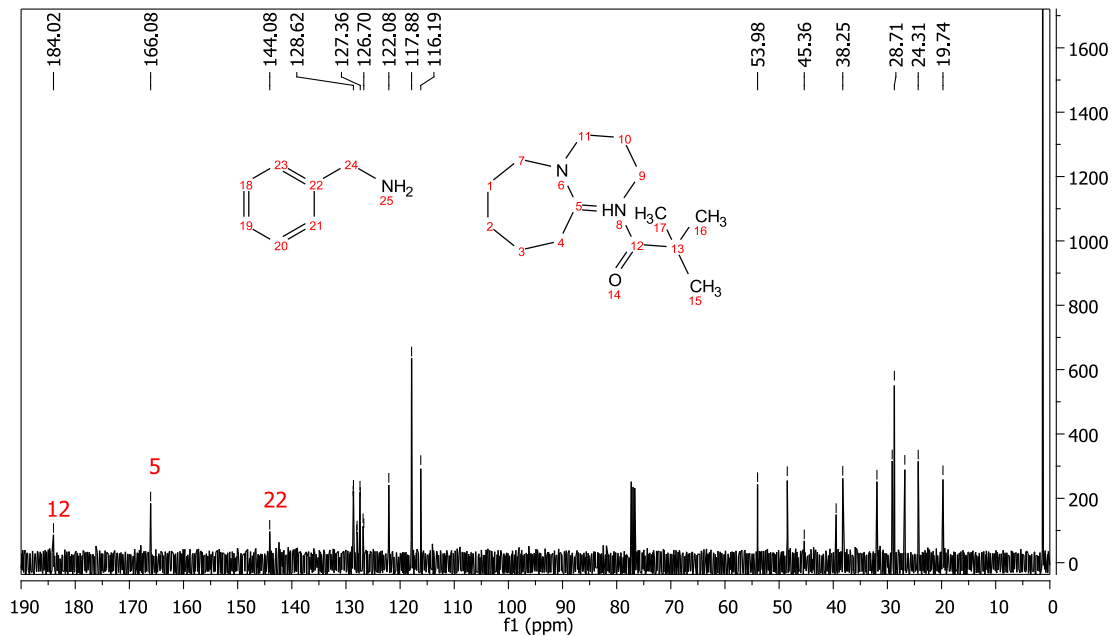
Figure 3.39. ^{13}C NMR of the reaction of CO$_2$-protected benzylamine using DBU and pivaloyl benzotriazole

3.4.4.3 Nucleophilic Acyl Substitution with Isopropenyl Acetate

Isopropenyl acetate has been reported in literature as an inexpensive, mild acylating agent.[32] The reaction of isopropenyl acetate with an amine can proceed under catalyst-free conditions, and the only byproduct formed is prop-1-en-2-ol which quickly tautomerizes to acetone. Shown in Figure 3.40 is the ^{13}C NMR of the reaction between isopropenyl acetate and benzylamine after 6 hours. A significant quantity of N-benzylacetamide was observed.
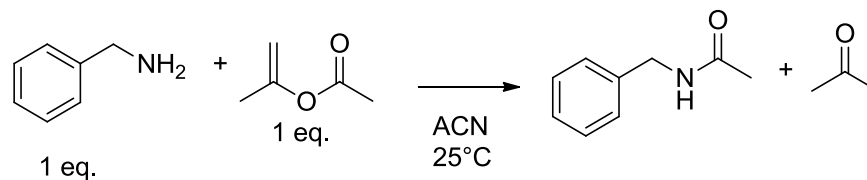
Figure 3.40. Control reaction of isopropenyl acetate with benzylamine
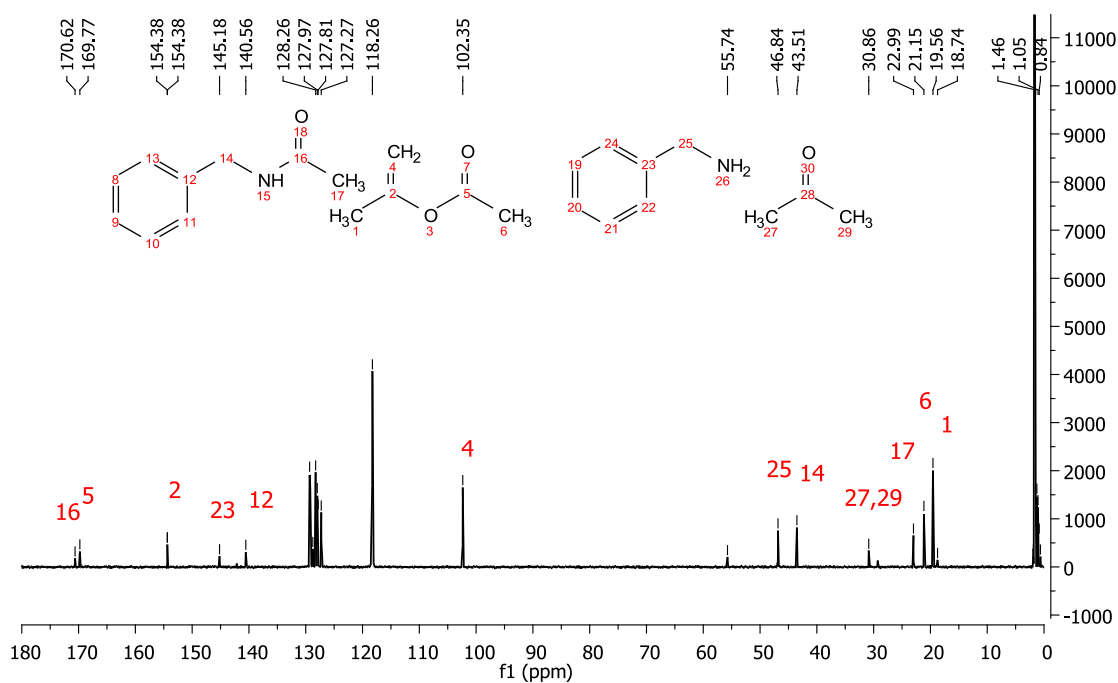
Figure 3.41. ^{13}C NMR control reaction of unprotected benzylamine with isopropenyl acetate

After confirming the reactivity of isopropenyl acetate with benzylamine, the reaction was then completed with CO_2 protection. The CO_2-protected benzylamine was prepared as previously described with 1.1 equivalents DBU. 1 equivalent of isopropenyl acetate was then added at room temperature. The reaction was stirred for 6 hours, and a sample taken for NMR analysis. The ^{13}C NMR indicated that the isopropenyl acetate did not react with the DBU. The benzylamine remained protected by CO_2, and no reaction was observed by ^{13}C NMR (Figure 3.42).
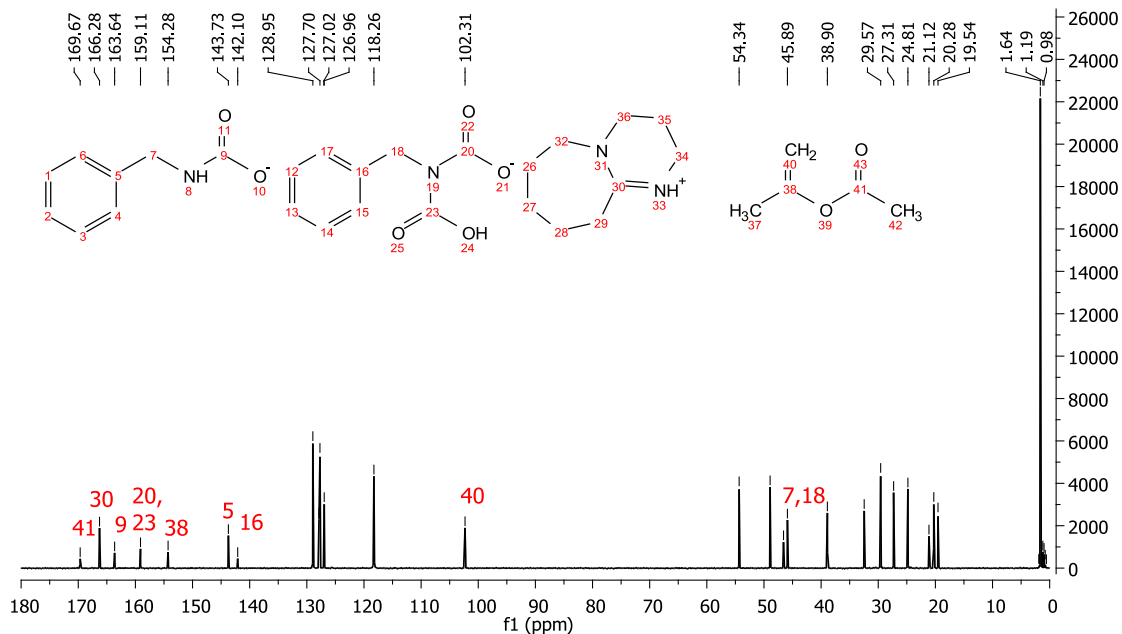
Figure 3.42. ^{13}C NMR of model reaction with CO$_2$ protection

Isopropenyl acetate was an attractive acylating agent for these reactions because it is less reactive than pivaloyl chloride. The goal however is not only to protect the amine functionality, but also to direct the reaction to an alternative site during a chemoselective reaction. To determine the reactivity of isopropenyl acetate with other functional groups, an equimolar quantity of benzyl alcohol was added to the benzylamine and DBU solution prior to protection with CO$_2$. 1 equivalent of isopropenyl acetate was added to the solution and stirred for 6 hours at room temperature; then a ^{13}C NMR sample was taken (Figure 3.43). No reaction of the CO$_2$-protected benzylamine was observed; however, only a small amount of phenyl acetate was produced from the reaction of benzyl alcohol and isopropenyl acetate. Control reactions of the benzyl alcohol with isopropenyl acetate indicated that the reactivity was much higher in the presence of DBU. An excess of DBU (above that for required for amine protection) in the CO$_2$ protected

reaction would likely result in increased protection of the hydroxyl site, so an alternative catalyst was investigated.[33]
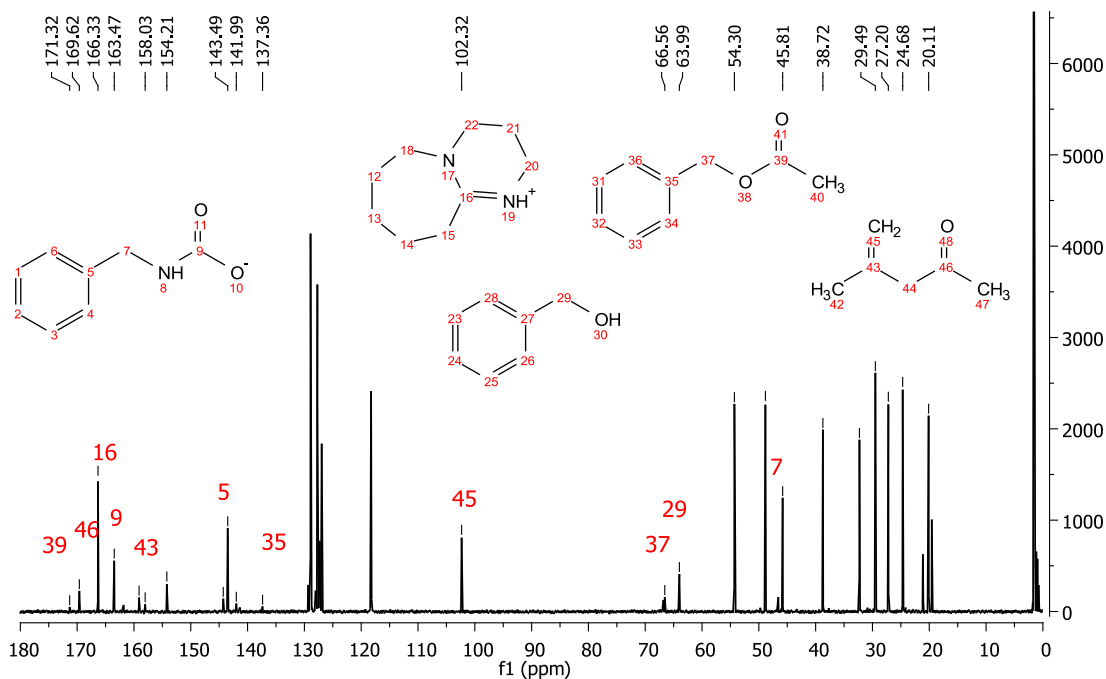
Figure 3.43. ^{13}C NMR of reaction between CO$_2$-protected benzylamine using DBU and benzyl alcohol with isopropenyl acetate

1,2,4-Triazole anion has been successfully used as an acyl transfer catalyst.[34] In the reaction of benzyl alcohol with isopropenyl acetate, 0.5 mol% triazole was shown to catalyze the reaction effectively. With the successful protection of benzylamine during an acylation reaction, the next logical step was to complete the reaction on a bifunctional molecule containing both an amine and hydroxyl functionality. The bifunctional molecule 4-(aminomethyl)-phenyl methanol was used. A control reaction was run first with the bifunctional molecule and isopropenyl acetate (1.7 equivalents). The first NMR sample was taken after 6 hours. The reaction, shown in Figure 3.44 can proceed at the

amine site, the hydroxyl site or both. By NMR analysis (Figure 3.45), 100% of the available amine reacted and 70% of the hydroxyl group reacted.
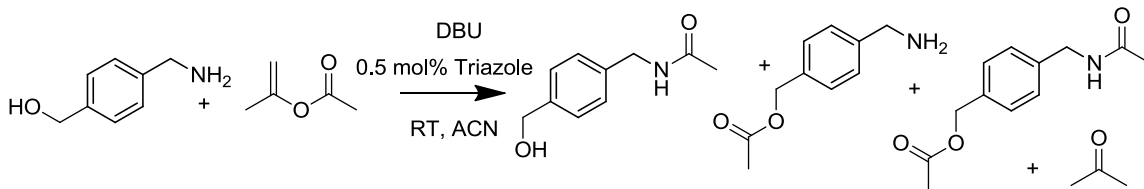
Figure 3.44. Control reaction scheme of 4-(aminomethyl)-phenyl methanol with isopropenyl acetate
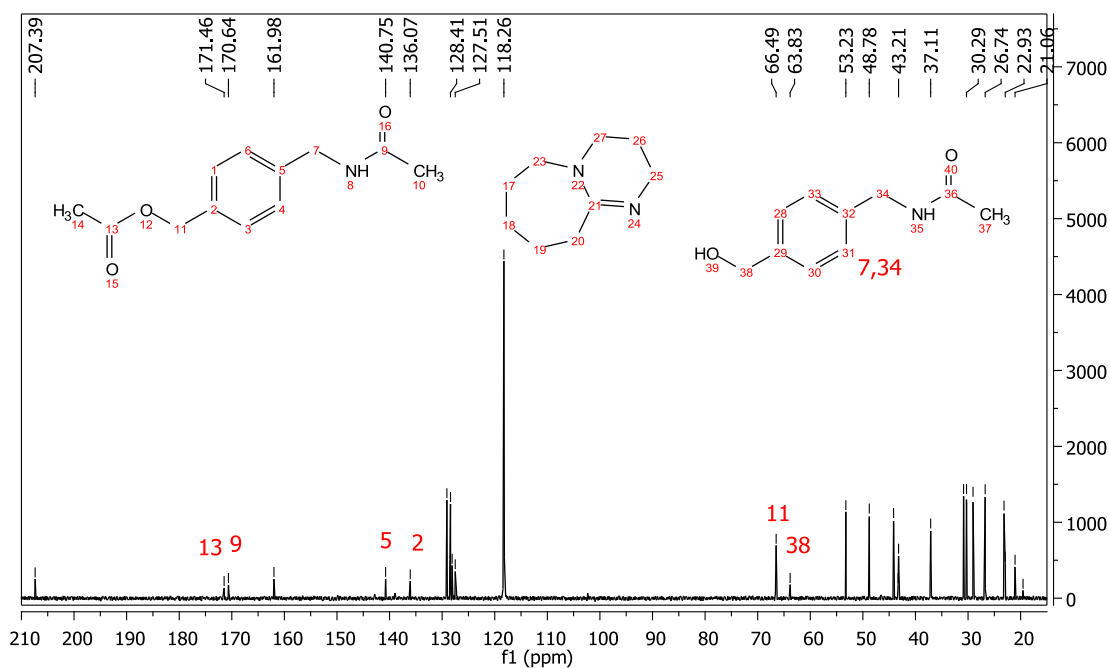
Figure 3.45. ^{13}C NMR control reaction of unprotected 4-(aminomethyl)phenyl methanol in the presence of isopropenyl acetate and DBU (no CO$_2$)

The reaction was then completed with CO$_2$ protection. The reaction scheme is shown in Figure 3.46.
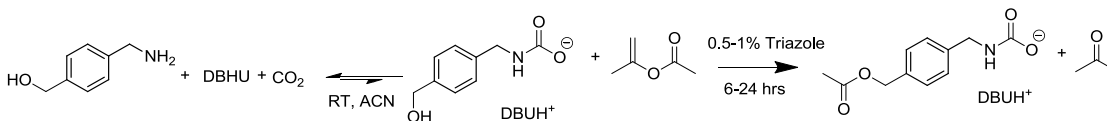
Figure 3.46. Reaction scheme of CO$_2$-protected 4-(aminomethyl)-phenyl methanol using DBU with isopropenyl acetate after 24 hours of reaction

Following the reaction of 4-(aminomethyl)-phenyl methanol with CO_2 and DBU, 1.7 equivalents of isopropenyl acetate and 0.5 mol% catalyst were added. After 6 hours of reaction, NMR analysis showed 30% of the hydroxyl group had reacted while the amine remained CO_2-protected. From these results it appears that the CO_2 protection at the amine site slows the acylation reaction at the hydroxyl group. Recent literature supports our initial findings on the ability to protect the amine in-situ with CO_2 and DBU; however the reported reaction used two compounds, benzylamine and benzyl alcohol.[35] In the literature report, benzyl alcohol was completely reacted to the benzyl acetate in 5 hours with 0.5 mol% catalyst. Clearly, the demonstration of a chemoselective reaction using a bifunctional molecule is not only novel, but more applicable to industrial applications. To promote the reaction of the hydroxyl group, 1 mol% catalyst was added and the reaction was carried out for 24 hours. At this time, NMR analysis (Figure 3.47) showed 80% of the hydroxyl group reacted while only trace amounts of the amine reacted.
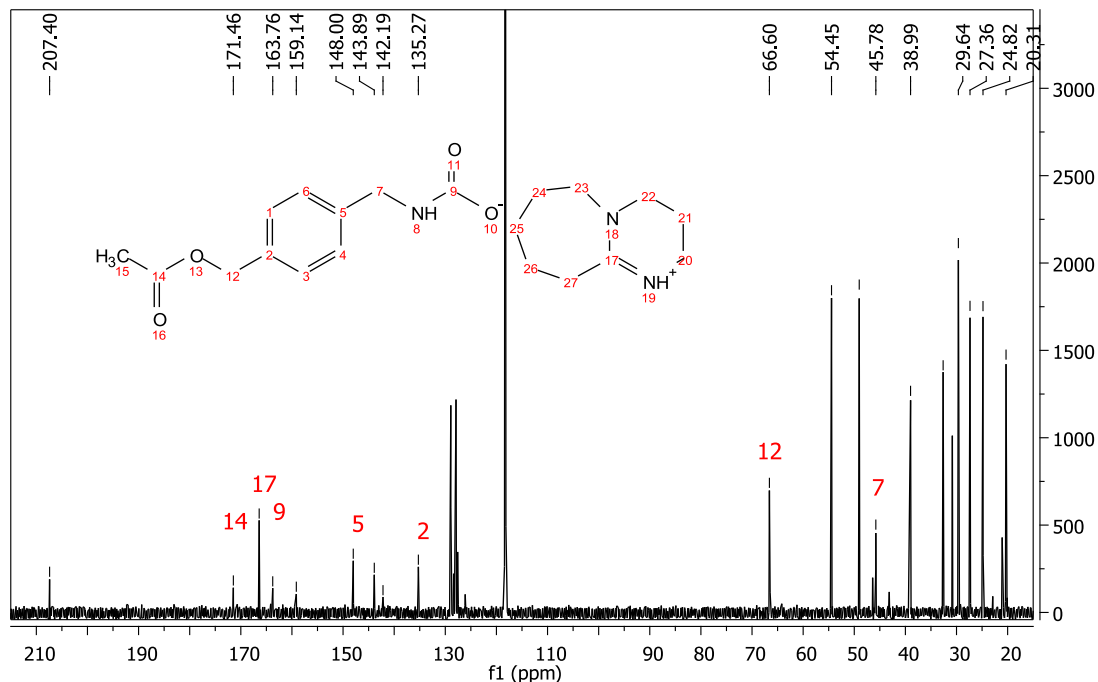
Figure 3.47. ^{13}C NMR of reaction CO$_2$-protected 4-(aminomethyl)phenyl methanol using DBU in the presence of isopropenyl acetate

3.5 Conclusions

We present the successful *in-situ* protection of an amine-containing compound. Three amine protection strategies were investigated: (1) reaction of CO$_2$ with benzylamine to form the ammonium carbamate salt, (2) reaction of benzylamine in DMSO/DMF with CO$_2$ to form the stabilized carbamic acid, and (3) reaction of benzylamine with CO$_2$ in the presence of an added base to form a carbamate – protonated base species. Of the strategies studied, the most successful and the most developed was the addition of an amidine or guanidine base to form the carbamate-protonated base ion pair.

114

The reaction of CO_2 with benzylamine in the presence of an amidine or guanidine base results in the formation of a complex carbamate-diadduct species that is stabilized via a hydrogen bonded network.

Nucleophilic acyl substitution reactions were carried out using CO_2-protected benzylamine and DBU to demonstrate the utility of the amine protection strategy. (4-(aminomethyl)phenyl)methanol was used as a model compound during a chemoselective reaction with and without CO_2 protection using isopropenyl acetate as the acylating agent. The selective reactivity of the bifunctional molecule was altered by temporarily blocking the amine site during an acylation reaction; effectively allowing the reaction to proceed at the hydroxyl group. This *in-situ* amine protection strategy using CO_2 has far reaching applications including endothermic reactions, preventing amine-metal complexation during metal catalyzed reactions and electronically affecting reactivity of aromatic substituents.

3.6 References

1. March, J., *Advanced Organic Chemistry Reactions, Mechanisms, and Structures*. 4th ed.; John Wiley & Sons Inc.: United States, 1992.

2. Carey, F. A.; Sunberg, R. J., *Advanced Organic Chemistry, Part B: Reactions and Synthesis*. 3rd ed ed.; Plenum Press: New York, NY, 1990; Carey, F. A., *Organic Chemistry*. 5th ed.; McGraw-Hill: New York, NY, 2003.

3. Wuts, P. G. M., *Greene's protective groups in organic synthesis*. 4th ed. / ed.; Wiley-Interscience: Hoboken, N.J. :, 2007.

4. Liu, N.; Liu, C.; Jin, Z. L., Poly(ethylene glycol)-functionalized imidazolium salts-palladium-catalyzed Suzuki reaction in water. *Green Chemistry* **2012,** *14* (3), 592-597.

5. Wuts, P., G. M.; Greene, T. W., *Greene's Protective Groups in Organic Synthesis*. Fourth Ed. ed.; John Wiley & Sons Inc.: Hoboken, NJ, 2007.

6. Agami, C.; Couty, F., The reactivity of the N-Boc protecting group: an underrated feature. *Tetrahedron* **2002,** *58* (14), 2701-2724.

7. Wittmann, K.; Wisniewski, W.; Mynott, R.; Leitner, W.; Kranemann, C. L.; Rische, T.; Eilbracht, P.; Kluwer, S.; Ernsting, J. M.; Elsevier, C. L., Supercritical carbon dioxide as solvent and temporary protecting group for rhodium-catalyzed hydroaminomethylation. *Chemistry-A European Journal* **2001,** *7* (21), 4584-4589.

8. Leitner, W., Supercritical carbon dioxide as a green reaction medium for catalysis. *Accounts of Chemical Research* **2002,** *35* (9), 746-756.

9. Furstner, A.; Ackermann, L.; Beck, K.; Hori, H.; Koch, D.; Langemann, K.; Liebl, M.; Six, C.; Leitner, W., Olefin metathesis in supercritical carbon dioxide. *Journal of the American Chemical Society* **2001,** *123* (37), 9000-9006.

10. Suzuki, A., Recent advances in the cross-coupling reactions of organoboron derivatives with organic electrophiles, 1995-1998. *Journal of Organometallic Chemistry* **1999,** *576* (1-2), 147-168; Miyaura, N.; Suzuki, A., Palladium-Catalyzed Cross-Coupling Reactions of Organoboron Compounds. *Chemical Reviews* **1995,** *95* (7), 2457-2483.

11. Czech, B. P.; Bartsch, R. A., Effect of Amines on O-Benzyl Group Hydrogenolysis. *Journal of Organic Chemistry* **1984,** *49* (21), 4076-4078.

12. Caron, S.; Massett, S. S.; Bogle, D. E.; Castaldi, M. J.; Braish, T. F., An Efficient and Cost-Effective Synthesis of 2-Phenyl-3-aminopyridine. *Organic Process Research & Development* **2001,** *5* (3), 254-256.

13. Karpf, M.; Trussardi, R., New, azide-free transformation of epoxides into 1,2-diamino compounds: Synthesis of the anti-influenza neuraminidase inhibitor oseltamivir phosphate (Tamiflu). *Journal of Organic Chemistry* **2001,** *66* (6), 2044-2051.

14. Dunetz, J. R.; Ciccolini, R. P.; Froling, M.; Paap, S. M.; Allen, A. J.; Holmes, A. B.; Tester, J. W.; Danheiser, R. L., Pictet-Spengler reactions in multiphasic supercritical carbon dioxide/CO2-expanded liquid media. In situ generation of carbamates as a strategy for reactions of amines in supercritical carbon dioxide. *Chemical Communications* **2005,** (35), 4465-4467; Matsuda, T.; Harada, T.; Nakamura, K., Organic synthesis using enzymes in supercritical carbon dioxide. *Green Chemistry* **2004,** *6* (9), 440-444; Campestrini, S.; Tonellato, U., Selective catalytic oxidations in supercritical carbon dioxide. *Current Organic Chemistry* **2005,** *9* (1), 31-47; Jessop, P. G.; Hsiao, Y.; Ikariya, T.; Noyori, R., Homogeneous catalysis in supercritical fluids: Hydrogenation of supercritical carbon dioxide to formic acid, alkyl formates, and formamides. *Journal of the American Chemical Society* **1996,** *118* (2), 344-355.

15. Kainz, S.; Brinkmann, A.; Leitner, W.; Pfaltz, A., Iridium-catalyzed enantioselective hydrogenation of imines in supercritical carbon dioxide. *Journal of the American Chemical Society* **1999,** *121* (27), 6421-6429.

16. Furstner, A., Olefin metathesis and beyond. *Angewandte Chemie-International Edition* **2000,** *39* (17), 3012-3043; Trnka, T. M.; Grubbs, R. H., The development of L2X2Ru = CHR olefin metathesis catalysts: An organometallic success story. *Accounts of Chemical Research* **2001,** *34* (1), 18-29.

17. Kuchurov, I. V.; Vasil'ev, A. A.; Zlotin, S. G., The Suzuki-Miyaura cross-coupling of bromo- and chloroarenes with arylboronic acids in supercritical carbon dioxide. *Mendeleev Communications* **2010,** *20* (3), 140-142; Carroll, M. A.; Holmes, A. B., Palladium-catalysed carbon-carbon bond formation in supercritical carbon dioxide. *Chemical Communications* **1998,** (13), 1395-1396; Shezad, N.; Oakes, R. S.; Clifford, A. A.; Rayner, C. M., Use of fluorinated palladium sources for efficient Pd-catalysed coupling reactions in supercritical carbon dioxide. *Tetrahedron Letters* **1999,** *40* (11), 2221-2224; Shezad, N.; Clifford, A. A.; Rayner, C. T., Pd-catalysed coupling reactions in supercritical carbon dioxide and under solventless conditions. *Green Chemistry* **2002,** *4* (1), 64-67; Gordon, R. S.; Holmes, A. B., Palladium-mediated cross-coupling reactions with supported reagents in supercritical carbon dioxide. *Chemical Communications* **2002,** (6), 640-641; Prajapati, D.; Gohain, M., Recent advances in the application of supercritical fluids for carbon-carbon bond formation in organic synthesis. *Tetrahedron* **2004,** *60* (4), 815-833.

18. Rayner, C. M., The potential of carbon dioxide in synthetic organic chemistry. *Organic Process Research & Development* **2007,** *11* (1), 121-132.

19. Katritzky, A. R.; Akutagawa, K., Carbon-Dioxide-A reagent for the Protection of Nucleophilic Centers and the Simultaneous Activation of Alternative Locations to Electrophilic Attack. *Tetrahedron Letters* **1985,** *26* (48), 5935-5938.

20. Williams, J. M.; Brands, K. M. J.; Skerlj, R. T.; Jobson, R. B.; Marchesini, G.; Conrad, K. M.; Pipik, B.; Savary, K. A.; Tsay, F. R.; Houghton, P. G.; Sidler, D. R.; Dolling, U. H.; DiMichele, L. M.; Novak, T. J., Practical synthesis of the new carbapenem antibiotic ertapenem sodium. *Journal of Organic Chemistry* **2005,** *70* (19), 7479-7487.

21. Wilkerson, C. Benzotriazole-Mediated Synthesis of N-Acylbenzotriazoles and 2H-Azirines. University of Florida, Online, 2003.

22. Katritzky, A. R., Rachwal, Stanislaw, Hitchings, Gregory J., Benzotriazole: A novel synthetic auxiliary. *Tetrahedron* **1991,** *47* (16-17), 2683–2732.

23. Pignataro, L.; Boghi, M.; Civera, M.; Carboni, S.; Piarulli, U.; Gennari, C., Rhodium-Catalyzed Asymmetric Hydrogenation of Olefins with PhthalaPhos, a New Class of Chiral Supramolecular Ligands. *Chemistry-a European Journal* **2012,** *18* (5), 1383-1400.

24. Fischer, H.; Gyllenhaal, O.; Vessman, J.; Albert, K., Reaction monitoring of aliphatic amines in supercritical carbon dioxide by proton nuclear magnetic resonance spectroscopy and implications for supercritical fluid chromatography. *Analytical Chemistry* **2003,** *75* (3), 622-626.

25. Frankel, M.; Katchalski, E., Derivatives of N-carboxy-alpha-amino acid esters. *Journal of the American Chemical Society* **1943,** *65*, 1670-1674; Wright, H. B.; Moore, M. B., Reactions of Aralkyl Amines with Carbon Dioxide. *Journal of the American Chemical Society* **1948,** *70* (11), 3865-3866; George, M.; Weiss, R. G., Chemically reversible organogels: Aliphatic amines as "latent" gelators with carbon dioxide. *Journal of the American Chemical Society* **2001,** *123* (42), 10393-10394.

26. Masuda, K.; Ito, Y.; Horiguchi, M.; Fujita, H., Studies on the solvent dependence of the carbamic acid formation from omega-(1-naphthyl)alkylamines and carbon dioxide. *Tetrahedron* **2005,** *61* (1), 213-229.

27. Dijkstra, Z. J.; Doornbos, A. R.; Weyten, H.; Ernsting, J. M.; Elsevier, C. J.; Keurentjes, J. T. F., Formation of carbamic acid in organic solvents and in supercritical carbon dioxide. *Journal of Supercritical Fluids* **2007,** *41* (1), 109-114.

28. Dubey, A.; Kandula, S. R. V.; Kumar, P., Dimethyl sulfoxide pivaloyl chloride: A new reagent for oxidation of alcohols to carbonyls. *Synthetic Communications* **2008,** *38* (5), 746-753.

29. McGhee, W.; Riley, D.; Christ, K.; Pan, Y.; Parnas, B., Carbon-Dioxide as a Phosgene Replacement-Synthesis and Mechanistic Studies of Urethanes from Amines, CO2, and Alkyl Chlorides. *Journal of Organic Chemistry* **1995,** *60* (9), 2820-2830.

30. Jessop, P. G.; Heldebrant, D. J.; Li, X.; Eckert, C. A.; Liotta, C. L., Reversible nonpolar-to-polar solvent. *Nature* **2005,** *436*, 1102; Yamada, T.; Lukac, P. J.; Yu, T.; Weiss, R. G., Reversible, room-temperature, chiral ionic liquids. amidinium carbamates derived from amidines and amino-acid esters with carbon dioxide. *Chemistry of Materials* **2007,** *19* (19), 4761-4768; Yu, T.; Yamada, T.; Gaviola, G. C.; Weiss, R. G., Carbon dioxide and molecular nitrogen as switches between ionic and uncharged room-temperature liquids comprised of amidines and chiral amino alcohols. *Chemistry of Materials* **2008,** *20* (16), 5337-5344; Carrera, G.; da Ponte, M. N.; Branco, L. C., Synthesis and properties of reversible ionic liquids using CO2, mono- to multiple functionalization. *Tetrahedron* **2012,** *68* (36), 7408-7413.

31. Heldebrant, D. J.; Jessop, P. G.; Thomas, C. A.; Eckert, C. A.; Liotta, C. L., The reaction of 1,8-diazabicyclo[5.4.0]undec-7-ene (DBU) with carbon dioxide. *Journal of Organic Chemistry* **2005,** *70* (13), 5335-5338.

32. Pelagalli, R.; Chiarotto, I.; Feroci, M.; Vecchio, S., Isopropenyl acetate, a remarkable, cheap and acylating agent of amines under solvent- and catalyst-free conditions: a systematic investigation. *Green Chemistry* **2012,** *14* (8), 2251-2255.

33. Heldebrant, D. J.; Yonker, C. R.; Jessop, P. G.; Phan, L., Organic liquid CO2 capture agents with high gravimetric CO2 capacity. *Energy & Environmental Science* **2008,** *1* (4), 487-493; Heldebrant, D. J.; Koech, P. K.; Rainbolt, J. E.; Zheng, F.; Smurthwaite, T.; Freeman, C. J.; Oss, M.; Leito, I., Performance of single-component CO2-binding organic liquids (CO(2)BOLs) for post combustion CO2 capture. *Chemical Engineering Journal* **2011,** *171* (3), 794-800.

34. Yang, X.; Birman, V. B., Acyl Transfer Catalysis with 1,2,4-Triazole Anion. *Organic Letters* **2009,** *11* (7), 1499-1502.

35. Peeters, A.; Ameloot, R.; De Vos, D. E., Carbon dioxide as a reversible amine-protecting agent in selective Michael additions and acylations. *Green Chemistry* **2013,** *15* (6), 1550-1557.

CHAPTER 4 - REVERSIBLE IONIC LIQUIDS AS SWITCHABLE SURFACTANTS FOR GOLD NANOPARTICLE SYNTHESIS

4.1 Introduction

Nanoparticles have potential as advanced materials for a number of applications as a result of their magnetic, optic, thermal and catalytic properties.[1] Due to increasing nanoparticle use, significant attention has been focused on the synthesis and subsequent characterization of nanoparticles. The size, shape and degree of monodispersity strongly influence nanoparticle properties, and thus control of these factors during synthesis is of utmost importance.

Specifically, gold nanoparticles (AuNPs) are receiving considerable attention due to their biological compatibility, high surface-to-volume ratio and catalytic potential.[2] Gold nanoparticles are the most stable metal nanoparticles and unlike bulk gold, supported gold nanoparticles with a diameter of less than 10 nm may be used as oxidation catalysts.[3]

To achieve directed nanoparticle growth and prevent agglomeration, stabilizing agents are used to passivate the nanoparticle surface.[4] Typical gold nanoparticle syntheses in solution involve the dissolution of a gold precursor; the addition of stabilizing agents (alkanethiol, alkylcarboxylates or polysugars) and the addition of a reducing agent. In synthetic methodologies involving multiphasic systems (i.e., Brust-Schiffrin method) chloroauric acid is dissolved in water.[5] A phase transfer catalyst such as tetraoctylammonium bromide (TOAB) is dissolved in toluene, and shuttles the gold precursor to the organic phase through vigorous mixing. An aqueous solution of sodium

borohydride, which acts as the reducing agent for the chloroauric acid is added slowly and shaken vigorously. Finally the organic layer is separated and washed with a large amount of ethanol.[6] Although TOAB acts as a stabilizing agent in addition to being a phase transfer catalyst, the bond between the nanoparticles and TOAB is not strong, and the nanoparticles will agglomerate. To prevent this agglomeration, a stronger capping agent, such as dodecanethiol may be added prior to the reduction of the gold salt. Dodecanethiol, whose high affinity for the nanoparticles prevents agglomeration, forms a near-permanent bond between the thiol and the gold.[7] Hostetler et al. determined that the dodecanethiolate monolayer coverage can range from 24-64% on nanoparticles with diameters between 1-2.4 nanometers.[8] As a result, the stabilizing ligands compete with reactants and products for adsorption sites during catalytic reactions.[9] The most potent stabilizers such as thiols can negatively affect the activity of gold nanoparticles even when present in small quantities.[10] The removal of a capping agents or the post-functionalization of capped gold-nanoparticles results in significant waste from the use of solvent washes. Research focused on the sustainability aspects of the synthetic process is limited.[11, 12]

Strategies for the sustainable synthesis of metallic nanoparticles that achieve performance criteria are required.[13] An alternative approach to the use of capping agents during gold nanoparticle synthesis is the use of reverse micelles. Reverse (inverted) micelles are aggregates of surfactant molecules around a polar core in a nonpolar continuous phase. As shown in Figure 4.1, the nonpolar groups of the surfactant molecule extend into the continuous, nonpolar phase, while the polar groups of the surfactant molecule point inward.
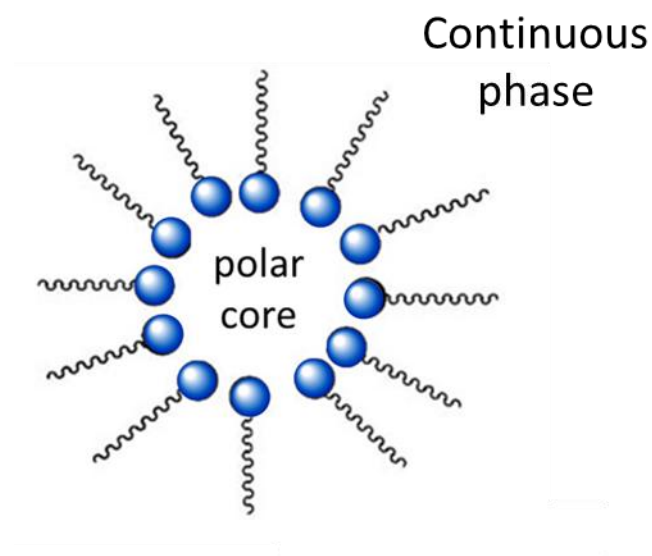
Figure 4.1. Schematic of a reverse (inverse) micelle with nonpolar groups extending into the nonpolar continuous phase

A commonly studied surfactant for reverse micelle formation is dioctyl sulfosuccinate sodium salt.[14] The structure of dioctyl sulfosuccinate sodium salt is shown below in Figure 4.2. The reverse micelle system is dynamic; the micelles collide via Brownian motion, percolate and break apart.[15] The stabilization provided by the surfactant prevents aggregation.[16, 17] Numerous studies have demonstrated the relationship between the radius of the reverse micelle and the surfactant to water ratio, pH and ionic interactions; however, there is conflicting evidence on the effect of reverse micelle size and resulting nanoparticle diameter.[14, 18]
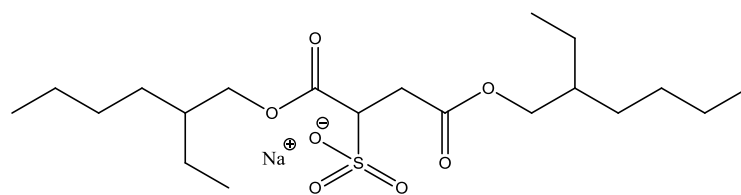
Figure 4.2. Structure of dioctyl sulfosuccinate sodium salt, a commonly used surfactant for reverse micelle synthesis

The opportunity to adjust the physico-chemical properties of tunable solvents such as gas expanded liquids (GXLs) provides a template for synthetic strategies that produce monodisperse nanoparticles with the potential for solvent recyclability.[19, 20] The template-directed synthesis of gold nanoparticles in supercritical carbon dioxide (scCO$_2$) has been reported.[21] A fluorinated surfactant, *N*-ethyl perfluorooctylsulfonamide, was used to stabilize reverse micelles with a guanidinium-based ionic liquid core in a continuous phase of supercritical CO$_2$. It was proposed that the micellar structure was stabilized via hydrogen bonding of the protonated guanidinium cation and the polar head of the surfactant.[21] Spherical gold nanoparticles were synthesized, albeit with a broad size distribution. Reversible ionic liquids, due to their low melting temperature and built-in "ionic switch" have successfully served as switchable surfactants for gold nanoparticle synthesis.

4.2 Experimental

4.2.1 <u>Materials</u>

All chemicals were purchased from Sigma-Aldrich and used as received unless otherwise noted. Chemicals used were: chloroauric acid trihydrate (HAuCl$_4$·3H$_2$O; 99.9+% metals basis); *n*-hexane (anhydrous, ≥99%); tetrahydrofuran (THF; anhydrous, inhibitor-free); acetonitrile (ACN; anhydrous); ethanol (≥99.5%, absolute) and methyl

orange (MO; ACS reagent, dye content 96%). Hydrazine (N_2H_4; anhydrous, 98%) was used as received and stored under inert atmosphere at 5°C. Spherical mesoporous silica (pore size 150 Å; diameter 75-200 μm) was obtained from Sorbant Technologies. Silylamines were synthesized as described in Appendix A and stored under dry nitrogen. TEM grids were purchased from Ted Pella. Carbon dioxide used was SFE grade from Airgas (99.999%).

4.2.2 Experimental Procedures

4.2.2.1 Reversible Ionic Liquid Formation

Reversible ionic liquids are formed from the silylamines by adding to a nitrogen purged vial 3-(aminopropyl)tripropylsilane (TPSA) or 3-(aminopropyl)trihexylsilane (THSA). TPSA R = propyl or THSA R = hexyl. The sample was sparged with CO_2 via a stainless steel needle (rotometer flowrate: 200 mL·min^{-1}) at 25°C and 1 bar for 75 minutes. Complete conversion of the neutral silylamine to the RevIL was verified by a gravimetric analysis.

4.2.2.2 Methyl Orange Studies

Methyl orange (5.24 mg) was added to TPSA RevIL (1.2413 g) and stirred in *n*-hexane (0.275 M solution) for one hour in a round bottom flask fitted with a condenser. A 1 mL sample was removed for UV-vis analysis. The solution was heated to 65°C for 30 minutes to trigger the reversal of the reversible ionic species. A 1 mL sample was removed for UV-vis analysis. The sample was then sparged with CO_2 for 75 minutes to reform the reversible ionic species, and again a 1 mL sample was taken for UV-vis analysis.

4.2.2.3 Surface Tension Measurements

Surface tension measurements were carried out using precision bore glass capillaries with an inner diameter of 0.254 mm purchased from Wilmad Labglass. Prior to each experiment, the capillaries were soaked in a 2 M HNO_3 solution overnight; rinsed with DI H_2O (18 MΩ·cm), acetone, and hexane; and stored in a drying oven at 120°C. The RevIL was formed as described above; complete conversion of the silylamine to the RevIL was confirmed with gravimetry. The RevIL was weighed directly into 25 mL volumetric flasks and then diluted to volume with hexane. The solutions were mixed thoroughly, and densities of the solutions were measured in triplicate at ambient temperature using a vibrating tube densitometer. The capillary tube was supported in a 4 dram glass vial with glass beads (diameter = 0.5 mm) added to a depth of approximately 5 mm. Approximately 1 mL of solution was added to the vial. To prevent solvent loss, the vial was closed using a lid with a small hole in the center. The height of the capillary rise was measured using a cathetometer after letting the liquid level equilibrate. Measurements were carried out in triplicate. A new sample of solution was added to the vial for each measurement.

4.2.2.4 Gold Nanoparticle Synthesis

$HAuCl_4$ (0.0034 g; 8.633 x 10^{-6} mol) was dissolved in the RevIL (0.5519 g TPSA; 1.162 mmol); 0.227 g of this homogeneous mixture was mixed with 2 mL of hexane (15.20 mmol) in a round bottom flask (the solution remained one phase). 0.1 mL of a 3.18 x 10^{-2} M solution of hydrazine in anhydrous inhibitor-free THF was added to the system (fast addition of the reducing agent) and stirred. The reaction was continued until there was no observable change in the λ_{max} as measured by UV-vis spectroscopy. The

λ_{max} is dependent on nanoparticle size and shape, and for these studies varied between 500 and 600nm. The resulting solution was diluted in absolute ethanol and deposited on transmission electron microscopy (TEM) grids by dropcasting. Sufficient time was allowed for the ethanol to evaporate prior to sample analysis using TEM.

4.2.2.5 Deposition of Gold Nanoparticles onto a Solid Support

A solid support (mesoporous silica) was added after the reduction of the gold salt and the heterogeneous mixture was stirred. The temperature at which neat TPSA and THSA RevIL release CO_2 and revert to the neutral silylamine has been reported to be $64\pm2°C$ and 51 ± 1 respectively.[20] The solution was heated to $65°C$ for one hour to reverse the reversible ionic species (i.e., release CO_2 and revert to the neutral silylamine) and to deposit the nanoparticles onto the solid support.

4.2.2.6 Instrumentation

UV-vis spectra were collected under ambient conditions using an Agilent Cary 100 UV-visible spectrophotometer. Transmission electron microscope (TEM) images were obtained using a Hitachi HF-2000 Field Emission Gun Transmission Electron Microscope, operated at 200kV. TEM images were analyzed using the ImageJ software package. At least 500 nanoparticles were sized to develop statistically relevant average sizes and distributions. Dynamic light scattering (DLS) measurements were performed using a Malvern Instruments Zetasizer Nano ZS in the laboratory of Dr. Sven Behrens. For DLS measurements, samples were added to a glass cuvette via a luer-lock syringe fitted with a 0.1 μm PTFE Millipore filter. The density measurements required for DLS measurements were completed in triplicate with an Anton Paar DMA 38 Laboratory

Density Meter. The water content of AOT and solvents was determined using a Metrohm 852 Titrando Karl Fischer titration system.

4.3 Results and Discussion

The focus of this research is to (1) streamline the synthetic process for the formation of nanoparticles, (2) minimize the need for stabilizing agents and (3) achieve desired physical characteristics -- size, shape and monodispersity -- of the resulting nanoparticles. In this regard we also sought to understand the mechanism of reversible ionic liquid-directed nanoparticle synthesis.

4.3.1 Structure of Reverse Micelles

Solutions of underivatized gold nanoparticles have been synthesized using a modified two-phase Brust method without the use of a strong capping agent.[21, 22] The phase-transfer reagents (a series of tetraalkylammonium bromides) are believed to provide stabilization through electrostatic and dispersion forces. Likewise, we speculate that the reversible ionic species interact with the gold salt, perhaps via ion exchange, stabilizing a reverse micelle structure as shown in Figure 4.3.[13, 23]
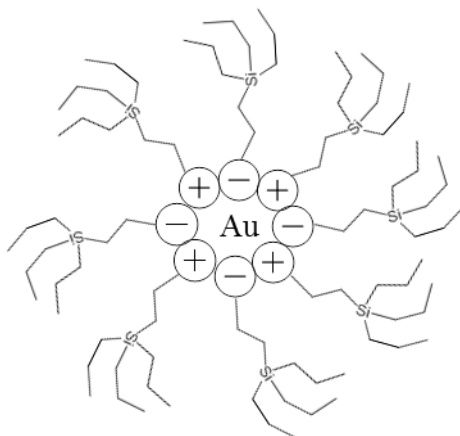
Figure 4.3. Reverse micelle formed through the use of reversible ionic liquids in a hydrocarbon continuous phase and metal core

The critical micelle concentration (CMC) is defined as the minimum amount of surfactant required to form the reverse micelle, above which monomers and micelles exist in equilibrium.[24, 25] A representation of the critical micelle concentration is shown in Figure 4.4.
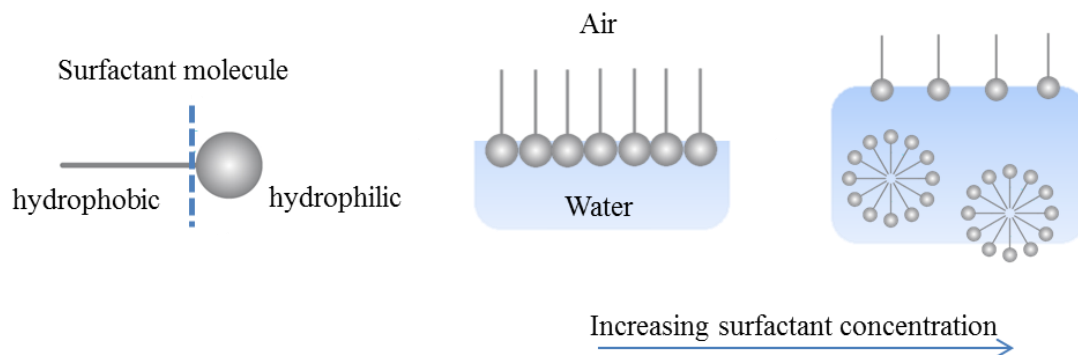
Figure 4.4. Critical micelle concentration in an aqueous solution

The surfactant molecules align at the air-water interface, with the hydrophilic heads orienting into the aqueous phase. At the critical micelle concentration, the interface is saturated with surfactant molecules and additional surfactant molecules result in the formation of micelles. When the critical micelle concentration is reached, some physical

properties including conductivity, surface tension and solution phase behavior change significantly.[24, 26] Surface tension is easily measured, and is one of the most common properties used to measure critical micelle concentrations for aqueous systems.[25] Unlike aqueous micelles, the primary forces that act as a driving force for reverse micelle formation are weak van der Waals forces.[27]

4.3.1.1 Surface Tension Measurements

The height to which a liquid will rise in a capillary is dependent on the surface tension of the liquid. Capillary rise results when the adhesive forces between glass (capillary wall) and the liquid, for example, exceed the cohesive forces internal to the liquid. The liquid is pulled up the capillary until the gravitational forces acting on the mass of liquid become greater than the adhesive forces. If the diameter of the capillary is less than 1 mm, the meniscus may be assumed hemispherical and surface tension calculated as follows:

$$\gamma = \frac{\rho g h r}{2}$$

Equation 4.1

In Equation 4.1, γ is surface tension, ρ is the density of the solution, h is the height of the liquid in the capillary (measured from the surface of the bulk solution), and r is the inner radius of the capillary.[28] To verify the experimental procedure, the surface tension of n-hexane was measured and compared to literature reports. The experimentally determined surface tension of n-hexane at 20°C was 17.7326±0.1229 mN·m^{-1}, which is in good agreement with the value of 17.90 mN·m^{-1} reported in literature.[29] RevIL concentration in hexane was varied from 0.1 to 0.0001 M. The density of each solution was measured at ambient temperature to determine surface tension at various RevIL concentrations.

Shown in Figure 4.5 is the typical surface tension response as a function of surfactant concentration in an aqueous solution.[30] There is no significant change in surface tension until the critical micelle concentration is reached. Following a drop in surface tension, additional surfactant molecules will result in the formation of aggregates.
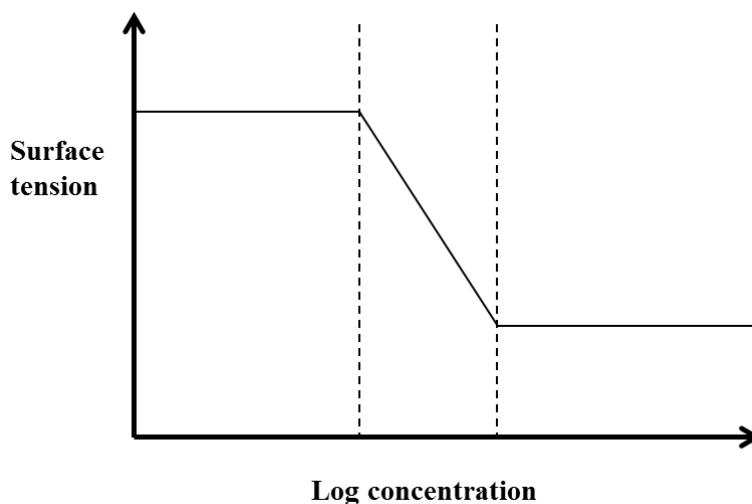
Figure 4.5. Surface tension as a function of surfactant concentration in an aqueous solution

As opposed to micelles in an aqueous solvent, the adsorption at the solution-air interface would be such that the polar head group would point outward, resulting in an increase in surface tension with increasing surfactant concentration.[31] Our system is expected to form reverse micelles in hexane, and thus one would expect an increase in surface tension with the further addition of RevIL. Presented in Figure 4.6 are the surface tension measurements as a function of TPSA RevIL concentration in hexane.
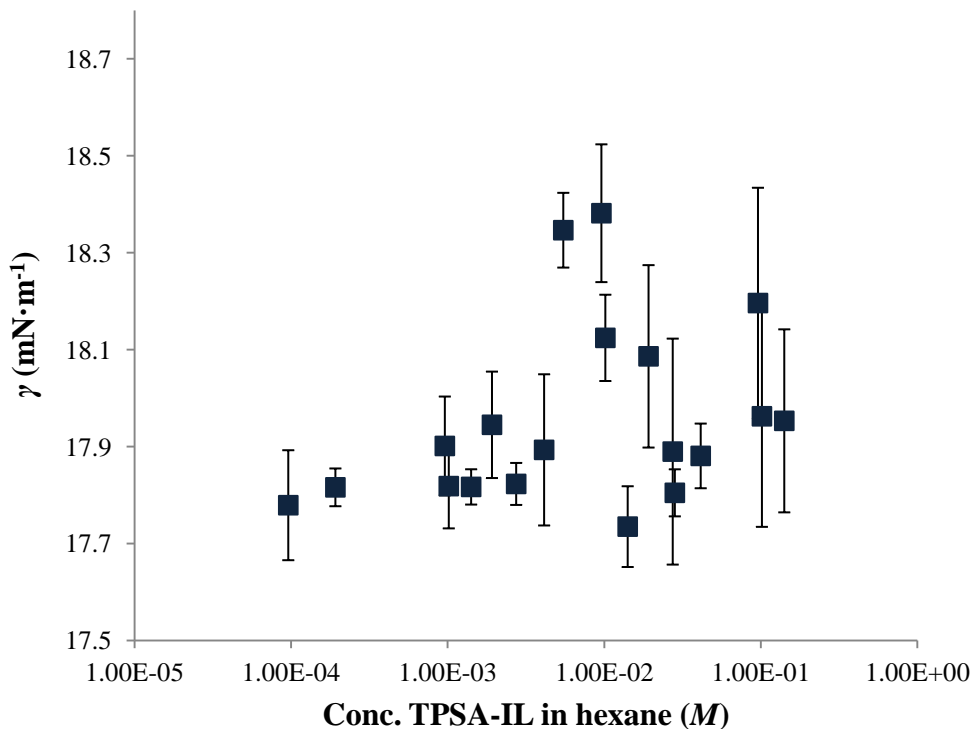
Figure 4.6. Surface tension measurements as a function of TPSA RevIL concentration in hexane measured via capillary rise

There is clearly no discernible trend in the data; and there are significant uncertainties in the surface tension measurements. The existence of a critical micelle concentration for a reverse micelle system is debated in literature.[25] It is believed that the aggregation process in an organic solvent is a continuous process as opposed to a sudden onset phenomenon.[32] As a result, one of the most common surfactant study methods, surface tension, may be largely ineffective. Despite the difficulty in measuring a critical micelle concentration, reported data indicates that many of the species that form reverse micelles in non-polar solvents have large, bulky hydrocarbon tails with a cross sectional area that exceeds that of the polar head group much like the RevILs presented here.[31]

4.3.1.2 Dynamic Light Scattering Studies

Reverse micelles in apolar solvents have also been studied using Dynamic Light Scattering.[33, 34] Many of the reverse micelles that have been reported in literature contain an aqueous core. The use of a polar disperse phase has been shown to facilitate control over the reverse micelle size, and in some reports researchers assert that a disperse phase is required for aggregation to occur.[32] The reactivity of our RevIL system with water to form bicarbonates precludes the use of water as the disperse phase in these studies. Acetonitrile was chosen instead to serve as the micelle core because it is largely insoluble with hexane and the successful use of acetonitrile as a non-aqueous polar solvent in a reverse micelle core has been reported.[35] To first study a conventional, highly studied system, AOT was used as the surfactant, isooctane as the continuous phase and water was used as the dispersed phase. Shown below in Table 4.1 are the experimentally determined values for the hydrodynamic radius of the reverse micelles measured using the Malvern Instruments Zetasizer Nano ZS. Also shown are literature values reported by Zulauf *et al.*[26] Viscosity and density measurements that were input into the Zetasizer software were taken from literature.[36]

Table 4.1. Experimental and literature values for the hydrodynamic radius (r_h) for AOT-water-isooctane system

mol AOT	Mol H_2O	$w_0 =$ [water]/[AOT]	Experimental r_h (nm)	Literature r_h (nm)
	0.124×10^{-3}	0.49	--	1.5
	4.901×10^{-3}	20.02	5.6	4.8
2.510×10^{-4}	9.997×10^{-3}	40.32	10.0	10.3
	12.167×10^{-3}	48.96	11.4	12.0

The water content is significant in dictating the hydrodynamic diameter of the reverse micelles, and thus the weight fraction of water in the AOT was determined using Karl-Fischer.[34, 37] The weight fraction of water in AOT was measured as 2 wt% and was accounted for in the values reported in Table 4.1. The experimentally determined values of r_h are in close agreement with literature values when the weight ratio of water/AOT was above 20.02. When no additional water was added to the system (i.e., the only water present was due to the 2% water in AOT), there was no detectable aggregation. It is believed that very small, spherical micelles are most favored in non-aqueous systems, and thus would not be detected using Dynamic Light Scattering.[31]

In an effort to deviate from the literature proceedings in a systematic way, the AOT was first replaced with the RevIL, again using isooctane as the continuous phase in our initial studies. The solubility of the RevIL in isooctane was high and thus would be a suitable solvent for our r_h measurements. Two solutions of TPSA RevIL and isooctane were prepared. The molecular weight of TPSA RevIL is close to that of AOT, however TPSA is bulkier molecule and therefore the solutions were visually inspected to ensure homogeneity. Unlike microemulsions, that appear clear; a solution that cannot support a microemulsion will appear cloudy.[38] The results of the preliminary DLS studies are shown in Table 4.2.

Table 4.2. Solubility of ACN in isooctane in the presence of TPSA RevIL

mol TPSA RevIL	Mol ACN	Mole fraction ACN in isooctane	$w_0 =$ [ACN]/[TPSA RevIL]	Homogeneous
6.340×10^{-4}	2.982×10^{-3}	0.020	4.70	Yes
	6.040×10^{-3}	0.040	9.53	Yes
	12.205×10^{-3}	0.080	19.25	No
	24.472×10^{-3}	0.162	38.60	No
5.152×10^{-4}	2.396×10^{-3}	0.040	4.65	Yes
	4.881×10^{-3}	0.081	9.48	No
	9.665×10^{-3}	0.159	18.78	No
	19.588×10^{-3}	0.323	38.02	No

The results of the Dynamic Light scattering experiments appeared to be consistent with the RevILs behaving as surfactants to support a microemulsion at w_o=4.7 and 9.53. However, further investigation revealed that the mole fraction of acetonitrile soluble in isooctane is 0.08.[35] Therefore, the homogeneity resulted from the solubility of acetonitrile in isooctane for mole fractions less than 0.08 rather than a solubilization effect via the addition of TPSA RevIL. The results of the dynamic light scattering studies indicate that there may be insufficient interaction between acetonitrile and the polar head of the RevIL. Dynamic light scattering studies did not provide significant information on the formation of reverse micelles with our system; however, a third approach using dye solubilization was investigated.

4.3.1.3 Dye Solubilization

An additional approach to study the presence of reverse micelles is dye solubilization. The use of malachite green, methylene blue and methyl orange has been described extensively in literature as probes into reverse micelle formation.[19, 27, 34, 39] In order to gain an understanding of the important parameters in the use of RevILs for nanoparticle synthesis, our initial investigations were carried out using the UV-active sodium salt methyl orange (MO); the structure shown in Figure 4.7.
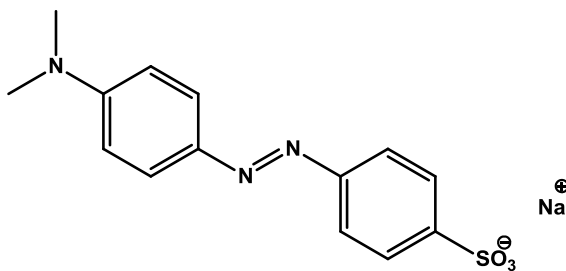
Figure 4.7. Structure of methyl orange

Methyl orange has a negligible solubility in a hydrocarbon such as hexane. In the presence of a micellar system, it becomes soluble in the hydrocarbon solvent. This is easily detected using UV-vis analysis. Methyl orange has a strong absorption at 430 nm in a [Bmim][BF$_4$]solution.[40, 27].

The RevIL was prepared by sparging a sample of TPSA silylamine with CO_2. Methyl orange (5.24 mg) was then added to the RevIL (1.2413 g) and stirred in *n-hexane* (0.275 M solution) for one hour. As shown in Figure 4.8, the solution assumed a bright orange color and was homogeneous. The solution was then heated at 65°C for 30 minutes to trigger the reversal of the ionic species. The initial solution, which was orange in the presence of the RevIL, became colorless upon heating, and orange solids precipitated from the solution.
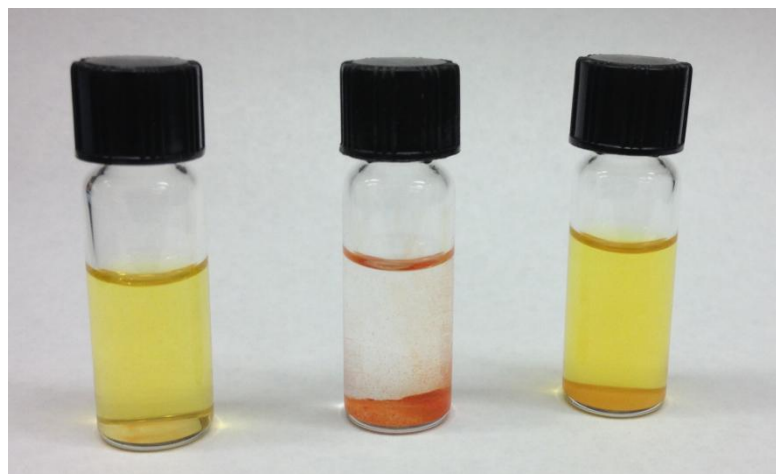
Figure 4.8. Methyl orange solubilized in a solution of TPSA RevIL and hexane (left); methyl orange solids that have precipitated out of solution after reversal of the RevIL (center); methyl orange resolubilized in solution after sparging with CO_2 and reforming the RevIL (right)

The UV-vis spectrum of the system is shown in Figure 4.9a. The λ_{max} of MO at 436 nm is consistent -- although slightly red shifted -- with the reported value of methyl orange [Bmim][BF$_4$]solution.[27, 40] Heating the solution to reverse the RevIL resulted in the disappearance of the methyl orange λ_{max} in the UV-vis spectrum (Figure 4.9b). To demonstrate recyclability of the system, CO_2 was then sparged through the solution for 75 minutes. The UV-vis spectrum provided support for the reformation of the reverse micelles with the reappearance of the methyl orange peak at 446 nm (Figure 4.9c).
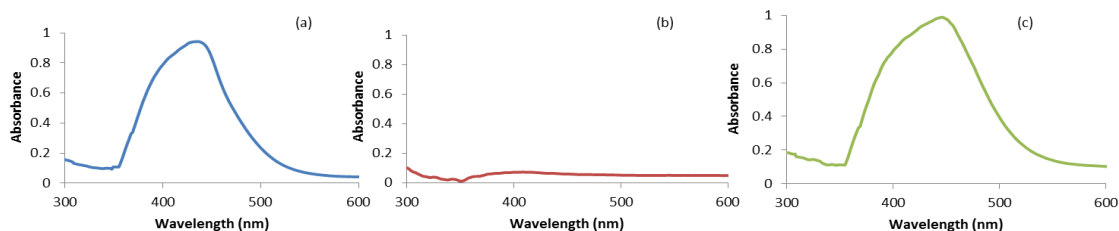
Figure 4.9. UV-vis spectra of methyl orange demonstrating (a) solubilization of methyl orange via reverse micelle formation, (b) reversal of the reversible ionic species and loss of methyl orange solubilization, and (c) reformation of the reversible ionic species and solubilization of methyl orange in hexane

136

These results are consistent with methyl orange stabilization in a hydrocarbon continuous phase through interaction of the reversible ionic species with methyl orange. We propose that this interaction between the polar head of the reversible ionic species and the methyl orange results in a reverse micelle structure in which the alkyl tails extend into the continuous phase (hexane). Furthermore, the micellar structure appeared to be fully reversible upon heating. We believe this behavior results from the loss in ionic character upon the heat-triggered reversal of the ionic liquid. This experiment also suggests that the neutral silylamine does not self-organize in a micellar-like structure capable of supporting an ionic precursor.

Although the results of these studies do not provide conclusive evidence of reverse micelles, the methyl orange studies were promising for the synthesis of gold nanoparticles in solution and the subsequent deposition onto a solid support following moderate heating.

4.3.2 Gold Nanoparticle Synthesis with Reversible Ionic Liquids

By analogy with the methyl orange, the gold precursor $HAuCl_4$ was solubilized within a Reversible Ionic Species (RevIS) micellar structure (Figure 4.10). The resulting reverse micelles provided templates in which the stabilized gold precursor can be reduced forming the stabilized nanoparticles. Through thermal treatment, the reversible ionic species would revert back to the silylamine, which is not capable of maintaining the reverse micelle structure and the gold particles would be released for the efficient deposition onto a support.
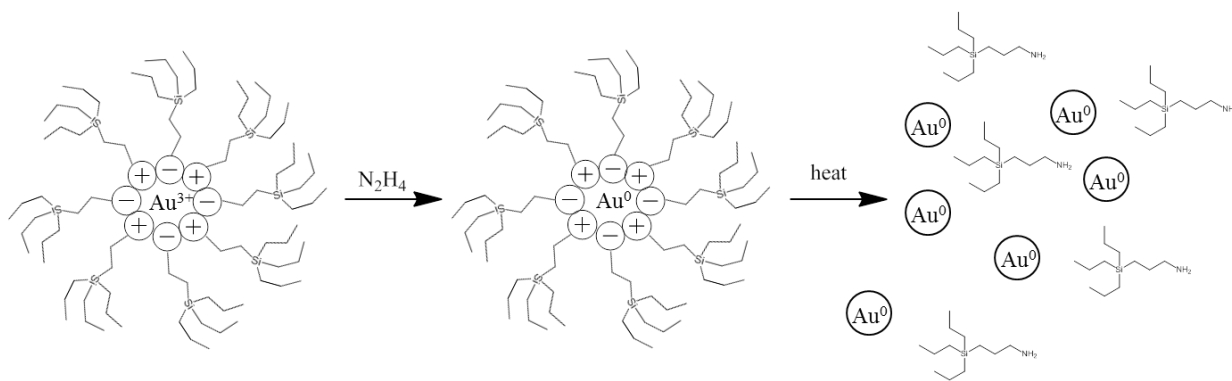
Figure 4.10. Gold nanoparticle synthesis using reversible ionic liquids, via a reverse micelle template

4.3.2.1 Formation of Gold Nanoparticles in Solution

A number of synthetic parameters were investigated and optimized for the preparation of RevIS-stabilized gold nanoparticles including the selection of a reducing agent solution. The use of a carousel reactor allowed us to run simultaneously up to 12 different reaction conditions. The factors that influence nanoparticle formation could be determined rapidly using UV-vis analysis. Shown in Figure 4.11 are the nanoparticles in solution synthesized with various conditions in the carousel reactor.

Figure 4.11. Gold nanoparticles in solution prepared simultaneously in a carousel reactor to study synthetic conditions

The surface plasmon band (SPR), which can be monitored by UV-vis and has been shown to be dependent on nanoparticle size, was measured as a function of hydrazine stoichiometry and delivery (solvent and time), reversible ionic liquid concentration and ratio of gold precursor to RevIL as shown in Figure 4.12 below.[41]
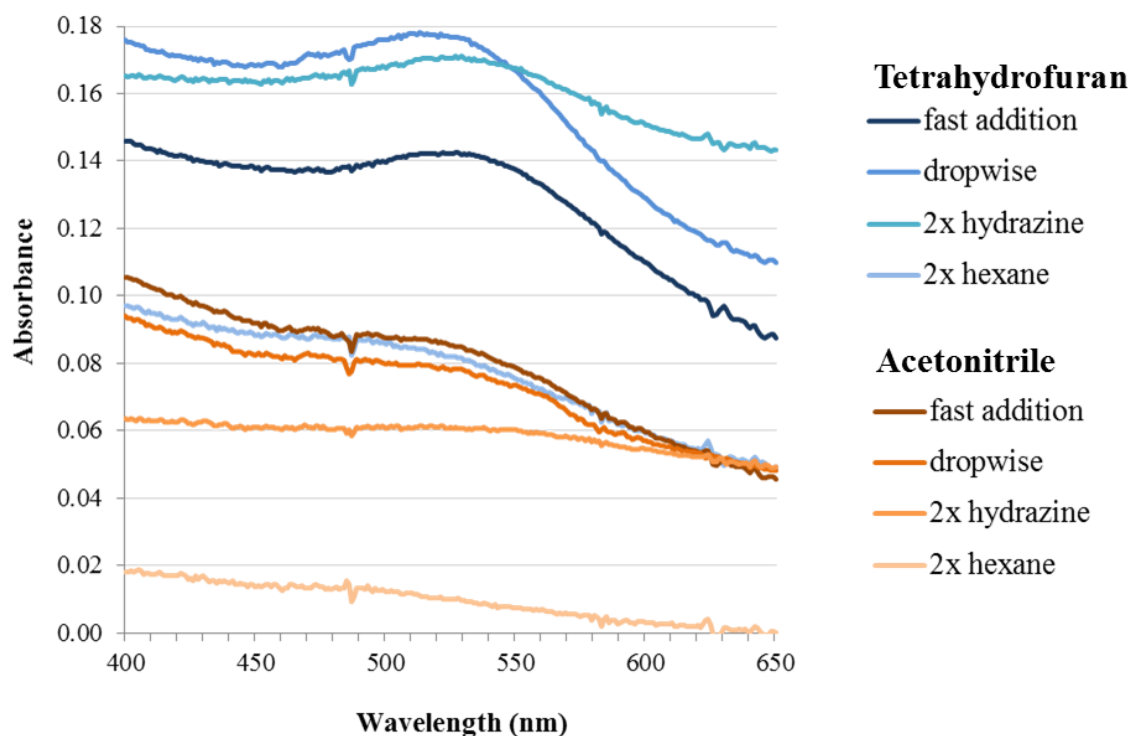
Figure 4.12. UV-vis spectra of gold nanoparticles synthesized in a carousel reactor

To control precisely the amount of hydrazine added, it was delivered as dilute solution in tetrahydrofuran or acetonitrile with a concentration of 3.18×10^{-2} M. The reducing agent and solvent were selected to avoid reaction with the reversible ionic species, as might be the case with aqueous solutions or other polar protic solvents.

The insolubility of acetonitrile in hexane resulted in a biphasic mixture following reduction. The acetonitrile phase quickly turned blue, indicating the nanoparticles were partitioning into the acetonitrile and agglomerating.[42] The amount of hydrazine added to the solution for reduction was also studied. The reduction of the gold precursor (Au^{III}) to elemental gold (Au^0) proceeds through the following reaction:

$$2HAuCl_4 + 2N_2H_4 \rightarrow 8HCl + 2Au^0 + 2N_2 + H_2 \qquad \textbf{Equation 4.2}$$

139

We observed that adding twice the amount of hydrazine (two times the stoichiometric amount) resulted in a broad absorption peak, indicating a more polydisperse sample. An excess amount of hydrazine may react with CO_2 forming the carbazic acid, shown in Figure 4.13.[43] As a result, the CO_2 in equilibrium with the RevIS is consumed, and the reaction equilibrium shifted toward the silylamine.

$$NH_2\text{-}NH_2 + CO_2 \rightleftharpoons N_2\overset{\oplus}{H}_5 \quad N_2H_3\overset{\ominus}{CO}_2$$
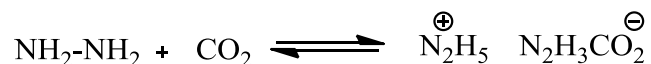
Figure 4.13. Reaction of CO₂ dissolved in hydrazine to give carbazic acid

A fast addition (added in less than 2 seconds) of a stoichiometric amount of a hydrazine solution in THF gave a narrow SPR band in the spectrum and was the delivery method consistently used thereafter.

Concentration of the reversible ionic liquid in the continuous phase and weight ratio of gold salt to reversible ionic liquid had a significant impact on the absorption peak in the UV-vis. Through a series of experiments, analyzed by UV-vis and TEM, the optimal weight ratio of gold salt to reversible ionic liquid (W_{HAuCl4}/W_{RevIL}) was 8.0 x 10^{-3}. The concentration of RevIL in hexane also influenced the absorption peak in the UV-vis spectrum. A solution of RevIL in hexane (2.56 x10^{-2}M) produced a narrower SPR band than a more dilute solution of RevIL (1.28 x10^{-2}M), indicating that a minimum concentration of RevIL is required to form the reverse micelles in solution. Once the optimal reduction (stoichiometric amount of a 3.18 x10^{-2} *M* solution in THF) and concentration conditions (2.56x10^{-2}M RevIL in hexane) were established as shown in Table 4.3, the effect of the structure of the reversible ionic liquid itself (TPSA and THSA RevIL) was investigated.

W_{HAuCl4}/W_{RevIL}	8.0×10^{-3}
RevIS concentration in hexane	2.56×10^{-2} M
Hydrazine concentration	3.18×10^{-2} M
Rate of Addition of hydrazine	<2 seconds

The effect of reversible ionic liquid structure on nanoparticle size and degree of monodispersity has proven to be significant. A TEM image of the nanoparticles synthesized at 25°C using THSA RevIL and deposited on grids with ethanol as co-solvent is shown in Figure 4.14.
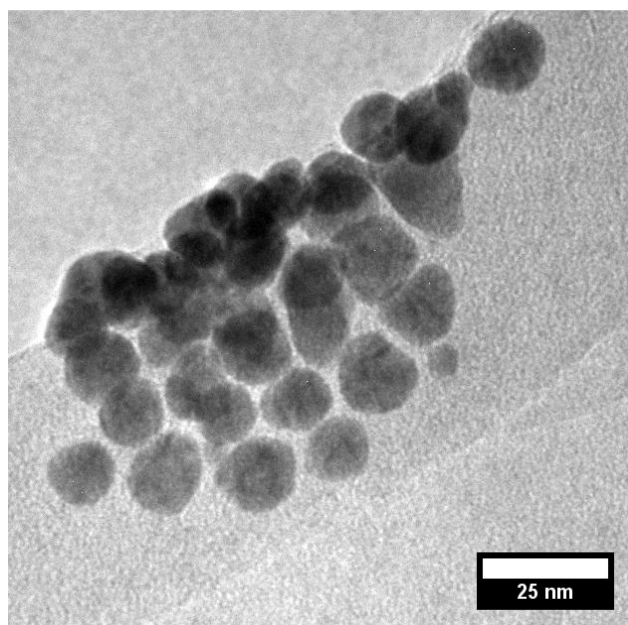
Figure 4.14. TEM image of gold nanoparticles synthesized using HAuCl₄, THSA RevIL and hexane

The nanoparticles synthesized using THSA RevIL were polydisperse and irregularly shaped. An ImageJ analysis was completed despite the irregularity of the nanoparticles, and it was found that the average diameter was 13.3 ± 3.0 nm. THSA RevIL is a bulky molecule, and reverse micelle formation may be hindered by the long alkyl chains extending from the silicon atom. TEtSA is a much smaller molecule, but the high viscosity of the RevIL (6,100 cP) is prohibitive during the dissolution of $HAuCl_4$ in the RevIL. TPSA is a smaller molecule than THSA, and it still has the physical properties that facilitate nanoparticle synthesis (i.e., moderate viscosity and reversal temperature). Nanoparticles synthesized with TPSA produced a red-purple solution following reduction with hydrazine as shown in Figure 4.15 below.
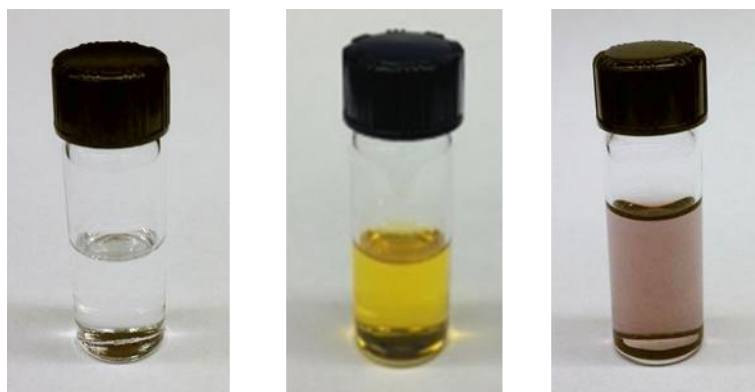
Figure 4.15. The prepared RevIL (left); mixture of $HAuCl_4$ in RevIL and gold nanoparticles in solution following reduction with hydrazine

A representative TEM image of the Au nanoparticles synthesized with TPSA RevIL is shown in Figure 4.16. In this case, the average diameter of the nanoparticles was found to be 6.1 ± 0.9 nm, as displayed in Figure 4.17.
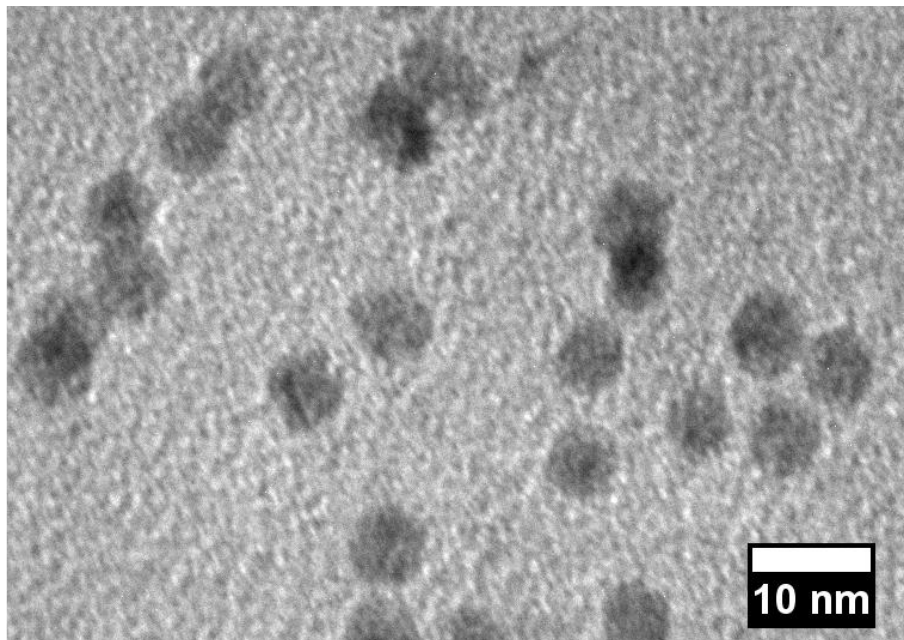
Figure 4.16. TEM image of gold nanoparticles synthesized using HAuCl₄, TPSA RevIL, and hexane
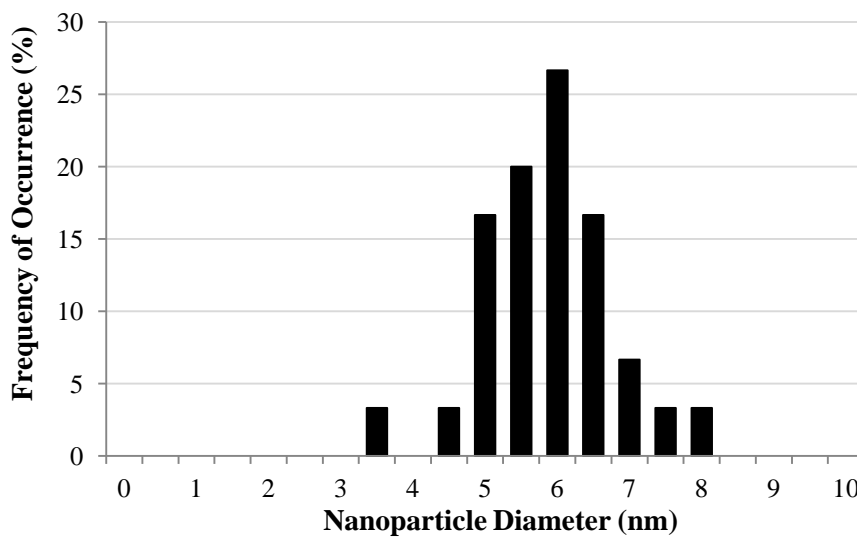
Figure 4.17. Size distribution of gold nanoparticles synthesized using HAuCl₄, TPSA RevIL and hexane

As expected, the structure of the RevIL plays a significant role in the average size of the

Au nanoparticles, likely due to differences in the length of the alkyl chain extending into

the continuous phase.[13, 21, 44] Nonetheless, these results demonstrate the RevIL mediated synthesis of monodisperse gold nanoparticles in hexane without the need of additional surfactants.

The nanoparticles presented above were in solution prior to the reversal of the RevIS. One of the key advantages of the reversible ionic liquid system presented here is the ability to switch off the ionic character of the RevIS by heating to moderate temperatures (less than 100°C).

4.3.2.2 Deposition of Gold Nanoparticles onto a Solid Support

The increasing interest in gold nanoparticle synthesis is in part due to the growing use of gold nanoparticles for heterogeneous catalysis. Initially, the focus of catalysis by gold was centered on oxidation reactions.[45] The successful use of gold nanoparticles (d=1-6 nm) on an oxide support has also been reported for the selective hydrogenation of 1,3-butadiene.[46] There are a number of deposition techniques for catalytic applications including deposition-precipitation,[47] impregnation,[48] and incipient wetness.[49] In contrast with traditional ionic liquids, the switchable nature of the reversible ionic liquids enables the facile deposition of the gold nanoparticles onto a solid surface. To first reverse the RevIL and release the nanoparticles from the reverse micelles, the solution was heated in an oil bath at 65°C for one hour. The reversal temperature of neat TPSA RevIL is 64 ±2°C. The initial deep purple solution became light purple upon heating. A TEM grid was prepared for analysis of the solution, and is shown in Figure 4.18 below.
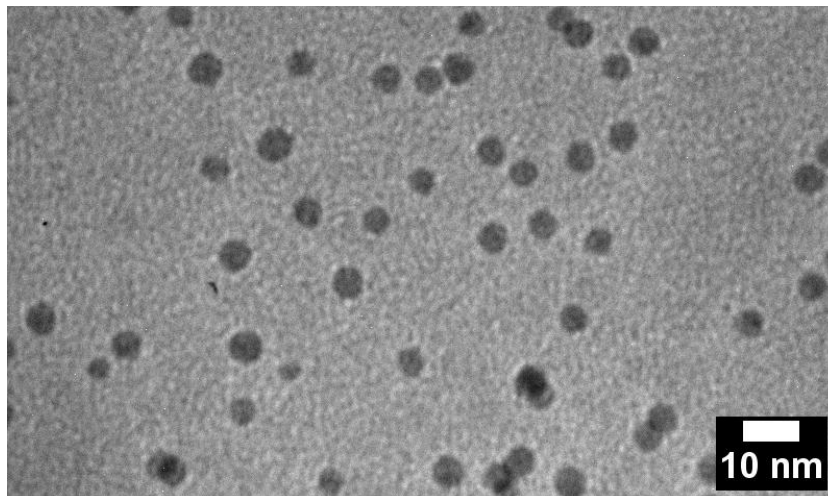
Figure 4.18. TEM image of gold nanoparticles formed using HAuCl4, TPSA RevIL, and hexane after thermal reversal of RevIL

The size distribution of the nanoparticles is presented in Figure 4.19. The average diameter of the nanoparticles in solution was 5.2±0.8 nm. Additionally, the distribution observed after heating has been shifted to smaller sizes.
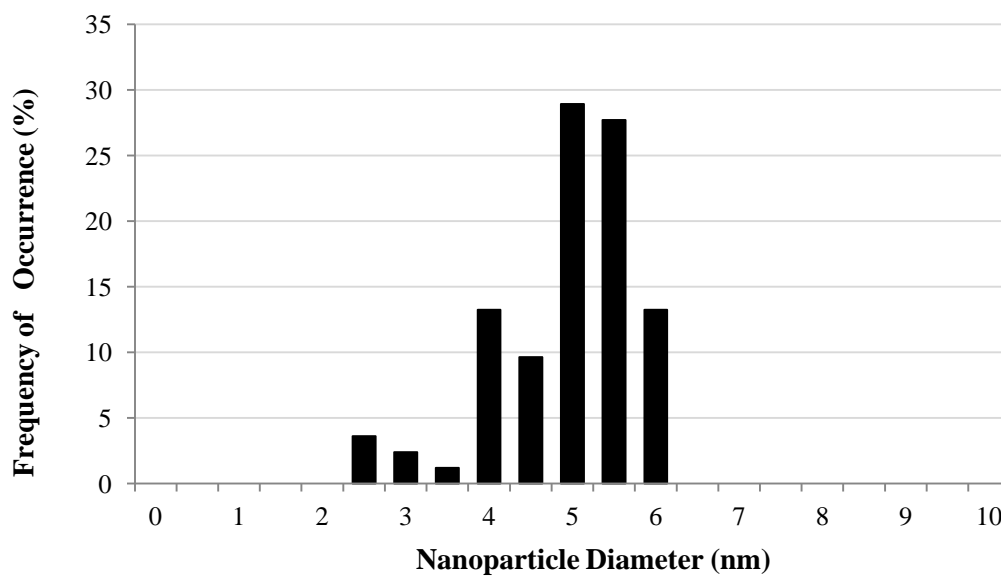
Figure 4.19. Size distribution of gold nanoparticles formed using HAuCl4, TPSA RevIL, and hexane after thermal reversal of RevIL

145

The TEM images of the solution indicate that the larger particles are destabilized as a result of heating and precipitate out of solution. The reversal procedure was repeated; heating at 65°C for 24 hours. Again, the solution had not fully become colorless, indicating that nanoparticles were still present in solution. Amines have been used in gold nanoparticle synthesis as reducing agents and stabilizers.[9, 50, 51] Literature reports of TGA/DTA analyses of amine-gold complexes indicate that the maximum weight loss occurs at 250°C, and results are in agreement with the number of bonded ligands determined by elemental analysis.[50, 52] The surface interaction has been described as a weak covalent bond that is highly dependent on solvent properties.[50] This coordination between the nanoparticle and amine may stabilize the nanoparticle in solution after the RevIL is reversed. To determine whether nanoparticle synthesis with an amine (replacing the RevIL) would support monodisperse nanoparticle formation, the procedure was repeated with the silylamines.

Preliminary experiments were completed using the silylamine rather than the RevIL in the synthetic procedure. The gold precursor was combined with the silylamine (using the same optimized conditions described above). The sample was then mixed with hexane, and the gold precursor reduced with the hydrazine solution. Upon addition of the reducing agent, the reaction mixed immediately turned a dark blue color indicating agglomeration, or large nanoparticles.[42] These initial studies indicate that the ionic nature of the RevIL is required to synthesize nanoparticles in the 5-10 nm range.

A facile method for the deposition of the gold nanoparticles on a solid support would be highly advantageous particularly for catalytic applications. The following studies were completed with silica (SiO_2) but other solid substrates that are used for

146

nanoparticle support are titania (TiO_2) or alumina (Al_2O_3).[53] The solid support was added

to the nanoparticle solution and heated to 65°C for one hour. As previously observed, the

solution did not become completely colorless upon heating. However, the solid support

did adopt the red-purple color of the nanoparticle solution as shown in Figure 4.20.

Figure 4.20. Gold nanoparticles deposited onto a silica support

4.4 Conclusions

Gold nanoparticles were successfully synthesized using reversible ionic liquids.

Preliminary dye solubilization studies indicate that the reversible ionic species form

reverse micelle structures in a hydrocarbon continuous phase. The reverse micelles

provide a template for monodisperse nanoparticle synthesis. The nanoparticles

synthesized using this approach were 6.1±0.9 nm; a diameter that has been shown to be

active in oxidation reactions.[45] The reversible ionic liquid system offers strong

advantages over the existing nanoparticle synthetic techniques in that it provides both

stabilization and size control, and an additional surfactant is not required. The unique,

reversible nature of the ionic liquids facilitated the deposition of the nanoparticles on a solid support by heating the solution.

4.5 References

1. Teranishi, T.; Hosoe, M.; Tanaka, T.; Miyake, M., Size Control of Monodispersed Pt Nanoparticles and Their 2D Organization by Electrophoretic Deposition. *The Journal of Physical Chemistry B* **1999,** *103* (19), 3818-3827.

2. Guo, S.; Wang, E., Synthesis and electrochemical applications of gold nanoparticles. *Analytica Chimica Acta* **2007,** *598* (2), 181-192.

3. Campelo, J. M.; Luna, D.; Luque, R.; Marinas, J. M.; Romero, A. A., Sustainable preparation of supported metal nanoparticles and their applications in catalysis. *Chemsuschem* **2009,** *2* (1), 18-45.

4. Daniel, M.-C.; Astruc, D., Gold Nanoparticles: Assembly, Supramolecular Chemistry, Quantum-Size-Related Properties, and Applications toward Biology, Catalysis, and Nanotechnology. *Chemical Reviews* **2003,** *104* (1), 293-346.

5. Brust, M.; Walker, M.; Bethell, D.; Schiffrin, D. J.; Whyman, R., Synthesis of thiol-derivatised gold nanoparticles in a two-phase Liquid-Liquid system. *Journal of the Chemical Society, Chemical Communications* **1994,** (7), 801-802.

6. Zhang, Z. P.; Wang, F.; Chen, F. E.; Shi, G. Q., Preparation of polythiophene coated gold nanoparticles. *Materials Letters* **2006,** *60* (8), 1039-1042; Sidhaye, D. S.; Prasad, B. L. V., Linear assembly of hexadecanethiol coated gold nanoparticles. *Chemical Physics Letters* **2008,** *454* (4-6), 345-349.

7. Haider, P.; Urakawa, A.; Schmidt, E.; Baiker, A., Selective blocking of active sites on supported gold catalysts by adsorbed thiols and its effect on the catalytic behavior: A combined experimental and theoretical study. *Journal of Molecular Catalysis a-Chemical* **2009,** *305* (1-2), 161-169; Martra, G.; Prati, L.; Manfredotti, C.; Biella, S.; Rossi, M.; Coluccia, S., Nanometer-sized gold particles supported on SiO2 by deposition of gold sols from Au(PPh3)(3)Cl. *Journal of Physical Chemistry B* **2003,** *107* (23), 5453-5459; Menard, L. D.; Xu, F. T.; Nuzzo, R. G.; Yang, J. C., Preparation of TiO2-supported Au nanoparticle catalysts from a Au-13 cluster precursor: Ligand removal using ozone exposure versus a rapid thermal treatment. *Journal of Catalysis* **2006,** *243* (1), 64-73.

8. Ghosh, P.; Han, G.; De, M.; Kim, C. K.; Rotello, V. M., Gold nanoparticles in delivery applications. *Advanced Drug Delivery Reviews* **2008,** *60* (11), 1307-1315.

9.   Quintanilla, A.; Butselaar-Orthlieb, V. C. L.; Kwakernaak, C.; Sloof, W. G.; Kreutzer, M. T.; Kapteijn, F., Weakly bound capping agents on gold nanoparticles in catalysis: Surface poison? *Journal of Catalysis* **2010,** *271* (1), 104-114.

10.   Murphy, C. J., Sustainability as an emerging design criterion in nanoparticle synthesis and applications. *J Mater Chem* **2008,** *18* (19), 2173-2176; Dahl, J. A.; Maddux, B. L. S.; Hutchison, J. E., Toward greener nanosynthesis. *Chem Rev* **2007,** *107* (6), 2228-2269; Eckelman, M. J.; Zimmerman, J. B.; Anastas, P. T., Toward green nano: E-factor analysis of several nanomaterial syntheses. *Journal of Industrial Ecology* **2008,** *12* (3), 316-328.

11.   Uskokovic, V.; Drofenik, M., Reverse micelles: Inert nano-reactors or physico-chemically active guides of the capped reactions. *Advances in Colloid and Interface Science* **2007,** *133* (1), 23-34.

12.   Bommarius, A. S.; Holzwarth, J. F.; Wang, D. I. C.; Hatton, T. A., Coalescence and Solubilate Exchange in a Cationic 4-Component Reversed Micellar System. *Journal of Physical Chemistry* **1990,** *94* (18), 7232-7239; Fletcher, P. D. I.; Howe, A. M.; Robinson, B. H., The Kinetics of Solubilisate Exchange Between Water Droplets of a Water-In-Oil Microemulsion. *Journal of the Chemical Society-Faraday Transactions I* **1987,** *83*, 985-1006.

13.   Eastoe, J.; Hollamby, M. J.; Hudson, L., Recent advances in nanoparticle synthesis with reversed micelles. *Advances in Colloid and Interface Science* **2006,** *128*, 5-15.

14.   Lopez-Quintela, M. A.; Tojo, C.; Blanco, M. C.; Rio, L. G.; Leis, J. R., Microemulsion dynamics and reactions in microemulsions. *Current Opinion in Colloid & Interface Science* **2004,** *9* (3-4), 264-278.

15.   Pileni, M. P., Reverse micelles as microreactors. *Journal of Physical Chemistry* **1993,** *97* (27), 6961-6973; Carpenter, E. E.; Seip, C. T.; O'Connor, C. J., Magnetism of nanophase metal and metal alloy particles formed in ordered phases. *Journal of Applied Physics* **1999,** *85* (8), 5184-5186.

16.   Bae, D. S.; Han, K. S.; Adair, J. H., Synthesis and microstructure of Pd/SiO2 nanosized particles by reverse micelle and sol-gel processing. *Journal of Materials Chemistry* **2002,** *12* (10), 3117-3120; Lin, J.; Zhou, W. L.; Kumbhar, A.; Wiemann, J.; Fang, J. Y.; Carpenter, E. E.; O'Connor, C. J., Gold-coated iron (Fe@Au) nanoparticles: Synthesis, characterization, and magnetic field-induced self-assembly. *Journal of Solid State Chemistry* **2001,** *159* (1), 26-31.

17.   Bhatt, A. I.; Mechler, A.; Martin, L. L.; Bond, A. M., Synthesis of Ag and Au nanostructures in an ionic liquid: thermodynamic and kinetic effects underlying nanoparticle, cluster and nanowire formation. *Journal of Materials Chemistry* **2007,** *17* (21), 2241-2250.

18.   Saunders, S. R.; Roberts, C. B., Size-selective fractionation of nanoparticles at an application scale using CO_2 gas-expanded liquids. *Nanotechnology* **2009,** *20* (47);

Anand, M.; You, S. S.; Hurst, K. M.; Saunders, S. R.; Kitchens, C. L.; Ashurst, W. R.; Roberts, C. B., Thermodynamic analysis of nanoparticle size selective fractionation using gas-expanded liquids. *Industrial & Engineering Chemistry Research* **2008,** *47* (3), 553-559; Liu, J. C.; Ruffini, N.; Pollot, P.; Llopis-Mestre, V.; Dilek, C.; Eckert, C. A.; Liotta, C. L.; Roberts, C. B., More Benign Synthesis of Palladium Nanoparticles in Dimethyl Sulfoxide and Their Extraction into an Organic Phase. *Industrial & Engineering Chemistry Research* **2010,** *49* (17), 8174-8179.

19.   Liu, J. H.; Cheng, S. Q.; Zhang, J. L.; Feng, X. Y.; Fu, X. G.; Han, B. X., Reverse micelles in carbon dioxide with ionic-liquid domains. *Angewandte Chemie-International Edition* **2007,** *46* (18), 3313-3315.

20.   Rohan, A. L.; Switzer, J. R.; Flack, K. M.; Hart, R. J.; Sivaswamy, S.; Biddinger, E. J.; Talreja, M.; Verma, M.; Faltermeier, S.; Nielsen, P. T.; Pollet, P.; Schuette, G. F.; Eckert, C. A.; Liotta, C. L., The Synthesis and the Chemical and Physical Properties of Non-Aqueous Silylamine Solvents for Carbon Dioxide Capture. *Chemsuschem* **2012,** *5* (11), 2181-2187.

21.   Fink, J.; Kiely, C. J.; Bethell, D.; Schiffrin, D. J., Self-organization of nanosized gold particles. *Chemistry of Materials* **1998,** *10* (3), 922-926.

22.   Brust, M.; Fink, J.; Bethell, D.; Schiffrin, D. J.; Kiely, C., Synthesis and reactions of functionalized gold nanoparticles. *Journal of the Chemical Society-Chemical Communications* **1995,** (16), 1655-1656.

23.   Porta, F.; Krpetic, Z.; Prati, L.; Gaiassi, A.; Scari, G., Gold-ligand interaction studies of water-soluble aminoalcohol capped gold nanoparticles by NMR. *Langmuir* **2008,** *24* (14), 7061-7064.

24.   Fulton, J. L.; Smith, R. D., Reverse Micelle and Microemulsion Phases in Supercritical Fluids. *Journal of Physical Chemistry* **1988,** *92* (10), 2903-2907.

25.   Dominguez, A.; Fernandez, A.; Gonzalez, N.; Iglesias, E.; Montenegro, L., Determination of critical micelle concentration of some surfactants by three techniques. *Journal of Chemical Education* **1997,** *74* (10), 1227-1231.

26.   Zulauf, M.; Eicke, H. F., Inverted Micelles and Microemulsions in the Ternary-System H2O-Aerosol-OT-Isooctane As Studied by Photon Correlation Spectroscopy. *Journal of Physical Chemistry* **1979,** *83* (4), 480-486.

27.   McFann, G. J.; Johnston, K. P.; Howdle, S. M., Solubilization in Nonionic Reverse Micelles in Carbon-Dioxide. *Aiche Journal* **1994,** *40* (3), 543-555.

28.   Adamson, A. W., *Physical Chemistry of Surfactants*. 5th ed.; Wiley: New York, 1990.

29. Perez-Gregorio, V.; Montano, D.; Giner, B.; Lafuente, C.; Royo, F. M., Surface and bulk behaviour of some (n-hexane plus chloroalkane) mixtures. *Journal of Chemical Thermodynamics* **2009,** *41* (4), 553-559.

30. Li, D., *Encyclopedia of Microfluidics and Nanofluidics*. Springer-Verlag: Boston, MA, 2008.

31. Myers, D., *Surfactant Science and Technology*. 3rd ed.; Wiley-Interscience: New Jersey, 2006.

32. Ravey, J. C.; Buzier, M.; Picot, C., Micellar Structures of Nonionic Surfactants in Apolar Media. *Journal of Colloid and Interface Science* **1984,** *97* (1), 9-25.

33. Bohidar, H. B.; Behboudnia, M., Characterization of reverse micelles by dynamic light scattering. *Colloids and Surfaces a-Physicochemical and Engineering Aspects* **2001,** *178* (1-3), 313-323; Blitz, J. P.; Fulton, J. L.; Smith, R. D., Dynamic Light-Scattering Measurements of Reverse Micelles in Liquid and Supercritical Ethane. *Journal of Physical Chemistry* **1988,** *92* (10), 2707-2710.

34. Zhu, D. M.; Wu, X.; Schelly, Z. A., Reverse Micelles and Water in Oil Microemulsions of Triton X-100 in Mixed Solvents of Benzene and n-Hexane-Dynamic Light Scattering and Turbidity Studies. *Langmuir* **1992,** *8* (6), 1538-1540.

35. Riter, R. E.; Kimmel, J. R.; Undiks, E. P.; Levinger, N. E., Novel reverse micelles partitioning nonaqueous polar solvents in a hydrocarbon continuous phase. *Journal of Physical Chemistry B* **1997,** *101* (41), 8292-8297.

36. Gomez-Diaz, D.; Mejuto, J. C.; Navaza, J. M., Density, viscosity, and speed of sound of solutions of AOT reverse micelles in 2,2,4-trimethylpentane. *Journal of Chemical and Engineering Data* **2006,** *51* (2), 409-411.

37. Maitra, A., Determination of Size Parameters of Water Aerosol OT Oil Reverse Micelles From Their Nuclear Magnetic-Resonance Data. *Journal of Physical Chemistry* **1984,** *88* (21), 5122-5125.

38. Harrison, K.; Goveas, J.; Johnston, K. P.; Orear, E. A., Water in Carbon Dioxide Microemulsions with a Fluorocarbon-Hydrocarbon Hybrid Surfactant. *Langmuir* **1994,** *10* (10), 3536-3541.

39. Qi, L. M.; Ma, J. M., Investigation of the microenvironment in nonionic reverse micelles using methyl orange and methylene blue as absorption probes. *Journal of Colloid and Interface Science* **1998,** *197* (1), 36-42.

40. Li, N.; Gao, Y. A.; Zheng, L. Q.; Zhang, J.; Yu, L.; Li, X. W., Studies on the micropolarities of bmimBF(4)/TX-100/toluene ionic liquid microemulsions and their behaviors characterized by UV-visible spectroscopy. *Langmuir* **2007,** *23* (3), 1091-1097.

41.   Amendola, V.; Meneghetti, M., Size Evaluation of Gold Nanoparticles by UV-vis Spectroscopy. *Journal of Physical Chemistry C* **2009,** *113* (11), 4277-4285; Jain, P. K.; Lee, K. S.; El-Sayed, I. H.; El-Sayed, M. A., Calculated absorption and scattering properties of gold nanoparticles of different size, shape, and composition: Applications in biological imaging and biomedicine. *Journal of Physical Chemistry B* **2006,** *110* (14), 7238-7248; Eustis, S.; El-Sayed, M. A., Why gold nanoparticles are more precious than pretty gold: Noble metal surface plasmon resonance and its enhancement of the radiative and nonradiative properties of nanocrystals of different shapes. *Chemical Society Reviews* **2006,** *35* (3), 209-217; Wilcoxon, J. P.; Williamson, R. L.; Baughman, R., Optical Properties of Gold Colloids Formed in Inverse Micelles. *Journal of Chemical Physics* **1993,** *98* (12), 9933-9950; Link, S.; El-Sayed, M. A., Size and temperature dependence of the plasmon absorption of colloidal gold nanoparticles. *Journal of Physical Chemistry B* **1999,** *103* (21), 4212-4217.

42.   Turkevich, J.; Garton, G.; Stevenson, P. C., The Color of Colloidal Gold. *Journal of Colloid Science* **1954,** *9* (6), S26-S35.

43.   Bellerby, J. M., The Chemical Effects of Storing Hydrazine Containing Carbon-Dioxide in Stainless-Steel Systems. *Journal of Hazardous Materials* **1983,** *7* (3), 187-197.

44.   Santra, S.; Tapec, R.; Theodoropoulou, N.; Dobson, J.; Hebard, A.; Tan, W. H., Synthesis and characterization of silica-coated iron oxide nanoparticles in microemulsion: The effect of nonionic surfactants. *Langmuir* **2001,** *17* (10), 2900-2906.

45.   Haruta, A., When gold is not noble: Catalysis by nanoparticles. *Chemical Record* **2003,** *3* (2), 75-87.

46.   Schimpf, S.; Lucas, M.; Mohr, C.; Rodemerck, U.; Bruckner, A.; Radnik, J.; Hofmeister, H.; Claus, P., Supported gold nanoparticles: in-depth catalyst characterization and application in hydrogenation and oxidation reactions. *Catalysis Today* **2002,** *72* (1-2), 63-78; Hugon, A.; Delannoy, L.; Louis, C., Supported gold catalysts for selective hydrogenation of 1,3-butadiene in the presence of an excess of alkenes. *Gold Bulletin* **2008,** *41* (2), 127-138.

47.   Zanella, R.; Delannoy, L.; Louis, C., Mechanism of deposition of gold precursors onto TiO2 during the preparation by cation adsorption and deposition-precipitation with NaOH and urea. *Applied Catalysis a-General* **2005,** *291* (1-2), 62-72; Haruta, M.; Tsubota, S.; Kobayashi, T.; Kageyama, H.; Genet, M. J.; Delmon, B., Low-Temperature Oxidation of CO Over Gold Supported on TIO2, Alpha-FE2O3, AND CO3O4. *Journal of Catalysis* **1993,** *144* (1), 175-192.

48.   Claus, P.; Bruckner, A.; Mohr, C.; Hofmeister, H., Supported gold nanoparticles from quantum dot to mesoscopic size scale: Effect of electronic and structural properties on catalytic hydrogenation of conjugated functional groups. *Journal of the American Chemical Society* **2000,** *122* (46), 11430-11439.

49. Bowker, M.; Nuhu, A.; Soares, J., High activity supported gold catalysts by incipient wetness impregnation. *Catalysis Today* **2007,** *122* (3-4), 245-247.

50. Leff, D. V.; Brandt, L.; Heath, J. R., Synthesis and characterization of hydrophobic, organically-soluble gold nanocrystals functionalized with primary amines. *Langmuir* **1996,** *12* (20), 4723-4730.

51. Newman, J. D. S.; Blanchard, G. J., Formation of gold nanoparticles using amine reducing agents. *Langmuir* **2006,** *22* (13), 5882-5887; Selvakannan, P.; Mandal, S.; Phadtare, S.; Gole, A.; Pasricha, R.; Adyanthaya, S. D.; Sastry, M., Water-dispersible tryptophan-protected gold nanoparticles prepared by the spontaneous reduction of aqueous chloroaurate ions by the amino acid. *Journal of Colloid and Interface Science* **2004,** *269* (1), 97-102; Aslam, M.; Fu, L.; Su, M.; Vijayamohanan, K.; Dravid, V. P., Novel one-step synthesis of amine-stabilized aqueous colloidal gold nanoparticles. *Journal of Materials Chemistry* **2004,** *14* (12), 1795-1797.

52. Kumar, A.; Mandal, S.; Selvakannan, P. R.; Pasricha, R.; Mandale, A. B.; Sastry, M., Investigation into the interaction between surface-bound alkylamines and gold nanoparticles. *Langmuir* **2003,** *19* (15), 6277-6282; Terrill, R. H.; Postlethwaite, T. A.; Chen, C. H.; Poon, C. D.; Terzis, A.; Chen, A. D.; Hutchison, J. E.; Clark, M. R.; Wignall, G.; Londono, J. D.; Superfine, R.; Falvo, M.; Johnson, C. S.; Samulski, E. T.; Murray, R. W., Monolayers in three dimensions: NMR, SAXS, thermal, and electron hopping studies of alkanethiol stabilized gold clusters. *Journal of the American Chemical Society* **1995,** *117* (50), 12537-12548.

53. Corma, A.; Garcia, H., Supported gold nanoparticles as catalysts for organic reactions. *Chemical Society Reviews* **2008,** *37* (9), 2096-2126; Arrii, S.; Morfin, F.; Renouprez, A. J.; Rousset, J. L., Oxidation of CO on gold supported catalysts prepared by laser vaporization: Direct evidence of support contribution. *Journal of the American Chemical Society* **2004,** *126* (4), 1199-1205.

CHAPTER 5 - CONCLUSIONS AND RECOMMENDATIONS

5.1 Overall Conclusions

Three industrially relevant projects have been presented; the research guided by the principles of green chemistry presented in Chapter 1. The use of reversible ionic liquids (RevILs) as switchable solvents for CO_2 capture from low and high pressure streams was first discussed. The goal of the project was to understand first the effect of silylamine structure on the properties of the RevILs pertinent to CO_2 capture. We then undertook the design of reversible ionic liquids for capture processes focused on maximizing CO_2 capture capacity while minimizing viscosity and energy required for regeneration.

The use of CO_2 as a protecting group during organic syntheses was presented in Chapter 3. Three strategies for the reversible protection of amines using CO_2 were developed and evaluated during a chemoselective reaction. By reversibly protecting the amine functionality of a bifunctional molecule, reaction was directed away from the amine and instead occurred at a less reactive site. This *in-situ* CO_2 protection technology offers significant advantages over traditional protection techniques through the elimination of separate protection and deprotection unit operations.

Reversible ionic liquids were again used in Chapter 4 as switchable surfactants for gold nanoparticle synthesis. Preliminary studies indicate that the reversible ionic liquid formed reverse micelles in a hydrocarbon continuous phase. The reverse micelle structure provided a template for the synthesis of monodisperse gold nanoparticles. The reversible

ionic liquid system offers significant advantages toward a greener and more sustainable synthesis and deposition of nanoparticles.

5.2 Recommendations

For each of the projects presented below, recommendations are given to continue or improve upon the completed research. A common recommendation for each project -- most specifically CO_2 capture and amine protection with CO_2 -- is the study of the economics of the process. Both of these projects have involved interaction with an industrial sponsor (Phillips 66 and Dow Chemical). The principles of green chemistry have guided the research to improve upon existing technologies, however, as presented in Chapter 1, there are three drivers for change: economic, environmental and social. It is important to consider each of these drivers in the development of sustainable technologies for industrial implementation.

5.3 Reversible Ionic Liquids for CO_2 Capture

5.3.1 Conclusions

To establish the effect of silylamine structure on reversible ionic liquid properties, over 15 silylamines were synthesized. Four significant changes were made to the silylamine structure shown in Figure 5.1, and each reversible ionic liquid was characterized.

$R_1 = C_2H_5, C_3H_7, C_6H_{13}$
$R_2 = CH_3, H$
$n = 1\text{-}4$
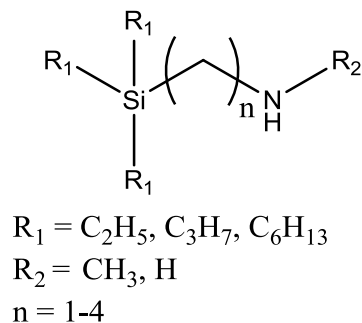
Figure 5.1. Trialkylsilylamine structure varying (1) alkyl chain length on the silicon atom; (2) proximity of silicon and nitrogen atom and (3) order of the amine

Several important conclusions are highlighted below.

- The CO_2 capacity exceeds the theoretical uptake if two moles of silylamine react with one mole of CO_2 to form the reversible ionic liquid. The enhanced capacity is the result of the formation of a stabilized carbamate-carbamic acid species.

- The reversal temperature and enthalpy of regeneration may be reduced through steric hindrance at the amine or by varying the order of the amine.

- The reversible ionic liquid viscosity is heavily influenced by silylamine structure, and can be controlled by limiting conversion (CO_2 uptake) of the silylamine to the RevIL. Unlike traditional or functionalized ionic liquids, the ability to control viscosity by limiting conversion is unique to switchable solvent systems such as ours. The effect of temperature (assuming that the flue gas enters at 40˚C) combined with limiting conversion results in a RevIL viscosity that has been deemed industrially viable.

- The optimal silylamine for CO_2 capture depends highly on capture conditions. For low pressure CO_2 capture (e.g. flue gas) it is critical to maximize chemical capacity while minimizing the enthalpy of regeneration. For CO_2 separation from high

156

pressure streams, capitalizing on the inlet CO_2 pressure through physical absorption results in enhanced capacity and a significant reduction in energy required for regeneration.

5.3.2 <u>Recommendations</u>

The CO_2 capture project with Phillips 66 is now finished, however, continued efforts to study reversible ionic liquids for CO_2 capture would benefit from the following recommendations. The ability to influence RevIL properties by making structural changes to the silylamine opens unlimited opportunities to optimize the CO_2 capture system. The screening of new potential molecules for CO_2 would be expedited drastically by complementing the synthesis of new molecules with predictive screening methods such as COSMO-RS. The characterization of the 15+ silylamines has produced two silylamines as optimal CO_2 capture solvents: *trans*-TEtSA and TEtMSA. TEtMSA is highly advantageous due to the low molecular weight (and therefore high CO_2 capture capacity) and low viscosity. This molecule could be improved by reducing the reversal temperature (78°C) via longer alkyl chain lengths on the silicon atom. The synthesis of this molecule is shown below in Figure 5.2.
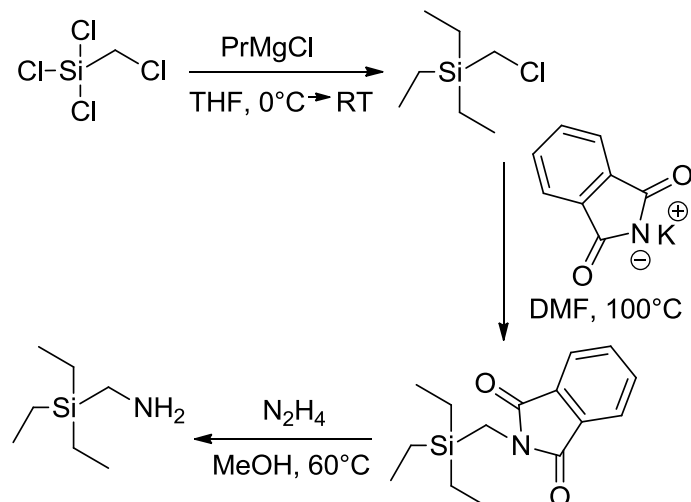
Figure 5.2. Synthetic scheme for (aminomethyl)tripropylsilane (TPSMA)

Secondary amines show strong potential for CO_2 capture.[1] The two secondary silylamines presented in Chapter 2 show significantly lower enthalpies of regeneration than the equivalent primary silylamine. A drawback of these molecules is the very low reversal temperature (below 40°C). To increase the reversal temperature of the secondary silylamines, N-methyl-3-(aminopropyl)dimethylethylsilane (SDMESA) or N-methyl-3-(triethylsilyl)propan-1-amine (STEtSA), the length of the tether between the silicon atom and amine could be shortened to an ethylene or methylene linker or lengthened to a butylene linker. This would be an instance in which predictive software would be advantageous for determining the best Si-NH$_2$ linker length to increase the reversal temperature of the secondary silylamines. The synthesis of TEtSBA is the easiest of the three linker lengths, and thus may prove to be the optimal candidate. N-methyl-4-(triethylsilyl)butan-1-amine may be synthesized as shown in Figure 5.3.
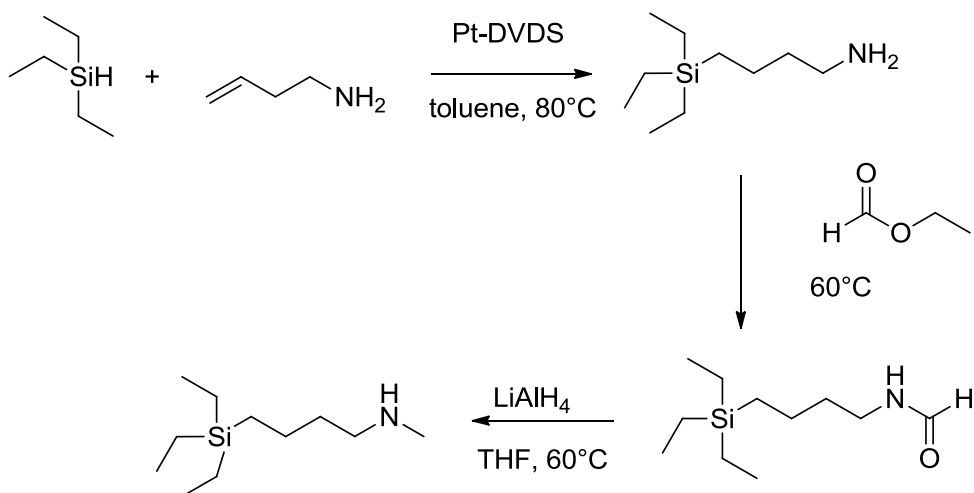
Figure 5.3. Proposed synthesis of N-methyl-4-(triethylsilyl)butan-1-amine

The reversible ionic liquid systems presented are non-aqueous capture solvents. However, residual water in the flue gas is certainly present and will likely influence the capture properties. Determining the amount of ionic liquid that is soluble in water is not straightforward, however there have been reports in literature that show the experimentally measured excess enthalpies for several ionic liquid-water systems.[2] The reactive nature of our RevIL system will add an additional level of complexity to these measurements. The solubility measurements of RevIL in water will also make the process simulation model of the system more robust. Preliminary modeling efforts have been completed by removing the water in the process stream. Incorporating RevIL properties will provide a more clear idea of the industrial viability of this capture system.

The properties of the reversible ionic liquids have been tuned by making structural changes to the silylamine. The next step toward implementation is the consideration of the CO_2 capture process using RevILs. Included in Appendix D is a proposal submitted to the Department of Energy (DOE) on developing a novel process for using reversible

159

ionic liquids in a CO_2 capture process with a spray atomizer. This proposal, submitted in collaboration with Dr. Andrei Fedorov in the Mechanical Engineering department, outlines the efficient delivery of the silylamine for CO_2 capture.

The use of the reversible ionic liquid system for alternative applications may also be considered. Initial high pressure CO_2 capture studies have been completed using high pressure ATR-FTIR and a sapphire cell to measure phase behavior at pressures up to 70 bar. These studies will prove to be helpful for developing solvents for CO_2 separation from methane. The switchable nature of the RevIL is highly advantageous for reactions and separations.

5.4 CO_2 as a Protecting Group in Chemical Syntheses

5.4.1 <u>Conclusions</u>

In-situ, reversible amine protection with CO_2 was presented in Chapter 3. Adding an amidine or guanidine base resulted in a carbamate-protonated base ion pair that was soluble in a polar aprotic solvent. Interestingly, the formation of a previously unreported species was observed and characterized. The reaction of CO_2 with a solution of 1,8-Diazabicyclo[5.4.0]undec-7-ene (DBU) and benzylamine formed a stabilized carbamate -diadduct species. The successful protection of an amine functionality was demonstrated during an acylation reaction. By protecting the amine functionality of a bifunctional molecule, we showed that CO_2 protection at the amine site could successfully direct the reaction to a less reactive site on the same molecule. *In-situ* amine protection with CO_2 offers a key advantage over traditional protecting groups in that it does not require separate unit operations for the protection, deprotection, and subsequent separation of the

160

protecting group. This amine protection strategy is highly applicable for industrial application and will serve as a model for our research partner, Dow Chemical.

5.4.2 Recommendations

The work presented in Chapter 3 was intended to serve as a proof of concept for amine protection using CO_2. The overarching goal of this project is to demonstrate amine protection during a Suzuki coupling reaction. This work is currently underway; however, due to the complexity of Suzuki coupling reactions, it was first necessary to establish the research using a model compound. In addition to applying the amine protection work to Suzuki coupling reactions, additional recommendations are as follows:

- In the investigation of amine protection strategies for Suzuki reactions, one important consideration is the reactivity of the amine-functionality. Our initial studies were focused on a benzylamine substrate; however, protection of anilines and pyridines is often desired in Suzuki coupling reactions. Due to the decreased nucleophilicity of the nitrogen, elevated CO_2 pressures may be required. In addition to demonstrating enhanced reaction yields of Suzuki reactions under CO_2 pressure, understanding the effect of CO_2 on all elements of the reaction would be valuable.

- Alternative bases should be investigated to supplement or replace DBU. Both amidine and guanidine bases such as DBU and tetramethyl guanidine (TMG) are expensive and difficult to separate, and therefore are not favored in industry. Inorganic bases that are currently used for Suzuki coupling reactions would be advantageous to streamline the entire coupling reaction. Preliminary studies using alternative organic bases indicate that solubility may be challenging, however the stability of the protected species during a model reaction has not been investigated.

- The presented work demonstrates amine protection during a chemoselective reaction to promote reaction at a less reactive site. This can be taken one step further to complete a total synthesis. As shown in Figure 5.4 below, the amine site would be temporarily blocked to allow reaction at the hydroxyl group. The amine could then be deprotected and reacted with an alternative reagent. The final step would include product isolation.
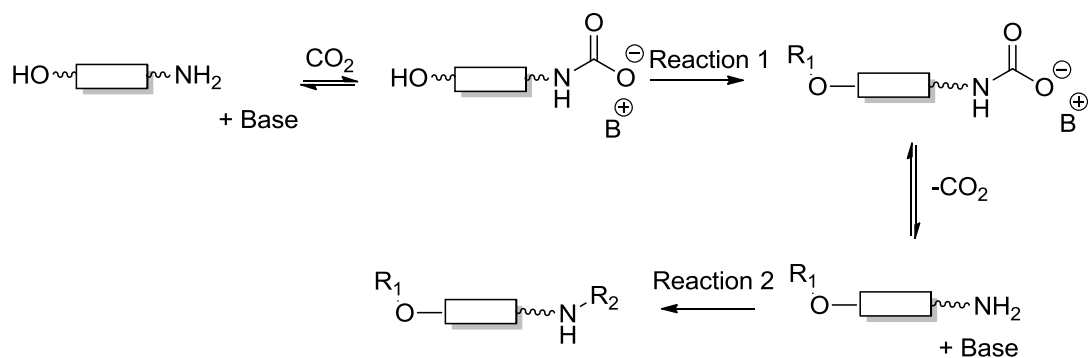
Figure 5.4. *In-situ* **amine protection during a chemoselective reaction**

- Alternative amine-containing reactions should be investigated. Nucleophilic acyl substitutions have been studied and future work will include Suzuki coupling reactions; however this amine protection strategy can be applied to a range of organic syntheses.

5.5 Reversible Ionic Liquids as Switchable Surfactants for Gold Nanoparticle

Synthesis

5.5.1 <u>Conclusions</u>

Gold nanoparticles were successfully synthesized using reversible ionic liquids. Methyl orange was used in our studies as a solubility probe and a mock gold precursor. Methyl orange has a negligible solubility in a hydrocarbon such as hexane; however it is known that methyl orange can become solubilized in hydrocarbon solvents when supported by a micellar system.[3] It is postulated that the reversible ionic species form reverse micelle structures in hexane that effectively solubilize methyl orange. Likewise, the reversible ionic species in hexane provides an effective template for the synthesis of monodisperse gold nanoparticles (6.1 +/- 0.9 and 13.3 +/- 3.0 nm with TPSA and THSA, respectively).Upon switching the ionic species to their neutral form by heating the solution to 65°C, the nanoparticles were deposited onto a solid support (silica). The reversible ionic liquid system offers two significant advantages toward a greener and more sustainable synthesis and deposition of nanoparticles: (1) an additional surfactant is not required, and (2) due to the reversible nature of the ionic liquids, a facile and waste-reduced deposition method exists.

5.5.2 <u>Recommendations</u>

It has not yet been shown conclusively that the RevIL in a hydrocarbon continuous phase forms reverse micelles. It is suggested in the literature that a disperse phase is needed to control the size of reverse micelles and achieve low polydispersity.[4] A disperse phase will need to be capable of dissolving $HAuCl_4$, but highly immiscible with the hydrocarbon continuous phase. The disperse phase must not react with the RevIL,

which eliminates many candidates. At this point, the most promising candidate is DMF; however, it is unclear if DMF as an additive will stabilize the carbamic acid species as presented in Chapter 3. The Dynamic Light Scattering experiments previously described should be repeated, using a RevIL-DMF-hydrocarbon system. Small angle x-ray scattering (SAXS) measurements would allow us to characterize smaller reverse micelles that do not contain a disperse phase in the core.

Despite heating the solution of gold nanoparticles and RevIL to 65°C for 24 hours, some nanoparticles remained in solution. To verify that the RevIL is completely reversed, FTIR studies of the solution of RevIL in hexane could be completed at 65°C to monitor the disappearance of the carbonyl peak of the RevIL. The second possibility is that the silylamine may act as an efficient capping agent. Elemental analysis of both the unsupported and supported nanoparticles should allow us to determine if silylamine is still present following solvent washes and drying.

The ultimate goal of this study is to determine the catalytic activity of the synthesized nanoparticles and compare with literature results. Supported gold nanoparticles have been used as catalysts in the hydrochlorination of acetylene, the epoxidation of propylene, and for the selective oxidation of alcohols.[5] The gold nanoparticles we have reproducibly synthesized have an average diameter of 5 nm, a size commonly used in oxidations.[6] A proof-of-concept reaction would be the oxidation of benzyl alcohol to benzaldehyde, as shown in Figure 5.5.
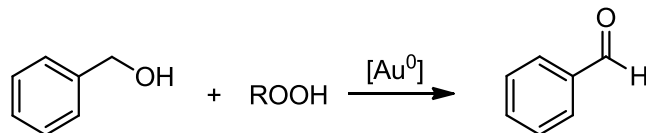
Figure 5.5. Proof-of-concept reaction for gold nanoparticles. Oxidation of benzyl alcohol to benzaldehyde with a peroxide oxidant and a gold nanoparticle catalyst.

The use of reversible ionic liquids as switchable surfactants for gold nanoparticle synthesis will serve as a model for future synthesis of metal nanoparticles. We plan to use our optimized reaction conditions from the gold nanoparticle synthesis to synthesize platinum and palladium nanoparticles; the resulting nanoparticles will be used in proof of concept reactions to test their activity and compare to reported values in the literature.[7]

5.6 References

1.   Dugas, R. E.; Rochelle, G. T., CO_2 absorption rate into concentrated aqueous monoethanolamine and piperazine. *Journal of Chemical & Engineering Data* **2011,** *56* (5), 2187-2195; Dang, H. Y.; Rochelle, G. T., CO_2 absorption rate and solubility in monoethanolamine/piperazine/water. *Separation Science and Technology* **2003,** *38* (2), 337-357; Rochelle, G. T., Amine Scrubbing for CO2 Capture. *Science* **2009,** *325* (5948), 1652-1654.

2.   Ficke, L. E.; Brennecke, J. F., Interactions of Ionic Liquids and Water. *Journal of Physical Chemistry B* **2010,** *114* (32), 10496-10501.

3.   Liu, J. H.; Cheng, S. Q.; Zhang, J. L.; Feng, X. Y.; Fu, X. G.; Han, B. X., Reverse micelles in carbon dioxide with ionic-liquid domains. *Angewandte Chemie-International Edition* **2007,** *46* (18), 3313-3315.

4.   Ravey, J. C.; Buzier, M.; Picot, C., Micellar Structures of Nonionic Surfactants in Apolar Media. *Journal of Colloid and Interface Science* **1984,** *97* (1), 9-25; Tanaka, R.; Yokoyama, T.; Sameshima, K.; Kawase, T., Growth of AOT reversed micelles and the solvent effect investigated by dielectric and light-scattering measurements. *Bulletin of the Chemical Society of Japan* **2005,** *78* (4), 599-603.

5.   Fierro-Gonzalez, J. C.; Gates, B. C., Catalysis by gold dispersed on supports: the importance of cationic gold. *Chemical Society Reviews* **2008,** *37* (9), 2127-2134;

Hutchings, G. J., Vapor-Phase Hydrochlorination of Acetylene-Correlation of Catalytic Activity of Supported Metal Chloride Catalysts. *Journal of Catalysis* **1985,** *96* (1), 292-295; Stangland, E. E.; Stavens, K. B.; Andres, R. P.; Delgass, W. N., Characterization of gold-titania catalysts via oxidation of propylene to propylene oxide. *Journal of Catalysis* **2000,** *191* (2), 332-347; Corma, A.; Garcia, H., Supported gold nanoparticles as catalysts for organic reactions. *Chemical Society Reviews* **2008,** *37* (9), 2096-2126; Abad, A.; Concepcion, P.; Corma, A.; Garcia, H., A collaborative effect between gold and a support induces the selective oxidation of alcohols. *Angewandte Chemie-International Edition* **2005,** *44* (26), 4066-4069.

6.   Haruta, A., When gold is not noble: Catalysis by nanoparticles. *Chemical Record* **2003,** *3* (2), 75-87; Haruta, M., Catalysis of gold nanoparticles deposited on metal oxides. *Cattech* **2002,** *6* (3), 102-115; Liu, Y. M.; Tsunoyama, H.; Akita, T.; Tsukuda, T., Size Effect of Silica-supported Gold Clusters in the Microwave-assisted Oxidation of Benzyl Alcohol with H2O2. *Chemistry Letters* **2010,** *39* (3), 159-161; Oliveira, R. L.; Kiyohara, P. K.; Rossi, L. M., High performance magnetic separation of gold nanoparticles for catalytic oxidation of alcohols. *Green Chemistry* **2010,** *12* (1), 144-149; Choudhary, V. R.; Dumbre, D. K.; Bhargava, S. K., Oxidation of Benzyl Alcohol to Benzaldehyde by tert-Butyl Hydroperoxide over Nanogold Supported on TiO2 and other Transition and Rare-Earth Metal Oxides. *Industrial & Engineering Chemistry Research* **2009,** *48* (21), 9471-9478.

7.   Ikeda, S.; Ishino, S.; Harada, T.; Okamoto, N.; Sakata, T.; Mori, H.; Kuwabata, S.; Torimoto, T.; Matsumura, M., Ligand-free platinum nanoparticles encapsulated in a hollow porous carbon shell as a highly active heterogeneous hydrogenation catalyst. *Angewandte Chemie-International Edition* **2006,** *45* (42), 7063-7066; Ley, S. V.; Stewart-Liddon, A. J. P.; Pears, D.; Perni, R. H.; Treacher, K., Hydrogenation of aromatic ketones, aldehydes, and epoxides with hydrogen and Pd(0)EnCat (TM) 30NP. *Beilstein Journal of Organic Chemistry* **2006,** *2*.

APPENDIX A - ADDITIONAL INFORMATION ON SILYLAMINES AS REVERSIBLE IONIC LIQUIDS FOR CARBON DIOXIDE CAPTURE

A.1 Introduction

This appendix provides additional information referenced in Chapter 2. It includes the synthesis of the silylamines presented. Syntheses were primarily performed by chemists in the Eckert-Liotta research group.

A.2 Synthesis of Silylamines

A.2.1 Materials

All chemicals were purchased from Sigma-Aldrich and used as received unless otherwise noted. Chemicals used were: triethylsilane (99%); tripropylsilane (99%); trihexylsilane (99%); allylamine (99+%); platinum(0)-1,3-divinyl-1,1,3,3-tetramethyl disiloxane complex solution in xylene (Karstedt's catalyst; 2 wt% Pt) (Pt-DVDS); toluene (anhydrous, 99.8%); 0.5 *M* 2,8,9-triisobutyl-2,5,8,9-tetraaza-1-phospha bicyclo[3.3.3]undecane in diethyl ether; dimethylethylsilane (98%); 4-amino-1-butene (97%); tetrahydrofuran (THF; anhydrous, inhibitor-free, ≥99.9%); 3-chloro-1-butene (96%); potassium phthalimide (98%); hydrazine (anhydrous, 98%); 2-methyl-3-butyn-2-amine (95%); N-vinylphthalimide (99%); Pd on activated charcoal (5 wt% Pd basis); Celite 545; hexanes (anhydrous, mixture of isomers, ≥99%); and methanol (anhydrous, 99.8%). Propargylamine (95%) was acquired from TCI America, used as received, and stored in the dark under inert atmosphere at 5°C. 2-methylallylamine (97%) was purchased from Acros Organics and used as received. All chemicals were stored under

inert dry atmosphere. The CO_2 employed was SFC grade from Airgas, certified to contain less than < 250 ppb H_2O with a purity of 99.9999%.

A.2.2 3-(aminopropyl)triethylsilane (TEtSA), 3-(aminopropyl)tripropylsilane (TPSA), and 3-(aminopropyl)trihexylsilane (THSA)
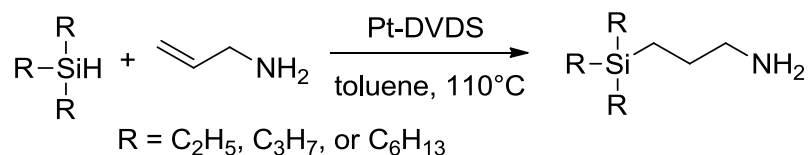
Figure A.1. Synthesis of TEtSA, TPSA, and THSA

Trialkylsilane (80 mmol, 1 eq.) and Pt-DVDS (0.8 mmol, 0.001 eq.) were placed into a 3 neck round-bottom flask under nitrogen atmosphere at RT. The solution was dark yellow. Anhydrous toluene was then added (40 mL) under stirring. Allyl amine (160 mmol, 2 eq.) was added in one portion (reddish color was first observed to then quickly turn dark brown). The reaction mixture was heated to reflux (110°C). ^{1}H NMR was used to monitor the disappearance of starting trialkylsilane. Upon complete reaction, the reaction solution was cooled to RT and the toluene and excess allyl amine were evaporated under vacuum. The crude material was then distilled under reduced pressure to afford the pure, desired silylamine.
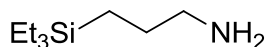
Figure A.2. 3-(aminopropyl)triethylsilane (TEtSA)

Yield: 89%, Distillation temperature/pressure: 75°C at 4 mmHg.

^{1}H NMR (400.13 MHz, CDCl$_3$), δ: 2.63 (t, 2H), 1.39 (m, 2H), 1.08 (s), 0.90 (t, 9H), 0.49 (q, 6H),0.49 (t, 2H)

^{13}C NMR (400.13 MHz, CDCl$_3$), δ: 45.47, 27.88, 7.90, 6.95, 2.87

168

Calculated % for C$_9$H$_{23}$NSi (MW: 173.37 g·mol^{-1}): C(62.35), H(13.37), N(8.08) Found: C(62.41), H(13.42), N(7.94)

$$Pr_3Si \diagup\diagdown\diagup NH_2$$
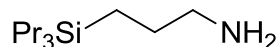
Figure A.3. 3-(aminopropyl)tripropylsilane (TPSA)

Yield: 96%, Distillation temperature/pressure: 84°C at 0.3 mmHg.

^{1}H NMR (400.13 MHz, CDCl$_3$), δ: 2.63 (t, 2H), 1.39 (m, 2H), 1.30 (m, 6H), 1.05 (s, 2H), 0.93 (t, 9H), 0.48 (m, 8H)

^{13}C NMR (400.13 MHz, CDCl$_3$), δ: 45.85, 28.30, 18.63, 17.45, 15.27, 9.55

Calculated % for C$_{12}$H$_{29}$NSi (MW: 215.45 g·mol^{-1}): C(66.90), H(13.57), N(6.50) Found: C(66.74), H(13.64), N(6.35)

$$Hex_3Si \diagup\diagdown\diagup NH_2$$
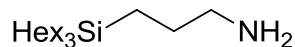
Figure A.4. 3-(aminopropyl)trihexylsilane (THSA)

Yield: 92%, Distillation temperature/pressure: 155°C at 3 mmHg.

^{1}H NMR (400.13 MHz, CDCl$_3$), δ: 2.62 (t, 2H), 1.37 (m, 2H,), 1.25 (s(br)), 1.17 (s, 2H), 0.86 (t, 9H), 0.47 (m, 8H)

^{13}C NMR (400.13 MHz, CDCl$_3$), δ: 45.87, 33.58, 31.53, 28.34, 23.84, 22.61, 14.11, 12.40, 9.45

Calculated % for C$_{21}$H$_{47}$NSi (MW: 341.69 g·mol^{-1}): C(73.82), H(13.86), N(4.10) Actual: C(72.87), H(13.59), N(4.07)

A.2.3 3-(aminopropyl)dimethylethylsilane (DMESA)
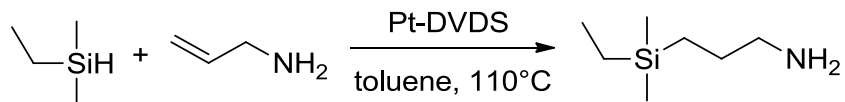
Figure A.5. Synthesis of DMESA

To a 3-neck 250 mL round bottomed flask fitted with a condenser and magnetic stir bar under inert atmosphere was added anhydrous toluene (80 mL, 0.751 mol), dimethylethylsilane (10.56 mL, 80 mmol), and 2 wt% Pt-DVDS in xylenes (1.82 mL; 1.60×10^{-4} mol Pt; 0.20% catalyst loading wrt silane). This was allowed to stir at room temperature for approximately five minutes, at which point allylamine (12 mL, 0.160 mol) was added and the reaction was heated to 110°C overnight. Reaction progress was monitored via ^{1}H NMR for the disappearance of the silane proton (~3.7 ppm). When this peak was no longer present, the reaction mixture was allowed to cool to room temperature; the solvent and excess allylamine was then removed via rotary evaporator. The product 3-(aminopropyl)dimethylethylsilane (58% isolated yield) was distilled from the catalyst under reduced pressure (bp: 38°C at 2.5 mmHg).

^{1}H NMR (400.13 MHz, CDCl$_3$, 25°C) δ = 2.61 (t, 2H), 1.37 (m, 2H), 1.15 (br, 2H), 0.44 (m, 4H), -0.09 (s, 6H)

^{13}C NMR (100.57 MHz, CDCl$_3$, 25°C) δ = 45.61, 28.22, 11.74, 7.24, 6.77, -4.04

Calculated % for C$_7$H$_{19}$NSi (MW: 145.32 g·mol^{-1}): C(57.86), H(13.18), N(9.64), Si(19.33); found: C (57.50), H(13.01), N(8.94)

A.2.4 (aminomethyl)triethylsilane (TESMA)
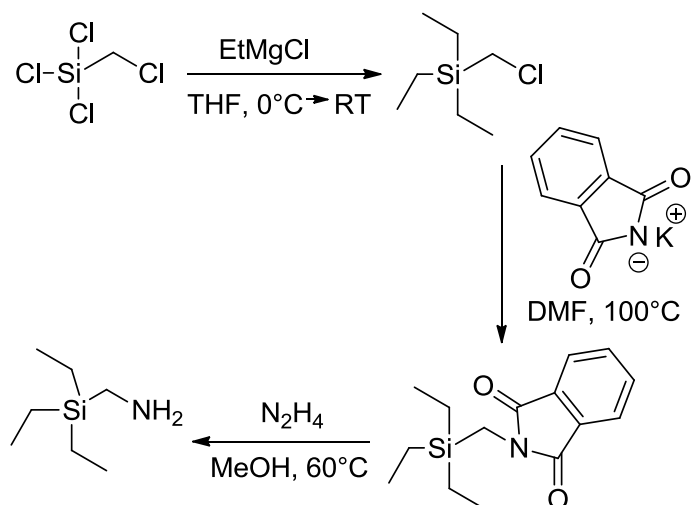
Figure A.6. Synthesis of TESMA

2-((Triethylsilyl)methyl)isoindoline-1,3-dione (25.92 g, 0.0945 mol) was dissolved in anhydrous MeOH (315 mL) under an inert atmosphere and stirred with mechanical stirring. Anhydrous hydrazine (8.9 mL, 0.284 mol) was added in one portion to the MeOH solution and the temperature of the solution was brought to 60°C. During the course of the reaction, phthalylhydrazide formation was evidenced by a cloudy-gel like precipitate. After 5 hours of reaction, the solution was cooled and 2M HCl was added until a solid white precipitate was formed in the single aqueous phase. The solid was filtered under vacuum and washed with more 2M HCl. The collected liquid layer was then basified with 1M NaOH until a pH of 14 was reached. Diethyl ether was added to extract the amine product. The ether was then washed with brine, dried over MgSO4 and removed at 45°C by distillation. The crude (aminomethyl)triethylsilane was attempted to be distilled under argon but it was noticed that as the temperature increased to 170°C a yellow sludge formed in the distillation flask. The heat was removed and the crude

distilled at 25°C at 0.6 mmHg to give 3.63 g of pure (aminomethyl)triethylsilane in a 27% isolated yield.

^{1}H NMR (400 Hz, CDCl$_3$) 2.24 (s, 2H), 1.74 (s, 2H), 0.95 (t, 9H), 0.57 (q, 6H)

^{13}C NMR (400 Hz, CDCl$_3$) 26.68, 7.36, 2.10

Calculated % for C$_7$H19NSi (MW: 145.32 g·mol^{-1}): Expected: C(57.86), H(13.18), N(9.64) found: C(56.56), H(13.28), N(9.13)

A.2.5 2-(aminoethyl)triethylsilane (TEtSEtA)
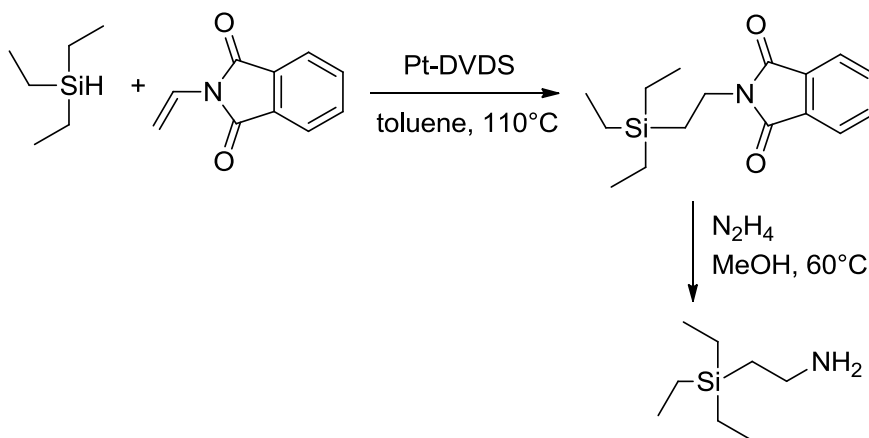
Figure A.7. Synthesis of TEtSEtA

Triethylsilane (72.8 g, 0.626 mol) and Pt-DVDS (3.0 mL of 2 % Pt solution in xylene, 0.29 mmol) were added to a 3-neck round bottom flask fitted with a reflux condenser under inert atmosphere. To the mixture was transferred N-vinylphthalimide (25 g, 0.144 mol) dissolved in 250 mL anhydrous toluene using a double-tipped needle. The mixture was brought to 110 °C and stirred for 2 days. After cooling, the reaction mixture was filtered through Celite and toluene was removed using a rotary evaporator. To the crude product was added hydrazine solution (35 wt. % in H$_2$O, 200mL, 2.16mol) and methanol 200 mL. The solution was heated to 60°C for 24 hours. After cooling, 150

mL of methanol was removed by distillation at atmospheric pressure, and the solution pH was adjusted to 1 using 6 N HCl aqueous solution at 0°C. The solution was filtered through Celite, and the mother liquor pH was adjusted to 12 using 30 % NaOH aqueous solution at 0°C. It was extracted using Et_2O (300 mL, 6 times). The combined ether solution was dried over anhydrous $MgSO_4$, and ether was removed by evaporation. The residual crude was distilled under reduced pressure (bp: 30°C at 1mmHg) to give 2-(triethylsilyl)ethanamine (5.75g) in 25 % yield (2 steps).

^{1}H NMR (400 MHz, $CDCl_3$), δ (ppm): 2.73 (t,2H), 1.16 (broad, 2H), 0.92 (t,9H), 0.77 (t, 2H), 0.50 (q, 6H)

^{13}C NMR (100 MHz, $CDCl_3$), δ (ppm): 38.40, 17.83, 7.53, 3.56

Calculated % for $C_8H_{21}NSi$ (MW: 159.34 g·mol^{-1}): C(60.30), H(13.28), N(8.79), Si(17.63) found: C(59.89), H(13.24), N(8.65)

A.2.6 4-(aminobutyl)triethylsilane (TEtSBA)
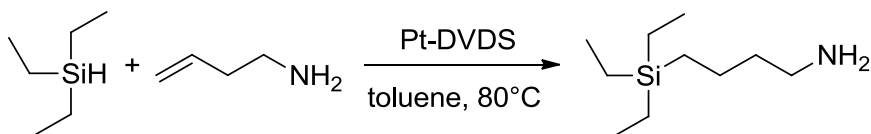
Figure A.8. Synthesis of TEtSBA

To a 3-neck 250 mL round bottomed flask fitted with a condenser and magnetic stir bar under inert atmosphere was added 2 wt% Pt-DVDS in xylenes (0.6% catalyst loading wrt silane, 8.01 mL, 0.7 mmol) and triethylsilane (12.21 g, 105 mmol); the solution turned dark yellow. To this was added anhydrous toluene (40 mL) and 4-amino-1-butene (5.0 g, 70.3 mmol). The solution was heated to 80°C for 20 hours. Reaction progress was monitored via ^{1}H NMR for the disappearance of the silane proton (~3.7 ppm). When this peak was no longer present, the reaction mixture was allowed to cool to

room temperature; the solvent and excess triethylsilane was then removed via rotary evaporator. The product 4-(aminobutyl)triethylsilane was distilled from the catalyst under reduced pressure (bp: 68°C at 1.95 mmHg) for an isolated yield of 66% (8.67 g; 46.3 mmol).

^{1}H NMR (400.13 MHz, CDCl$_3$, 25°C) δ = 2.62 (t, 2H), 1.40 (p, 2H), 1.27 (s, 2H), 1.17 (s, 2H), 0.86 (t, 9H), 0.44 (q, 8H)

^{13}C NMR (100.57 MHz, CDCl$_3$, 25°C) δ = 41.83, 37.95, 21.04, 11.09, 7.32, 3.16

Calculated % for C$_{10}$H$_{25}$NSi (MW: 187.40 g·mol^{-1}): C(64.09), H(13.45), N(7.47), Si(14.99); found: C(62.34), H(13.33), N(7.47)

A.2.7 4-(triethylsilyl)-butyl-2-amine (αMe-TEtSA)
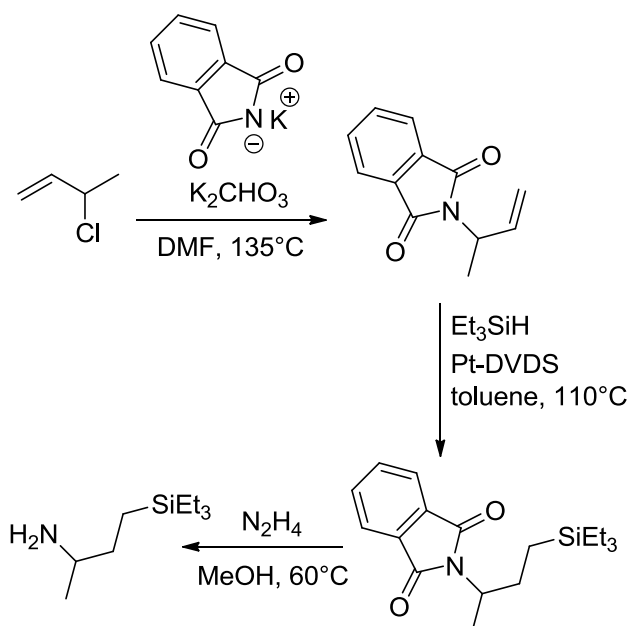
Figure A.9. Synthesis of αMe-TEtSA

Gabriel Synthesis

A typical synthesis of αMe-TEtSA was achieved via the series of reactions detailed below. In a round-bottomed flask fitted with a condenser, 3-chloro-1-butene

174

(9.05 g, 100 mmol), potassium phthalimide (24.17 g, 130 mmol), and potassium carbonate (4.14 g, 30 mmol) were added to DMF (90 mL, 0.969 mol) and heated at reflux overnight. The reaction mixture was then poured over ice, forming a brown precipitate, which was isolated via vacuum filtration. The solid was washed with 1 M NaOH (200 mL, 0.2 mol), distilled water (100 mL, 5.6 mol), 1 N HCl (100 mL, 0.1 mol), and distilled water (100 mL, 5.6 mol); it was then vacuum dried, resulting in a 67% yield of the desired 3-phthalimido-1-butene (mp: 76-79°C).

^{1}H NMR (400.13 MHz, CDCl$_3$, 25°C) δ = 7.82 (m, 2H), 7.70 (m, 2H), 6.19 (m, 1H), 5.23 (d, 1H), 5.15 (d, 1H), 4.93 (p, 1H), 1.58 (d, 3H)

^{13}CNMR (100.57 MHz, CDCl$_3$, 25°C) δ = 167.92, 136.80, 133.84, 133.02, 123.11, 116.33, 48.93, 18.21

Hydrosilylation

In a 250 mL 3-neck round-bottomed flask fitted with a condenser, the isolated 3-phthalimido-1-butene (20.1 g, 100 mmol) and 2 wt% Pt-DVDS in xylenes (1.54 mL, 1.35 x 10^{-4} mol Pt, 0.104% loading wrt silane) was added to anhydrous toluene (60 mL, 0.563 mol) under inert atmosphere. The reaction mixture was then heated to 50°C, at which point the protected amine became soluble. Triethylsilane (20.7 mL, 130 mmol) was then added to the reaction mixture, which was then heated to 110°C and kept at that temperature overnight. The reaction was allowed to cool; the solvent was removed via rotary evaporator and the crude 3-(phthalimidobutyl)triethylsilane was distilled under reduced pressure with a 75% yield of the desired product 3-(phthalimidobutyl)triethylsilane (bp: 120°C at 0.7 mmHg).

^{1}H NMR (400.13 MHz, CDCl$_3$, 25°C) δ = 7.82 (m, 2H), 7.70 (m, 2H), 4.23 (s, 1H), 2.01 (m,1H), 1.72 (m,1H), 1.46 (d, 3H), 0.88 (trip, 9H), 0.48 (q,7H), 0.37 (t of d, 1H)

^{13}C NMR (100.57 MHz, CDCl$_3$, 25°C) δ = 168.61, 133.73, 132.01, 123.01, 50.58, 28.14, 18.30, 8.42, 7.37, 3.10

Ing-Manske Deprotection

3-(phthalimidobutyl)triethylsilane (16.9 g, 53 mmol) was dissolved in anhydrous methanol (250 mL, 6.172 mol). Anhydrous hydrazine (5 mL, 187 mmol) was slowly added and the reaction mixture was heated at 60°C for 4 hours. A cloudy white network formed, which was precipitated via addition of 2 M HCl. The resulting solid was removed from the desired liquid product mixture via vacuum filtration and washed with distilled water (100 mL, 5.6 mol). The solvent was removed via rotary evaporator and NaOH was added to the crude product until the pH was greater than 9. Extraction with ether, drying with MgSO$_4$, and distillation under reduced pressure yielded the pure product, 4-(triethylsilyl)-butan-2-amine in 62% yield (bp: 73°C at 2.7 mmHg).

^{1}H NMR (400.13 MHz, CDCl$_3$, 25°C) δ = 2.74 (s, 1H), 1.26 (m, 2H), 1.16 (s, 2H), 1.03 (d, 3H), 0.90 (t, 9H), 0.49 (q and m overlapping, 8H)

^{13}C NMR (100.57 MHz, CDCl$_3$, 25°C) δ = 49.71, 34.18, 23.25, 7.48, 7.37, 3.14

Calculated % for C$_{10}$H$_{25}$NSi (MW: 187.40 g·mol^{-1}): C(64.09), H(13.45), N(7.47), Si(14.99); found: C(63.03), H(13.47), N(7.39)

A.2.8 2-methyl-4-(triethylsilyl)-butyl-2-amine (α,αDMe-TEtSA)

Figure A.10. Synthesis of α,αDMe-TEtSA

Hydrosilylation

A 3-neck 250 mL round bottomed flask was fitted with a condenser and stir bar and placed under argon. To this was added 2 wt% Pt-DVDS in xylenes (13.75 mL, 1.205 x 10^{-3} mol Pt; 1.268% catalyst loading wrt silane) and 0.5 M 2,8,9-triisobutyl-2,5,8,9-tetraaza-1-phosphabicyclo[3.3.3]undecane solution in diethyl ether (2.4 mL, 1.200 x 10^{-3} mol). The reaction mixture was heated at 60°C for 10 minutes. After cooling to room temperature, anhydrous inhibitor-free THF (80 mL, 0.9865 mol) was added to the flask, which was then cooled to approximately -10°C in an ice-and-brine bath. Triethylsilane (21.25 mL, 0.133 mol) was then added dropwise to the flask and allowed to stir for approximately 5 minutes. 2-methyl-3-butyn-2-amine (10 mL, 9.503 x 10^{-2} mol) was then added dropwise to the reaction mixture, which was kept in the ice bath until the large exotherm had ceased. The reaction was then allowed to stir at room temperature overnight; reaction progress was monitored by the disappearance of the terminal alkyne carbon in the ^{13}C NMR (approximately δ91). The solvent and unreacted silane were removed via rotary evaporator. Distillation under reduced pressure yielded the alkene

product 2-methyl-4-(triethylsilyl)but-3-en-2-amine as a clear oil (bp 60°C at 5 mmHg; 4.7772 g, 79.8% yield).

^{1}H NMR (400.13 MHz, CDCl$_3$, 25°C) δ = 6.10 (d, 1H), 5.55 (d, 1H), 1.17 (s, 2H), 1.14/1.13 (s overlapping, (6H)), 0.88 (t of d, 9H), 0.52 (q of d, 6H)

^{13}C NMR (100.57 MHz, CDCl$_3$, 25°C) δ = 157.50, 118.58, 52.24, 30.20, 7.28, 3.47

Hydrogenation

Hydrogenation of the alkene was carried out in a Parr reactor. The reactor was first loaded with 5 wt% Pd/C (0.1367 g, 6.42 x 10^{-5} mol Pd; 0.11% catalyst loading wrt alkene) and then purged several times with dry nitrogen. Anhydrous ethanol (30 mL, 0.513 mol) and 2-methyl-4-(triethylsilyl)but-3-en-2-amine (11.9032 mL, 59.69 mmol) were added to the reactor, which was then pressurized with hydrogen (80 psi) and heated at 50°C for 12 hours. Upon cooling, excess H$_2$ was vented, and the catalyst was removed from the reaction mixture via filtration with Celite. ^{1}H NMR of the product mixture revealed the total absence of any alkene peaks, indicating that the reaction had gone to completion. Removal of the solvent via rotary evaporator yielded the desired saturated crude product, which was then distilled at reduced pressure to yield 2-methyl-4-(triethylsilyl)-butyl-2-amine as a clear oil (9.1850 g, bp 65°C at 1.5 mmHg; 76.4% isolated yield).

^{1}H NMR (400.13 MHz, CDCl$_3$, 25°C) δ = 1.24 (m 2H), 1.09 (s, 2H), 0.99 (s, 6H), 0.86 (t, 9H), 0.42 (q, 8H)

^{13}C NMR (100.57 MHz, CDCl$_3$, 25°C) δ = 50.20, 39.02, 29.81, 7.59, 5.22, 3.30

Calculated % for C$_{11}$H$_{27}$NSi (MW: 201.42 g·mol^{-1}): C(65.59), H(13.51), N(6.95), Si(13.94); found: C(64.03), H(13.51), N(6.67)

A.2.9 2-methyl-3-(triethylsilyl)propylamine (βMe-TEtSA)
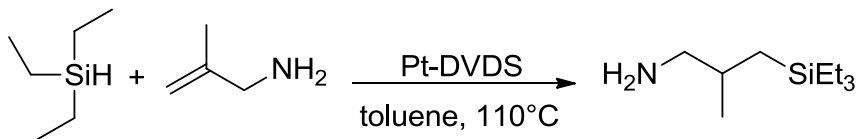
Figure A.11. Synthesis of βMe-TEtSA

A 3-neck 250 mL round-bottomed flask was fitted with a condenser and stir bar and placed under argon. Anhydrous toluene (40 mL, 0.376 mol) was added to the flask, followed by triethylsilane (16.5 mL, 103 mmol; 2.58 M) and 2 wt% Pt-DVDS in xylenes (2.70 mL, 2.395 x 10^{-4} mol Pt; 0.23% loading wrt silane). The reaction mixture was allowed to stir at room temperature for several minutes; 2-methylallylamine (5 g, 70.3 mmol; 1.75 M) was then added and the reaction mixture was heated at 110°C for 24 hours. Reaction progress was checked via ^{1}H NMR for disappearance of the vinyl peaks of 2-methylallylamine. The solvent was removed via rotary evaporator and the product distilled under reduced pressure to yield 10.0744 g product (53.7 mmol; 76.4% isolated yield).

^{1}H NMR (400.13 MHz, CDCl$_3$, 25°C) δ = 2.51 (m, 1H), 2.43 (m, 1H), 1.54 (m, 1H), 1.11 (s, 2H), 0.91 (t, 9H), 0.90 (d, 3H), 0.51 (q, 6H), 0.61 (d of d, 1H), 0.32 (d of d, 1H)

^{13}C NMR (100.57 MHz, CDCl$_3$) δ = 51.75, 32.79, 20.39, 16.69, 7.46, 4.01

Calculated % for C$_{10}$H$_{25}$NSi (MW: 187.40 g·mol^{-1}): C(64.09), H(13.45), N(7.47), Si(14.99); found: C(63.31), H(13.54), N(7.33)

A.2.10 (*trans*)-3-(Triethylsilyl)prop-2-en-1-amine (*trans*-TEtSA)
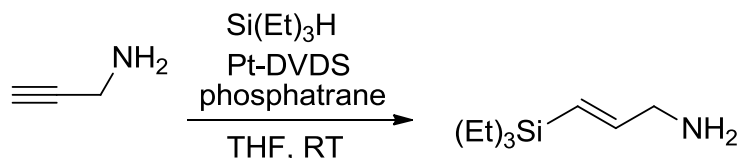
Figure A.12. Synthesis of trans-TEtSA

A typical reaction was carried out as follows. In a 3-neck 250 mL round bottomed flask fitted with a condenser under inert atmosphere, 17.8 mL 2% Pt-DVDS in xylenes (1.560×10^{-3} mol Pt; 1.00% loading wrt silane) was combined with 3.1 mL 0.5 M 2,8,9-triisobutyl-2,5,8,9-tetraaza-1-phosphabicyclo[3.3.3]undecane solution (1.625×10^{-3} mol) in diethyl ether. The reaction mixture was heated at 60°C for 10 minutes and then allowed to cool to room temperature. 100 mL anhydrous inhibitor-free THF (1.233 mol) was added to the flask, which was then cooled to approximately -10°C in an ice-and-brine bath. 27.5 mL triethylsilane (0.172 mol) was then added dropwise to the flask and allowed to stir for approximately 5 minutes. 10 mL of propargylamine (0.156 mol) was then added dropwise to the reaction mixture, which was kept in the ice bath until the large exotherm had ceased. The reaction was then allowed to stir at room temperature overnight; reaction progress was monitored by the disappearance of the terminal alkyne carbon in the ^{13}C NMR (approximately δ91). The solvent and excess triethylsilane were then removed via rotary evaporator, and the product was distilled under reduced pressure (bp: 75°C at 6 mmHg) to yield 12.1926 g of the trans-isomer only (0.0711 mol; 45.57% yield).

^{1}H NMR (400.13 MHz, CDCl$_3$, 25°C) 6.13 (dt, J = 18.8, 4.8 Hz, 1H), 5.67 (dt, J = 18.9, 1.8 Hz, 1H), 3.33 (dd, J = 4.8, 1.8 Hz, 2H), 1.12 (s, 2H) 0.98 (t, J = 7.9 Hz, 9H) 0.57 (q, J = 7.9 Hz, 6H)

^{13}C NMR (100.57 MHz, CDCl$_3$, 25°C) 149.10, 124.22, 47.19, 7.55, 3.70

Calculated % for $C_9H_{21}NSi$ (MW: 171.36 g·mol^{-1}): C(63.08), H(12.35), N(8.17), Si(16.39); found: C(62.34), H(12.36), N(7.67)

A.2.11 (*trans*)-2-methyl-4-(triethylsilyl)but-3-en-2-amine (*trans*-α,αDMe-TEtSA)

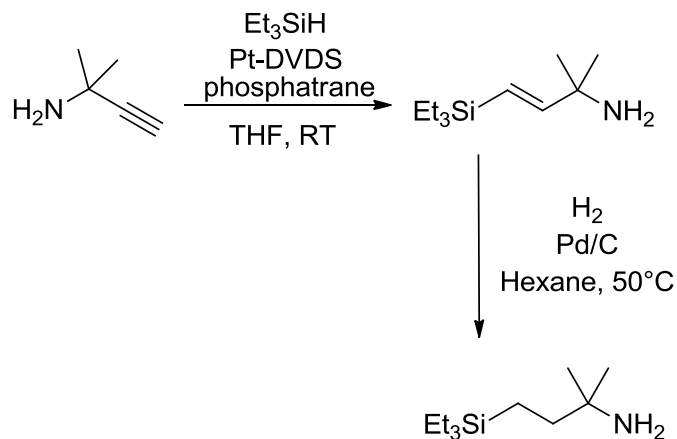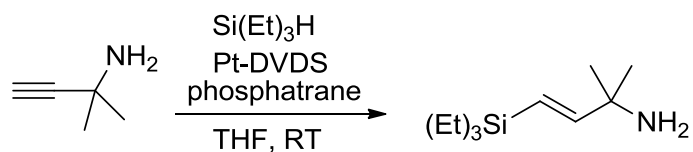**Figure A.13. Synthesis of trans-α,αDMe-TEtSA**

A 3-neck 250 mL round bottomed flask was fitted with a condenser and stir bar and placed under argon. To this was added 2 wt% Pt-DVDS in xylenes (13.75 mL, 1.205 x 10^{-3} mol Pt; 1.268% catalyst loading wrt silane) and 0.5 M 2,8,9-triisobutyl-2,5,8,9-tetraaza-1-phosphabicyclo[3.3.3]undecane solution in diethyl ether (2.4 mL, 1.200 x 10^{-3} mol). The reaction mixture was heated at 60°C for 10 minutes. After cooling to room temperature, anhydrous inhibitor-free THF (80 mL, 0.9865 mol) was added to the flask, which was then cooled to approximately -10°C in an ice-and-brine bath. Triethylsilane (21.25 mL, 0.133 mol) was then added dropwise to the flask and allowed to stir for approximately 5 minutes. 2-methyl-3-butyn-2-amine (10 mL, 9.503 x 10^{-2} mol) was then added dropwise to the reaction mixture, which was kept in the ice bath until the large exotherm had ceased. The reaction was then allowed to stir at room temperature overnight; reaction progress was monitored by the disappearance of the terminal alkyne carbon in the ^{13}C NMR (approximately δ91). The solvent and unreacted silane were removed via rotary evaporator. Distillation under reduced pressure yielded the alkene product 2-methyl-4-(triethylsilyl)but-3-en-2-amine as a clear oil (bp 60°C at 5 mmHg; 4.7772 g, 79.8% yield).

^{1}H NMR (400.13 MHz, CDCl$_3$, 25°C) δ = 6.10 (d, 1H), 5.55 (d, 1H), 1.17 (s, 2H), 1.14/1.13 (s overlapping, (6H)), 0.88 (t of d, 9H), 0.52 (q of d, 6H)

^{13}C NMR (100.57 MHz, CDCl$_3$, 25°C) δ = 157.50, 118.58, 52.24, 30.20, 7.28, 3.47

Calculated % for C$_{11}$H$_{25}$NSi (MW: 199.41 g·mol^{-1}): C(66.25), H(12.64), N(7.02), Si(14.08); found: C(64.81), H(12.41), N(6.55)

A.2.12 (*trans*)-2-methyl-4-(tripropylsilyl)-butyl-2-amine (*trans*-α,αDMe-TPSA)
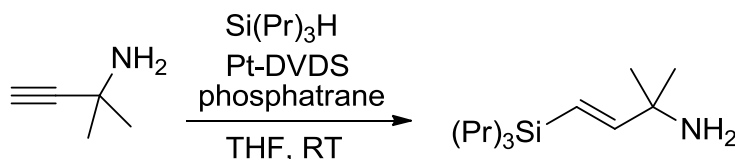
Figure A.14. Synthesis of trans-α,αDMe-TPSA

Synthesized in the same manner as trans-α,αDMe-TEtSA. A 3-neck 250 mL round bottomed flask was fitted with a condenser and stir bar and placed under argon. To this was added 2 wt% Pt-DVDS in xylenes (13.75 mL, 1.205 x 10^{-3} mol Pt; 1.268% catalyst loading wrt silane) and 0.5 M 2,8,9-triisobutyl-2,5,8,9-tetraaza-1-phosphabicyclo[3.3.3]undecane solution in diethyl ether (2.4 mL, 1.200 x 10^{-3} mol). The reaction mixture was heated at 60°C for 10 minutes. After cooling to room temperature, anhydrous inhibitor-free THF (80 mL, 0.9865 mol) was added to the flask, which was then cooled to approximately -10°C in an ice-and-brine bath. Tripropylsilane (21.25 mL, 0.133 mol) was then added dropwise to the flask and allowed to stir for approximately 5 minutes. 2-methyl-3-butyn-2-amine (10 mL, 9.503 x 10^{-2} mol) was then added dropwise to the reaction mixture, which was kept in the ice bath until the large exotherm had ceased. The reaction was then allowed to stir at room temperature overnight; reaction progress was monitored by the disappearance of the terminal alkyne carbon in the ^{13}C NMR (approximately δ91). The solvent and unreacted silane were removed via rotary

evaporator. Distillation under reduced pressure yielded the alkene product 2-methyl-4-(tripropylsilyl)-butyl-2-amine as a clear oil (68.1% yield).

^{1}H NMR (400.13 MHz, CDCl$_3$, 25°C) δ = 5.85 (d, 1H), 5.35 (d, 1H), 1.06 (s (br) overlapping sex, 8 H), 0.88 (s, 6H), 0.67 (t, 9H), 0.29 (d overlapping t, 6H)

^{13}C NMR (100.57 MHz, CDCl$_3$, 25°C) δ = 156.74, 119.31, 51.84, 29.79, 18.12, 17.01, 15.10

Calculated % for C$_{14}$H$_{31}$NSi (MW: 241.49 g·mol^{-1}): C(69.63), H(12.94), N(5.80), Si(11.63); found: C(68.93), H(12.96), N(5.29)

A.2.13 N-methyl-3-(triethylsilyl)propan-1-amine (STEtSA)
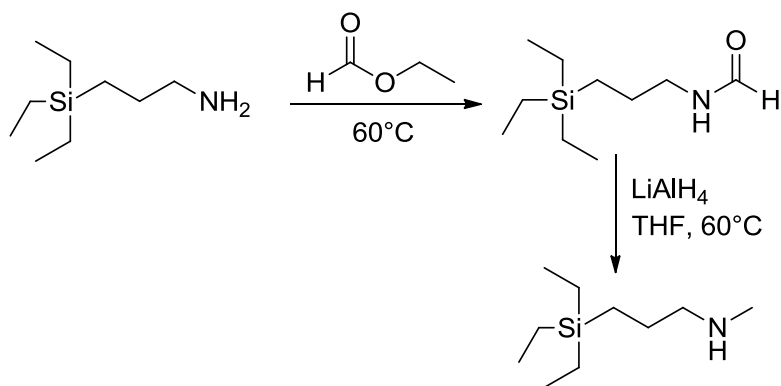
Figure A.15. Synthesis of STEtSA

Formylation

To a round bottomed flask fitted with a condenser and magnetic stir bar under inert atmosphere was added 3-(aminopropyl)triethylsilane (8.69 g, 50 mmol). This was cooled to 10°C; ethylformate (5.25 mL, 65 mmol) was added then added dropwise over 15 minutes. The solution was then heated to 60°C and stirred for 3 hours. The byproduct EtOH and excess ethylformate were then removed under reduced pressure to yield 9.72 g (48.27 mmol) of the desired product N-(3-(triethylsilyl)propyl)formamide in 97% yield.

^{1}H NMR (400.13 MHz, CDCl$_3$, 25°C) δ = 8.13 (s)/8.01 (d)(1H), 5.96 (s, 1H), 3.23 (q)/3.15 (q) (2H), 1.47 (s, 2H), 0.89 (t, 9H), 0.48 (q, 8H)

183

^{13}C NMR (100.57 MHz, CDCl$_3$, 25°C) δ = 161.19, 41.43, 24.09, 8.51, 7.37, 3.13

Reduction

To a round bottomed flask fitted with a condenser and magnetic stir bar under inert atmosphere was added anhydrous THF (80 mL, 0.9865 mol) and N-(3-(triethylsilyl)propyl)formamide (8.49 g, 42 mmol). This solution was heated to 60°C, and LiAlH$_4$ in THF (50.7 mL, 50.7 mmol, 1 M) was added slowly over 45 minutes. An exotherm was observed. The reaction mixture was stirred for 18 hours at 60°C, at which point the resulting mixture was cooled to room temperature. DI H$_2$O (2.5 mL, 0.139 mol) and 10% NaOH (5 mL, 1.25 mmol) were added. An additional aliquot of H$_2$O (10.5 mL, 0.58 mol)) was then added; the mixture was filtered through Celite, then washed with hexane and MeOH. The organic layer was separated; the aqueous layer was washed with hexane, which was then combined with the previous organic layer. The solution was then washed with brine and dried with MgSO$_4$. The solvents were removed via rotary evaporator. The resulting liquid was distilled under reduced pressure at 1 mmHg and 48°C to provide N-methyl-3-(triethylsilyl)propan-1-amine (5.68 g, 30.3 mmol), corresponding to a 73% isolated yield.

^{1}H NMR (400.13 MHz, CDCl$_3$, 25°C) δ = 2.54 (t, 2H), 2.42 (s, 3H), 1.46 (s, 2H), 1.37 (s, 1H), 0.91 (t, 9H), 0.50 (q, 8H)

^{13}C NMR (100.57 MHz, CDCl$_3$, 25°C) δ = 55.70, 36.37, 24.09, 8.73, 7.42, 3.23

Calculated % for C$_{10}$H$_{25}$NSi (MW: 187.40 g·mol^{-1}): C(64.09), H(13.45), N(7.47), Si(14.99); found: C(63.12), H(13.47), N(7.47)

A.2.14 <u>N-methyl-3-(aminopropyl)dimethylethylsilane (SDMESA)</u>
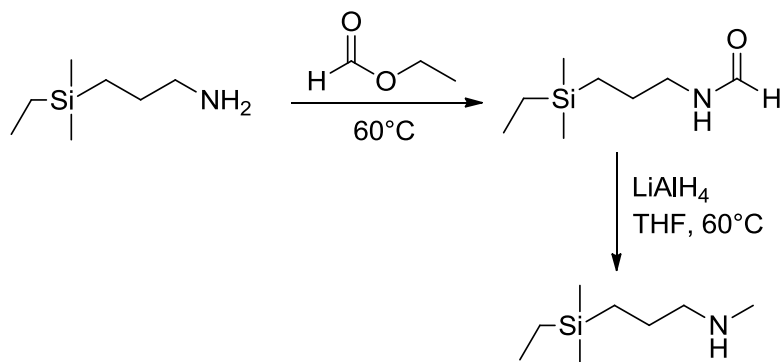
Figure A.16. Synthesis of SDMESA

Formylation

3-(Aminopropyl)dimethylethylsilane (DMEtSA) (7.3 g, 0.05 mol) was added to a RB flask under argon. Ethylformate (5.25 mL, 0.065 mol) was added dropwise over 15 minutes at 10°C. The temperature of the solution was increased to 60°C and stirred for 4 hours. The solution was then cooled and rotovapped to remove the by-product, EtOH, and excess ethylformate to provide 8.47 g of N-(3-(dimethylethylsilyl)propyl)formamide in 98% yield.

^{1}H NMR (400 Hz, CDCl$_3$) 8.14 (s)/ 8.00 (d) (1H), 5.79 (s, 1H), 3.25 (q)/3.16(q) (2H), 1.48 (s, 2H), 0.89 (t, 3H), 0.47 (q, 4H), -0.06 (s, 6H)

^{13}C NMR (400 Hz, CDCl$_3$) 161.11, 41.28, 24.12, 11.92, 7.25, 6.68, 4.07

Reduction

N-(3-(dimethylethylsilyl)propyl)formamide (7.83 g, 0.0452 mol) was added to 120 mL of anhydrous THF under an inert atmosphere in a RB flask. The solution temperature was brought to 60°C and solid LiAlH$_4$ (3.091 g, 0.081 mol) was added

slowly via solid addition arm over 30 minutes. After stirring for 18 hours at 60°C, the resulting mixture was cooled with a dry/ice acetone bath to keep the temperature at about 0°C. To it was added 3 mL H_2O followed by 6 mL of a 10% NaOH solution. 12 mL of H_2O were then added and the entire mixture was filtered through a pad of Celite and washed with THF and H_2O. The collected solution was then introduced into a separatory funnel and heavily brined with NaCl. The organic layer was separated. The aqueous layer was washed with hexane and the organic layer was combined with the previous. They were both washed with brine and dried over $MgSO_4$. The solvents were removed via rotovap distillation. The resulting liquid was distilled under reduced pressure at 3.4 mmHg and 36°C to provide 3.54 g of the N-methyl-3-(dimethylethylsilyl)propan-1-amine corresponding to a 49% isolated yield.

^{1}H NMR (400 Hz, CDCl3) 2.47 (t, 2H), 2.35 (s, 3H), 1.40 (s, 2H), 1.00 (s, 1H), 0.84 (t, 3H), 0.40 (q, 2H), -0.12 (s, 6H)

^{13}C NMR (400 Hz, CDCl3) 55.47, 36.32, 24.10, 12.15, 7.21, 6.73, -4.10

Expected: C(60.30), H(13.28), N(8.79), Si(17.63) found: C(58.97), H(13.17), N(8.42)

APPENDIX B - QUANTITATIVE REFLECTANCE SPECTROSCOPY: THEORY AND APPLICATION

B.1 Introduction

Reflectance spectroscopy is a powerful tool for measuring both qualitatively and quantitatively the characteristic absorption of a chemical species. Infrared spectroscopy is a low-cost, versatile technique that is used for the analysis of pure compounds and mixtures. As a result, nearly all researchers have access to a Fourier Transform Infrared (FTIR) Spectrophotometer.

B.2 Background

Spectroscopy is the study of the behavior of the molecules upon exposure to radiation. The range of frequencies of electromagnetic radiation falls on an electromagnetic spectrum and is classified as follows:
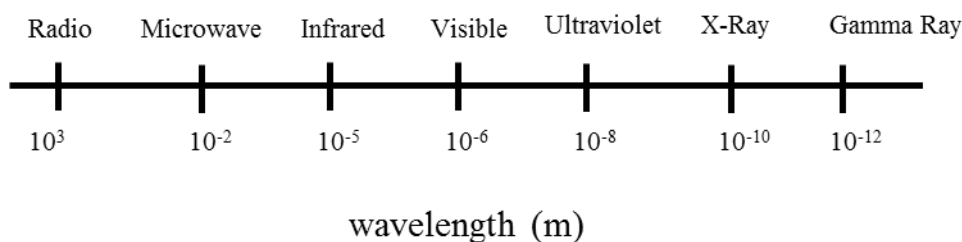
Figure B.1. The electromagnetic spectrum

The radiation is split into three regions: far (100-30μm); mid (30-2.5 μm) and near (2.5-0.8 μm). The mid-IR region is used for the studies reported here with a standard deuterated L-alanine doped triglycine sulphate (DLaTGS) detector. The detection of the signal after it has been absorbed by the sample produces the IR spectra. Infrared radiation

is absorbed by a molecule and converted into energy of molecular vibration at temperatures above absolute zero. The specific vibrations correspond to the configuration of the atoms and bonds that comprise the molecule. For example, there are six major modes of vibration in the mid-IR region: scissoring (sci), symmetric and asymmetric stretching (str), rocking (rock) wagging (wag), bending (bend) and twisting (twi). [1]

The assignments for stretching frequencies may be approximated using Hooke's law. Like a spring, two atoms are connected by a bond that may be treated as a simple harmonic oscillator as shown in Equation B.1.[2]

$$\upsilon = \frac{1}{2\pi c} \sqrt{\frac{f}{(M_x M_y)/(M_x + M_y)}} \qquad \textbf{Equation B.1}$$

where υ is vibrational frequency (cm^{-1}), c is the velocity of light (cm·s^{-1}), f is the bond force constant (dyne·cm^{-1}), and M_x and M_y are the masses (g) of atom x and atom y, respectively. The bond force constant can be correlated with bond order and bond strength, so as bond strength decreases, the frequency of the bond vibration will also decrease. To observe a vibration in the IR spectrum, the vibrations must result in rotation, or a change in the dipole. Examples of "IR inactive" vibrations are found in diatomic gases, and the symmetric stretch of CO_2. Approximations of stretching frequencies for a selection of vibrations are shown below in Table B.1 calculated using Hooke's law. [1] Also shown in Table B.1 are the observed absorption regions, which in some cases vary from the calculated values due to coupled interactions and both inter- and intra-molecular interactions.

Table B.1 IR absorption regions calculated using Hookes's law and observed values

Bond Type	Force Constant (f) [dyne/cm]	Absorption Region (cm^{-1})	
		Calculated	Observed
C - O	5.0 x 105	1113	1300-800
C - C	4.5 x 105	1128	1300-800
C - N	4.9 x 105	1135	1250-1000
C = C	9.7 x 105	1657	1900-1500
C = O	12.1 x 105	1731	1850-1600
C ≡ C	15.6 x 105	2101	2150-2100
C - D	5.0 x 105	2225	2250-2080
C - H	5.0 x 105	3032	3000-2850
O - H	7.0 x 105	3553	3800-2700

Based on these calculated and observed absorption regions, the presence of certain bond types, or functional groups may be identified in the IR spectrum.

B.3 Attenuated Total Reflectance Spectroscopy

Reflectance spectroscopy is particularly useful for samples that may not be analyzed using transmission spectroscopy. Application of the Beer-Lambert Law (Equation B.2) demonstrates that the absorbance is directly proportional to the concentration and the pathlength of the sample.

$$A = log\frac{1}{T} = \varepsilon bc$$ **Equation B.2**

Samples that are too dense will essentially saturate the detector, and as a result, the spectrum will appear as a flat line. To overcome this challenge, reflectance spectroscopy may be used without the need for further sample preparation or modification. Reflectance spectroscopy can be divided into two categories—internal or external reflectance. For this work Attenuated Total Reflectance was used for internal reflectance measurements, shown in Figure B.2 below.
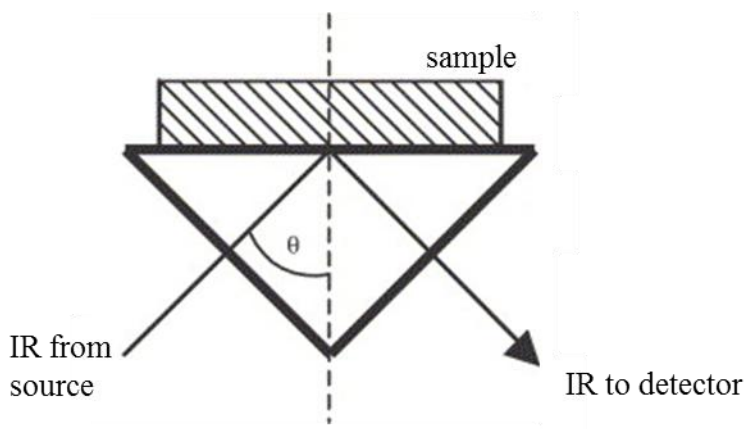
Figure B.2. Schematic of single reflectance ATR-FTIR spectroscopy

Internal reflectance occurs when the ATR crystal is a highly refractive infrared transmitting material. The internal reflectance results in an evanescent wave at the crystal surface that extends into the sample. The depth of penetration is dependent on the crystal material and angle of incidence for the IR beam travelling through the crystal to the sample interface. Although there are a number of materials that may be used as ATR-FTIR crystals, the material that was chosen for the application described here is diamond. Diamond, although the most expensive crystal, is resistant to water, acid, bases and mechanical stress. For the study of amine-based systems, it was critical that the ATR-FTIR crystal be resistant to corrosive materials particularly at elevated temperatures.

190

B.3.1 <u>Calculation of Pathlength</u>

The use of ATR for quantitative analysis involves a series of equations, and in some cases assumptions. Unlike transmission IR where the pathlength is equivalent to the distance the radiation travels in a closed cell; internal reflectance spectroscopy results in the complete reflection of the propagating wave. The evanescent electric field that penetrates into the sample following internal reflectance of the IR beam at the crystal and sample interface undergoes an exponential decay in intensity shown in Equation B.3[3, 4]

$$E = E_o \cdot e^{-z/d_p}$$
<div align="right">**Equation B.3**</div>

where E is the electric field amplitude at a penetration distance into the sample, z; E_o is the electric field amplitude at the interface and d_p is the penetration depth given by:

$$d_p = \frac{1}{\gamma} = \frac{\lambda_1}{2\pi(n_1^2 \sin^2\theta - n_2^2)^{1/2}}$$
<div align="right">**Equation B.4**</div>

In Equation B.4, λ is the wavelength of the incident beam, ϑ is the incident angle and n_1 and n_2 are the refractive indices of the crystal and sample respectively. To effectively use the Beer-Lambert law for quantitative calculations, a path length that would produce an equal value for absorbance as it does transmission is required.[5] This term has been referred to as the effective thickness and was developed by Harrick *et al.*[3] Harrick proposed that the evanescent wave was made up of two waves: one parallel to the plane

of incidence and one perpendicular. The wave that travels perpendicular to the plane is calculated as follows:

$$(d_e)_S = \frac{(n_2/n_1)\lambda_1 \cos\theta}{\pi(1-(n_2/n_1)^2)(\sin^2\theta - (n_2/n_1)^2)^{1/2}} \qquad \text{Equation B.5}$$

The terms in this equation are similar to those in the equation for d_p. The polarized wave parallel to the plane is calculated using the following equation:

$$(d_e)_P = \frac{(n_2/n_1)\lambda_1(2\sin^2\theta - (n_2/n_1)^2)\cos\theta}{\pi(1-(n_2/n_1)^2)[(1+(n_2/n_1)^2)\sin^2\theta - (n_2/n_1)^2](\sin^2\theta - (n_2/n_1)^2)^{1/2}} \qquad \text{Equation B.6}$$

The average effective thickness is taken as the average of the two,

$$d_e = \frac{(d_e)_s + (d_e)_p}{2} \qquad \text{Equation B.7}$$

The successful use of the above equations for the calculation of the effective thickness has been reported in literature.[5, 6] The dynamic nature of our system further necessitates the use of the above equations to account for the change in refractive index as a result of temperature and conversion of the silylamine to the RevIL. Shown below in Figure B.3 is

d_p and d_e calculated as a function of refractive index, keeping all other variables constant (λ_1=2400 cm^{-1}, ϑ=45°C and n_1 = 2.4).
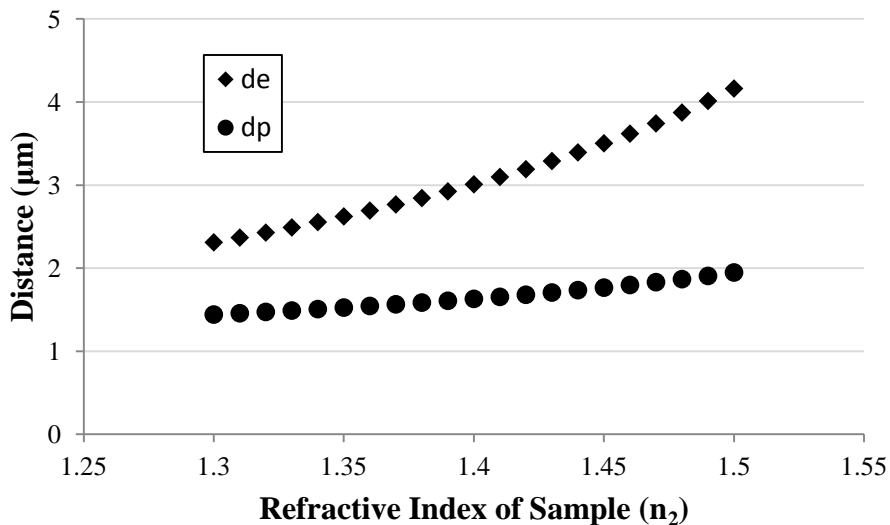
Figure B.3. Penetration depth (dp) and effective thickness (de) as a function of refractive index of the sample

The error associated with using d_p over d_e is greater than 5% for a change in refractive index equal to 0.03 as the refractive index of the sample approaches that of the diamond crystal. As shown in the table below, the refractive index of the silylamine and the RevIL vary by approximately 0.01 .

Table B.2. Refractive index of select silylamine and RevILs at 25°C

	Silylamine RI	RevIL RI
TEtSA	1.45396	1.45655
TPSA	1.45389	1.47015
THSA	1.45917	1.46755

Furthermore the effect of temperature on the silylamine and the RevIL refractive index may be seen in Figure B.4-Figure B.6 below for TEtSA, TPSA and THSA.
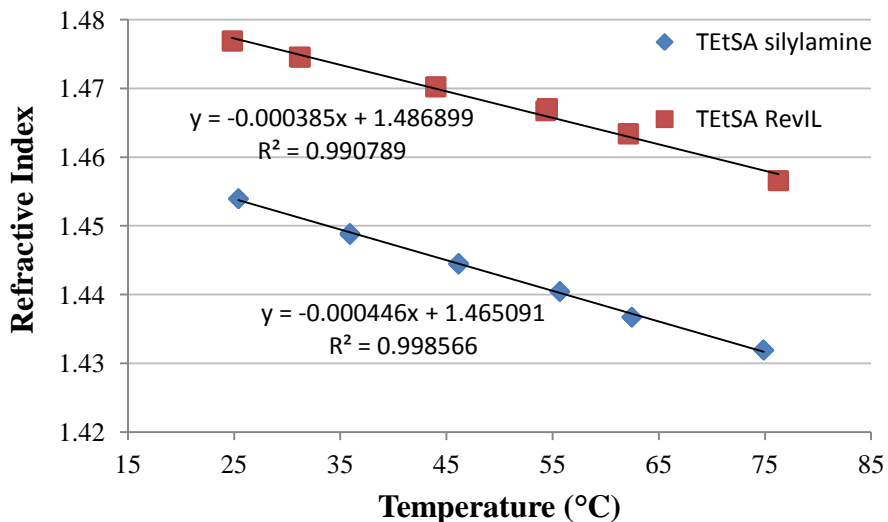
Figure B.4. TEtSA silylamine and RevIL refractive index as a function of temperature
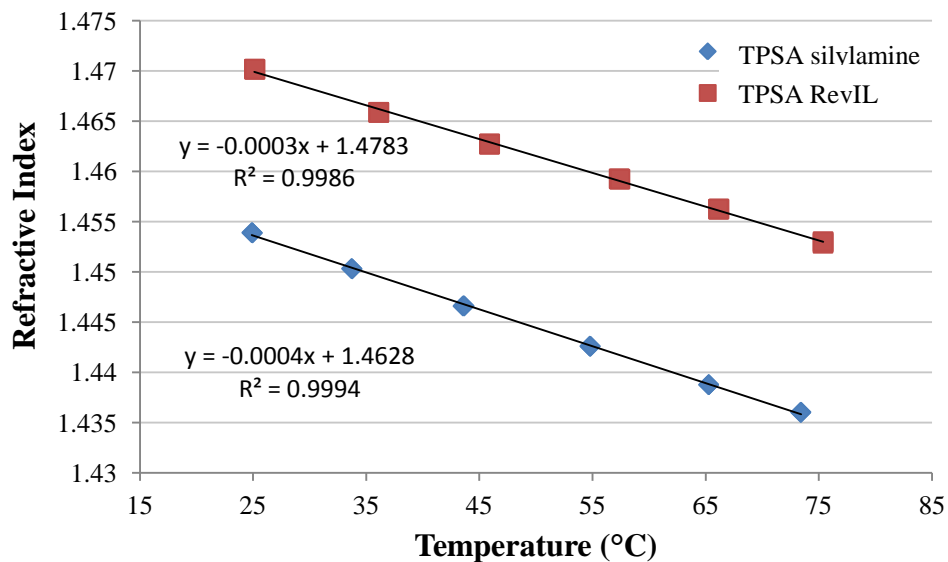
Figure B.5. TPSA silylamine and RevIL refractive index as a function of temperature
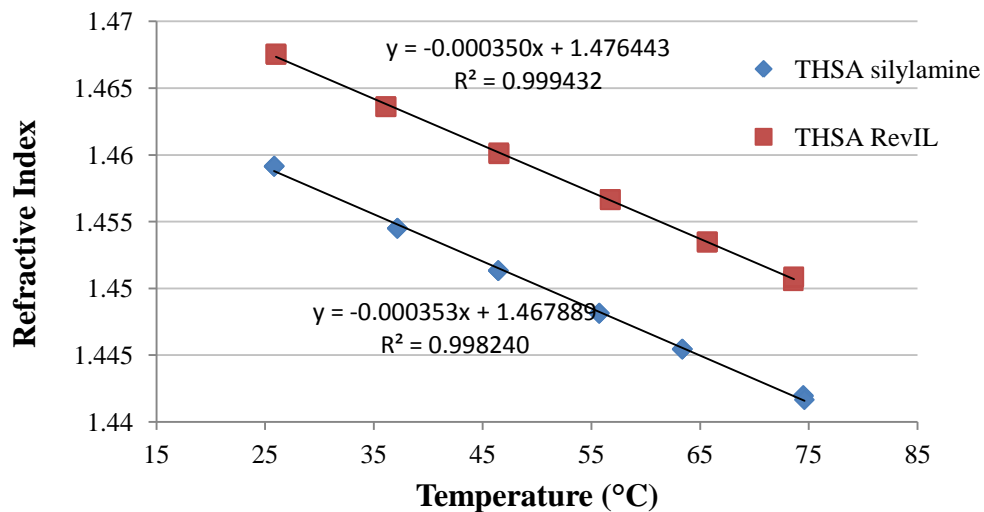
Figure B.6. THSA silylamine and RevIL refractive index as a function of temperature

B.3.2 Absorbance Measurements

Absorbance measurements may be recorded either as a peak maximum or an integrated peak area for application to the Beer-Lambert Law. In the ATR-FTIR spectrum of TPSA, the peak maximum of the asymmetric CO_2 stretch will increase accordingly with an increase in CO_2 absorbed in the RevIL.

195
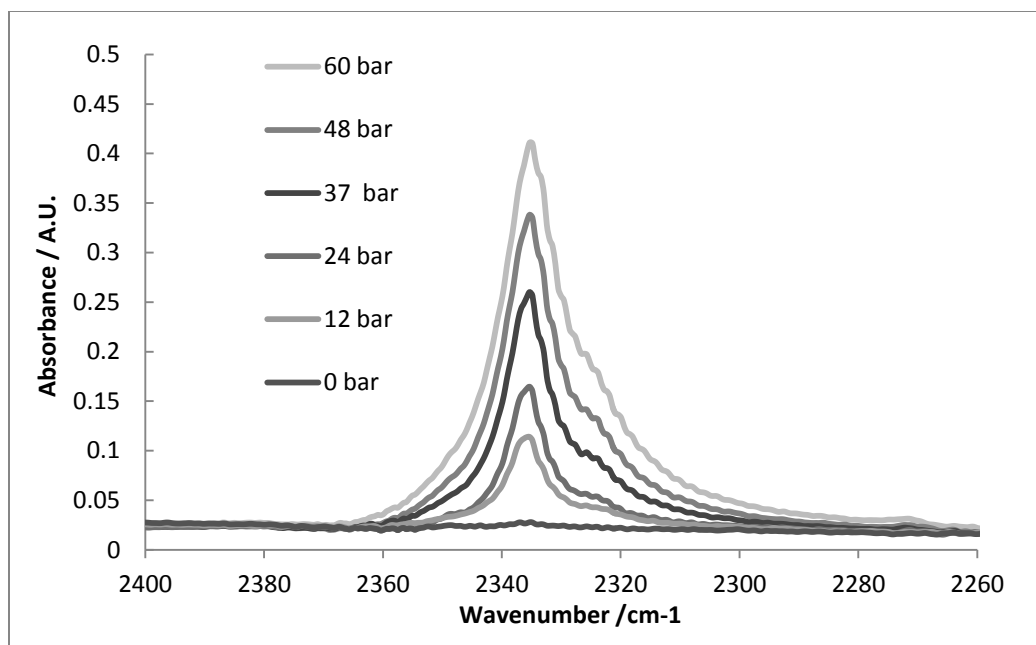
Figure B.7. Asymmetric CO_2 stretch in the ATR-FTIR spectra at 25°C

However, for very broad peaks (e.g., the ammonium peak) measuring a peak maximum may be difficult. Furthermore, the wavelengths of the IR peaks are strongly influenced by their environment, and thus measuring the peak area is more logical approach for this dynamic system. The IR spectra of the silylamine and RevIL were divided into three regions:

- Region I (3100-2600 cm-1): C-H stretch vibration and NH_3^+ vibration (IL)

- Region II (2400-2600 cm-1): Asymmetric CO_2 stretch

- Region III (1740-1520): Asymmetric CO_2^- stretch of the carbamate anion and the carbonyl stretch of the carbamic acid

A MatLab trapezoidal method was used to approximate the peak areas.

B.3.3 <u>Molar Absorptivity of the Silylamine and RevIL</u>

The molar extinction coefficient or molar absorptivity is the measure of how strongly a species absorbs radiation at a given wavelength. The extinction coefficient was calculated from experimental data of the silylamine, RevIL and CO_2-swollen RevIL. For example the extinction coefficient of the C-H stretch of the silylamine and RevIL were calculated from the absorbance and pathlength of the silylamine as shown in Equation B.8 below:

$$\varepsilon_{C-H} = \frac{A_I MW_{silylamine}}{b_I \rho_{silylamine}}$$

Equation B.8

where A_I is the measured absorbance of Region I and b_I is the effective pathlength for region I. The calculation of the N-H stretch was calculated similarly by measuring the absorbance of Region III, which contains only the N-H stretch of the silylamine.

$$\varepsilon_{N-H} = \frac{A_{III} MW_{silylamine}}{b_{III} \rho_{silylamine}}$$

Equation B.9

where A_{III} is the measured absorbance of Region III and b_{III} is the effective pathlength for Region III. The extinction coefficient of the ammonium stretch was calculated by measuring the absorbance of the RevIL and subtracting the area that is contributed by the silylamine as shown in Equation B.10.

$$\varepsilon_{NH_3^+} = \frac{(A_{I,RevIL} - A_{I,silylamine})}{b_I \rho_{RevIL}} \cdot MW_{RevIL}$$

Equation B.10

In the above equation, $A_{I,RevIL}$ and $A_{I,silylamine}$ are the measured absorbance values in Region I, and b_I is the pathlength of the RevIL calculated also for Region I. Finally, the

197

extinction coefficient of the asymmetric stretch of the carbamate was measured as follows:

$$\varepsilon_{C=O} = \frac{(A_{III,RevIL} - A_{III,silylamine})}{b_{III}\rho_{RevIL}} \cdot MW_{RevIL}$$

Equation B.11

where $A_{III,RevIL}$ and $A_{III,silylamine}$ are the measured absorbance values in Region I, and b_{III} is the pathlength of the RevIL calculated also for Region I. The density of the silylamine and the RevIL must be determined for each of the calculations presented above. The density of three selected silylamine and RevIL systems at 25°C is shown below in Table B.3.

Table B.3. Silylamine and RevIL density at 25°C for three select systems

Molecule	Silylamine density (g·cm⁻³)	RevIL density (g·cm⁻³)
TEtSA	0.828	0.922
TPSA	0.824	0.912
THSA	0.830	0.884

The silylamine and RevIL density as a function of temperature are shown below in Figure B.8-Figure B.10 for TEtSA, TPSA and THSA.
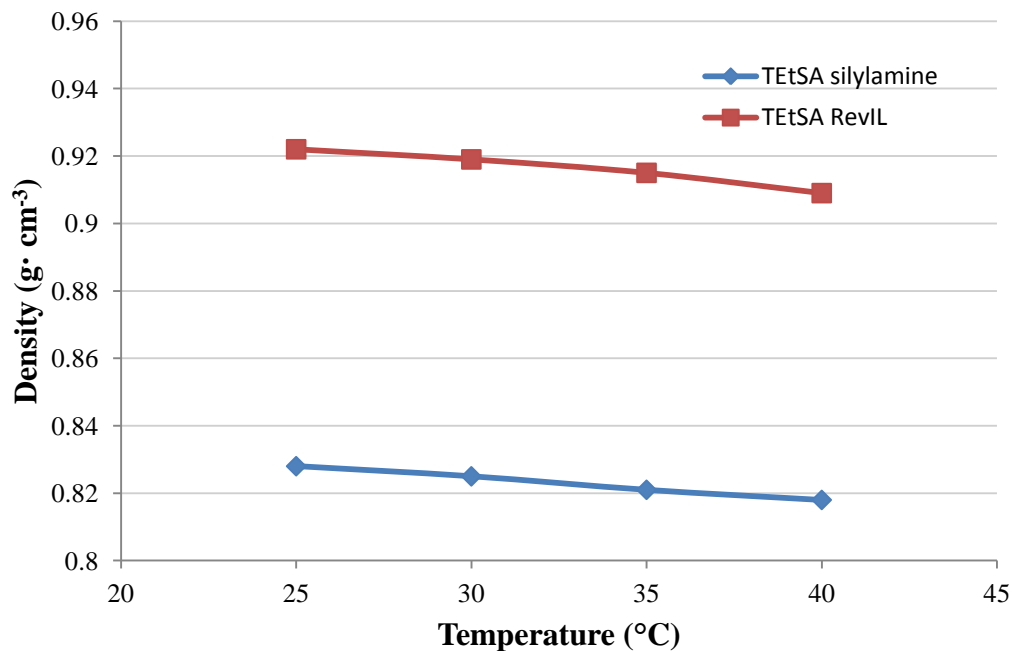
Figure B.8. TEtSA silylamine and RevIL density as a function of temperature
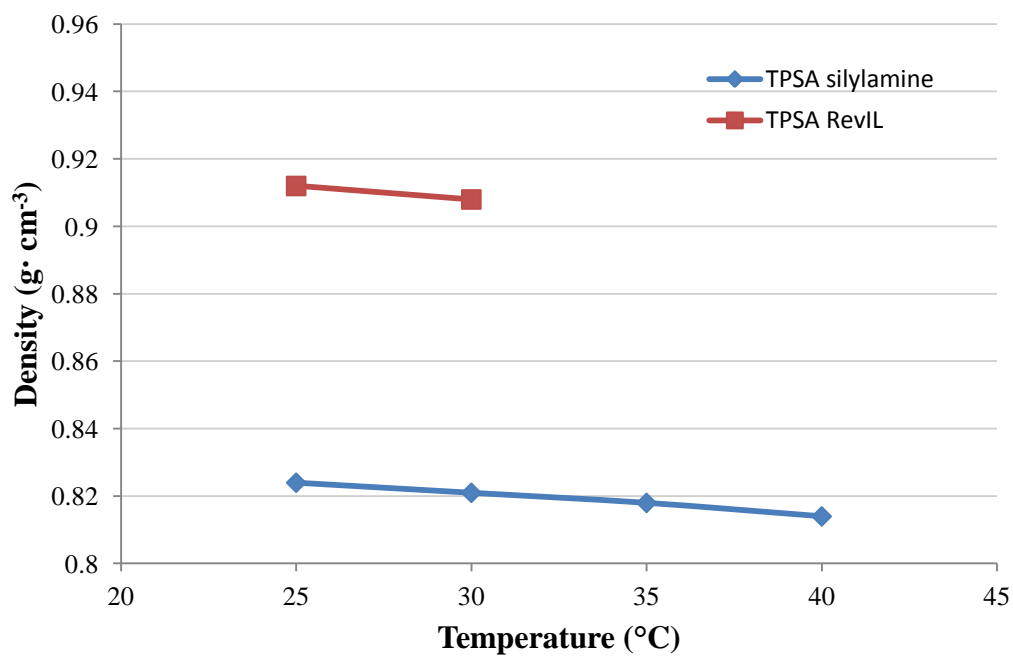
Figure B.9. TPSA silylamine and RevIL density as a function of temperature

199
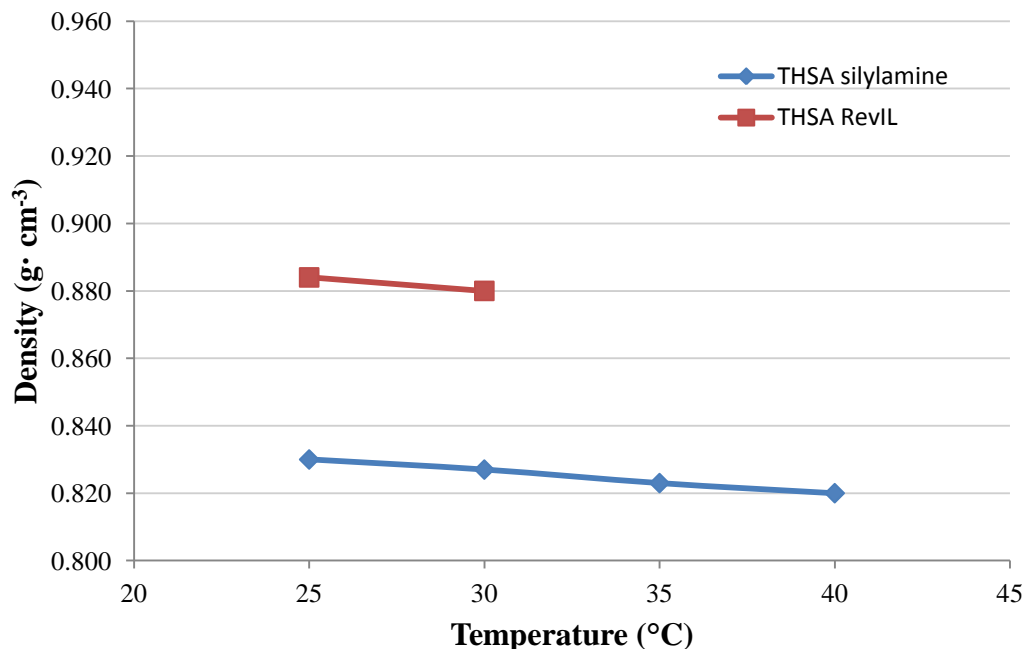
Figure B.10. THSA silylamine and RevIL density as a function of temperature

The density measurements of TPSA and THSA RevIL were limited to two temperatures as the densitometer was unable to converge on a density measurement at temperatures above 30°C. This is likely due to CO_2 bubbles forming in the RevIL from vibrations of the densitometer and the lower reversal temperature of TPSA and THSA compared to TEtSA.

B.3.4 Molar Absorptivity of the Asymmetric CO_2 Stretch

The molar absorptivity of the asymmetric CO_2 stretch was determined experimentally in a system of methanol for which the solubility of CO_2 has been widely reported.[7] Accounting for the refractive index of methanol at 35°C, the absorbance of the asymmetric CO_2 stretch was plotted as shown in Figure B.11 below.
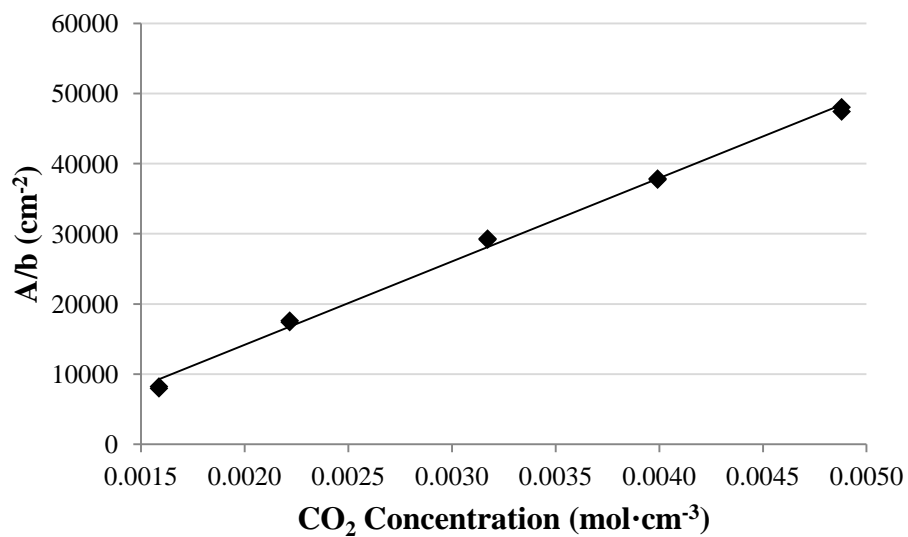
Figure B.11. Determination of extinction coefficient (ε, cm•mol^{-1}) by calibration of absorbance area (A, cm^{-1}) as a function of known concentrations of carbon dioxide in methanol at 35°C

Based on the calibration plot, an extinction coefficient for the asymmetric CO_2 stretch was found to be 1.187 x 10^{7}cm·mol^{-1}. To verify the validity of this procedure, the extinction coefficient was used to calculate the concentration of CO_2 in water (grams of CO_2 per gram of water) as a function of CO_2 pressure. The experimental data was compared to published data by Wiebe and Gaddy.[8]
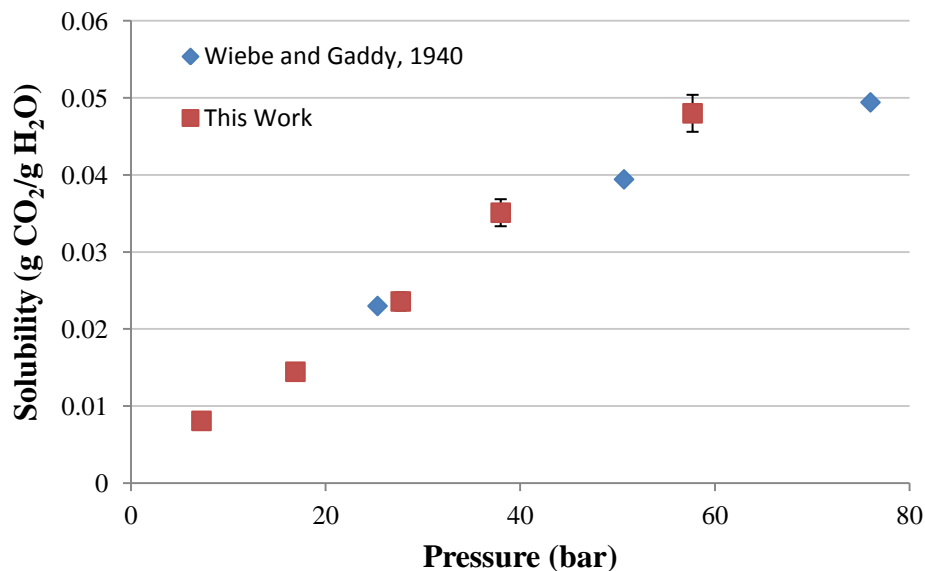
Figure B.12. Experimental and literature values for CO$_2$ solubility in water as a function of CO$_2$ pressure

The experimentally determined extinction coefficient produces concentration measurements that agree very closely with literature values.

B.4 Conclusions

A useful spectroscopic technique has been presented for the measurement of chemical and physical absorption capacity of CO$_2$ by the RevIL system. Through a series of experimental measurements of physical properties (e.g., density and refractive index) and calculations derived from the Beer Lambert Law, the concentration of silylamine and RevIL may be calculated as a function of temperature. Furthermore, the physical absorbance of CO$_2$ as a function of pressure may be quantified by using an experimentally determined extinction coefficient with the measured absorbance of the asymmetric CO$_2$ stretch.

B.5 References

1. Silverstein, R. M.; Webster, F. X.; Kiemle, D. J., *Spectroscopic Identification of Organic Compounds*. 7th ed.; John Wiley & Sons: New Jersey 2005.

2. Silverstein, R. M.; Webster, F. X.; Kiemle, D. J., *Spectrometric identification of organic compounds*. Seventh ed.; John Wiley & Sons, Inc.: 2005; p 502.

3. Harrick, N. J., Internal Reflection Spectroscopy. Harrick Scientific Corporation: New York, 1987.

4. Urban, M. W., *Attenuated Total Reflectance Spectroscopy of Polymers*. American Chemical Society: Washington D.C., 1996.

5. Flichy, N. M. B.; Kazarian, S. G.; Lawrence, C. J.; Briscoe, B. J., An ATR-IR study of poly (dimethylsiloxane) under high-pressure carbon dioxide: Simultaneous measurement of sorption and swelling. *Journal of Physical Chemistry B* **2002,** *106* (4), 754-759.

6. Mirabella, F. M., Jr., *Internal reflection spectroscopy: Theory and applications*. Marcel Dekker, Inc.: 1993; Vol. 15, p 374; Mirabella, F. M., Strength of interaction and penetration of infrared radiation for polymer-films in internal-reflection spectroscopy. *Journal of Polymer Science Part B-Polymer Physics* **1983,** *21* (11), 2403-2417.

7. Chang, C. J.; Day, C. Y.; Ko, C. M.; Chiu, K. L., Densities and P-x-y diagrams for carbon dioxide dissolution in methanol, ethanol, and acetone mixtures. *Fluid Phase Equilibria* **1997,** *131* (1-2), 243-258.

8. Wiebe, R.; Gaddy, V. L., The solubility of carbon dioxide in water at various temperatures from 12 to 40 degrees and at pressures to 500 atmospheres - Critical phenomena. *Journal of the American Chemical Society* **1940,** *62*, 815-817.

APPENDIX C - SAFE ASSEMBLY AND OPERATING PROCEDURE FOR THE HIGH PRESSURE SAPPHIRE CELL APPARATUS

C.1 Introduction

The high pressure sapphire cell apparatus is a unique tool to measure phase behavior without sampling. Using a cathetometer, very precise volume measurements can be recorded to measure liquid expansion, and phase composition.

C.2 Apparatus

The equilibrium cell consists of a hollow sapphire cylinder (50.8 mm O.D. $\times$ 25.4$\pm$0.0001 mm I.D. $\times$203.2 mm L). The cell is divided into two chambers separated by a piston. The bottom cell contains water used as a pressurizing fluid and the top cell contains the equilibrium components. In Figure C.1 is the sapphire cell with sample in the top chamber. In the bottom cell is water with blue dye for demonstration purposes.
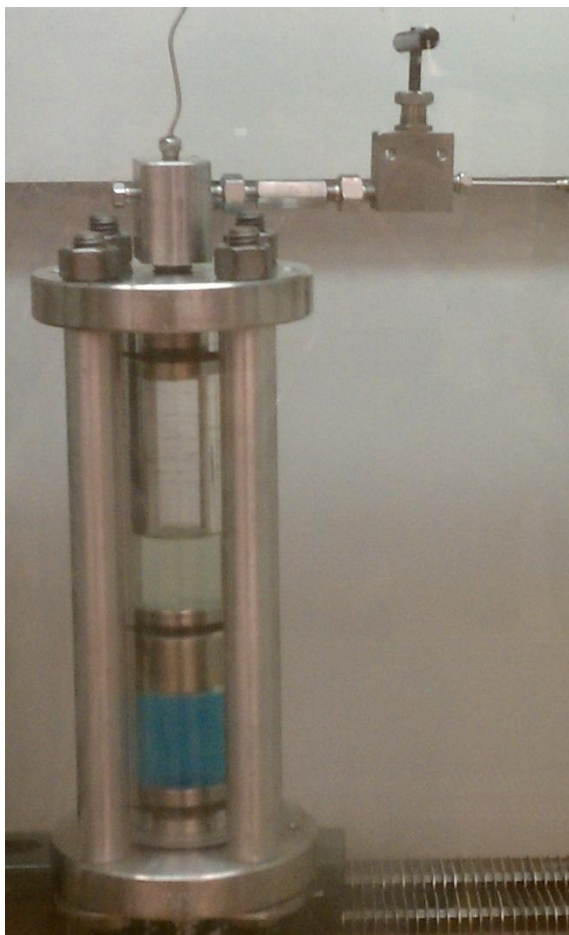
Figure C.1. Sapphire cell apparatus

The cell is placed inside a temperature controlled airbath which is maintained with a digital temperature controller (Omega CN76000). The temperature of the airbath is monitored with thermocouples (Omega Type K) and digital readouts (HH-22 Omega). There is an additional thermocouple (Omega Type K) at the top of the sapphire cell that is also monitored with a digital readout. The pressures were measured with a pressure transducer and digital readout (Druck, DPI 260, PDCR 910). Two Isco pumps (Model 500D) were required for operation. The first Isco pump contains water that is used to pressurize the system. The second Isco pump (Model 500D) was used to introduce CO_2 (or other gas) to the system. The gas inlet is at the top of the sapphire cell. The pressure is

controlled with the Isco pump to achieve an equilibrium pressure on both sides of the piston. The sapphire cell is placed on a movable shaft to allow for mixing.

C.3 Safe Handling of the Sapphire Cell

There are important considerations to be aware of while handling the sapphire cell. Because this is a high pressure apparatus, periodical pressure testing must be completed. It is recommended the sapphire cell is pressure tested every four months or 12 pressure cycles (increasing the pressure above atmospheric and then depressurizing). Pressure testing should be completed with the operating side full of water.

The sapphire cell should never be handled with bare hands. The transfer of oil from skin can result in micro-cracks or scratches. Do not place the sapphire cell on the lab bench unprotected. The hard surface will likely scratch the cell, or there is risk of the cell rolling. Prior to use, inspect the cell for any cracks or defects.

Finally, whenever the sapphire cell is under pressure, the air bath must be down. The airbath serves two purposes, and one of them is to provide a barrier between you and the pressurized contents of the cell if there was a rupture.

C.4 Assembly of the Sapphire Cell

1) Place a 116 size backing ring and 210 size O-ring onto the piston. The current O-ring is Kalrez. This O-ring is recommended for any experiments with corrosive materials. Research the compatibility of the materials with the O-ring prior to assembly. Some backing rings have a flat and a curved edge. Place the flat edge down and the curved edge against the O-ring. Using a rod with a threaded tip (Figure C.2), thread rod into the bottom of the piston.

206

Figure C.2. Threaded rod for piston removal

2) Wrap the rod with a layer of towel to prevent scratching while inserting the piston into the cell. Inserting the piston will be difficult, so force must be used. However, it is important to ensure that only the O-ring comes in contact will the cell wall.

3) Place a 8210 size backing ring and 210 size O-ring onto the top and bottom end cap. The bottom end cap is the water side with the fitting attached. While inserting the end caps, take caution that only the O-ring comes in contact with the cell wall.

Figure C.3. Bottom (left) and top (right) end caps of sapphire cell

4) Align end camps and insert two bolts through the UNISTRUT mounting bracket and through the aluminum spacers. Loosely attach nuts.

5) Insert the remaining two bolts through aluminum spacers and end cap holes. Loosely attach nuts.

6) Tighten all nuts to 8-10 ft/lbs torque.

7) Mount assembled cell to bracket on rotating shaft. Attach all fittings and thermocouple to top and bottom end cap.

C.5 Operation of the Sapphire Cell Apparatus

1) Fill the ISCO pump approximately half full with water. The amount of water that will be required will be determined by the pressures at which the experiment will be run. Do not completely fill the ISCO so that the system may be depressurized if required. Run the Isco pump so that a few drops of water leave the tubing. Attach the tubing to the sapphire cell fitting. This is to ensure no air is in the line prior to connection. Open the gas inlet valve and fill the cell with water until the piston is at a level that liquid height may be measured with the cathetometer. *If the gas inlet valve is not open the system will become pressurized.

2) Make sure the gas inlet valve is now closed. Attach an air-tight syringe to the sample inlet connection (open) and evacuate the cell by pulling back 10 mL. Close the sample inlet valve. Inject a volume of sample by again using an airtight syringe attached to the sample inlet. Apply slight pressure on the airtight syringe while slowly opening the sample inlet valve. Close the valve. Depending on the syringe size, the sapphire cell may need to be inverted on the rotating shaft as the airbath cannot be raised completely above the cell. The amount of sample can be measured by recording the mass of the syringe before and after addition. There is error associated with this method due to an unknown amount of sample left in the tubing and fittings.

3) Once the sample is injected, and airbath temperature set, allow sample to come to equilibrium prior to taking first height measurement with the cathetometer. Repeat as necessary.

4) Add CO_2 by first running to Isco to eject any air from the line, and then attaching the tube to the gas inlet valve. Open the gas inlet valve to the sapphire cell. The amount of CO_2 added to the system may be measured by recording the volume of the Isco before and after CO_2 addition.

5) The pressure may now be controlled using the pressurizing fluid. Check that the flowrate on the water Isco pump is zero (after equilibrium is reached) to ensure there are no leaks.

C.6 Cleaning the Sapphire Cell

Following the completion of the experiment the sapphire cell needs to be cleaned. In some cases this will require disassembly. However, for most experiments the cell may be cleaned by repeatedly washing with solvents. To do this, inject approximately 10 mL of solvent in which the sample is soluble. Shake the cell on the rotating shaft to clean the walls and piston. Invert the sapphire cell and open the sample inlet valve to empty the contents of the cell. Repeat procedure, ending with acetone. Once the cell has been rinsed with acetone, it may be dried by opening all valves and heating the airbath.

C.7 Disassembling the Sapphire Cell

1) Remove the tubing from the fittings. Water will drain from the bottom of the sapphire cell. Removing the piston from the sapphire cell is difficult if it is halfway up the cell once the system is dismantled. If this is the case, the water first needs to be run back into the Isco pump. First close the sample inlet valve

and pressurize the cell with CO_2. The Isco may now be refilled (<5 mL/min). Do not refill the Isco if the cell is not pressurized. If the cell is still pressurized after running the water back to the Isco, open the gas inlet valve to vent into the hood. Now the tubing supplying the water may be removed from the sapphire cell.

2) Loosen the nuts and the spacer bolts.

3) Take out the bolts, ensuring that no metal comes in contact with the cell. If the bolts do not come out easily, you may tap them. Take the end caps straight off without touching the cell.

4) Remove the piston with the threaded rod wrapped in a towel.

APPENDIX D - INTEGRATING REVERSIBLE IONIC LIQUIDS WITH ATOMIZER TECHNOLOGY FOR EFFICIENT CO₂ CAPTURE

D.1 Introduction

This appendix presents a proposal that was submitted to the Department of Energy (DOE) for continued funding on the project presented in Chapter 2 detailing the use of silylamines for CO_2 capture. The proposal presents novel atomizer technology for silylamine introduction into the absorption tower, outlining its potential advantages. The atomizer portion of the proposal was to be conducted with Dr. Andrei Fedorov of the School of Mechanical Engineering at Georgia Teach. The proposal was not acted on but is included for reference.

D.2 Abstract

The use of reversible ionic liquids for CO_2 capture from existing coal-fired power plants offers many advantages over conventional processes. We propose to bring our process nearer to commercialization by optimizing conditions and applying a powerful atomizer technology to eliminate limitations for heat and mass transfer. At the end of this project, (1) the method will be ready for pilot scale demonstration, (2) the process for large-scale manufacture of the solvent will have been defined, and (3) the economic and energy benefits will have been demonstrated.

Silylamine solvents are uncharged molecules which react with CO_2 to form reversible ionic liquids with moderate viscosity. Subsequently, modest heating reverses the reaction, yielding pure CO_2 for sequestration and pure solvent for reuse. The lower solvent viscosities reduce the water requirement and hence the parasitic energy penalty and the lower regeneration temperatures mitigate the energy requirements of the process.

Further, we propose bench-scale demonstration of these solvents using a state of the art atomizer unit, capable of producing uniform droplets only a few microns in diameter with minimum power input. Miniaturization of the droplets greatly increases the surface area to volume ratio to help overcome the heat and mass transfer limitations and reduce the residence times in the absorber. The droplets can be given a charge to prevent agglomeration. The net result is to render the CO_2 capture process highly efficient and cost-effective.

In parallel to our efforts towards improved capture technology through atomizer technology, we are also actively collaborating with our two industrial partners Evonik and ConocoPhillips. Through these collaborations, we propose (1) to determine the important design parameters and scale-up conditions for the industrial scale manufacture of our silylamines and (2) address corrosion, degradation, and toxicity issues related to our silylamines.

D.3 MRC 1: Scientific and Technical Merit

D.3.1 Background

We have developed a new class of solvent systems which we have termed reversible ionic liquids (RevIL). These switchable organic solvents can be taken reversibly from a relatively nonpolar state to an ionic liquid state by contact with ambient CO_2. Reversal back to the nonpolar state is accomplished by simply heating the ionic liquid to remove the CO_2. Such fluids have been applied to a host of reactions and separations.[1-4] In recent years, we have successfully demonstrated that these reversible

ionic liquids also offer an alternative to the existing ethanolamine based CO_2 capture systems in coal-fired power plants.[1,3]

Figure D.1 illustrates the reversible reaction of our silylamines with CO_2. CO_2 is efficiently captured as an ammonium carbamate liquid salt. The subsequent release of the CO_2 is easily accomplished by modest heating. The unique feature of our amine solvent systems is the presence of the silyl group which (1) allows the tuning of the temperature range for the release of the captured CO_2 and (2) aids in the control of the viscosity of the system.[3-5]
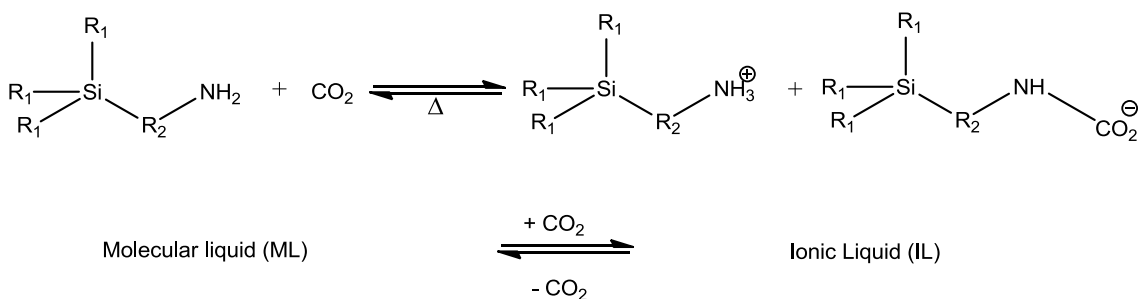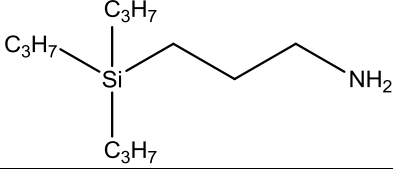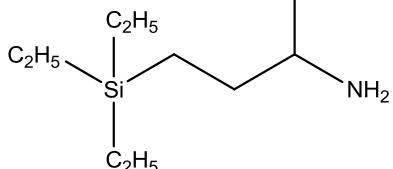
Figure D.1. Reaction of silylamine with CO_2 to form a reversible ionic liquid

Through a systematic study of structure property relationships, we have determined that the three solvent systems listed in Table D.1 represent those systems with optimum properties with respect to CO_2 capture and release, viscosity, stability, and ease of synthesis. Table D.2 tabulates the critical properties of each of these solvent systems.

Table D.1. Three silylamine solvents proposed in this project

Acronym	Compound	Structure
ML1	(3-aminopropyl) triethylsilane	

213

ML2	(3-aminopropyl) tripropylsilane	
ML3	4-(triethylsilyl) butan-2-amine	

D.3.1.1 *Effect of water*

One of the major challenges in the ethanolamine based CO_2 capture solvent systems is the large quantities of water (70-80% by weight) used to bring down the viscosity and minimize amine degradation.[6] This results in large parasitic energy (165 KJ/mol of CO_2)[6] for heating water during regeneration as well as for separating CO_2 and steam in the exit stream of the stripper. However, some water will always be present because of water in the flue gas. In fact, in our method small quantities of water prove beneficial in improving the CO_2 capture capacity due to the formation of extra bicarbonate (HCO_3^-) and carbonate ions (CO_3^{2-}).

At STP, the solubility of water in our pure MLs prior to CO_2 capture is between 10-15 weight %, while less than 0.3 weight % of our MLs are soluble in the water phase. Thus our MLs have much lower water solubility than MEA, and they require far less water than MEA for corrosion prevention and for viscosity reduction. The viscosity of our neat ionic liquids (without water) varies between (400-2000cP at 40 ºC), significantly lower than that of MEA (8200cP). Therefore there are substantial processing advantages of our silylamines relative to MEA in minimizing the need for excess water, thus

reducing the energy requirement for water separation in the cycle. For this proposal, as a standard working solution, we shall use 95% (by weight) ML/water solution.

Table D.2. State-point data table

	Units	ML1 M/E P	ML1 PP	ML2 M/E P	ML2 PP	ML3 M/E P	ML3 PP
Pure Solvent							
Molecular Weight	mol^{-1}	173		215		187	
Normal Boiling Point	^oC	168		180		160	
Normal Freezing Point	^oC	< -77		< -77		< -77	
Vapor Pressure @ 15^oC	bar	$1x10^{-3}$		$0.5x10^{-3}$		$0.7x10^{-3}$	
Working Solution							
Concentration	kg/kg	0.95		0.95		0.95	
Specific Gravity $(15^oC/15^oC)$	-	0.82		0.83		0.82	
Specific Heat Capacity @ STP	kJ/kg-K	2.20		2.21		2.20	

		ML1		ML2		ML3	
Viscosity @ STP	cP	2.2		2.19		1.97	
Surface Tension @ STP	dyn/cm	24.8		23.74		24.3	
		ML1		**ML2**		**ML3**	
Absorption	**Units**	**M/E P**	**PP**	**M/E P**	**PP**	**M/E P**	**PP**
Pressure	bar	0.15		0.15		0.15	
Temperature	^{o}C	40		40		40	
Equilibrium CO_2 Loading	mol/mol	0.4		0.36		0.28	
Heat of Absorption	kJ/mol CO_2	123.0		156		152	
Solution Viscosity	cP	910		632		319	
Desorption							
Pressure	bar	1.2		1.2		1.2	
Temperature	^{o}C	109		86		94	
Equilibrium CO_2 Loading	mol/mol	< 0.01		< 0.01		< 0.01	
Heat of Desorption	kJ/mol CO_2	123.0		156		152	

M/E P: Measured/ Estimated Performance	**PP: Projected Performance**

Small improvements to the properties are possible during the course of this project.

D.3.1.2 *Description of sources of data in Table D.2*

Normal Boiling point – Experimentally obtained using Differential Scanning Calorimetry (Q20 TA instruments machine) by heating the RevILs at 5ºC/minute.

Normal freezing point – Solvents remained liquids at dry ice/acetone temperatures, (-78 °C).

Vapor pressure @ 15ºC – Estimated using a combination of Wilson-Jasperson Method[7] for critical point, and Ambrose-Walton Corresponding States Method[7] for accentric factor and vapor pressure.

Working Solution: Measurements are obtained for a 95-5% RevIL-water solutions, while the estimates are obtained by linear interpolation of the pure water and pure RevIL properties.

Specific gravity – Data obtained using a vibrating tube densitometer (Anton Paar DMA 38) at multiple points between $25^{o}C$ and $55^{o}C$ and extrapolated to $15^{o}C$.

Specific heat capacity – Estimated using method of Ruzika and Domalski.[7]

Viscosity – Measured using a Rheosys Merlin II rotational cone and plate viscometer

Surface tension – Measured using Ramé-Mart Model 250 goniometer.

Absorption

Experiments were performed by sparging a water-saturated gas mixture of ($CO_2:N_2$ 15:85) through our solvent-water mixtures maintained at 40 ºC for 75 minutes. The gas was pre-saturated with water using water bubblers maintained at 40 ºC.

Equilibrium CO_2 loading –Measured gravimetrically as weight gain upon CO_2 sparging.

Heat of absorption – Approximated to be same as heat of desorption (see below).

Solution viscosity - By a Rheosys Merlin II rotational cone and plate viscometer.

<u>*Desorption:*</u>

Pressure –Estimated by comparing to pressures of regeneration with MEA corrected for the lower regeneration temperatures with our RevILs.

Temperature – Experimentally obtained using Differential Scanning Calorimetry DSC (Q20 TA instruments machine). Preformed ionic liquid (~2mg) ramped up from -40 ℃ 400 ℃ at a rate of 5 ℃/minute with a convective nitrogen flow of 50 mL/min.

Equilibrium CO_2 loading – The samples were reversed by heating at the respective regeneration temperatures. Subsequent NMR and refractive index measurements showed that the amount of CO_2 in the reversed molecular liquid was below the detection limit (< 1%).

Heat of desorption - Measured by DSC.

Structure-property relationships

We have extensively studied a wide variety of silylamines with respect to structure-property relationships. In this section we summarize results for the three chosen silylamines in the absence of water.

<u>*Thermodynamics:*</u> The thermodynamics of the capture process can be described by:

The reaction equilibrium constant K which determines the extent of reaction. High K values at absorption temperatures and low K values at regeneration temperatures would

be ideal for the entire carbon capture process. The silylamines in Table D.1 possess these properties.

1. The heat required to raise the ionic liquid to regeneration temperature is expressed by the following equation: $Q = mC_p\Delta T$. This quantity depends on (1) the mass and hence the absorption capacity, (2) the heat capacity, C_p, which is nearly same for all three MLs (2.1 KJ/kg-K), and (3) the regeneration temperature T_{reg} ($\Delta T = T_{reg} - 40$) which ranges from 81-104°C for the three compounds used here.

2. The enthalpy of reaction ΔH_{rxn} which we expect to vary little for the three molecules (~110 KJ/mol of CO_2 as they follow the same reaction scheme (Scheme 1).

Capacity: All our RevILs contain single amine functionality. Hence the capacity (in mol CO_2/kg solvent) depends on the molecular weight and the extent of reaction. All three of our solvents showed complete conversion at room temperature and which goes down with increasing temperature.

Kinetics: For all our RevILs the amine reaction was found to be mass transfer limited. The actual reaction of the silylamine with CO_2 is almost instantaneous. Detailed analysis of this is given below.

Viscosity: Viscosities at complete conversion (at room temperature) decreased from 7600cP to 4000 cP as we increased the size of the substituent chain from ethyl to propyl in RevIL1 and RevIL2, respectively. The introduction of a methyl group in the alpha position of the amine functionality reduced the viscosity to 1900 cP. Viscosities under

the operating conditions of the particular silylamine will depend on temperature, extent of conversion, and water content.
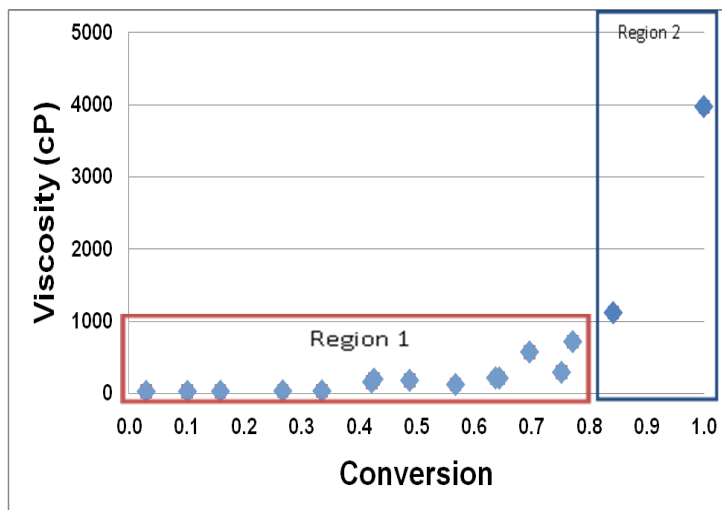
Figure D.2. Effect of conversion on ionic liquid viscosity for RevIL2

Viscosity and extent of conversion: Figure D.2 above shows the viscosity as a function of conversion from ML2 to RevIL2 upon reacting with CO_2. Two regions are highlighted: region 1 (where viscosity varies slightly with conversion) and region 2 (where viscosity is highly dependent on conversion). The viscosity of the RevIL2 system remains relatively low up to 80% conversion; however, beyond 80% conversion small increments in conversion result in viscosity increase from 300cP to 4000cP (region 2). We shall use these results to our advantage to get a significant reduction in pumping costs as well as to minimize the water requirement with very small compromise in capacity. We expect similar behavior at a capture temperature of 40 ºC.

D.3.1.3 *Recyclability*

We have demonstrated recyclability by alternately reacting ML2 with CO_2 and subsequently releasing CO_2 from RevIL2 over 5 cycles. The procedure we use to

demonstrate this is quite simple. We first expose ML2 to CO_2 through at 1 bar and room temperature to capture the CO_2. This is followed by heating the resulting RevIL2 to approximately 100°C for 1 hour in order to release the CO_2. The capture and release behavior is shown over 5 cycles in Figure D.3. NMR spectra show no changes in structure or appearance of new peaks that would be indicative of possible degradation between the first and the fifth cycle.
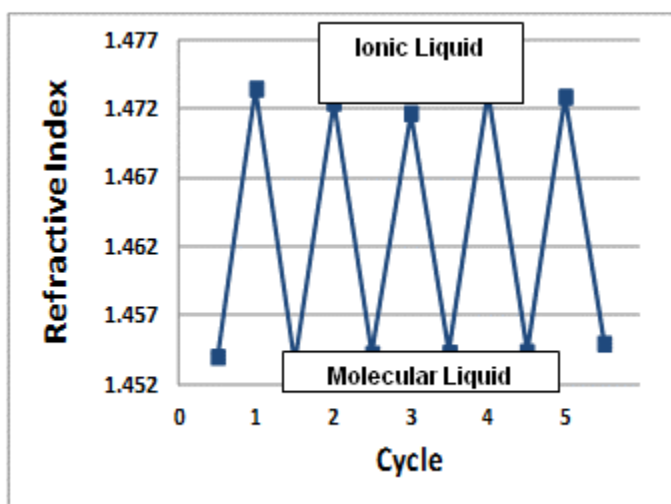
Figure D.3. Recyclability of RevIL2

D.3.1.4 *Interactions with other flue gas components (SO$_2$)*

We have demonstrated that our silylamines will reversibly react with SO_2.
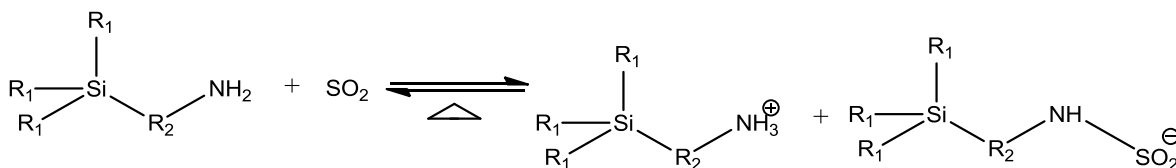
Figure D.4. Reaction of silyl-amines with SO$_2$

Our experiments conducted with pure SO_2 at STP showed that our silylamines have similar absorption capacities for both SO_2 and CO_2. Infrared spectra of RevIL1 bubbled with SO_2 showed asymmetric and symmetric S=O stretches in the 1000-1300 cm^{-1} region, confirming the reaction. Therefore, we expect our silylated amines to capture both SO_2 and CO_2. Based on our data, release of the two would occur at different temperatures.

D.3.2 <u>Proposed work I: Efficient solvent dispersion by ultrasonic atomizer</u>

D.3.2.1 *Motivation*

A major adavantage of our silylamine compounds is the extremely short reaction times with CO_2, with reaction half lives less than a second ($t_{rxn} \sim$ 1s). However, the total absorption time depends on three processes in series: (a) gas phase mass transfer from flue gas bulk to the solvent interface, (b) reaction kinetics and (c) CO_2 mass transfer through the ionic liquid skin into the bulk molecular liquid. The slowest of these dictates the absorption time. Although a detailed CFD (computational fluid dynamics) simulation would be required to model the dynamics of these processes accurately, a simple order of magnitude estimate can be easily obtained.

For CO_2, the gas-phase diffusivity D_{gas} is *~16 mm^2/s* at STP while the diffusivity in the ionic liquid D_{IL} (estimated from Stokes-Einstein equation) is *3.1x10^{-6}mm^2/s*. The diffusion time scales can be related to diffusivity by ($t \sim \delta^2/D$), where δ is the characteristic diffusion path length. For a representative (target) droplet radius of r~20μm, the diffusion length in gas phase δ_{gas}~r [8], which gives $t_{diff,gas}$ ~25μs. Even if we consider a limiting case where the thickness of the ionic liquid layer is as small as the of

222

vapor side interface $\delta_{IL} = \delta gas$, the diffusion time scale for CO_2 across ionic liquid layer will be $t_{diff,IL} \sim 131s$, making the <u>mass transfer of CO_2 in the IL the rate-limiting step</u>. Also note that an *<u>order of magnitude reduction in the size of the liquid layer will bring down the diffusion times by two orders of magnitude</u>* (since $t \sim \delta^2/D$). Therefore, in this project we propose miniaturization of molecular liquid into micron size droplets to achieve faster absorption cycles. The three competing processes affecting the mass transfer in a liquid droplet are depicted in Figure D.5.
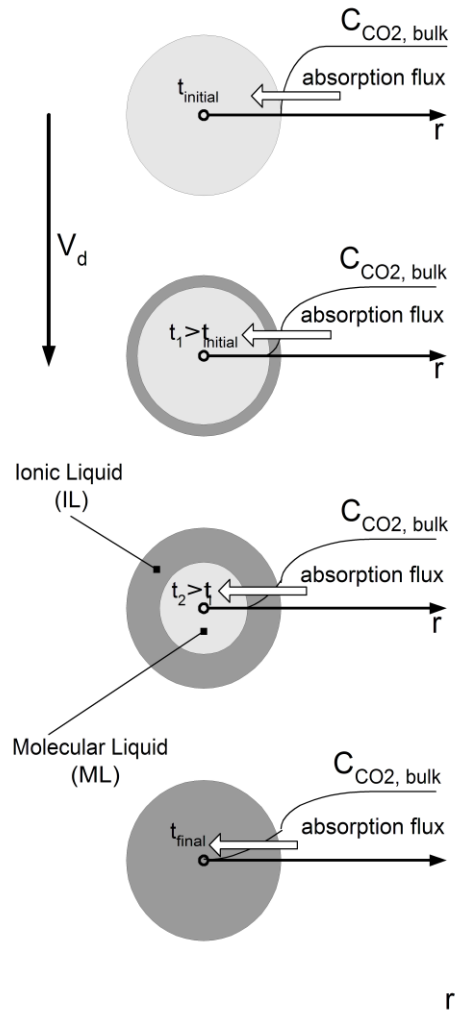
Figure D.5. Mass transfer and reaction across a molecular liquid droplet

Supporting experimental evidence for the dependence of absorption times on the mass transfer between the gas and liquid phase can be seen in Figure D.6, which shows the extent of CO_2 capture for two modes of gas introduction into molecular liquid at room temperature for 1 minute with constant CO_2 flowrate of 200 ml/min . For the first case, the pure CO_2 is bubbled through a molecular liquid using an 18 gauge needle while for the second case CO_2 is introduced using a fritted glass tube providing much better mass transfer than a needle. It can be seen that the reaction extent was almost three times higher with better mass transfer.
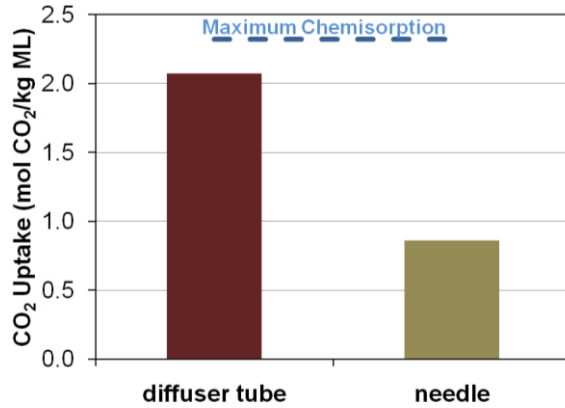
Figure D.6. Effect of mass transfer on absorption times

The amine-CO_2 reaction is highly exothermic, which could elevate the system temperature and trigger the reverse reaction. Adequate heat transfer is essential to achieve high conversion. The time scales of heat dissipation depend on the thermal diffusivities in the gas phase (α_{gas} ~$1.8x10^{-5}m^2/s$) and in the ionic liquid (α_{IL}~$7.4x10^{-8}m^2/s$) $t_{HT,total} \sim t_{HT,IL} + t_{HT,gas} \sim \delta_{IL}^2/\alpha_{IL} + \delta_{BL}^2/\alpha_{gas}$. For the target case of 20μm in radius droplets, $t_{HT,total}$ ~$0.05s$ which is four orders of magnitude lower than the diffusion time scales. The calculation illustrates two key characteristics of the systems (1) *mass transfer in our systems is more limiting than the heat transfer*, thus allowing higher conversion

rates without reversion, and (2) similar to mass transfer, the heat transfer time scales are proportional to square of the radius of the droplets, therefore *efficient dispersion of the solvent into an ultra-fine mist would also make the heat transfer highly efficient*.

D.3.2.2 *Atomizer*

To address the rate-determining mass transfer we propose to incorporate a novel ultrasonic atomization technique for converting our molecular precursors to fine droplets prior to CO_2 exposure. By enhancing the surface area available for CO_2 adsorption we decrease the characteristic time for gas phase heat and mass transfer processes, thus eliminating the mass transfer limitations in the gas phase. In addition, since the time scale for CO_2 transport into a droplet depends on the length scale, ultra-fine droplets will reduce the CO_2 diffusion times down to microseconds, thus removing the transport limitations in the liquid phase, as well.

Conventional fluid atomization techniques have severe limitations to their application in a CO_2 capture system: (1) they produce much larger than optimal droplets with diameter in hundreds of micrometers; (2) the size distribution of liquid droplets is broad and therefore puts severe constraints on design and operating conditions for the absorber with difficulty in fine-tuning for optimal mass transfer conditions; (3) the power required for fluid dispersion using conventional atomization techniques is large. The proposed ultrasonic atomization device overcomes all of the above practical limitations of conventional atomization devices.

The key enabling technology for the proposed CO_2 capture system is an array of ejectors capable of *high-throughput, scalable* generation of a mist of *microscopic*

droplets of suitable size at *low power input*. It is based on the novel microelectromechanical systems (MEMS)-enabled ultrasonic atomization technology[9] that ejects fluid from micro-scale (3–50 μm) nozzles with incorporated electrodes for manipulation of electro-active fluids. Four aspects enable the superior ejection performance of this atomization technology: (1) ultrasonic frequency of operation, resulting in high throughput (high flow rate) atomization, (2) resonant operation enabling efficient power transfer from the transducer to the ejected liquid, resulting in minimum power input required for atomization, (3) acoustic wave focusing for localized delivery of mechanical (wave) energy bursts, resulting in peak pressure gradient right at the tip of the nozzle and hence enabling ejection of even very high viscosity liquids, and (4) a parallel format (arrayed device) with precisely-controlled (via MEMS fabrication) size of all ejecting nozzles, resulting in scalability of throughput and size uniformity of the mist.

This unique combination of features not only enables ejection of fluids that other droplet generators fundamentally cannot eject, but also brings about the critical operating advantages such as an increased power-efficiency of ejection (reduced power consumption), high throughput from a compact device (ejection of large liquid volumes by a single small-form-factor array), and linear scalability of technology (via adding identical nozzle arrays) to match a wide range of application requirements.
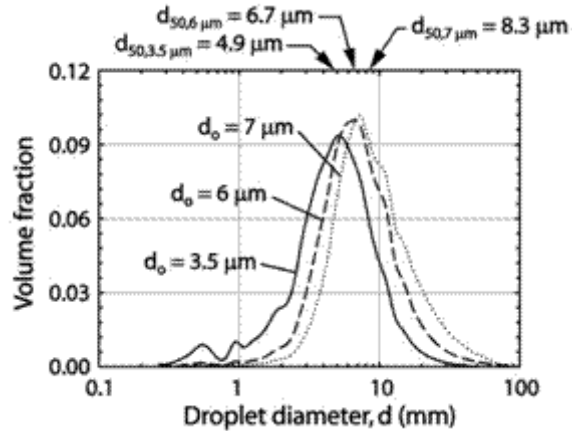
Figure D.7. Size distribution of water droplets with atomizer

In the course of the past seven years of focused research, we have <u>demonstrated a number of key atomizer capabilities</u>, which are relevant to the proposed effort and offer significant advantages over the conventional droplet formation techniques:

- Controlled ejection of droplets of uniform diameter between 5 and 50 μm, as governed by the operating frequency, fluid properties, and nozzle orifice size;[10] [11] (Figure D.7 above shows the unimodal size distribution of water droplets)

- High throughput due to ultrasonic frequency of operation up to 1.5 L/min (for 50 μm droplets at ~1.2 MHz frequency from a 400 active nozzle array in 1"x1" footprint), which is linearly scalable by increasing the number of nozzles and multiplexing; [12]

- Low power input for multi-nozzle array (sub-Watt level to power 400 nozzle devices) with diminishing extra-power-cost associated with adding new nozzles to the array;[13]

- Simple, scalable, low-cost batch microfabrication of ejector nozzle array in silicon;[10]

227

- High droplet ejection velocity of 5-25 m/s, controlled independently of the flow rate;[11]

- Capability to eject ionic conductors and dielectric fluids with the record large viscosities (0.7–3000 mN-s/m2) and significant variation in surface tensions (~25–73 mN/m);[14]

- Capability to operate in drop-on-demand (DOD) or continuous-jet-ejection mode

- Capability to charge droplets upon ejection to avoid post-ejection coalescence;[15,16]

- Device operation independent of orientation relative to the gravity field, with fast start-up and shut-down (~1 μsec) to respond to transient loads, and the ejector utilizes ultrasonic waves for droplet generation, resulting in ultrasonic cleaning (anti-clogging).

In the course of this project, we shall adopt and refine the ultrasonic atomizer for dispersion of our silyl-amines for efficient CO_2 capture. Our efforts will include an optimized atomizer design, aiming to minimize the specific power input (i.e., per unit flow rate of atomized liquid), and in-depth experimental characterization and modeling of the acoustics and fluid mechanics of device operation, targeting the necessary/desired flow rates (system throughput) and droplet size(s). Details about the device components and fabrication, atomizer design and operation, and description of the bench-scale apparatus for CO_2 capture with atomizer are discussed in MRC2.

D.3.2.3 *Preliminary Results for CO₂ Capture Using Atomizer*

A first generation prototype of the bench-scale device was constructed to demonstrate the higher efficiency of using the atomizer for solvent dispersion in CO_2 capture. We observed 90% conversion with use of atomizer, while only 14% conversion

without it, clearly illustrating a significant advantage of using solvent atomization in improving the capture process efficiency. A detailed schematic of the device and the operating conditions are discussed in detail in MRC2.
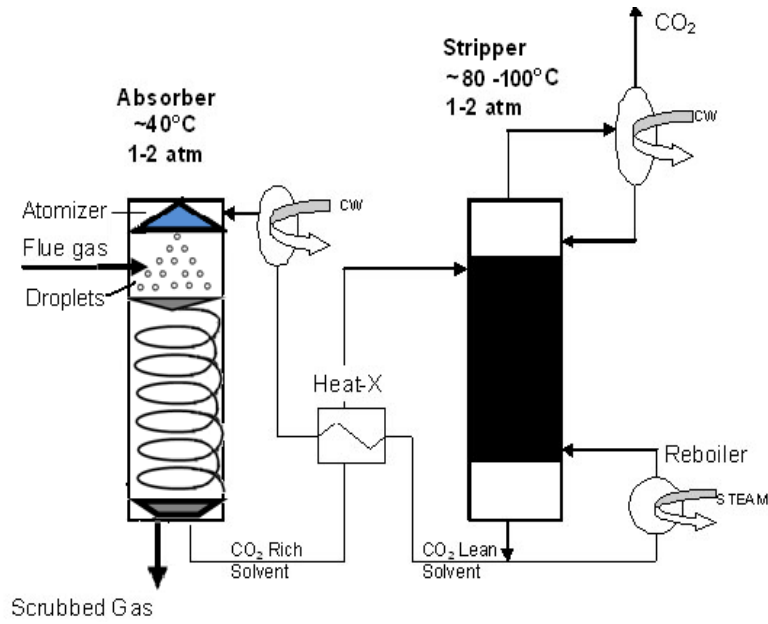
Figure D.8. Block Diagram of CO$_2$ capture with Atomizer

D.3.2.4 *Block flow diagram*

A simple block diagram depicting the CO$_2$ absorption process from a flue gas stream using the atomizer technology is shown in Figure D.8. The atomizer disperses the molecular liquid droplets from the top of the absorption tower. Traditional absorption towers use a countercurrent operation of the solvent and the flue gas stream. However, in a tower equipped with atomizer, such an arrangement might lead to unsatisfactory conversion levels and solvent losses. To address this, we envision absorber geometries that will have a swirl flow of the flue gases within the capture chamber, into which the atomized ultra-fine solvent droplets will ejected from the top and carried to the bottom

collection tray (for CO_2-saturated solvent) along an extended path with an optimally designed residence time to maximize the CO_2 capture efficiency per unit pumping power input. The helical shape of the chamber will allow optimum utilization of the available absorber volume. The molecular liquid droplets, once converted to ionic liquid at 40 ℃ are collected at the bottom of the helical chamber while the scrubbed gas is vented out. The CO_2 rich ionic liquid is then pumped to the stripping tower via a heat exchanger for molecular liquid regeneration. The regeneration temperatures (as reported in state-point data table) will depend of the particular choice of RevIL. These temperatures are lower than 120 ℃ used for conventional MEA processes. Once regenerated the hot lean solvent is cooled by transferring heat to the counter flowing ionic liquid and a cooler unit and subsequently reintroduced in the absorber for the next CO_2 capture cycle.

D.3.3 Proposed work II: Bulk/commercial scale synthesis of the MLs/RevILs:

For CO_2 capture, a 500 MW power plant requires ~350 tons of initial solvent loading with additional 180 tons of solvent annually for make-up.[17] With nearly 8000 power plants in the U.S. alone,[18] the market for CO_2 capture solvents is of the order of several million metric tons. Therefore we shall show that the proposed solvent is relatively inexpensive and can be efficiently produced in bulk quantities. We are working with Evonik (formerly Degussa), who have extensive experience in research, scale-up, and manufacture of silyl compounds. We will work with Evonik on process scale-up in order to develop an inexpensive, reliable, and environmentally benign industrial process. This is described in greater detail in MRC2.

D.3.4 Proposed work III: Stability of MLs/RevILs and determination of important industrial parameters

The stability of our RevILs against corrosion and degradation is important for determining their applicability in the actual CO_2 capture process. A systematic stability study is essential for determining (a) equipment construction materials and solvent additives, (b) recyclability of the solvent over multiple cycles (c) potential environmental, health and safety concerns and (d) the overall economics of the process. ConocoPhillips, one of our industrial partners in this project, has many years of experience in corrosion and degradation testing in the oil and gas industry and will provide both expertise and facilities in this area. The company will also help in the evaluation of key performance parameters such as absorption kinetics, process recyclability, and spray contactors. The range of tests and analyses to be performed during this collaborative effort is listed in the Statement of Process Objectives.

D.3.5 <u>Advantages of the technology</u>

Table D.3. Comparison of pure RevILs post CO_2 capture with MEA

	RevIL1	RevIL2	RevIL3	MEA	30 % MEA aq. solution
Reaction time for complete conversion at R.T., 1 bar CO_2 at 200 ml/min	2 min	2 min	2 min	10 hours	15 minutes
Regeneration temperature	104	95	81	120	120

The work proposed integrates reversible silylamine ionic liquids and the ultrasonic atomization technology, to achieve synergistically the target of 90% CO_2 capture with less than 35% increase in the cost by the year 2020. As shown in Table D.3, our RevILs demonstrate much more promising properties than pure MEA and 30% MEA

aqueous solution. In the absence of water our silylamines show much faster kinetics and lower regeneration temperatures. In addition, the lower regeneration temperatures of our RevILs also ensure that lower energy inputs are required for CO_2 release, *thus enabling a more efficient usage of the existing steam in the power plant*. Due to faster kinetics, the *absorber residence time* for our RevILs will be significantly *shorter* than that for MEA. The residence times will further improve due to the enhanced mass transfer from the atomizer. The ML systems proposed herein exhibit less reactive sites susceptible to undergo degradative chemistries, thus minimizing make-up and waste streams.

The atomizer unit proposed is a highly efficient (from input power prospective) and a cost-effective alternative to the conventional solvent dispersion systems, especially when used for producing essentially monodisperse mist of ultra-fine (<50 μm in diameter) droplets. The ultrasonic atomizer is a resonant device that exploits operation at judiciously matched resonant frequencies of the array of liquid horns and the piezoelectric transducer to enable low-power operation. In our most recent experiments, at a power consumption of *only 85 mW*, stable ejection of 10 μm water droplets with an estimated ejection flow rate of 100 mL/min was achieved while maintaining the transducer temperature below 30°C. An incremental increase of the array size driven by a single piezoelectric transducer comes at a significantly diminishing cost (a fraction of a percent) of additional power input, due to improved power utilization with an increase in the array size. The device also has a self-pumping capability by the flexing piezoelectric transducer, thus requiring *no additional pumping costs* for continuous operation.

The reduced energy penalty for solvent regeneration, decreased water usage, shorter residence times with efficient heat and mass transfer, and minimal solvent

232

makeup needs contribute in *significantly bringing down the process costs* for CO_2 capture compared to current technology.

D.3.6 Anticipated technical challenges

Our group is a unique collaboration between three academic faculties with expertise in chemistry, chemical engineering, and mechanical engineering. Our two industrial partners have great strengths in silicon-based chemical synthesis and global energy solutions, making us highly capable of successfully addressing technical challenges during the course of the project. Below we list some of the challenges that we currently anticipate with the respective remedial strategies.

D.3.6.1 *Droplet coalescence and collection*

In-flight coalescence is a common problem encountered with dispersed solvents, and directing the mist of droplets towards the collection tray is also challenging. We have shown that putting a net charge of the same sign on the droplets can easily prevent coalescence, while a small opposite sign charge on the collection tray will help direct the drops towards the tray. This can be conveniently achieved in the ultrasonic atomizer, at very low bias DC potentials (V_{ext}) or even in purely AC mode of the piezoelectric transducer's operation (V_{PZT}) through the intrinsic coupling of electric and mechanic fields, by using a locally arranged set of electrodes in the vicinity of the nozzle array surface. [16]

D.3.6.2 *Device design and optimum integration of silyl-amine RevILs and atomizer for*

   CO_2 capture

Our preliminary experiments have shown that the two technologies can be successfully integrated. One challenge could be device design to ensure the desired conversion levels. We shall use extensive heat and mass transfer calculations to guide our device design. In addition, we shall explore absorber geometries with helical chambers with co-current solvent and flue gas streams.

D.3.6.3 *Stability of RevILs*

Our RevILs will be less susceptible to degradation than MEA because they contain less reactive sites. For instance, the absence of hydroxyl groups is expected to minimize or eliminate oxidations and intra-cyclization reactions which are observed in the case of MEA as a major source of parasitic side reactions. We will use the ConocoPhillips expertise for developing solvent additives that will improve the solvent stability.

D.3.6.4 *Availability of RevILs in bulk quantities*

The RevILs proposed here are not now commercially available. Our collaboration with Evonik will help us in optimizing the reaction pathways for bulk manufacture of the silylamines. Yields, cost, and environmental impact will be of prime importance.

D.3.7 Environmental, health and safety

The EH&S assessment will address two distinct areas of the technologies being developed in the proposal, per se the atomization process and the silylamine solvents.

(1) Atomization unit: Ultrasonic atomizers use standard electronic components (signal generators and RF power amplifier), which are extensively used in industrial practice and operated via well-established standard operating procedures. The driving voltage amplitude is modest (under 200V peak-to-peak after amplification) and transducer heating never exceeds 100°C, which is monitored using thermocouples. The personnel in the power plant are expected to be familiar, equipped and trained to safely handle such voltage levels safely. In addition, ~20 μm atomized droplets can potentially increase irritation by inhalation (entering respiratory tracks up to the bronchial tree). Large scale process involving atomized droplets are established and will be used as a basis to develop a risk assessment and safety operative protocol for the atomizer unit.   For example, engineering controls that would provide a secondary filter of the particles prior to any accidental release could be installed to prevent aerosolized RevILs being present in the working atmosphere.

(2) Silylamine solvents: A preliminary assessment of the proposed silylamines highlighted that these materials may be flammable and irritants. The silylamines proposed are novel solvents; as a result, there is little to no information to realistically estimate their level of flammability and health concerns (rating from 0-4) at this time. TWe propose to compile the data to establish MSDS (Material Safety Data Sheets) for our solvents. These MSDS will be used to develop a rigorous and realistic EHS assessment of large scale operations involving these systems. The proposed silylamine RevILs have less reactive sites susceptible to undergo degradative chemistries than monoethanolamine (current technology), therefore preventing the formation of large degradation by-products stream. As a result, we anticipate the waste streams resulting

from solvent's purification and make-up streams to be minimized. In addition, RevILs have low water solubility (less than 0.3wt%), limiting aqueous-contaminated streams. In compliance with current federal regulations, the EH&S assessments and safety handling procedures of the final process will be established in collaboration with Georgia Tech's Department of Environmental Health and Safety team, ConocoPhillips and Evonik. An existing relationship exists with ConocoPhillips and letters of support from Georgia Tech EH&S and Evonik are included in the Appendices.

D.4 MRC2. Technical Approach and Understanding

D.4.1 Capture agents

D.4.1.1 *Current preparation of silylated amines*

The amines being investigated are currently synthesized by reaction of trialkylsilanes with allyl amine (or in the case of ML3, a substituted allyl amine) using a catalytic amount of platinum-divinyldisiloxane in refluxing toluene.[19] For ML3, before hydrosilylation we must make the 3-amino-1 butene hydrochloride salt through a Gabriel synthesis from 3-chloro-1-butene.[20] This hydrochloride salt requires neutralization prior to hydrosilylation, therefore increasing the number of steps from commercially available materials in the formation of ML3. Due to the expense of platinum catalysts, which would require further functionalization to recycle, and the multistep reactions required for

the formation of ML3 precursor, we have developed a common method for the scalable preparation of all three MLs proposed.

D.4.1.2 *Scale-up synthesis of silylated amines*

We propose an environmentally-conscious synthesis for the multi-scale manufacturing of silylated amines. The synthesis requires the formation of silylpropylchlorides from inexpensive trialkylsilanes (triethyl and tripropylsilane) and readily available allyl chloride and methallyl chloride, followed by a simple amination to yield the target silylamines. The silylalkylchlorides can be obtained in quantitative yields from trialkylsilanes with both substituted and unsubstituted allyl chlorides.[21] Through scaling the amine syntheses to volumes on the order of hundreds of milliliters, a blueprint can be developed for future scaling to industrial volumes. We propose to use Aspen HYSYS to calculate costs associated with the bulk manufacture of our proposed amine solvent.

The process chosen for scale up involves a much more benign and facile two-step reaction sequence. Figure D.9 shows the proposed synthesis of the intermediate (trialkylsilyl)propylchlorides through a hydrosilylation reaction run under neat conditions with an inexpensive copper acetate catalyst. Copper(I) salts have also been shown to have very limited solubility in most solvents, theoretically allowing for complete catalyst recycle, which will be investigated in our bench-scale formation of the silylatedpropylchlorides.

Amination of alkyl chlorides is a classic substitution reaction (Figure D.10).[22] We propose the amination of silylated propylchlorides by reaction with excess liquid

ammonia, followed by a mildly basic aqueous wash to provide the desired silylamines. The reaction of the chlorides in excess liquid ammonia provides an opportunity for recycling the remaining amount of ammonia through evaporation and recondensation. We have noted the hydrophobicity of the target RevILs, thus providing an facile extraction from the aqueous wash required (unpublished results in our laboratory).
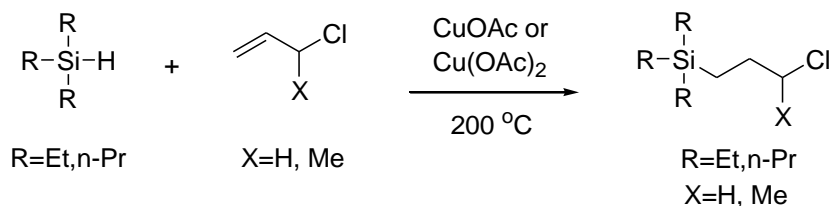
Figure D.9. Hydrosilylation to desired silylpropylchlorides
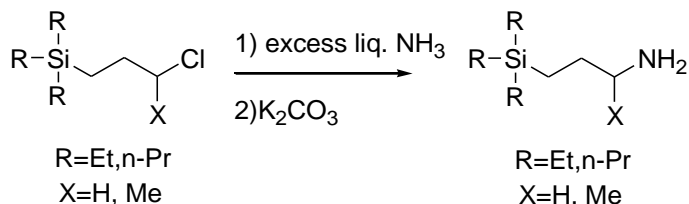
Figure D.10. Amination of the silylpropylchloride to yield target silylamines

D.4.1.3 *Synthesis of (trialkylsilyl)propylchlorides*

Following a literature procedure, either triethylsilane or tripropylsilane will be mixed in optimized concentrations with allyl chloride or methallyl chloride and subsequently added to dry Cu(OAc) or Cu(OAc)$_2$ in a pressurizable glass tube at -40 $^{\circ}$C through the use of a polyethylene glycol chiller.[21] The tube will be sealed and heated to 200 $^{\circ}$C for an optimal amount of time and then cooled back down to room temperature. The resulting mixture of reactants and heterogeneous catalyst will be filtered and the solution will then be analyzed by LC, GC and ^{1}HNMR for product purity. Any remaining starting materials will be distilled from the product chlorides. Complete characterization

through GC, ^{1}HNMR, ^{13}CNMR, MS, and elemental analysis of the chloride products will be conducted. Variables that will be taken into consideration for optimization of the formation of (3-chloropropyl)triethylsilane, (3-chloropropyl)tripropylsilane, and (3-chlorobutyl)triethylsilane will be reaction temperature, catalyst loading, reaction time, and starting material concentration. The optimized reaction conditions will then, with consultation with our research partner, Evonik, be used to scale the reaction to the order of 100 mL batches, which can be used as a model to get more information for commercial-scale production.

D.4.1.4 *Synthesis of (trialkylsilyl)propylamines*

The amination reaction will be conducted by reacting isolated and purified chlorides mentioned above with excess liquid ammonia. These reactions will be done by first condensing ammonia gas through a dry ice condenser into a reaction flask at -40$^{\text{o}}$C. The liquid chloride starting materials will then be added with efficient stirring. The product, once isolated, will be characterized by ^{1}HNMR, ^{13}CNMR, LC, MS, and elemental analysis. We shall consider reaction time, temperature, and ammonia concentration in order to scale the reactions to 100 mL batches.

The synthetic reaction conducted at 100 mL quantities will provide (1) materials for carbon capture and release for the bench-scale experiments, and (2) critical information for the development of synthesis scale-up to the tonnage quantities required for broad use in CO_2 capture facilities. In collaboration with Evonik and Environmental Health and Safety at Georgia Tech, we propose to demonstrate the viability of an industrial scale up procedure for the formation of our three target reversible CO_2

capturing silylamines. Additional proposed experimental details and timelines are included in the Standard Operating Procedures (SOPO) in MRC4.

D.4.2 <u>Atomizer device and operation</u>

Concurrently to the ML silylated amine studies, the CO_2 capture atomization unit will be designed, built and implemented for CO_2 capture in the laboratory. The CO_2 absorption tower design comprises two components: (1) the absorption tower and (2) the atomization device and ancillary equipment. The details are described below.

D.4.2.1 *Components*

The atomizer concept described in MRC1 is realized by (1) creating an array of resonant fluid cavities, (2) making each cavity focus acoustic waves when driven at appropriate resonant frequencies, and (3) selecting a piezoelectric transducer material and geometry for the most efficient operation in the desired frequency range. This conceptual framework has been used to design the droplet generator.[9] A representative device comprises of a fluid reservoir that is formed between a piezoelectric transducer and an array of liquid horn structures (nozzles) in the cover plate. Two power wires on the piezoelectric transducer connect to an external signal amplifier to power the device. A thermocouple is attached to monitor temperature of the piezoelectric transducer as well as the nozzle plate. A small stainless steel line fits into the side of the rubber spacer and is connected to an external device syringe pump to provide a feed for the molecular liquid. To protect the device, silicone gaskets are used on the top and bottom of the sandwich structure to provide a flexible cushion for device assembly and packaging. The device is held together by a custom stainless steel clamp and compression (sealing) of the package

device is controlled by four peripherally located bolts. A sketch of the device (without the surrounding stainless steel clamp) is shown in Figure D.11.
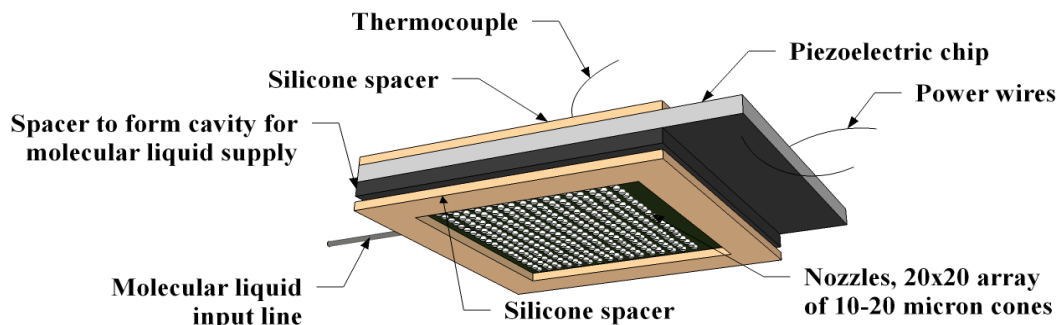

Figure D.11. Schematic of the atomizer device highlighting integral components

There are three pieces of equipment required to operate the atomizer. The 300 MHz synthetic function generator (Model DS 345) is manufactured by Stanford Research Systems. The function generator provides control of the frequency and amplitude of the driving signal, as well as the number of pulses and pulse frequency (period) when operating at less than 100% duty cycle. Signal gain was set using an ULTRA Series RF power amplifier. To monitor the sinusoidal wave generated, a Tektronix TPS 2014 oscilloscope is used.

D.4.2.2 *Atomizer operation*

The atomizer generates liquid droplets by utilizing cavity resonances in the 1–3 MHz range along with the acoustic wave focusing properties of pyramidal liquid horns formed by a silicon wet etching process. The liquid horn structure, cavity size, and the speed of sound within the ejection fluid dictate the device resonances and thus the operating frequencies of the device.[10,13] Inexpensive and commonly available lead zirconate titanate (PZT-8) ceramic is used for the piezoelectric transducer. When the

piezoelectric transducer is driven at the fundamental cavity resonant frequency or any of the higher cavity modes, a standing acoustic wave develops, and constructive interference in the pyramidal nozzles focuses the wave so that the peak pressure gradient occurs near the tip of the nozzles.

Selective operation of the atomizer can be in either drop-on-demand (DOD) or continuous-jet-ejection mode.[11,12] These different modes adapt to the requirements of specific tasks such as droplet-gas contact time, solvent consumption, etc. Regardless mode, the produced droplets/jets are highly uniform in size, which is an important consideration for achieving efficient and reproducible performance of any system relying on the "quality" of fluid dispersion.

Putting a net charge of the same sign is often beneficial in aerosol formation avoid in-flight coalescence of generated droplets in the dispersed phase. We do this in the atomizer, at very low bias DC potentials or even in purely AC mode of the piezoelectric transducer's operation through the intrinsic coupling of electric and mechanic fields in the ultrasonic atomizer, by using a locally arranged set of electrodes in the vicinity of the nozzle array surface.[16]

The atomizer is a resonant device that enables low-power operation, a critically-important consideration. An incremental increase of the active number of nozzles (array size) driven by a single piezoelectric transducer comes at a significantly diminishing cost (a fraction of a percent) of an additional power input due to improved power utilization with an increase in the array size.

D.4.2.3 *Absorption tower*

The tower, constructed of Plexiglas to verify ejection of molecular liquid and monitor experiment progress, will stand one meter tall and contain a collection tray on the bottom and the atomizer device mounted to the top. The atomizer device will be mounted to a Plexiglas disk attached to a custom clamp to allow for adjustment of the effective tower height. Beside the atomizer, a baffle will be mounted to direct the flow of the atomized molecular liquid as well as the flue gas to a mixing zone below the baffle. The atomizer will sit on one side of the baffle while the flue gas injection port will sit on the other. The design and placement of the baffle will be optimized using CFD simulations and supporting experiments in order to direct the atomized molecular liquid downward while allowing sufficient mixing. The tower will be completely sealed, to prevent escape of atomized molecular liquid. The device is shown below in Figure D.12.
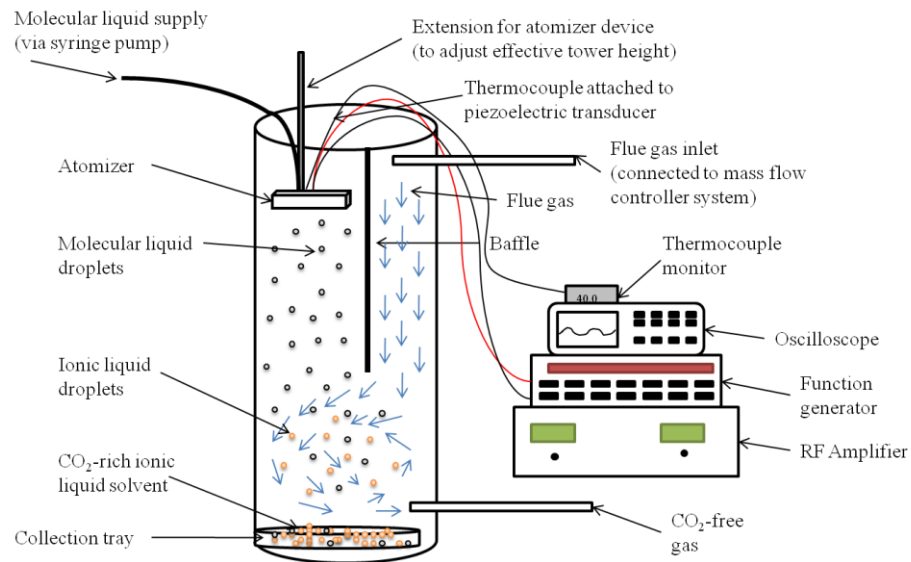

Figure D.12. Schematic of atomizer, absorption tower and ancillary equipment

D.4.2.4 *Overall operation*

The ML is fed to the atomizer device as described above. The driving voltage signal is sent from the function generator, which produces a sinusoidal wave at a specified frequency and amplitude. The signal is amplified by the RF power amplifier and sent to the piezoelectric transducer (the voltage signal on the piezoelectric is in-situ monitored via an oscilloscope). The frequency used is the resonance frequency of the fluid filled device and the amplitude used is the minimum that provides sufficient ejection (to minimize power requirements). Prior to performing CO_2 capture experiments, the ML atomization process will be experimentally characterized for power input required for ML ejectability, nozzle aperture size and operating frequencies as a function of ML properties. These results will be used in the CO_2 capture process as well as further power requirement (using ANYSYS) and fluid flow modeling (using FLUENT). Once the atomization properties have successfully been set, the molecular liquid will be atomized into the column with the simulated flue gas that enters and flows downward on the opposite side of the baffle. The simulated flue gas is to be created using mass flow controllers and gas cylinders. Studies in Budget Period (BP) 1 will use simple simulations of 13%CO_2/N_2. BP2 will involve utilizing a more realistic gas mixture at also includes H_2O and SO_x. As the atomized molecular liquid and flue gas meet at the bottom of the baffle, a mixing zone will be created. The molecular liquid droplets absorb the CO_2 in the stream and fall to the collection tray at the bottom of the tower as RevIL. As the experiment progresses, the product gases will be monitored with a residual gas analyzer. After the runtime has expired, the collection tray will be removed and the ionic liquid formed will be analyzed.

D.4.3 <u>Analysis and Data Integrity</u>

D.4.3.1 *Post-experimental analysis*

To quantify the extent of conversion of the molecular liquid to the reversible ionic liquid, a sample of the formed RevIL will be taken from the bottom of the tower. Using a Reichert Arias 500 Abbe-style refractometer, the sample refractive index will be measured and used to calculate conversion of the molecular liquid to the ionic liquid and ultimately CO_2 capture. Additionally, the collected RevIL and regenerated ML will be analyzed by NMR, LC and GCMS to detect the possible formation of degradation products. Successful atomization of ML in the CO_2 absorption column with measurable conversion to RevIL will indicate success at the go/no-go decision point.

The reversible ionic liquid collected from the bottom of the absorption tower will also be analyzed to measure viscosity and study desorption. Viscosity plays an important part in determining the operating costs and as shown in MRC1, we can have sufficiently low viscosities (300cP) with fairly high conversion levels (80%). Desorption temperatures will be studied using a TGA. Potential loss of the ML as a result of elevated temperatures for desorption will be determined.

To eliminate variability as a function of the sampling location, ionic liquid samples will be collected from multiple locations at the bottom of the tower. This will allow for an accurate value of conversion to be calculated as well as any deviation or error that may be present. Calculation of standard deviation of the sample conversion will further allow us to optimize the system and achieve a uniformly converted ionic liquid for

desorption and subsequent regeneration. At the end of BP1, a single ML/RevIL will be identified for further experimentation and analysis for commercial-scale CO_2 capture simulation.

D.4.3.2 *Variables*

Tower height and experiment duration will be varied to determine the optimal time of flight and contact time with CO_2 for the ejected droplets. Smaller droplets will lead to greater gas-to-solvent contact area, shorter diffusion paths, slower rate of fall (greater residence time), which yield higher CO_2 uptake. Increased CO_2 uptake for greater conversion of ML to RevIL will give an increase in viscosity. This would impose a pumping power overhead on the overall energy efficiency of the system. The optimum level of CO_2 capture and ML-to-RevIL conversion during the solvent transport are important design variables which we shall optimize.

In the course of this program, we shall also adopt and refine the ultrasonic atomizer for unique requirements of dispersing the molecular liquids. Our efforts will include an optimized atomizer design, aiming to minimize the specific power input (i.e., per unit flow rate of atomized liquid), and in-depth experimental characterization and modeling of the acoustics and fluid mechanics of device operation, targeting the necessary/desired flow rates (system throughput) and droplet size(s). The device performance will be tested with simulated flue gas, and the system-level results will be used to further enhance the ultrasonic atomizer design and performance. The effect of flue gas flow direction (co-, counter- or cross-current) and flow rate will be determined for optimal mass transfer in conjunction with atomizer parameters.

To establish a complete absorption / desorption capture system it will also be necessary to define the variables that influence the desorption process. The effect of desorption temperature and heating rate will be examined to achieve complete reversal of the ionic liquid to the molecular liquid and minimal solvent losses.

To perform these tasks we shall use the state-of-the-art simulation and experimental tools and manufacturing processes we have already used and described in the previous sections of the proposal, and will develop new tools and techniques, as necessary.

By altering the dimensions of the absorption tower, we can observe the effect of scale-up for our process. At bench-scale our lab can supply a flue gas for simulation with the composition and temperature of power plant flue gas after desulfurization.

D.4.4 Environmental health and safety

We have a long standing collaboration with the department of Environmental Health and Safety of the Georgia Institute of Technology. We will continue our collaboration to anticipate and evaluate the hazards of our proposed process at the bench-scale and as we progress towards the commercial process. We propose to approach the hazard assessment for the scale up of the carbon dioxide capture plant in a similar fashion to the way we have been doing for the laboratory bench-scale model. At this stage, we already have established chemical hazard assessments of all reactants and standard operating procedures (SOP) for the synthesis of the RevILs system 1, 2 and 3 and for operating the bench-scale atomizer model. In the final assessment, we will identify the hazards of all the reactants (including catalysts), products and by products/wastes. This would include chemical hazards and physical hazards such as flammability, heat, or

247

cryogenic hazards. Also, we will consider the final disposition of all the products, wanted and unwanted, and determine how they will be dealt with, such as collect to recycle, or dispose of per local, state and federal regulations.

Additional proposed experimental details, activities and timelines are included in the Standard Operating Procedures (SOPO) in MRC4.

D.4.5 Scale-up and Simulation

D.4.5.1 *A. Analysis of ML/RevIL corrosion and degradation behavior*

Determining the corrosive behavior of liquids to be used in CO_2 capture is important for three reasons: selection of unit operation materials of construction, handing considerations and determination of degradation pathways. Many chemical degradation pathways are promoted by the presence of metal ions in the solvent that are a result of corrosion of the processing equipment by the solvent. ConocoPhillips, who are well-equipped and experienced in corrosion testing, will be aiding in the corrosion testing and interpretation.   Once the corrosion properties have been analyzed, the degradation pathways will be investigated for the ML and resulting RevIL from CO_2 capture. Analysis of the ML/RevIL after cycling will be performed by FTIR, LC-MS, GC-MS and NMR. After identification of any degradation products has occurred, we shall seek to delineate potential degradation pathways, again consulting our partners ConocoPhillips and Evonik. Model reactions will also be performed to test the hypotheses. These may be implemented into the synthesis of the ML or as an additive step later.

D.4.5.2 *Establish critical parameters for pilot scale phase*

We shall work on design of a large scale system suitable for scale-up, including development of a design strategy for (1) integration of many atomization units into a large scale array with suitable solvent delivery and distribution system and (2) collection of ionic liquid, regeneration and return to the atomization unit to close the loop. This will require choosing the design and sizing of heat exchanger components and coupling with external heater/chiller system (optimally using being the utilities already available in a coal-fired power plant) for efficient heat supply/rejection to the capture system.

To transition to large scale demonstration, we shall address the issues of costs and manufacturability of components. Our baseline strategy is to use silicon micromachining to fabricate the nozzle arrays. Since these nozzle arrays are made using a standard 2-mask batch process, it is scalable to production of large quantities at reasonably low cost. The cost estimates have been prepared in consultation with the microfabrication service companies (Micralyne and MEMSCAP) and suggests a cost of 6-8 cents per nozzle is readily achievable.

D.4.5.3 *Modeling*

The atomization process will be analyzed for optimized power inputs using ANSYS and fluid flow of the droplets using computational fluid dynamics (CFD/ FLUENT software). Additionally, we will use the combination of simple analytical models and CFD simulations to evaluate and optimize the heat and mass transfer in the ML-CO_2-RevIL system. We have significant experience with such analytical tools, including validation on laboratory systems, with applications to a wide range of reaction-transport systems, including adsorption CO_2 capture and catalysis.[23] The goal of these simulations will be to design an optimal system configuration and develop operating

guidelines that result in highest heat and mass transfer rates to/from solvents in order to reach near-intrinsic kinetics of CO_2 absorption and desorption during solvent regeneration, while minimizing the parasitic losses due to pumping power and heat rejection to the environment.

The results obtained from experiment and modeling of the atomization and CO_2 capture process along with EH&S analysis will be integrated into the final process simulation of a commercial-scale CO_2 capture system using Aspen HYSYS. The end result of the project will be a system simulated for CO_2 capture with information available for process costs and power needs. With the results obtained in this project, the proposed technology will be ready for scale-up to pilot scale in a future project.

D.5 References

1. Blasucci, V.; Dilek, C.; Huttenhower, H.; John, E.; Llopis-Mestre, V.; Pollet, P.; Eckert, C. A.; Liotta, C. L. *Chemical Communications* **2009**, 116.

2. Blasucci, V. M.; Hart, R.; Pollet, P.; Liotta, C. L.; Eckert, C. A. *Fluid Phase Equilibria* **2010**, *294*, 1.

3. Blasucci, V.; Hart, R.; Mestre, V. L.; Hahne, D. J.; Burlager, M.; Huttenhower, H.; Thio, B. J. R.; Pollet, P.; Liotta, C. L.; Eckert, C. A. *Fuel* **2010**, *89*, 1315.

4. Hart, R.; Pollet, P.; Hahne, D. J.; John, E.; Llopis-Mestre, V.; Blasucci, V.; Huttenhower, H.; Leitner, W.; Eckert, C. A.; Liotta, C. L. *Tetrahedron* **2010**, *66*, 1082.

5. Shirota, H.; Edward W. Castner, J. *Journal of Physical Chemistry B* **2005**, *109*, 21576Crosthwaite, J. M.; Muldoon, M. J.; Dixon, J. K.; Anderson, J. L.; Brennecke, J. F. *Journal of Chemical Thermodynamics* **2005**, *37*, 559Chuit, C.; Corriu, R. J. P.; Reye, C.; Young, J. C. *Chemical Reviews* **1993**, *94*, 1371.

6. Yeh, J. T.; Pennline, H. W.; Resnik, K. P. *Energy & Fuels* **2001**, *15*, 274.

7. Poling, B. E. *The properties of gases and liquids*; 5th ed. ed.; McGraw-Hill: New York :, 2001.

8.   Eckert, E. R. G.; Drake, R. M. *Analysis of Heat and Mass Transfer*; McGraw Hill, New York.

9.   Fedorov, A. G.; Degertekin, F. L. USA, 2007Fedorov, A. G.; Degertekin, F. L. USA, 2009Degertekin, F. L.; Fedorov, A. G. USA, 2007.

10.   Meacham, J. M.; Ejimofor, C.; Kumar, S.; Degertekin, F. L.; Fedorov, A. G. *Review of Scientific Instruments* **2004**, *75*, 1347.

11.   Meacham, J. M.; Varady, M. J.; Degertekin, F. L.; Fedorov, A. G. *Physics of Fluids* **2005**, *17*.

12.   Forbes, T. P.; Degertekin, F. L.; Fedorov, A. G. *Review of Scientific Instruments* **2007**, *78*.

13.   Meacham, J. M.; Varady, M. J.; Esposito, D.; Degertekin, F. L.; Fedorov, A. G. *Atomization and Sprays* **2008**, *18*, 163.

14.   Meacham, J. M.; O'Rourke, A.; Yang, Y.; Fedorov, A. G.; Degertekin, F. L.; Rosen, D. W. *Journal of Manufacturing Science and Engineering-Transactions of the Asme* **2010**, *132*.

15.   Aderogba, S.; Meacham, J. M.; Degertekin, F. L.; Fedorov, A. G.; Fernandez, F. M. *Applied Physics Letters* **2005**, *86*.

16.   Forbes, T. P.; Dixon, R. B.; Muddiman, D. C.; Degertekin, F. L.; Fedorov, A. G. *Journal of the American Society for Mass Spectrometry* **2009**, *20*, 1684Forbes, T. P.; Degertekin, F. L.; Fedorov, A. G. *Journal of the American Society for Mass Spectrometry* **2010**, *21*, 501.

17.   DOE/NETL-2010/1397, 2010.

18.   Development, C. f. G. In *Science Daily*, 2007; Vol. November 15.

19.   Marzinke, M.; MacMillan, J. H.; August, T. F.; Telepchak, M. J.; United Chemical Technologies, Inc.: United States, 2001.

20.   Wang, H.; Matsuhashi, H.; Doan, B. D.; Goodman, S. N.; Ouyang, X.; Clark, W. M. J.; Tetrahedron, 2009; Vol. 65.

21.   Nguyen, B. T.; Dow Corning: United States, 2004.

22.   Shreve, R. N.; Burtsfield, D. R. *Journal of Industrial and Engineering Chemistry* **1941**, *33*, 218.

23.   Damm, D. L.; Fedorov, A.; Industrial & Engineering Chemistry Research, 2008; Vol. 47 Damm, D. L.; Fedorov, A.; Industrial & Engineering Chemistry Research, 2009; Vol. 48Fedorov, A.; Viskanta, R.; International Journal of Heat and Mass

Transfer, 1999; Vol. 42Fedorov, A.; Viskanta, R.; Thermal Science and Engineering, 1999; Vol. 5Fedorov, A.; Viskanta, R.; Chemical Engineering Communications, 1999; Vol. 171Kaisare, N. S.; Lee, J. H.; Fedorov, A., *AIChE Journal*, Vol. 51 (8), pp. 2254-2264.; AIChE Journal, 2005; Vol. 51Kaisare, N. S.; Lee, J. H.; Fedorov, A.; Industrial & Engineering Chemistry Research, 2005; Vol. 44Kim, Y. J.; Joshi, Y.; Fedorov, A.; Journal of Mechanical Science and Technology, 2008; Vol. 22.

APPENDIX E - ADDITIONAL INFORMATION ON CO$_2$ AS A PROTECTING AGENT

E.1 Standard NMRs

The NMRs included below are for reference to those presented in Chapter 3.
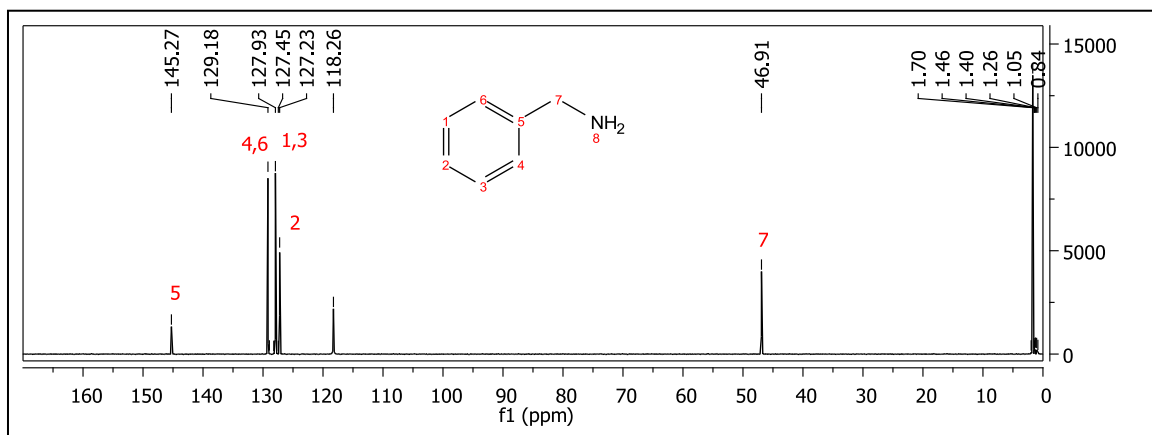
Figure E.1. 13C NMR spectrum of benzylamine in deuterated acetonitrile
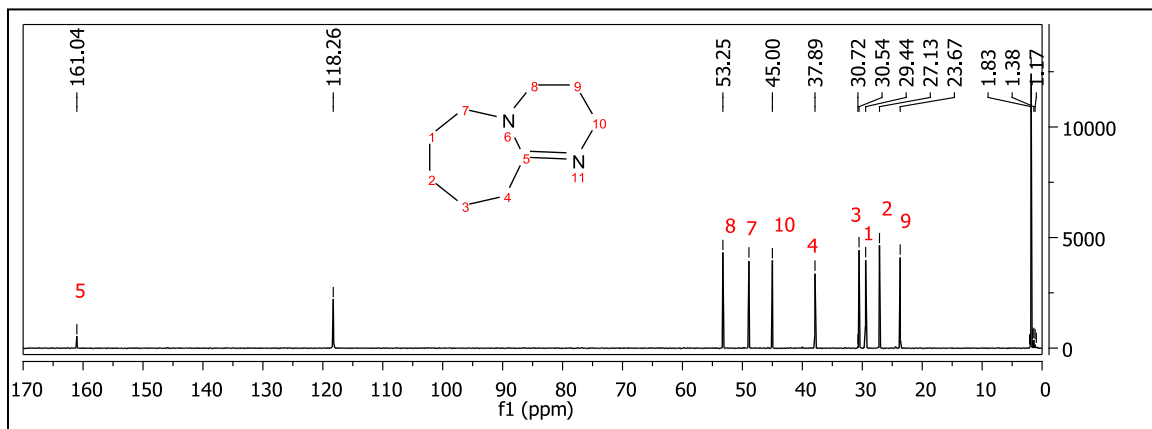
Figure E.2. ^{13}C NMR spectrum of DBU in deuterated acetonitrile
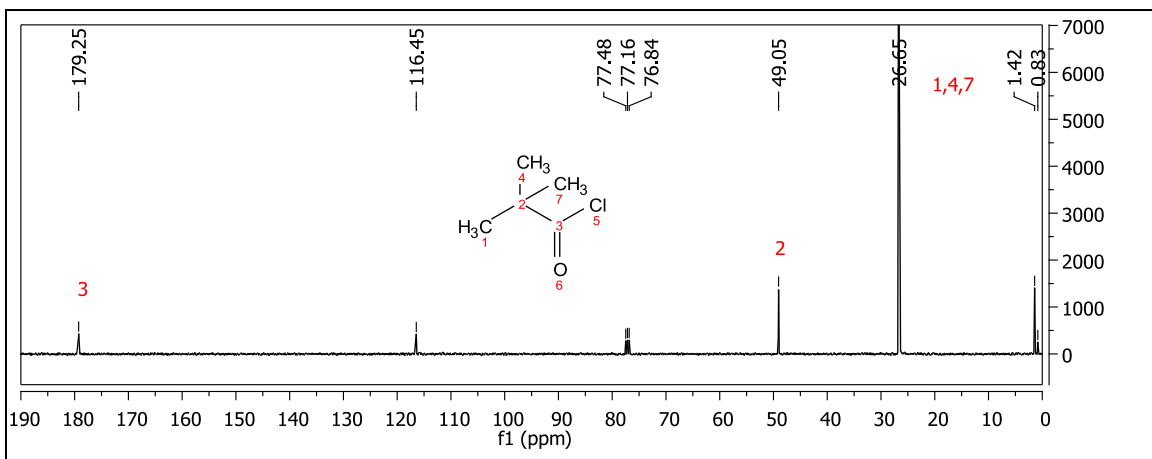
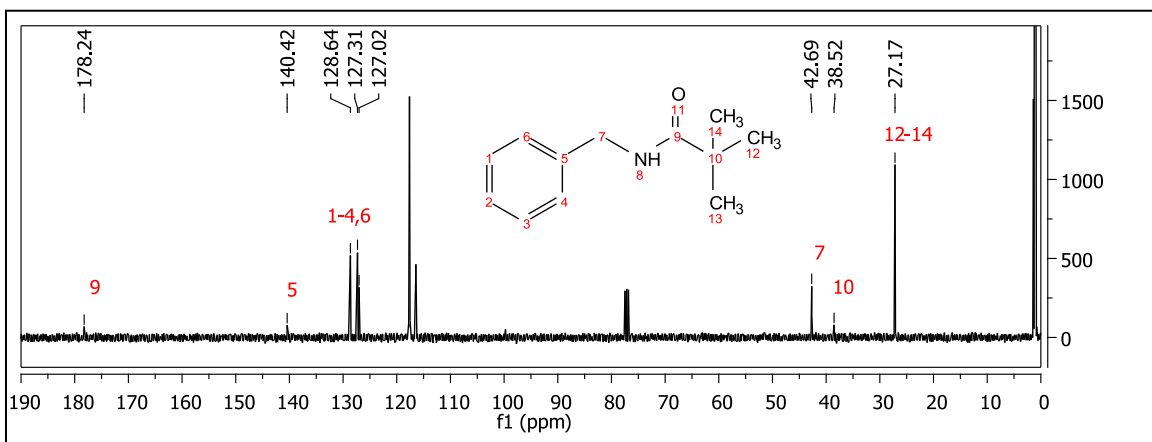**Figure E.3.** ^{13}C NMR spectrum of pivaloyl chloride with a deuterated chloroform capillary

Figure E.4. ^{13}C NMR spectrum of benzylpivalamide with a deuterated chloroform capillary
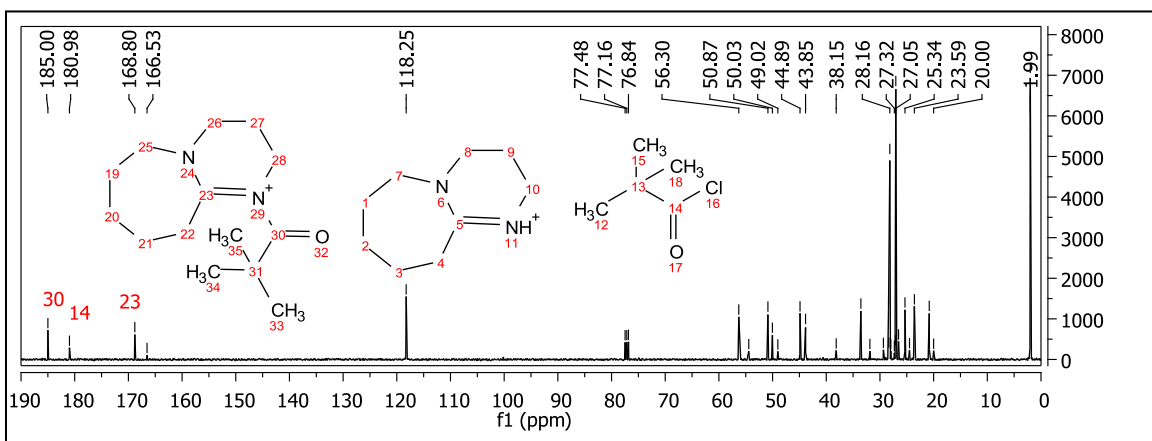
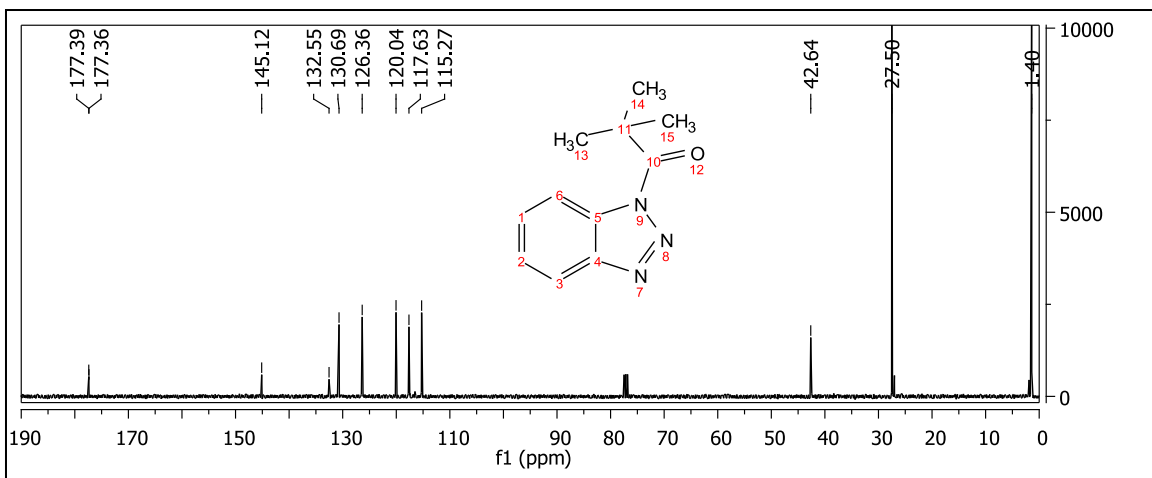**Figure E.5.** ^{13}C NMR spectrum of pivaloyl chloride and DBU – reaction observed

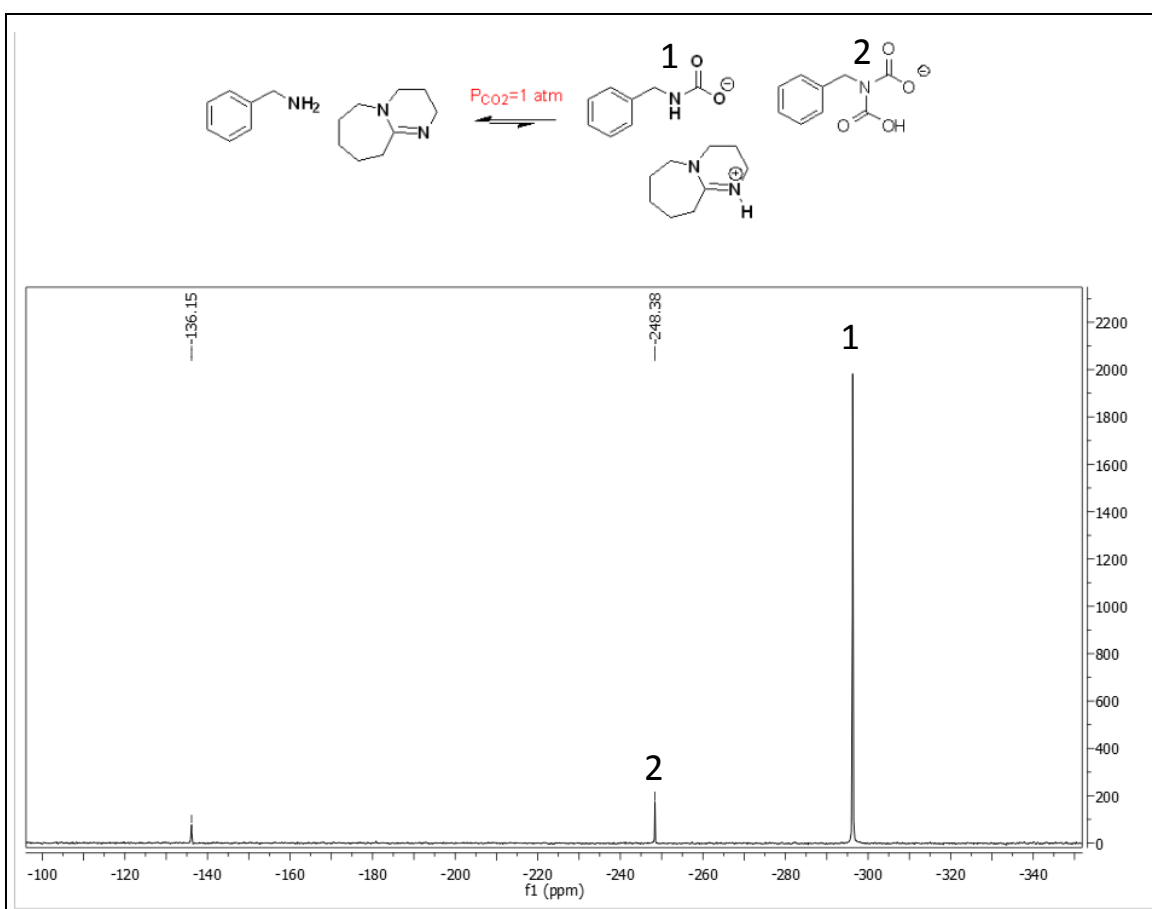**Figure E.6.** ^{13}C NMR spectrum of pivaloyl benzotriazole in deuterated chloroform

Figure E.7. ^{15}N NMR of CO_2-protected benzylamine (^{15}N labeled) using DBU, nitrogen atoms are labeled above
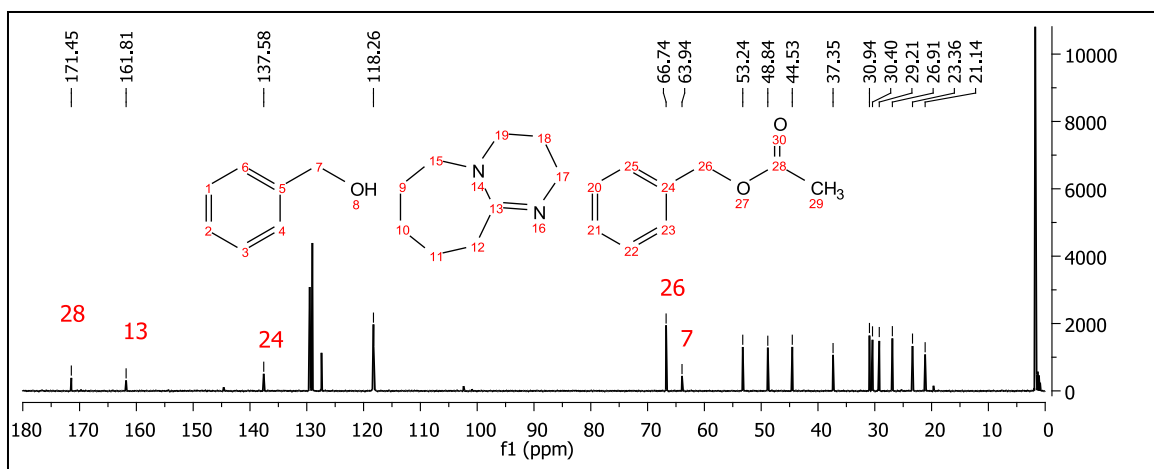
Figure E.8. ^{13}C NMR showing reaction products from benzyl alcohol and isopropenyl acetate in the presence of DBU
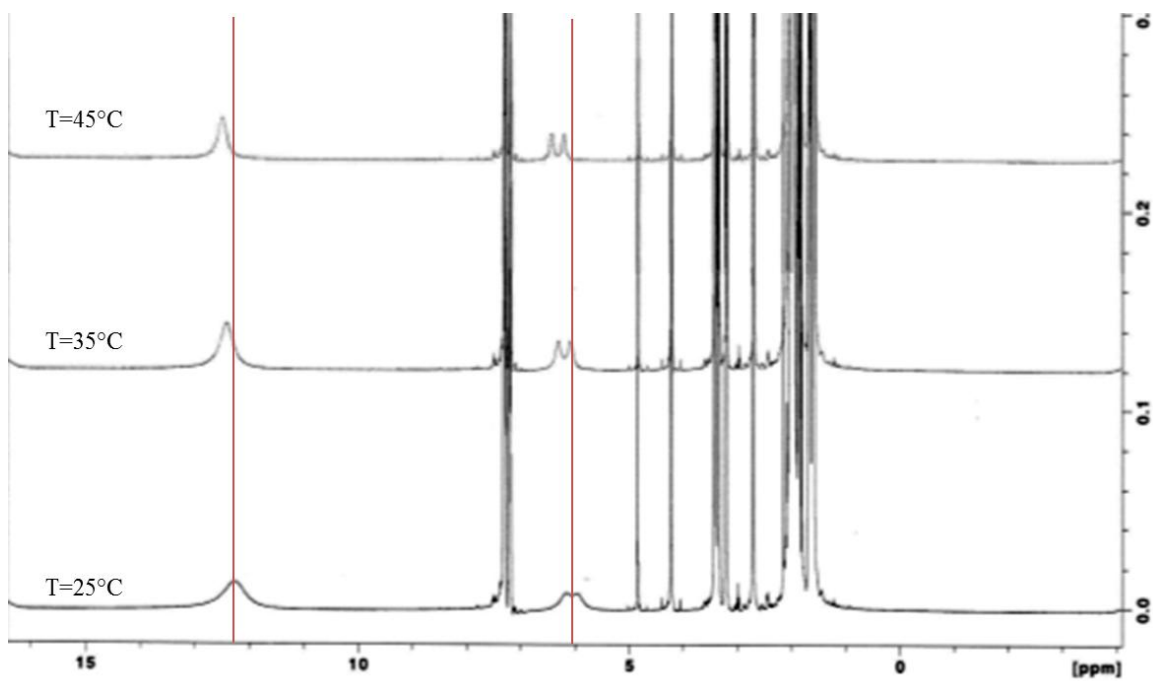

Figure E.9. ^{1}H NMR showing the effect of temperature on proton exchange of the protected benzylamine

256

VITA

Amy Ethier (née Rohan) was born in October 1985. Raised in Columbia, CT she attended Windham High School. After graduating from high school in 2003, Amy pursued an undergraduate degree in chemical engineering at the University of Connecticut. At the University of Connecticut, she conducted research under Dr. Robert Weiss. After graduating in 2007, she accepted a position as a research engineer at Saint-Gobain. While at Saint-Gobain, she decided to pursue an advanced degree. She began her doctoral study at the Georgia Institute of Technology in the Chemical & Biomolecular Engineering department in 2009. During that time, she has completed research as a member of the Eckert-Liotta research group, and was actively involved with Society of Women Engineers as the outreach coordinator for the Atlanta area. She will continue her career with BASF Chemical Co. in the Professional Development Program.